A FIELD, PETROLOGICAL AND GEOCHEMICAL STUDY
OF THE MASIRAH OPHIOLITE, OMAN.

by .

IAN LLOYD ABBOTTS

A thesis submitted for the degree of Doctor of Philosophy under
the general regulations of the Faculty of Science and Engineering,
University of Birmingham.

UNIVERSITY^{OF}BIRMINGHAM

University of Birmingham Research Archive

e-theses repository

SYNOPSIS

A reconnaisance survey of the 1000 Km^2 of Masirah Island, Oman,
has revealed a fully-developed ophiolite complex which is believed to represent
a fragment of Cretaceous ocean crust and upper mantle generated at a
constructive plate margin. The complex consists of mantle serpentinites,
plutonic rocks ranging from dunite to trondhjemite, a sheeted dyke complex
and pillow lava-sediment sequences, all of which have been chemically and
petrographically analysed.

Several belts of serpentinite occur within the ophiolite associated with
major fault-lines. The serpentinites are clearly derived from depleted
harzburgitic mantle and their field relations suggest that some were emplaced
in the oceanic environment.

The chemistry of the plutonic rocks suggests that they are products of
dominantly open-system fractional crystallisation of tholeiitic liquid(s),
possibly in several discrete magma chambers. Modelling of trace and RE
elements suggests that moderate degrees of mantle peridotite melting were
involved in production of the magma chamber parental liquid(s).

At a higher crustal level sheeted dyke-massive gabbro relationships are
interpreted in a model of roof underplating, which causes a decreasing frequency
of dyke injection. Metamorphism of the sheeted dykes and lavas is interpreted
as sub-sea floor in origin and its effect on whole-rock chemistry is assessed.
The dykes and lavas have a chemistry largely typical of present-day ocean
tholeiites and the relative contributions of the processes of partial melting and
fractional crystallisation to that chemistry are evaluated.

Two localised volcanic groups were identified, which appear to have
enriched chemistries compatible with origin at off-axis oceanic islands.

A major tectonic zone cross-cuts the ophiolite units and has features
reminiscent of the modern oceanic transform faults. The importance of this
structure, both in the oceanic environment and during the process of ophiolite
emplacement, is assessed.

Intrusive into the ophiolite is a granite whose trace and RE element chemistry is alien to the oceanic environment and suggests melting of continental crust.

Finally, a synthesized model of the former constructive margin is produced and an attempt is made to define the type of spreading centre represented. Comparison of the Masirah Ophiolite with the Semail Ophiolite of the Oman Mountains suggests that their former correlation may be ill-founded. An assessment of late Mesozoic-early Tertiary plate motions indicates an origin during Cretaceous sea-floor spreading of an early Indian Ocean. Several features may indicate a slow-spreading, much-faulted, constructive margin.

Frontispiece

General view southeastwards from Jabal Hamra showing typical
rugged topography of the plutonic rocks. Paler outcrops are
gabbroic, darker are olivine gabbros or troctolites.

DEDICATION

I would like to dedicate this work to Anne for

her continual support.

ACKNOWLEDGEMENTS

CONTENTS   Page

<u>LIST OF TEXT FIGURES</u>   <u>After Page</u>

LIST OF PLATES After Page

CHAPTER 1

INTRODUCTION

The desert island of Masirah, which lies 24 km off the SE coast of Oman at the margin of the Indian Ocean, is formed predominantly of an ophiolite complex of mafic and ultramafic rocks. There is wide acceptance that such complexes represent oceanic lithosphere generated at constructive margins (Coleman, 1977; Gass and Smewing, 1978). Consequently this thesis is argued on the premise that ophiolite studies give an insight into the processes operating at oceanic spreading centres. The magmatic supply rate from mantle to spreading centre is greater and more continuous than that of any other tectonic environment. It follows that study of ophiolite complexes will also aid in understanding the evolution of the mantle-crust system.

1A. Previous studies and scope of the present work

There have been few geological studies on Masirah. The first by Lees (1928) described the occurrence of gabbros and serpentinites, noted that they were overlain by Eocene limestone and correlated them with similar rocks in the Semail Nappe of the Oman Mountains. Moseley (1969) noted that the mafic-ultramafic rocks were intruded by a late-stage potassic granite whilst Glennie et al. (1974) recorded the presence of the complete ophiolitic assemblage and its close association with Lower-Middle Cretaceous sediments. The last workers concluded:

"there is no direct correlation (of the basic
and ultrabasic rocks of Masirah Island)with
the Hawasina and Semail apart from lithological
similarity."

Field work was undertaken during the winters of 1975-76 and
1976-77 when a reconnaissance survey of the 1000 sq.km of
Masirah Island was conducted, together with collection of
approximately 800 rock specimens for petrological, geochemical
and palaeomagnetic studies. The help and hospitality provided
by the personnel of R.A.F. Masirah ensured two pleasant visits
and meant that 54 days on the island resulted in 52 full days
in the field, both for the writer and for Dr F. Moseley.
Though a reconnaissance approach was dictated by the large area
and lack of previous survey, an attempt was made to quickly
define the problem areas and to map these in more detail on a
1:12000 scale. The high degree of exposure and good vertical
air photograph cover, at 1:12000 and 1:60000, facilitated these
designs.

1B. Geomorphology of Masirah

The island has maximum dimensions of 65 km from NNE to
SSW and 16 km perpendicular to this and rises to a height of
245 m in the north. Solid rocks are almost continuously exposed
over much of the island and over 95% belong to the ophiolite
complex. Gabbros and sheeted dyke complex form the higher
ground of the north and south of the island respectively. The
low-lying waist of the island is floored mainly by pillow lavas
and serpentinites. Locally in the north the ophiolite is
overlain unconformably and topographically by gently warped

Lower Tertiary (? Eocene) limestone.

The solid geology is partially concealed by coastal gravel fans, particularly well developed along the north-west coast, and by wadi sands and gravels composed of ophiolite and limestone debris. The latter are incised to a depth of 8-10 m by wadis of the present erosion cycle and the resulting terraces testify to recent uplift (late Quaternary : Carney and Welland, 1974).

1C. Definition of an ophiolite

Coleman (1977) notes that the term ophiolite is derived from the Greek root "ophi" meaning snake or serpent and was originally used to describe serpentinites (Brongniart, 1827). The currently accepted definition is that proposed by the 1972 Penrose conference which describes an ophiolite as an assemblage of ultrabasic and basic rocks as set out in Table 1 (see overleaf):

Table 1. An idealized complete ophiolite (modified from Gass, 1977)

TOP

        Mafic volcanics   Commonly pillowed, overlying sediments may include ribbon cherts, thin shale interbeds and minor limestone.

- - - - - - - merging into - - - - - - -

        Mafic sheeted dyke complex

- - - - - - - - - - - - - - - - - - -

                                        Trondhjemites
                                        Gabbros
        Gabbro complex,   Olivine gabbros
        usually cumulate   Peridotites*
                                          Dunites* (commonly with chromite)

- - - - - - - - - - - - - - - - - - -

        Harzburgite* (sometimes lherzolite and dunite) usually with metamorphic tectonic fabric

BASE

---

    * Commonly serpentinized

1D.   Ophiolite complexes as ocean crust

The Penrose conference also states:

> "although ophiolites generally are interpreted
> as oceanic crust and upper mantle the term
> should be independent of supposed origin."

Ophiolite complexes are common along the Tethyan region from Yugoslavia to Oman (Dewey et al, 1973) and also throughout the Circum-Pacific (e.g. California : Bailey et al, 1970; Papua : Davies, 1969; Macquarie Island : Varne and Rubenach, 1973). Both areas have been interpreted as sites of oceanic plate consumption. Preservation of the complexes varies from the extensively disrupted and dismembered examples (e.g. California coast ranges : Bailey, op.cit) to those that are stratigraphically complete and intact (e.g. Troodos : Gass, 1968; Moores and Vine, 1971).

Seismic profiles of the large and intact Troodos and Oman Ophiolites compare quite favourably with those of the oceanic lithosphere (Fig.1.1). Moreover, direct sampling of the ocean crust has revealed a rock suite which is broadly similar in petrological, geochemical and metamorphic characteristics to that of the ophiolite complexes (Miyashiro et al, 1971; Pearce and Cann, 1971; Saunders et al, 1978). Stable isotope studies of the ophiolite metamorphic rocks indicate a sea-water induced metamorphism whilst metallogenic deposits found in both ophiolitic and oceanic environments appear to result from similar patterns of rock-sea water interaction (Spooner et al, 1974; Scott et al, 1974 and 1976; Smewing et al, 1977).
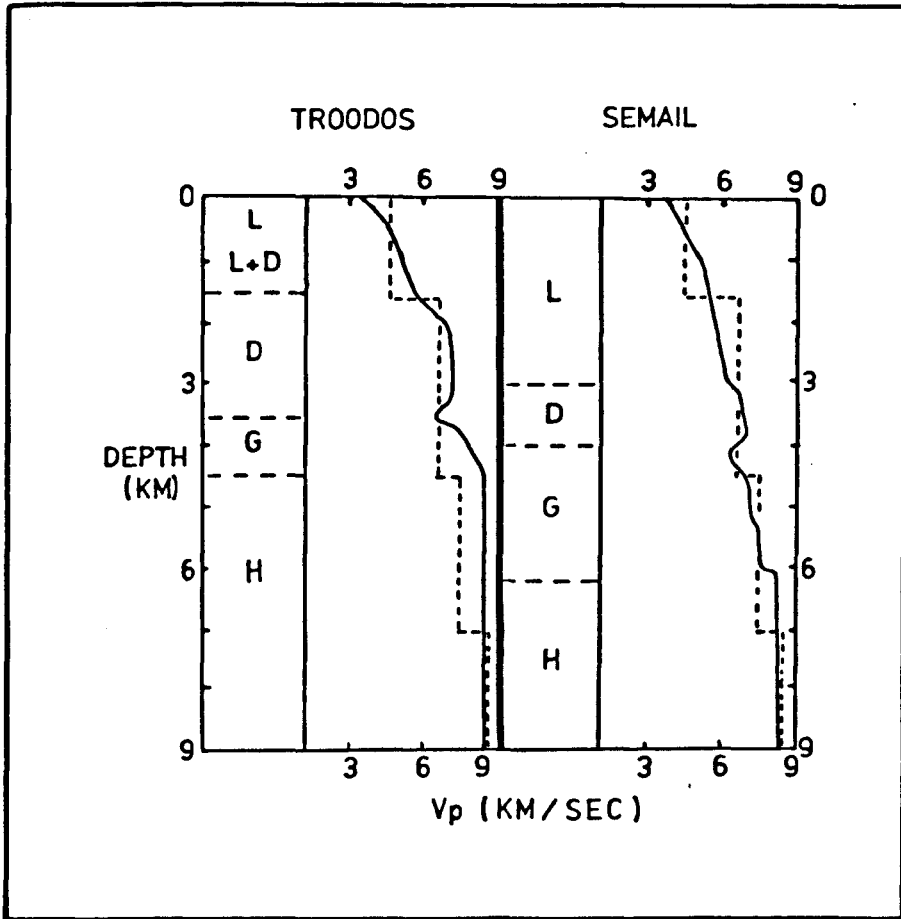
FIG.1.1. Simple stratigraphic columns and estimated seismic velocity profiles for the Troodos and Semail ophiolites. Modified from Christensen, 1978. (L = lava, D = dolerite, G = gabbro complex, H = harzburgite). For comparison the dashed lines show the Sonobouy type 2 ocean crust profile of Christensen and Salisbury (1975).

Table 1.2 sets out the environmental indicators of the various ophiolite units. (see overleaf).

The evidence of Table 1.2 strongly suggests that ophiolite generation occurs in a marine environment, which was under a tensional tectonic regime and was dominated by basic magmatism. The similarity to the present-day constructive plate margin seems inescapable and has been cogently argued by many, including Moores and Vine (1971), Dewey and Bird (1971), Gass (1977), Salisbury and Christensen (1978) and Gass and Smewing (1978).

1E. Regional setting of the Masirah Ophiolite

1. On-land geology of the adjacent Oman Mountains

The broad similarity of the Masirah Ophiolite and the Oman Ophiolite found within the Semail Nappe of the Oman Mountains led to their correlation and the postulated dextral displacement of Masirah along the Batain Coast (Fig.1.2; Morton, 1959; Laughton, 1966). However Glennie et al (1974) note:

> "It cannot be demonstrated that the basic and
> ultrabasic rocks of Masirah form a nappe. The
> term Semail Nappe is therefore avoided ...
> the stratigraphic relationships of the
> scattered pre-Tertiary sediments (of Masirah)
> to those of the Oman Mountains are not
> understood."

The suggestions that the correlation of the two ophiolites may be ill-founded is expanded within this thesis. Nevertheless a

Table 1.2. Environmental indicators of the ophiolite units (modified from Gass, 1977)

ROCK TYPE	Sediments (commonly radiolarian cherts).	Lavas (commonly mafic and pillowed).	Sheeted dykes (mafic)	Gabbros	Harzburgites
ENVIRONMENT	Marine bathyal.	Sub-aqueous, lack of intercalated sediments indicates distance from land-mass or rapid extrusion. Little or no vesicularity indicates deep water.	Extensional. No sialic host rock to this or any other of the units.	Layering and cumulate textures suggest large basic magma chamber(s).	Deformation textures suggest solid shearing.
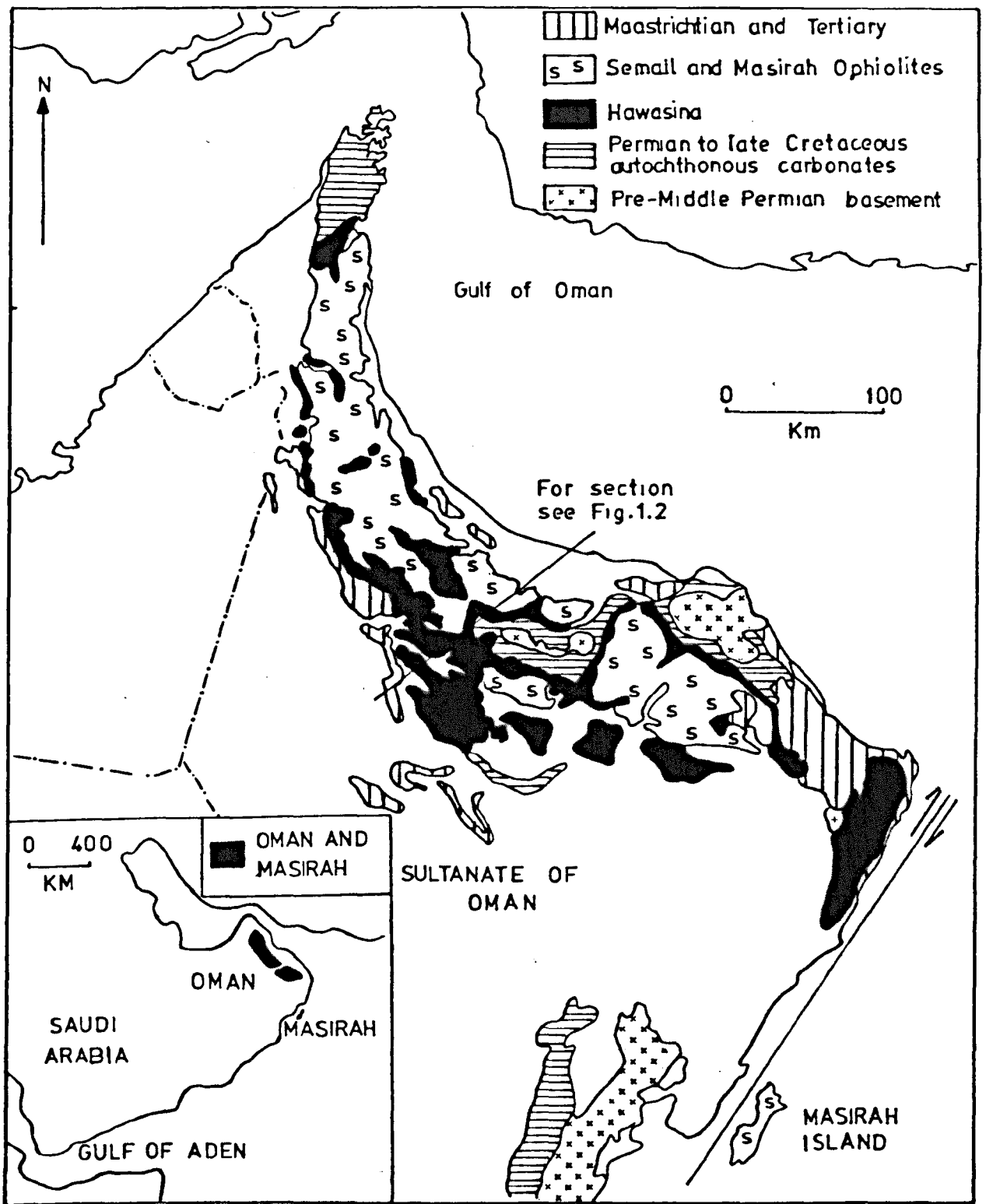
FIG.1.2. Geological map of the Oman Mountains. Simplified from Fig.2.1.1., Glennie et al (1974). For clarity Neogene-Recent deposits are not shown.

brief description of the relationships within the Semail Nappe
are presented here to help the reader to make an independent
assessment.

An introductory account of the Oman Mountains geology is
given by Glennie et al (1974) who described five major rock
sequences. The relationships of these are set out in Table 1.3
and Figs.1.1, 1.3, 1.4.

Glennie et al (1974) suggest that the Oman Ophiolite
represents ocean lithosphere produced during Late Cretaceous
sea-floor spreading to the NE of the Arabian platform. The
Hawasina is believed to represent the partial sedimentary cover
of that lithosphere. Both units are considered to have reached
their present position / on the Arabian continental margin by nappe
emplacement from the north-east (Reinhardt, 1969; Allemann and
Peters, 1972; Glennie et al, 1973, 1974; Carney and Welland,
1974).

2. The Oman Ophiolite

The full ophiolite sequence has been described from the
Oman Ophiolite (Fig. 1.4, adapted from Smewing et al, 1977;
Coleman, 1977). The basal peridotite, dominantly harzburgitic,
is pervasively serpentinized (FIFTY per cent: Coleman, 1977)
and also sheared along the horizontal basal thrust. Olivine,
plagioclase and diopside are the dominant cumulus phases in the
gabbros. These are commonly banded, particularly toward their
base, and late trondhjemitic differentiates are found in their
upper levels. Extensive dyke swarms occur which feed overlying

Table 1.3. Simplified geological succession in the Oman Mountains (adapted from Glennie et al, 1974)

	UNIT	LITHOLOGY	AGE	RELATIONSHIPS
TOP	E	Shallow marine carbonates.	Maastrichtian - early Tertiary.	Unconformable on A-D.
	D	Intact, fully-developed Oman Ophiolite.	Upper Cretaceous	Nappe derived from the NE.
	C	Hawasina Formation: turbidites, limestones, cherts, (pillow lavas, serpentinites) of continental margin - open ocean environment.	Permian to Cretaceous	Several nappes derived from the NE, exposed in reversed age order.
	B	Shallow marine carbonates.	Permian to Cretaceous	Autochthonous unconformable on A.
BASE	A	Crystalline basement	Folded in pre Mid-Permian orogeny.	
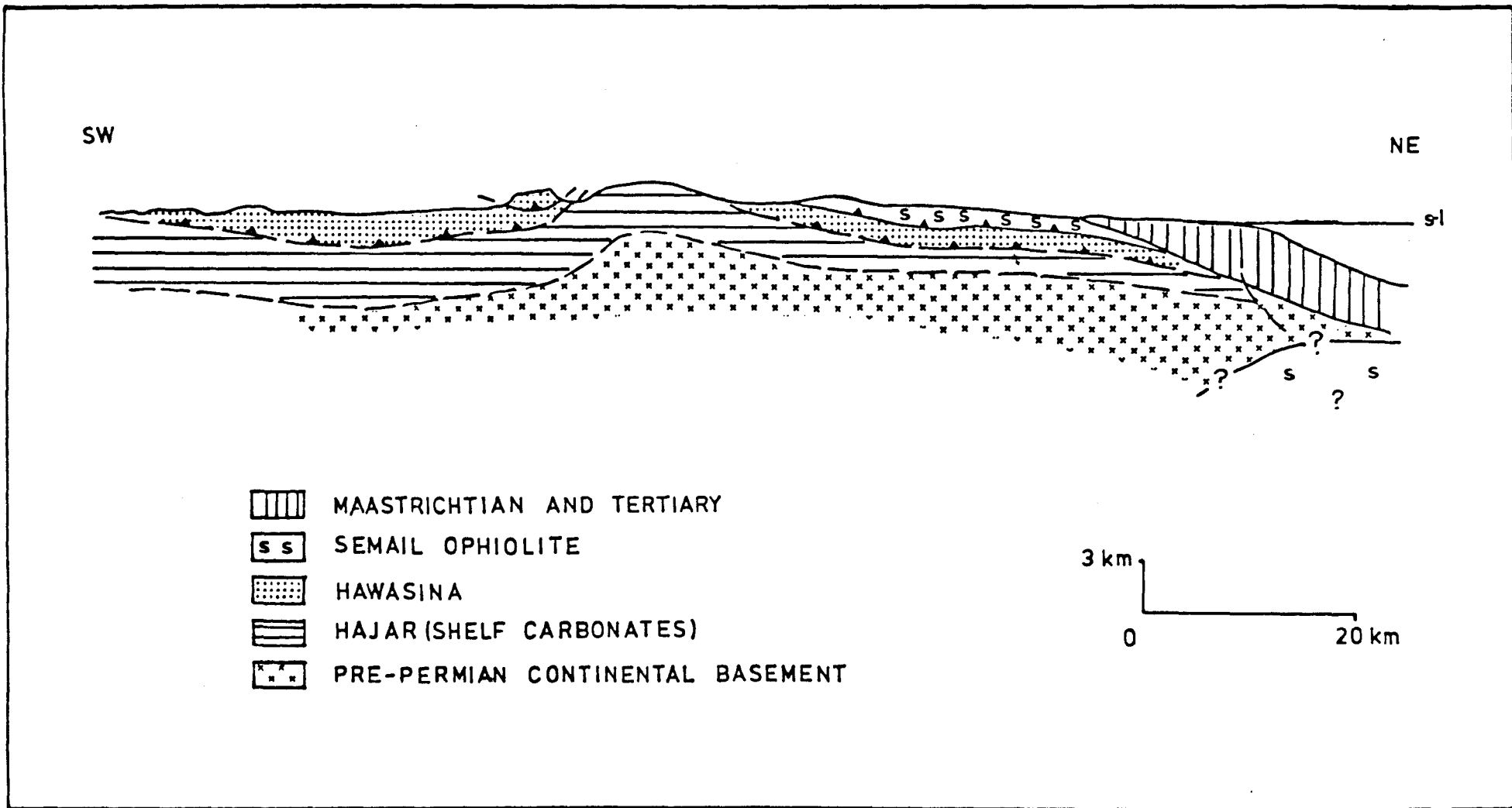
FIG. 1.3. Cross-section through the Oman Mountains. Simplified from Fig. 2.2.1., Glennie et al (1974). For line of section see Fig. 1.1.

FIG.1.4.
Disposition of the nappe units within the Oman Mountains. Copied from Fig.1., Smewing et al, 1977.

Maestrichtian limestones (autochthonous)

Olistoliths of the Hawasina Formation
Ophiolite sediments – laminated mudstones
Pillow lavas, sills, massive flows

Lava host rock

No host rock = 100% dykes

Plutonic rock host rock

Sheeted Intrusive Complex

Trondhjemite, tonalite and quartz diorite

High-level gabbro

High-level intrusives

Laminated pyroxene gabbro

Banded gabbro and peridotite

Cumulate Sequence

SEMAIL NAPPE

Mantle sequence: harzburgite and dunite

1 km

Upper Cretaceous

Metamorphic sheet – greenschists and amphibolites

Hawasina Nappes

Permian to Mid-Cretaceous

Flysch

Platform limestones

Autochthonous sediments

Permian to Upper Cretaceous

Pre-Permian crystalline basement

pillow lavas. The dykes possess a N-S trend in part of the northern Oman Mountains near Sohar (Smewing et al, 1977).
The lavas, dykes and a portion of the gabbros have undergone a thermal metamorphic event attributed to hydrothermal spreading-centre circulation (Coleman, 1977). Sulphide mineralization of the pillow lavas is believed to have a similar cause (Smewing et al, 1977). A metamorphic sheet occurs along the basal thrust and is thought to have developed during ophiolite emplacement (Glennie et al, 1973; Woodcock and Robertson, 1977).

3. <u>Adjacent Arabian Sea Geology</u>

The basement geology of the Arabian Sea (Fig.1.5) is obscured by the thick terrigenous sediments of the Oman Basin and the Indus Cone (Geol.and Geophys.Atlas of the Indian Ocean, 1975; Farhoudi and Karig, 1977). These sediments have prevented   clear documentation of the early Gondwanaland fragmentation and initial Indian Ocean plate motions.

Cretaceous-Lower Tertiary ocean lithosphere is thought to underlie much of the Arabian Sea adjacent to Masirah for the following reasons: (1) Lower Tertiary basement was penetrated along the Owen Fracture in D.S.D.P. holes 223-4 (Whit narsh et al, 1974); (2) there are recognisable Upper Cretaceous-Lower Tertiary magnetic anomalies to the east of the Owen Fracture. The oldest, anomaly 28, is dated at
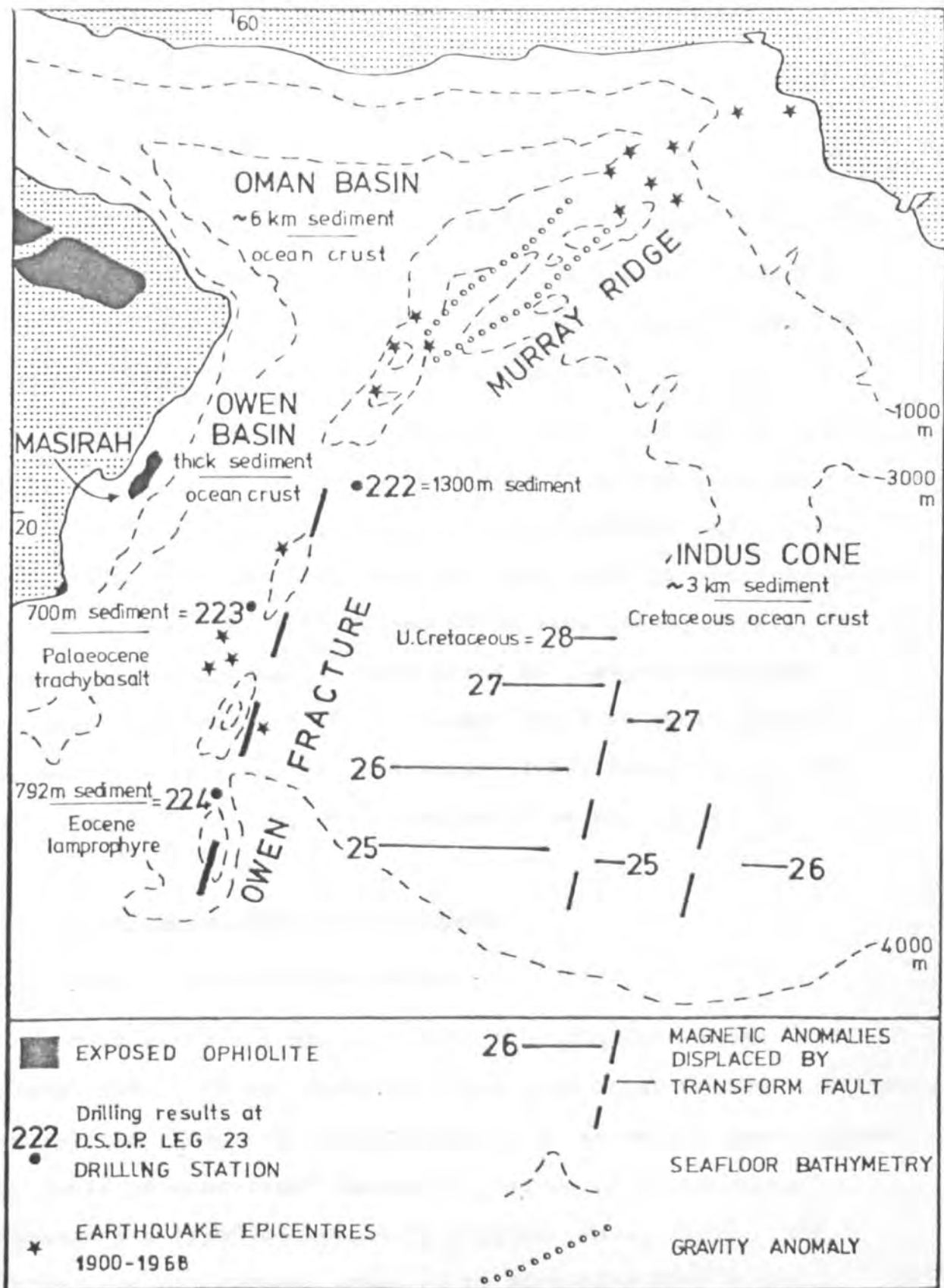
FIG.1.5. Map of the northern Arabian Sea. Data sources:
(a) magnetic anomalies and transform faults (McKenzie and
Sclater, 1971; Whitmarsh and others, 1974), (b) D.S.D.P.
stations and results (Whitmarsh and others, op.cit.),
(c) bathymetry, gravity anomalies and earthquake epicentres.
(Geological and geophysical atlas of the Indian Ocean, 1975),
(d) seismic refraction studies and estimates of sediment
thickness (White and Klitgord, 1976; Farhoudi, 1977).

68 m.y. B.P. and suggests that crust further north may be Middle Cretaceous (Le Pichon and Heirtzler, 1968; McKenzie and Sclater, 1971; Whitmarsh et al, 1974); (3) ocean lithosphere appears to underlie the thick Oman basin sediments (Taylor, 1968; Geol.and Geophys. Atlas of the Indian Ocean, 1975; White and Klitgord, 1976; Farhoudi and Karig, 1977).

Early spreading in the Indian Ocean, from 100 to 50 m.y. B.P., is believed to have occurred along an E-W axis and to have driven India northwards (Fig.1.6; McKenzie and Sclater, 1971). During the Eocene the spreading axis jumped from this E-W orientation to the present NW-SE line (Rona, 1978). The Owen Fracture appears to have acted as a major transform accommodating much of the northward drift of India from at least 75 to 10 m.y. B.P. (Matthews, 1966; Ewing et al, 1969; McKenzie and Sclater, 1971; Whitmarsh et al, 1974).

1F. Outstanding Ophiolite Problems

(i) Type of constructive margin

Most earth-scientists accept the ophiolite-ocean crust correlation. It is, however, often less clear whether individual ophiolites represent crust generated at major mid-ocean ridges, at "Gulf of Aden-type" spreading centres or at back-arc "Scotia Sea-type" constructive margins (Gass, 1977). The island arc environment proposed by Miyashiro (1973) can generally be eliminated as a contender. Field evidence for the spreading centre environment, such as the presence of an extensive sheeted dyke complex, or alternatively trace element geochemical discrimination can both be used in this context.
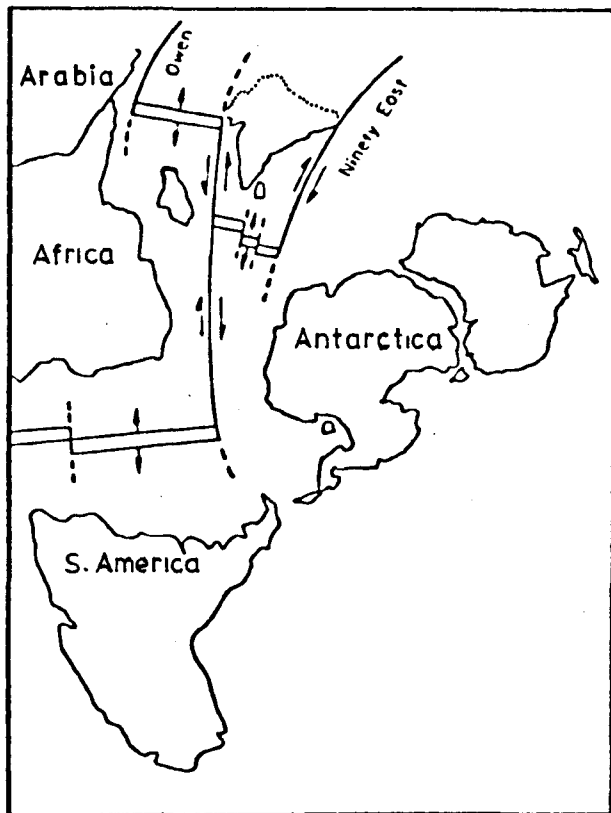
FIG.1.6. Taken from Fig.47, McKenzie and
Sclater (1971). Simplified sketch-map of
active plate boundaries between 75 and 55
m.y. B.P.

The back-arc environment has been suggested as a likely ophiolite source. The sandwiched position of the ocean crust between arc and continent, the shallow sea, and the possibility of buoyant mantle beneath, could all help to explain ophiolite obduction (Dewey, 1974 and 1976; Hawkins, 1974 and 1976; Saunders et al, 1978). However Gass (1975) notes a possible problem with the back-arc setting when he writes:

> "the lack of andesitic debris contemporaneous with the presumed spreading age of many of the Mesozoic Alpine-Himalayan ophiolites suggests that the oceans were not back-arc basins ... They are thought to be small (oceans) because of the general lack of andesitic volcanism associated with their emplacement."

The metamorphic aureole common along the basal contact of many ophiolites (Woodcock and Robertson, 1977) indicates emplacement of young hot lithosphere and may suggest a small ocean environment, of either back-arc or Gulf of Aden type.

At the present time geochemical studies have not aided significantly in the discrimination of the various environments. The wide chemical variation found within mid-ocean ridge basalts (e.g. Tarney et al, 1978), the relative lack of data on back-arc volcanics, and the altered state of many ophiolite sections are significant problems in this context.

(ii) Ophiolite emplacement

Despite much study, the mechanism of ophiolite emplacement onto continental crust is still a poorly defined process. It is difficult to visualize the dense, 10 km thick, slab of the

Oman Ophiolite "sliding" into position, on the apparently passive Arabian continental margin (Coleman, 1977). As Gass (1975) notes "what should normally go down goes up".

Some of the more practical attempts to define the emplacement mechanism are illustrated in Fig.1.7. and include:

(a) the subduction of a spreading centre (Fig.1.7.B; Christensen and Salisbury, 1975);

(b) the attempted subduction of a continental margin (Dewey and Bird, 1971). This might follow spreading-centre subduction as in the model for the Oman Ophiolite (Fig.1.7.A: Welland and Mitchell, 1977). Ophiolite elevation and exposure is affected by isostatic recovery of the continental margin;

(c) dehydration of subducting ocean crust-sediments which causes serpentinization in the overlying mantle. Serpentinization could cause diapirism and vertical uplift, as in the Troodos model (Fig.1.7.C1: Gass, 1977), or regional uplift and emplacement by gravity-sliding (Fig.1.7.C2: Gass, 1977);

(d) the scraping of slivers from the subducting slab (Fig. 1.7.C3: Gass, 1977). This process might be facilitated by significant relief in the oceanic crust and could produce the more disrupted types of ophiolite.

Coleman (1977) estimates that the preserved Phanerozoic ophiolites represent approximately 0.001% of the ocean lithosphere formed during that period, while Christensen and Salisbury (1975) point out that very often there appears to be only a short time-period between igneous formation and tectonic ophiolite emplacement. These relationships may suggest that
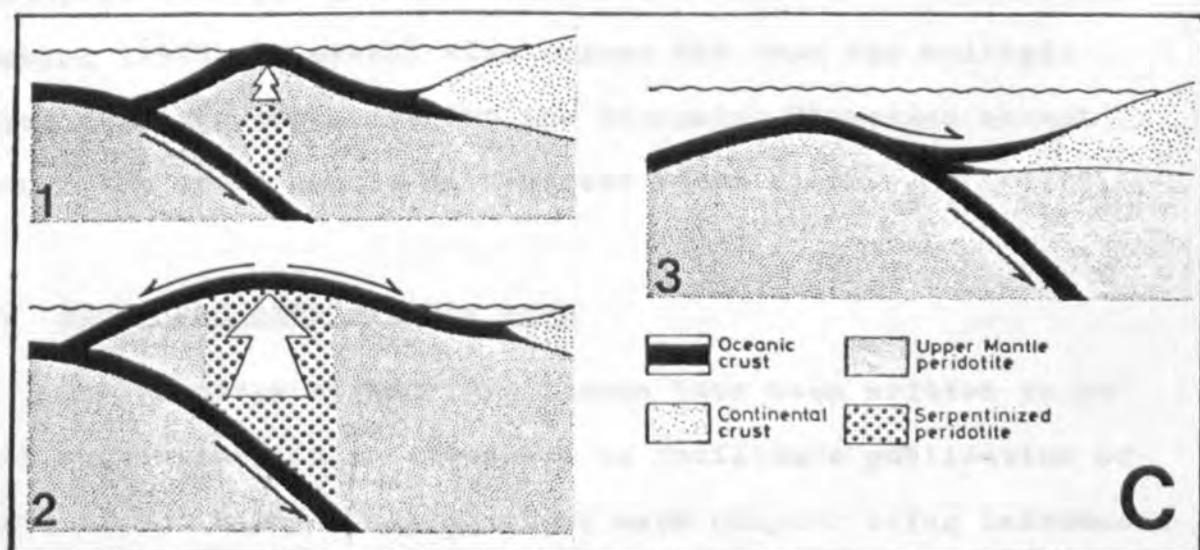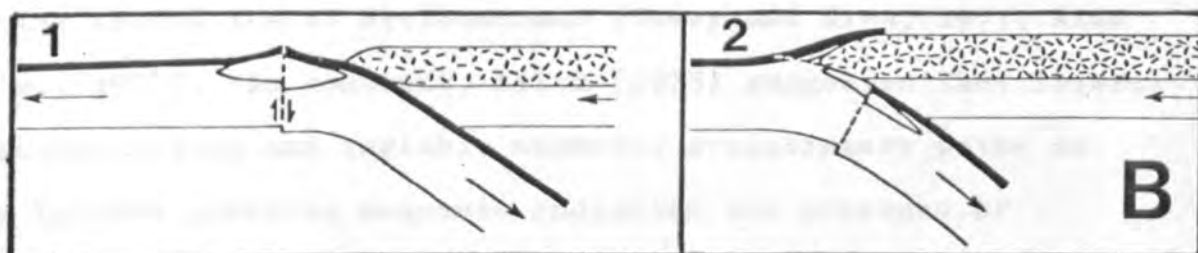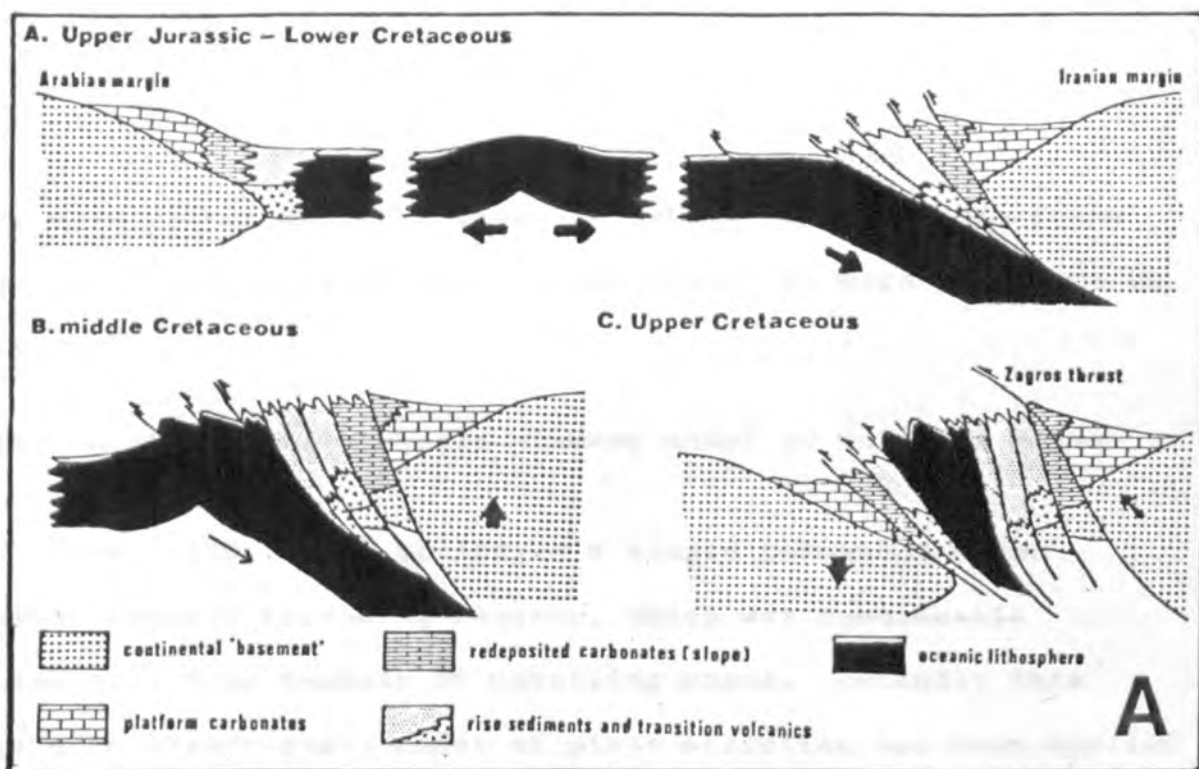
FIG.1.7. Schematic models of possible mechanisms of ophiolite emplacement.
(A) modified from Fig.6., Welland and Mitchell (1977) for the Semail Ophiolite, Oman: spreading centre subduction followed by attempted continental margin subduction.
(B) modified from Fig.21., Christensen and Salisbury (1975): partial spreading centre subduction.
(C) taken from Fig.3., Gass (1977): (1) serpentinite diapirism causing ocean plate uplift, Troodos Ophiolite model,
(2) serpentinization causing regional uplift and gravity sliding
(3) elevation before subduction, again causing gravity sliding.

old, cold mid-ocean ridge crust is subducted whilst the young
immature lithosphere of small ocean basins is more likely to be
preserved.

(iii)   A steady-state single chamber model or multiple magma
        chambers?

Cann (1970, 1974) envisaged a single permanent magma
chamber beneath spreading-centres, which was continually
replenished from beneath by upwelling magma. Recently this
idea of a steady-state model of plate accretion has been applied
to the ophiolites of Newfoundland (Dewey and Kidd, 1977; Kidd
et al, 1978). In contrast, Allen (1975) suggested that lateral
discontinuities and variable magmatic evolutionary paths in
the Troodos plutonic sequence indicated the presence of
multiple, small, magma chambers. In a recent review Gass and
Smewing (1978, in press) also argued the case for multiple
magma chambers encouraged by the irregular Stokesian ascent
though the upper mantle of discrete magma diapirs.

1G.   Scope and Aims of this work

The chapters within this thesis have been written to be
self supporting, in an endeavour to facilitate publication of
parts of the work. This involves each chapter being introduced
and concluded and has reduced the need for an extensive
introduction and conclusion. Any repetition involved has been
kept to a necessary minimum.

It has seemed apparent throughout this work that there
are two possible origins for the Masirah Ophiolite. It could
have been generated in a small ocean to the NE of Arabia, as was

the Oman Ophiolite or it could have formed during spreading of an early Indian Ocean Ridge, an environment contrary to the normally postulated small ocean basin. Consequently a common theme running through the following chapters is an attempt to define the nature of the former constructive margin and so discriminate between these alternatives.

Chapter 2 considers the occurrence of serpentinites within the ophiolite in the light of recent work which shows them to be of common occurrence in much of the oceanic crust (e.g. Bonatti and Honnorez, 1976). The subsequent chapter describes the plutonic crystallisation sequence from dunite to trondhjemite and considers the merits of the alternatives of steady state model or multiple magma chambers. Chapter 4 examines the structural, metamorphic and intrusive relationships of the sheeted dyke complex. The relative influence of the partial melting and fractional crystallisation processes on the whole rock chemistry of the dykes and overlying pillow lavas is then considered. There are three distinct volcanic groups within the ophiolite and Chapter 6 attempts briefly to define their origin in terms of present oceanic crustal structure. Initial mapping discovered the exposure of what appears to represent a major oceanic transform fault and the importance of this feature is examined, both in the oceanic environment and during the processes of ophiolite emplacement. Chapter 8 briefly describes the intrusion of the ophiolite by highly-potassic granite magma . The short concluding chapter synthesizes all of the available data into a model of the constructive margin processes which produced the Masirah Ophiolite.

Included within the appendices are the petrographical, micro-probe, and XRF data upon which this thesis is based; the location of all analysed samples; and the details of the techniques, precision and accuracy of the various analytical techniques. 55 oriented palaeomagnetic samples were collected during the fieldwork. These have been processed within the Department of Geological Sciences, University of Birmingham, and are now being interpreted by staff competent in this field.

The final aspect of this work is the enclosed geological map of Masirah Island. This covers the whole area of the island and provides a reconnaissance appraisal upon which any detailed economic or academic studies could be based. Production seemed relevant in the light of recent discoveries of constructive margin metallogenesis (e.g. Smewing et al, 1977).

1H. Future Research

It is felt that the reconnaissance studies embodied here were reasonably successful in the results they produced. Two areas might repay more detailed work. Firstly, a more detailed field and mineral chemistry study of the plutonic sequence might allow: (i) a more rigorous appraisal of the alternative hypotheses of single-state model or multiple magma chambers; (ii) better constraint of the processes which produced the volumetrically insignificant late trondhjemitic differentiates. The general occurrence of these rocks in ophiolite complexes has however been the subject of a recent PhD study by AJ diss (1978) at the Open University. Secondly, knowing the extent of

the localized "off-axis" volcanics might allow a specific collection to be made and more information concerning their origin to be forthcoming.

CHAPTER 2

SERPENTINITES IN THE MASIRAH OPHIOLITE: OCEAN CRUST PROTRUSION OR OPHIOLITE EMPLACEMENT PHENOMENA?

1. INTRODUCTION

Masirah Island lies on the SE edge of Arabia and is composed of a fully-developed but partially disrupted ophiolite complex. It probably represents Cretaceous ocean lithosphere emplaced during the late-Cretaceous-early Tertiary (Moseley, 1969; Glennie et al, 1974).

The site of the former constructive margin is equivocal and is discussed by Moseley and Abbotts (1978) and Abbotts (1978b). Previously the Masirah Ophiolite has been correlated with the Semail Complex, Oman (e.g. Morton, 1959; Laughton, 1966) which would suggest an origin in the late-Mesozoic ocean to the NE of Arabia in which the Semail was generated (Glennie et al, 1974; Carney and Welland, 1974). However study of the literature on the Semail suggests discrepant features between the two ophiolites which include (i) different sheeted-dyke trends (Abbotts, op.cit.), (ii) different relations to associated Cretaceous sediments (Glennie et al, op.cit.), and (iii) different modes of emplacement (Glennie et al, op.cit., Moseley and Abbotts, op.cit.). Thus it has recently been suggested that an alternative origin for the Masirah Ophiolite may be as ocean crust formed during early Indian Ocean spreading (Moseley and Abbotts, op.cit; Abbotts, op.cit.)

Within the ophiolite occur several narrow belts of serpentinite. Some of these appear to have analogues in their distribution with serpentinite protrusions found in the ocean crust near the slow spreading Mid-Atlantic Ridge (M.A.R.) (Bonatti, 1976 and 1978; Bonatti and Honnorez, 1976).

2. DISTRIBUTION AND FIELD RELATIONS OF THE VARIOUS SERPENTINITES

Serpentinite which is formed from mantle-derived rocks and does not include the partially serpentinized ultramafic cumulate occupies approximately 8% (56 sq.km) of the exposed Masirah Ophiolite. The original harzburgitic nature is evident even in hand-specimen where bronze bastite-serpentines, replacing orthopyroxene, are prominent in a green-black serpentine matrix. The serpentinites are exposed in a series of linear belts with trends which vary from E-W in the north of the island to NE-SW toward the south. (Fig.2.1). These sub-divide on a tectonic basis into 3 groups.

2A. Serpentinite Group 1

Serpentinites "b" and "d" are bounded by major sub-vertical dislocations on their SSE sides, where they occur adjacent to sub-vertical, red pillow lavas (Fig.2.1). The much weathered and easily eroded nature of both lithologies leaves the actual contact obscured. Their NNW contacts, with crudely-layered ultramafic cumulates, are conformable with the 30-40° NNW dip of the layering in those rocks. The actual contacts, of lithologies of differing competence, are obscured both by minor ("d") to extensive shearing (east end of "b") and by intrusion of pegmatitic gabbros and dolerites (west end of "b"). Nevertheless the sequence of layered black and light grey cumulates overlying stratigraphically and topographically the brown deeply-weathered, serpentinite "d" is clearly visible from the SSE. Assuming the gabbro dip of 30°in these homogeneous serpentinites there is a maximum thickness of 1.2 km exposed
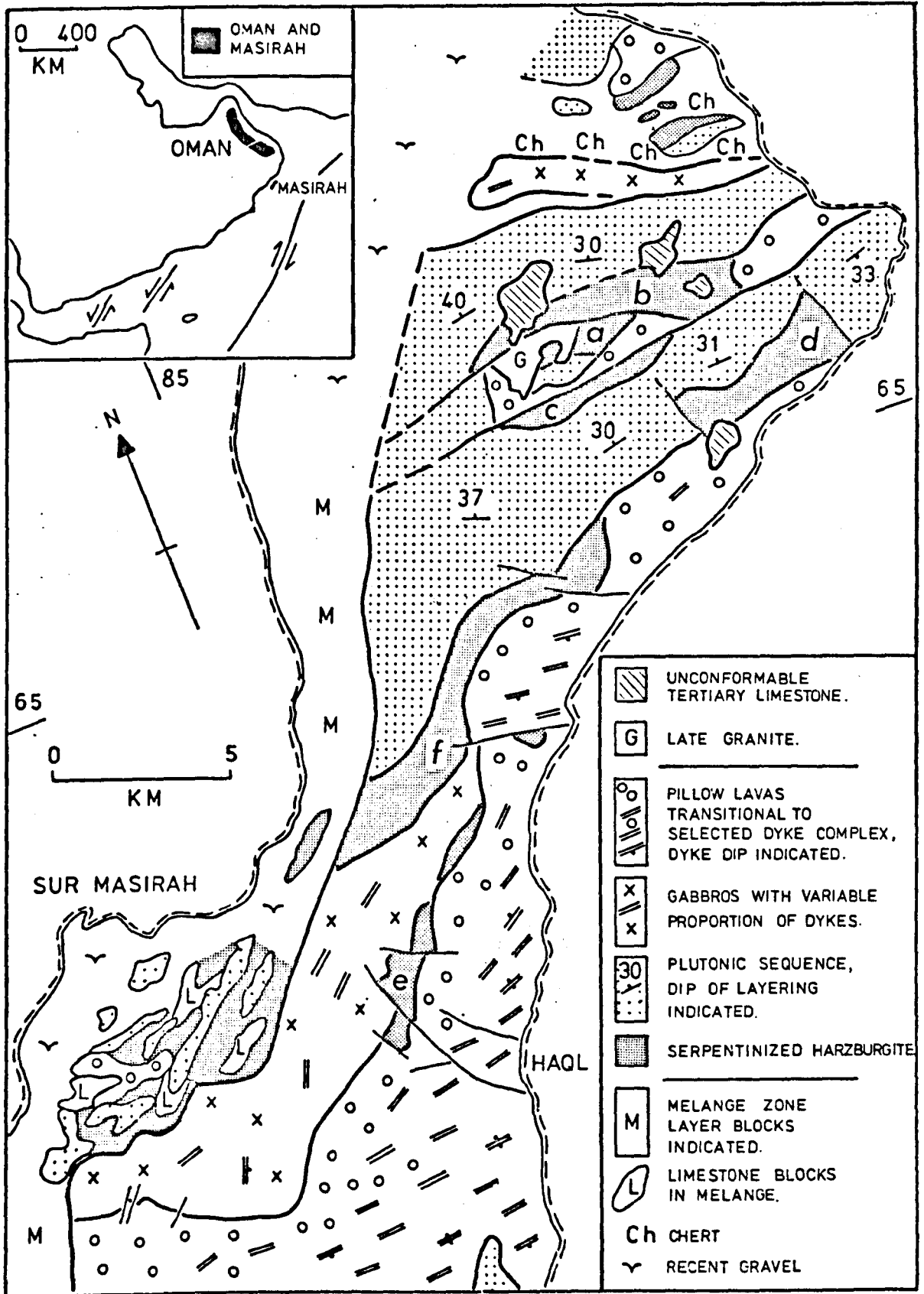
FIG.2.1. Geological map of the central part of Masirah Island showing the location of the various serpentinized harzburgite outcrops.

in "d". Both "b" and "d" contain a lineament visible on the
1:12000 aerial photographs but because of the complete
serpentinization and extremely weathered outcrop, such that
2m are removed to obtain even coherent samples, the nature of
this lineament was not discovered. It parallels the strike
of "d" but trends NE-SW and is obique to the E-W striking
serpentinite "b". In other (fresher) ophiolite harzburgites a
banding caused by variation in the ol:opx ratio has been
recorded but Coleman (1977) notes the problems of assigning
an origin when serpentinization is advanced. Serpentinite " f "
occupies an analogous position to "d" but relations along its
NNW contact are much obscured by dolerite intrusion in the
form of small irregular stocks.

2B. Serpentinite Group 2

Group 2 is composed of serpentinites outcropping in the
melange zone on the west of the island (Fig.2.1). This zone
has been described elsewhere (Moseley and Abbotts, op.cit.),
where it was suggested that it may have developed at an ocean
ridge transform fault. It has a minimum width of 5 km and is
composed of blocks, up to 2 sq.km, of limestones, chert,
pillow lava, sheeted dolerite dykes, and layered gabbros-
ultramafics often set in a serpentinite matrix. A similar
wide lithological range is commonly sampled along the MAR
transforms (Bonatti and Honnorez, 1976). The zone trends N-S
in the south of the island, swinging to a more NE-SW trend
in the centre and north (Fig.2.1). It cuts off all the

ophiolite units, including 20 km of sheeted dykes which have
an ENE-WSW strike, almost perpendicular to its own trend. A
perpendicular ridge axis-transform relationship is thus in
evidence. The exposed melange-sheeted dyke contact is vertical,
marked firstly by 20-30 m of sheared serpentinite with a vertical
foliation parallel the contact, and then by tectonic mixing of
serpentinite, gabbro and dolerite. It is frequently the site
of copper mineralisation in brecciated zones, 4-5 m wide.
Similar tectonism and metallogenesis are found on the oceanic
transforms (Bonatti et al, 1976). In the extreme south of the
zone there occurs extensive serpentinite breccias, with fragments
30-100 cm in diameter, whilst all the other lithologies are
frequently similarly brecciated. The serpentinite blocks in
the extreme N of Fig.2.1 show similar brecciation, are associated
with blocks of a similar wide lithological range, and may
possibly mark the melange continuation on a deflected trend.
An extensive coastal gravel fan development prevents proof of this
continuity.

2C. Serpentinite Group 3

The serpentinites "c", "e", and probably "a", are bounded
by major sub-vertical, parallel faults on both sides and
separate pillow lavas from gabbro sequences with variable
proportions of dolerite dykes (Fig.2.1). Serpentinite "e",
though disrupted by E-W and NW-SE faulting, swells and thins
markedly along strike. Subsequent granite intrusion has
obscured the relations of "a". The southern contact of "c"
with massive leucogabbros is a line of tectonic shearing.

5-6 m. of sheared foliated serpentinite, the foliation rather

irregular but approximately parallel the contact, are in

contact with weathered leucogabbro which is much granulated

and veined by epidote.

3. OUTCROP CHARACTERISTICS

All outcrops are almost completely (99-100 per cent)

serpentinised, a process probably encouraged by: (1) their

common occurrence either along, or within 1 km of, major faulting;

(2) the presence of abundant, close joints, less than a cm.

apart and occasionally lined by white near-amorphous calcite;

(3) olivine grain boundaries and cracks, which direct the

serpentinization on the miscroscopic scale and result in the

final "mesh-texture".Intermediate stages of the serpentinization

process are seen in the partially-serpentinized, cumulate

mela-olivine gabbros. The brown-weathering serpentinite is

monotonously homogeneous in the field except for (i) spherical

structures, 30-50 cm. in diameter, which may result from

differential weathering of the joint-directed serpentinization

process or possibly slow serpentinite flowage. (ii) common

gabbroic intrusions which are described below. The extreme

serpentinization and weathering has obscured any igneous or

tectonic variation but their homogeneity and spinel-harzburgite

origin is obvious in their modal composition (Table 2.1.,

Fig. 2.2). Serpentinization perfectly pseudomorphs the

scattered orthopyroxene grains which are commonly associated

with the spinel phase (c.f. Aumento and Loubat, 1971, who noticed
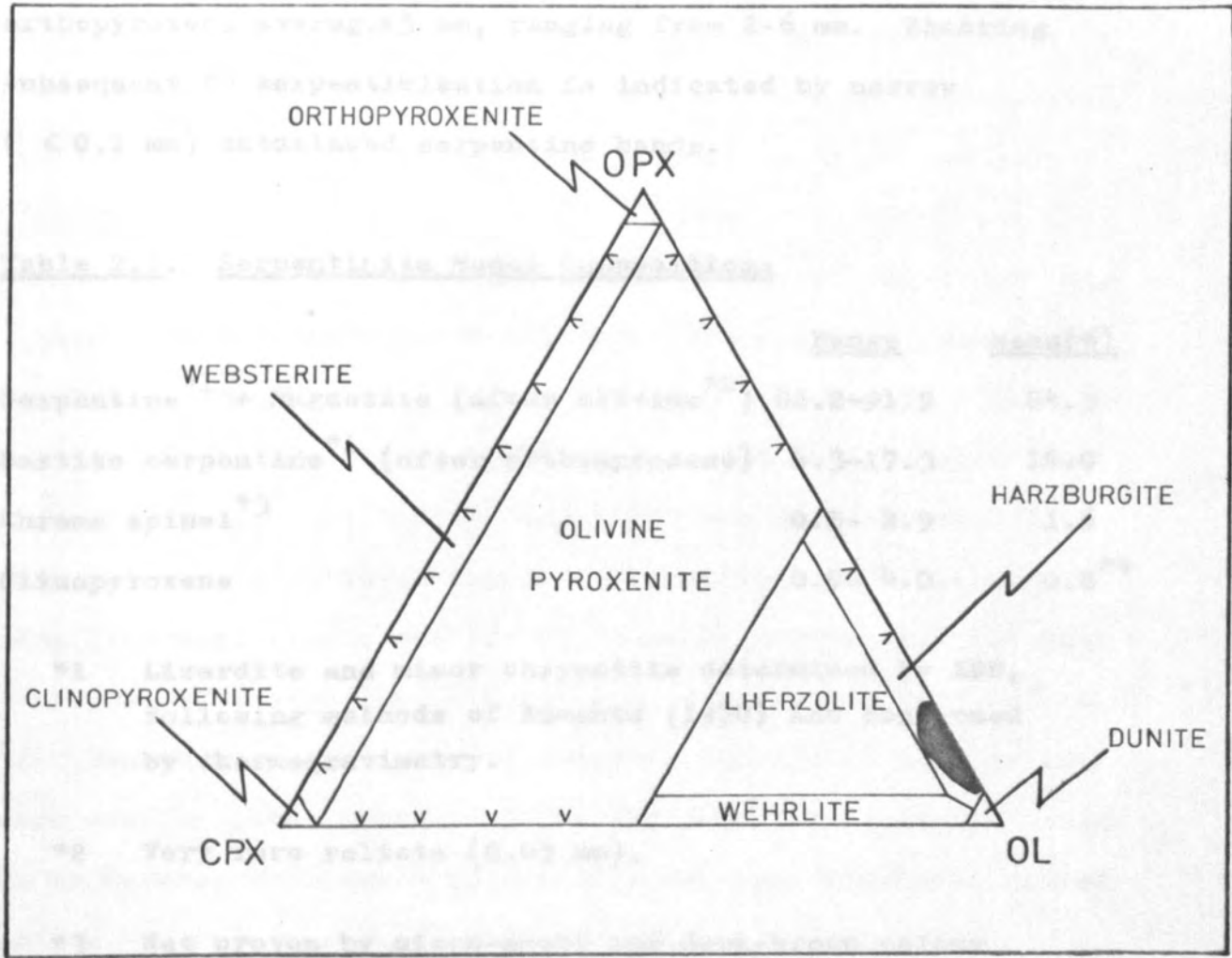
FIG.2.2. Uniform harzburgitic nature of the Masirah serpentinites illustrated by the Ternary modal diagram of Moores (1972).

a similar feature in M.A.R. serpentinites.) Olivine texture
and grain-size is obscured by serpentinization though the
orthopyroxene averages 5 mm, ranging from 2-6 mm. Shearing
subsequent to serpentinization is indicated by narrow
(< 0.1 mm) cataclased serpentine bands.

Table 2.1. Serpentinite Modal Compositions

	Range	Mean(6)
Serpentine[1] + Magnetite (after olivine[2])	82.2-91.9	84.3
Bastite serpentine[1] (after orthopyroxene)	4.3-17.3	14.0
Chrome spinel[3]	0.5- 2.9	1.6
Clinopyroxene	0.9- 4.0	0.8[4]

[1]   Lizardite and minor chrysotile determined by XRD,
       following methods of Aumento (1970) and confirmed
       by thermogravimetry.

[2]   Very rare relicts (0.05 mm).

[3]   Not proven by micro-probe but dark-brown colour
       and whole rock content of 3500 ppm Cr suggests
       chrome-spinel (Irvine and Findlay, 1972).

[4]   Clinopyroxene only present in 2 of 17 sections
       studied.

4. MINOR INTRUSIONS

The homogeneity of the serpentinite outcrop is frequently masked by complex and cross-cutting systems of veins, dykes and pods of gabbro, gabbro pegmatite, less common anorthosite, the latter two with a 5-15 cm grain-size, dolerite and rarer clinopyroxenite. The proportions of these vary widely: a large area at the E end of the serpentinite "b" contained only 2 narrow gabbro dykes whereas locally areas of "e" contain 50-70 per cent intrusive gabbro and gabbro pegmatite. An average of all field observations gives 78% serpentinite and 22% minor intrusions. Dykes and veins are commonly 2-60 cm wide and can be followed for 0.5-50 m whilst the pods and more irregular intrusions occupy areas of 2-30 sq.m. All have sharp contacts with the serpentinized harzburzite host and no textures reminiscent of insitu partial melting or segregation were seen. Coarse grain-sizes in the pegmatites, even in veins 10 cm across, indicate a hot environment when intruded. There exists a complete variation in this pegmatitic facies to anorthositic intrusions with only minor amphibole. All of the intrusions are frequently granulated and show varying degrees of saussuritization-uralitization but they do not appear to show the effects of the rodingitization processes recorded in M.A.R. ocean floor equivalents (Honnorez and Kirst, 1976). In contrast plagioclase is frequently quite fresh whereas the larger poikilitic clinopyroxene is uralitized. Some recrystallisation is indicated by very fresh, triple-junctioned plagioclase.

There seems to be all transitions from completely irregular, cross-cutting, intrusions (e.g. in the W. of the in-place serpentinite "b") to some alignment of the veins and pods parallel to the strike of the serpentinites "e" and "f". One larger gabbro in "f" is cut by dolerite dykes which terminate against the host serpentinite and is clearly an incorporated tectonic block, as seen in the melange zone.

Minor intrusives cutting the harzburgite-dunite-lherzolite component are common recorded in the ophiolite literature (Reinhardt, 1969; Irvine and Findlay, 1972; Allemann and Peters, 1972; Menzies and Allen, 1974). Allemann and Peters (op.cit) note common gabbro-gabbro pegmatite-dolerite-anorthosite-orthopyroxenite-clinopyroxenite intrusions in the top 500 m. of the Semail harzburgite.

5. SERPENTINITE WHOLE-ROCK CHEMISTRY

The uniform serpentinite chemistry is illustrated by the XRF analyses listed in Table 2.2. Table 2.3 compares the mean of these with 3 fresher harzburgites from other ophiolites and the ocean floor. In view of the difficulty of obtaining acceptable geochemical samples their coherence internally and with these harzburgites is quite good. There are discrepancies in Mg, Fe and Si between the fresher rocks and these Masirah samples; in particular the Masirah serpentinites have high SiO_2 and low MgO. The MgO/SiO_2 ratio of 0.85 compares with a mean of 1.02 quoted by Coleman (1977), who suggests that if serpentinization does not involve brucite formation it will be a

Table 2.2 : Representative analyses of Masirah Serpentinites

ROCK NO	X14	MA100	MA135	MA110	MA125	X152	MA108	MA31
SIO2	41.90	42.10	40.21	40.58	40.72	41.88	40.65	42.77
TIO2	0.01	0.01	0.01	0.01	0.01	0.01	0.01	0.01
AL2O3	1.51	1.37	0.58	0.36	0.52	0.48	0.37	0.48
FE2O3	1.16	1.20	1.18	1.19	1.16	1.26	1.18	1.17
FEO	7.63	7.92	7.81	7.84	7.62	8.31	7.79	7.60
MNO	0.00	0.00	0.12	0.17	0.11	0.15	0.17	0.10
MGO	34.74	32.93	35.45	34.07	35.65	34.22	34.35	38.44
CAO	0.49	0.58	0.18	0.73	0.23	0.22	0.52	0.15
NA2O	0.05	0.05	0.07	0.21	0.06	0.05	0.04	0.05
K2O	0.01	0.01	0.01	0.01	0.01	0.02	0.01	0.01
P2O5	0.00	0.00	0.00	0.00	0.00	0.00	0.00	0.00
H_2O*	13.21	13.46	13.76	14.15	13.90	14.90	15.37	10.12
TOTAL	100.71	99.63	99.38	99.82	99.99	101.50	100.46	100.99

TRACE ELEMENTS IN PPM

	X14	MA100	MA135	MA110	MA125	X152	MA108	MA31
NI	2077	2336	2505	2337	2556	2449	2390	2456
CR	3843	3100	3539	3453	3321	3243	3171	3478
ZN	30	33	44	37	57	42	42	35
GA	4	-2	-2	-2	-2	-2	-2	-2
RB	-1	-1	-1	-1	-1	-1	-1	1
SR	14	10	10	15	23	12	11	59
Y	-2	-2	-2	-2	-2	-2	-2	-2
ZR	1	1	3	3	4	4	5	2
NB	-1	-1	1	2	1	-1	2	-1
BA	11	-4	7	4	8	14	1	10
LA	-2	-2	1	1	2	2	3	2
CE	-3	3	7	3	5	8	7	6

Table 2.3   Mean Masirah serpentinite compared with other ophiolite and ocean-crust harzburgites

	A	1	2	3
SiO_2	47.31	43.72	42.41	47.91
TiO_2	0.01	0.01	0.06	0.03
Al_2O_3	0.81	0.47	0.48	0.91
FeO	10.10	8.19	8.28	6.35
MnO	0.15	0.15	0.16	n.d.
MgO	40.30	45.99	46.95	43.96
CaO	0.41	0.77	0.75	0.74
Na_2O	0.08	0.01	0.05	0.09
K_2O	0.01	0.00	0.01	0.01
P_2O_5	0.01	0.01	0.00	n.d.
NiO	0.31	0.27	0.30	n.d.
CrO	0.50	0.39	0.48	n.d.
Total	100.00	100.00	100.00	100.00

A   Avg 8 Masirah serpentinites, recalculated anhydrous

1   Avg 8 Troodos harzburgites (Allen, 1975)

2   Avg 7 Othris harzburgites (Menzies and Allen, 1974)

3   Mid-Atlantic Ridge 45°N, serpentinized harzburgite, recalculated anhydrous, (Christensen, 1972, AII-32-8-4)

n.d. not determined.

process of Mg loss and/or SiO_2 gain. XRD and thermogravimetric study, did not reveal the presence of brucite, suggesting that the extreme serpentinization may have involved minor chemical adjustment.

The complete serpentinization and possible element mobility precludes knowledge of the original chemistry and prevents use in quantitative modelling of the ophiolite petrogenesis.

5A. Residual Nature

The serpentinites are hydrated olivine-orthopyroxene rocks composed predominantly of Mg, Fe, Si and added OH. Combined, these 4 oxides form 98-99% of the serpentinites which are thus distinguished by their low levels of Ca, Al, Ti, K, Na, P, Rb, Sr, Ba, Y and the other incompatible trace elements, many of which approach the lower limits of detection of the XRF method (Table 2.2). The low CaO (0.15-0.73 per cent) and Al_2O_2 (0.36-1.51 per cent) reflect the absence of plagioclase and clinopyroxene. Orthopyroxene in harzburgite contains 0.6-1.6% Al_2O_3 and 1.3-1.4% CaO (Allen, 1975) and whole-rock contents in excess of orthopyroxene contribution are probably accommodated in the spinel (Al_2O_3) and the exsolved clinopyroxene (CaO) phases. Thus MA100, which has a slightly higher Al_2O_3 level, has a high modal spinel content and MA110, which contains minor clinopyroxene has higher CaO and Na_2O.

5B. The serpentinite-cumulate ultramafic discontinuity.

Levels of the compatible trace elements Ni (2077-2601 ppm) and Cr (3100-3843 ppm) are uniformally high in the serpentinites and a clear discontinuity, particularly of Ni, exists between them and the lower contents in the cumulate rocks (Fig.2.3). The pronounced fall in Ni levels to the most primitive cumulate with 1325 ppm Ni is significant because both rocks contain comparable amounts of olivine ($\sim$ 85 modal %). The high $K_D^{OL/L}{}_{Ni}$ value means that the element will be largely accommodated in that phase. The discontinuity between the serpentinites and the partially serpentinised early olivine cumulates is clearly shown in the levels of Ni, Mg, Ti and Al_2O_3 in Fig.2.4.

5C. CaO : Al_2O_3 ratio

The very low CaO and Al_2O_3 contents in the serpentinites are shown in Fig.2.5 to be only typical of this rock-type. It is noticeable however that the Masirah samples have a lower CaO : Al_2O_3 ratio than harzburgites from elsewhere; the mean ratio of 0.5 compares with 1.5 for the Troodos samples (Allen, 1975) and an overall range of 0.5 to 2.0. It is possible that the low ratio is the result of the complete serpentinization of these rocks. Locally joints in the serpentinite are calcite-lined which could indicate some Ca expulsion during serpentin-ization. The possibility of this has been suggested by Coleman and Keith (1971). However the low CaO/Al_2O_3 character-istic is reflected also in the mantle partial melts respresented
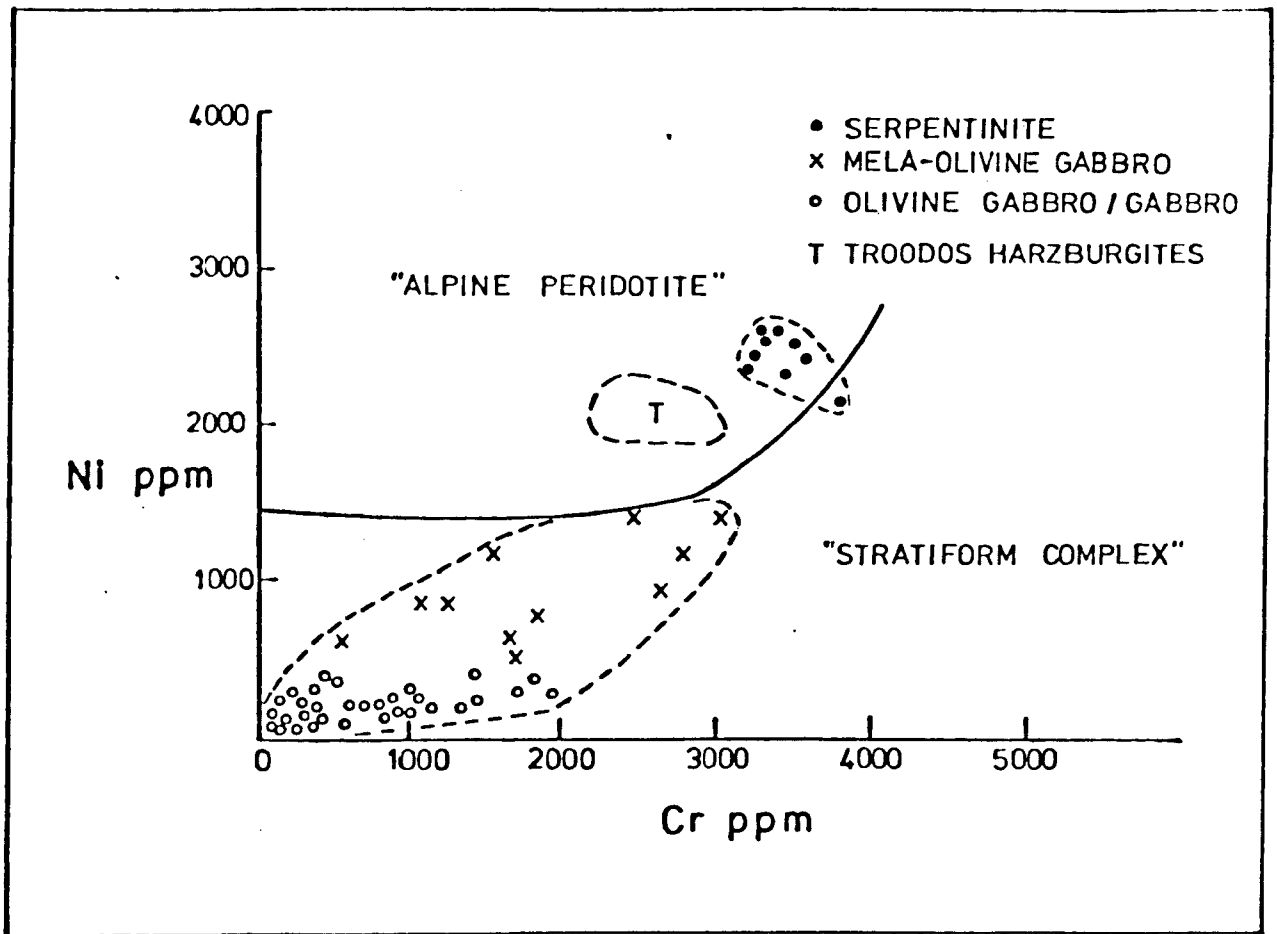
FIG.2.3. Ni-Cr plot incorporating the "alpine peridotite" (tectonite harzburgite-dunite-lherzolite) - "stratiform complex" (layered cumulates) discriminator of Irvine and Findlay (1972). The Troodos harzburgite field is taken from Allen (1975). The serpentinites are clearly discriminated from the other plutonic types.
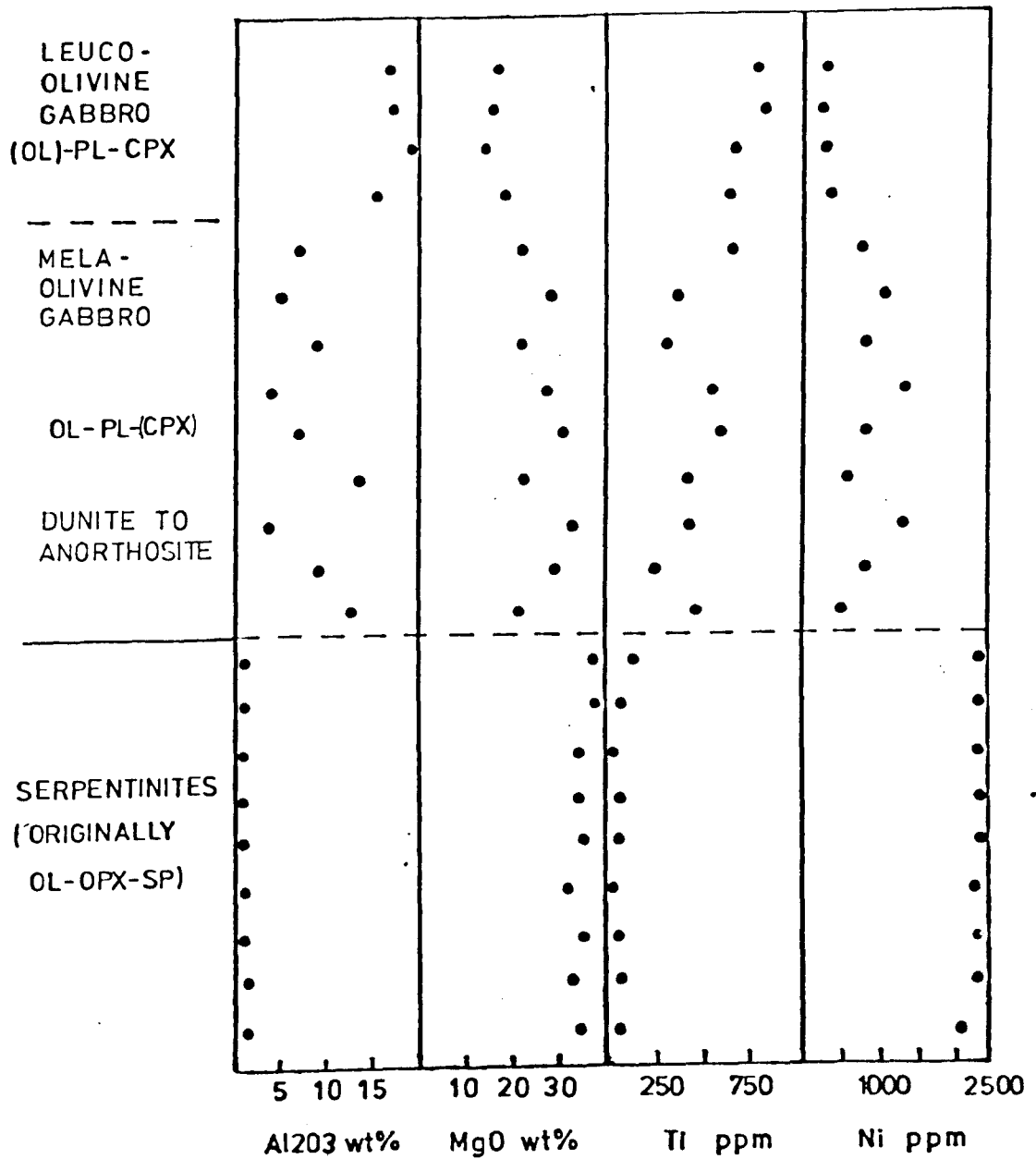
FIG.2.4. Variation in Al_2O_3 MgO, Ti and Ni in the Masirah serpentinites and olivine-bearing cumulate rocks. Note that the samples are arranged simply in order of increasing Zr content upwards and do not represent a strict stratigraphic section.
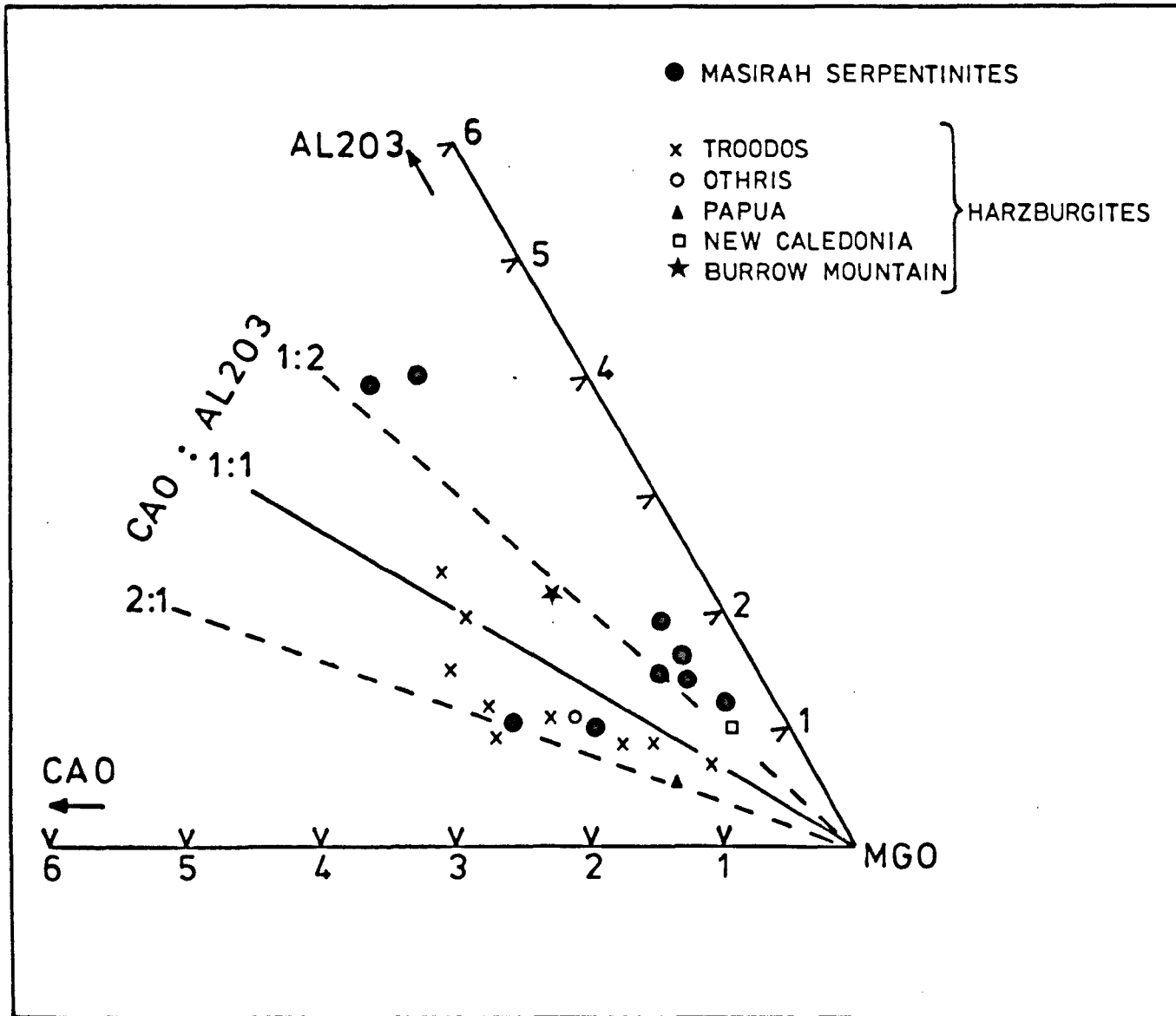
FIG.2.5. CaO-Al₂O₃-MgO ternary diagram of the Masirah serpentinites and other ophiolite mantle harzburgites. Data sources: Troodos (Allen, 1975); Othris (avg.of 7, Menzies and Allen, 1974); Papua (Davies, 1971); New Caledonia (avg.of 4, Guillon, 1975); Burrow Mt. California (avg.of 8, Loney et al, 1971). Note the generally low CaO/Al₂O₃ ratio in the Masirah samples compared to the other harzburgites.

by the gabbro-dyke-lava sequence on Masirah. These show an ol-pl-di crystallisation sequence in both the gabbros and the lava phenocryst phases. This indicates, because plagioclase precedes clinopyroxene, a low $CaO/CaO + Al_2O_3$ ratio in the basaltic liquid.

6. RESIDUAL MANTLE OR CUMULATE ORIGIN FOR THE SERPENTINITES

In recent years much experimental and field evidence has accumulated to support the hypothesis that partial melting of an aluminous peridotite in the upper mantle beneath spreading centres produces a basaltic/picritic melt and a (spinel) harzburgite residuum (Menzies and Allen, 1975; Smewing et al, 1975; Malpas, 1978). Quantitative evaluation of this hypothesis is not possible here because of the absence on Masirah of undepleted aluminous peridotite mantle.

The Masirah serpentinites are formed from spinel harzburgites (ol + opx + sp $\pm$ cpx). At present only two plausible explanations of such an assemblage are apparent : they might be early cumulate products of fractional crystal-lisation or they could represent residual mantle. A cumulate origin is discounted for the following reasons:

(1) Serpentinite "d" represents at least 1.2 km thickness of an olivine-orthopyroxene assemblage (Fig.2.1). To precipitate this thickness of/uniform ultramafic cumulate would require an impossibly large parent magma.

(2) The layered plutonic sequence overlying the serpentinites "a" and "d" shows the following sequence of cumulus phases:

(a) cr + ol (b) ol (c) ol + pl (d) ol + pl + di (e) pl + di.
Orthopyroxene does not occur as a cumulus phase and in
approximately 100 sections it was only seen 5 times as narrow
olivine reaction rims in mela-olivine gabbros. In contrast the
cumulates contain plagioclase and diopside and are Ne, and not
Hy, normative. It does not seem possible to fit the
harzburgites into this crystallisation sequence.

(3) Fig.2.4 shows no variability in the levels of Ni,
MgO, TiO_2 and Al_2O_3 in the serpentinite samples. There is a
marked serpentinite-cumulate sequence discontinuity and the
cumulates show the obvious effects of modal and cryptic
variation (e.g. Al_2O_3 and TiO_2 increase with incoming plagioclase
and diopside, MgO decreases with decreasing olivine content
and Ni is rapidly reduced by the early cumulus olivine with a
high $K_D{}^{OL/L}_{Ni}$). Fig.2.3 shows the serpentinites and the cumulates
plotting respectively in the "alpine peridotite" (= mantle
ultramafic) and "stratiform complex" (= low-P cumulates) fields
of Irvine and Findlay (1972).

(4) The olivine-orthopyroxene reaction relationships
below 6 kb anhydrous (Kushiro et al, 1968) does not allow
cotectic crystallisation of these phases in the proportions
in evidence in the serpentinites.

(5) Olivine-orthopyroxene residues are common in aluminous
peridotite systems (Green, 1970).

Points (1) - (5) are all compatible with the residual
mantle hypothesis. The extremely low levels of Al, Ca, K, Na,
P, Ti and other LIL elements and the uniformally high Cr, Ni

and Mg are all suggestive of a residuum depleted by partial
melt extraction. The serpentinites could not themselves produce
a tholeiitic liquid by the commonly suggested 10-20 per cent of
partial melting: for example the CaO ($<$ 0.73%) and TiO_2
($<$ 0.02%) contents suggest that a 20 per cent melt would contain
a maximum 3.65% (CaO) and 0.10% (TiO_2), a 10 per cent melt a
maximum 7.30% (CaO) and 0.20% (TiO_2). Clearly these figures
are too low for basalt production unless tholeiites can be formed
from rather lower (1-5%) percentages of partial melt than is
at present believed. Various geochemical parameters, and in
particular REE levels, do not support these low degrees of
partial melting for the formation of ocean tholeiites. Thus
it is suggested that these serpentinites represent residual
mantle derived by basalt extraction from less-depleted mantle.
The extracted basalt melt is represented by the gabbro-dyke-
lava sequence on Masirah. The less-depleted mantle probably
consisted of the plagioclase lherzolite seen in the Othris and
other mantle sequences (Menzies and Allen, 1974). A minimum
gabbro-dyke-lava thickness of 5.75 km is present on Masirah.
Assuming 10-20% partial melting, suggested later by REE
modelling, there will be over 23 km of harzburgite residue.
It therefore seems reasonable to suggest that the limited
serpentinite thickness (1.2 km) below the cumulates means that
sampling is confined to the top of the mantle sequence, where
basalt extraction and harzburgite production will be most
successful. Notwithstanding this, these uniform serpentinised
harzburgites, and the absence of the lherzolitic type, suggests
efficient partial melt segregation and/or extraction at an

established spreading centre. Dickey (1975) suggested that a zone-refining process "purifies" the harzburgite as it moves laterally out of the MOR thermal regime.

7. TIMING OF SERPENTINIZATION

The problem of the timing and process of serpentinite emplacement is probably inter-related with that of the timing of serpentinization of these upper mantle harzburgites. Wenner and Taylor (1971) and Coleman (1971) suggested that most serpentinization is affected by meteoric water during ophiolite emplacement whilst Barnes (1978) presents evidence that present-day serpentinization ($< 115^{\circ}C$) is occurring in the Semail Complex, Oman. However ocean-crust serpentinization caused by sea water penetration of fractures is also a well-documented process (Miyashiro et al, 1969 and 1970; Christensen, 1970 and 1971; Aumento and Loubat, 1971; Cann, 1974; Bonatti, 1976 and 1978; Bonatti and Honnorez, 1978). It appears that serpentinization can occur almost immediately adjacent to the spreading centre, during emplacement, or as a slow post-emplacement process.

Thermogravimetric and XRD studies of these serpentinites have failed to detect the presence of brucite in the lizardite-chrysotile assemblage. A similar absence of brucite was noted by Aumento (1970) in MAR dredged serpentinites. Shear bands through the serpentinite mesh texture suggest some tectonism subsequent to serpentinization.

8. TIMING OF SERPENTINITE EMPLACEMENT

Serpentinite emplacement within the Masirah sequence could have occurred : (1) near ridge, where analogy with the present oceanic crust indicates extensive serpentinite diapirism (e.g. Aumento, 1970; Thompson and Melson, 1972; Bonatti, 1976 and 1978; Bonatti and Honnorez, 1976); (2) during ophiolite emplacement; (3) some combination of both processes with the emplacement tectonics possibly influenced by major ocean-crust faults.

8A. Group 1 serpentinite emplacement

Serpentinites "b" and "d" appear to conformably underlie the cumulate sequence (Fig.2.1) and probably formed the magma-chamber floor on which the latter accumulated. The actual contact, the petrological Moho, is the site of minor shearing which may have occurred in the near-axis environment before cumulate consolidation, or during ophiolite emplacement. (More detailed study might discriminate between these possibilities). Emplacement of those serpentinites into their present position seems to involve ophiolite dislocation along NE-SW faults, which bound both "b" and "d" on their SE sides, and tilting of the ophiolite to dip $30-40^{\circ}$ to the NW. "D" is also confined by apparently earlier NNW-SSE faulting.

Serpentinite "f" occupies an analogous position to "d". Its SE contact is a vertical tectonic line and steps from pillow lava to gabbro cut by dolerite dykes. Additionally the tectonic incorporation within the serpentinite of a large gabbro

block cut by dolerite dykes was noted earlier. The NW contact is obscured by poor exposure and intrusion of massive dolerite.

8B.   Group 2 serpentinite emplacement

Extensive work on MAR serpentinites emplaced at a high-level in the oceanic crust (e.g. Bonatti, 1976 and 1978; Bonatti and Honnorez, 1976) has resulted in the following explanation of their emplacement: (1) sea-water penetrates the crust along both major transform faults which displace the ridge-axis and smaller faults which parallel the ridge-axis. Some of these faults are believed to extend to the upper mantle (Lister, 1972). (2) The sea-water causes hydration and serpentinization of the mantle peridotites. (3) The same faults are loci for upward serpentinite diapirism encouraged by (a) the low strength of serpentinite, relative to gabbro, at the temperatures of 3-400°C prevalent in the lower crust (Raleigh and Paterson, 1965; Paterson, 1967);   (b) the low density of serpentinite, relative to gabbro, and its consequent bouyancy; (c) complex patterns of compression and tension acting on the faults as they move from the ridge; (iv) some volume increase, during the near-isochemical serpentinization process. The potency of tectonic serpentinite diapirism is illustrated by Dickinson (1966) who records diapirism actually reaching land surface and resulting in serpentinite flowage.

Group 2 comprises the discontinuous serpentinite blocks and matrix in the western melange. The melange cross-cuts all of the ophiolite units, including juxtaposed serpentinised

harzburgite and "gabbro with dykes" E of Sur-Masirah. It is
suggested here, and argued at greater length elsewhere
(Moseley and Abbotts, 1978) that the melange represents a
transform fault and the serpentinites represent diapirism along
that fault. The resulting lubricated crustal suture may have
been utilized during ophiolite uplift and emplacement which
would explain its cross-cutting nature of vertically displaced
units. Fox et al (1976) note that in the N.Atlantic an
important transform occurs, approximately, every 55 km. Except
for that recorded by Simonian and Gass (1978) on Troodos, the
absence of transforms in the ophiolite literature could suggest
that (i) the tectonics of emplacement, except in intact ophiolites
such as Troodos, obscures their presence. (ii) most ophiolites
do not represent fragments of transform-faulted mid-ocean
ridge but instead the younger more ductile crust of small ocean-
basins or (iii) transformfaults, being common lines of weakness
in the ocean lithosphere, are thrust along and obscured during
ophiolite uplift and emplacement onto continental crust.

The Arakapas fault zone on Cyprus has recently been
convincingly described as a former oceanic transform (Simonian
and Gass, op.cit). The structure consists of mafic volcanics
and clastic sediments deposited along a trough within
brecciated basement, largely of sheeted dykes. There are some
similarities between the Arakapas transform zone and the
melange belt on Masirah which include: (1) their development
within sheeted dyke complex and a trend rotation within that
complex from perpendicular to the transform to parallelism
near the contact; (2) serpentinite emplacement near and along

the transform. The more important distinction of the structures is the much greater degree within the Masirah example of mechanical brecciation, serpentinite diapirism and serpentinite incorporation of blocks of the varied ophiolite lithologies.

8C. Group 3 serpentinite emplacement

Serpentinites "c" and "e" are bounded on both sides by major vertical faults. Both have contacts on one side with tilted cumulate gabbro blocks and on the other with pillow lavas (Fig.2.1). This suggests relative vertical displacement of at least 2-3 km because approximately 1.8 km of sheeted dykes and at least 0.5 km of massive gabbro are present on the island (Abbotts 1978b and d). The serpentinites have not incorporated any blocks of sediments-lavas-dykes but contain the common minor intrusions described above. The infrequent presence of coherent dolerite dykes, which can be followed as far as exposure allow (< 50 m), suggests intrusion into a cooler environment than that of the more common coarse gabbros-gabbro pegmatites. This, in turn, may suggest serpentinite protrusion upwards in a near-axis environment when limited magma was still available. (c.f. Dewey and Kidd, 1978). There is no thermal aureole development. From this evidence cold, fault-directed, protrusion appears to be suggested. The NE-SW strike of "e" and E-W of "c" approximately parallels that of the ENE-WSW sheeted dykes and thus also that of the original spreading-axis.

It was noted earlier that serpentinite distribution in
the present upper ocean crust of the MAR follows a roughly
orthogonal pattern, with serpentinites present along faults
both parallel and perpendicular to the axis. Bonatti (1976)
noted that the narrower serpentinite protrusions on the former
reach progressively higher levels at greater distance from the
ridge and calculated from the relationship that diapirism
occurs at approximately 1 mm/1 year.

The emplacement of these serpentinites might be as follows:
(1) deep faulting parallel to the spreading ridge allowed water
access to the upper mantle and resulted in local serpentinization.
The presence of faulting of this trend is suggested within the
sheeted dyke complex where faults of significant displacement,
but free of serpentinite, occur parallel to the dyke trend and
therefore the original spreading axis (Abbotts, 1978b);
(2) Serpentinization provoked upward diapirism largely along
the faults which allowed water entry; (3) During ophiolite
uplift and emplacement any accommodating movement, including
regional tilting of the gabbros, would have utilized these weak
lubricated zones.

The original geological relationships of serpentinite "a"
are obscured both by subsequent granite intrusion (Abbotts, 1978c)
and its position within an E-W zone of concentrated and complex
tectonic disruption (Fig.2.1). Significant vertical displacements
have occurred to place pillow lavas between serpentinites "a"
and "c" but whether wholly attributable to the tectonics of
ophiolite emplacement is not clear on present field evidence.

9. ORIGIN OF THE MINOR INTRUSIONS

Minor intrusives cutting harzburgite, and its serpentinised equivalent, have been commonly recorded in the ophiolite literature (e.g. Allemann and Peters, 1972; Irvine and Findlay, 1972; Menzies and Allen, 1974). The latter authors suggest that gabbro veins cutting the Troodos and Othris harzburites represent coalesced melt, generated during partial melting below the ocean ridges, which has not escaped into the overlying magma chamber(s).

Salient features of the minor intrusions in the Masirah serpentinites include:

(i) Sharp contacts with the serpentinites, no textures suggestive of insitu segregation and no evidence of chilling in the dominant gabbro varieties;

(ii) A variation in their degree of development from 1% of the outcrop in parts of the insitu "b" up to 70% in part of "e";

(iii) Pegmatitic gabbros occur in 15 cm wide veinlets and fire-grain dolerite in 30 cm wide dykes suggestive of variable environments of intrusion;

(iv) Generally a degree of shearing and cataclasis;

(v) In the insitu Group 1 serpentinites the dykes have irregular trends but in the Group 3 type ("e" and probably "f") there is some tendency for more discontinuous podiform gabbro development with an alignment parallel the strike of serpentinite belt.

The field evidence suggests a range in timing of intrusion. The pegmatitic gabbros and allied anorthosites probably represent coalesced partial melt generated under the spreading ridge which did not succeed in escaping into the overlying magma chamber(s). A hot axial environment is necessary to explain the coarse grain-size in narrow veins. Their invariably sharp contacts with the serpentinite suggest that all of the gabbros have left their regions of segregation and were arrested during ascent through the upper mantle. A possible alternative, suggested by the rarity of gabbros in the east part of the insitu serpentinite "b" and their concentration in the Group 3 type, are that some intrusion occurred during the suggested Group 3 serpentinite protrusion into the overlying gabbro units.

The aligned podiform gabbros, frequently granulated in section, may have been developed during serpentinite protrusion because of their stronger, more rigid, nature compared to the ductile serpentinite matrix.

10. SIGNIFICANCE OF THE SERPENTINITES, THEIR ASSOCIATED FAULTING, AND THE MELANGE

The common occurrence on Masirah of narrow serpentinite lenses occurring along major fault-lines has an analogue in the slow spreading, much faulted, MAR (Bonatti and Honnorez, 1976; Bonatti, 1978). The Group 3 serpentinites, which parallel the sheeted dyke trend, are on a smaller scale than the melange with its significant serpentinite component which cross-cuts the sheeted dyke trend. The latter has mechanically incorporated lithological blocks ranging from chert to ultramafic cumulate.

The contrasting scale and relationship to the spreading axis is again comparable to findings on the MAR (Bonatti, 1976). Cann (1974) suggests that the occurrence within an ophiolite of "fault sets of considerable throw and serpentinite diapirism" indicates a rifted constructive margin. The Masirah-MAR analogy may qualitatively suggest a faulted, slow spreading, constructive margin for the Masirah Ophiolite.

Plate 2.1

(a)   Typical low-lying exposure of serpentinised harzburgite.
Lighter pods are the minor intrusions of pegmatitic gabbro,
leucogabbro and anorthosite referred to in the text (P. 24.).
W of Macula   FT881582

(b)   Serpentinised harzburgite containing calcite veins. These
veins may indicate Ca expulsion during the serpentinization
process and explain the low CaO/Al_2O_3 ratios of the
serpentinites (P. 28).
The hammer is 30 cm long.
Jabal Hamra   FT935705

Plate 2.2

(a) The contact of a gabbro pegmatite vein in serpentinite. The
coarse grain-size in these minor intrusions suggests a hot
environment when they were intruded (P. 24.).
Jabal Hamra   FT930700

(b) Detail of minor intrusion of gabbro pegmatite in serpentinite.
Light mineral = plagioclase, dark mineral = clinopyroxene
Jabal Hamra   FT935705

CHAPTER 3

THE MASIRAH PLUTONIC ROCKS: OUTCROPS OF OCEANIC LOWER CRUST

1. INTRODUCTION

Masirah Island lies 25 km. off the SE coast of Oman, at the NW margin of the Indian Ocean, and is formed of a well-exposed ophiolite complex (Moseley, 1969; Glennie et al, 1974 Abbotts, 1978a). Emplacement tectonics have involved some disruption of the former ocean-crust stratigraphy but the gabbro-sheeted dyke and sheeted dyke-pillow lava relationships are clearly displayed (Abbotts, 1978b).

The ophiolite is associated with Lower to Mid-Cretaceous sediments (Glennie et al, 1974) and is unconformably overlain by Lower Tertiary limestone (Lees, 1928; Moseley, 1969). It is believed to represent Cretaceous ocean crust emplaced during Upper Cretaceous - Lower Tertiary times. This paper examines both the structural and intrusive relationships and the whole rock and mineral chemistry of the plutonic rocks and provides some information on the processes operative in the lower crust of constructive margins.

The igneous rock nomenclature of Streckeisen (1976) and where appropriate the layering terminology of Jackson (1967) are employed. For the sake of space, the general term "gabbro" is used to describe the complete plutonic assemblage.
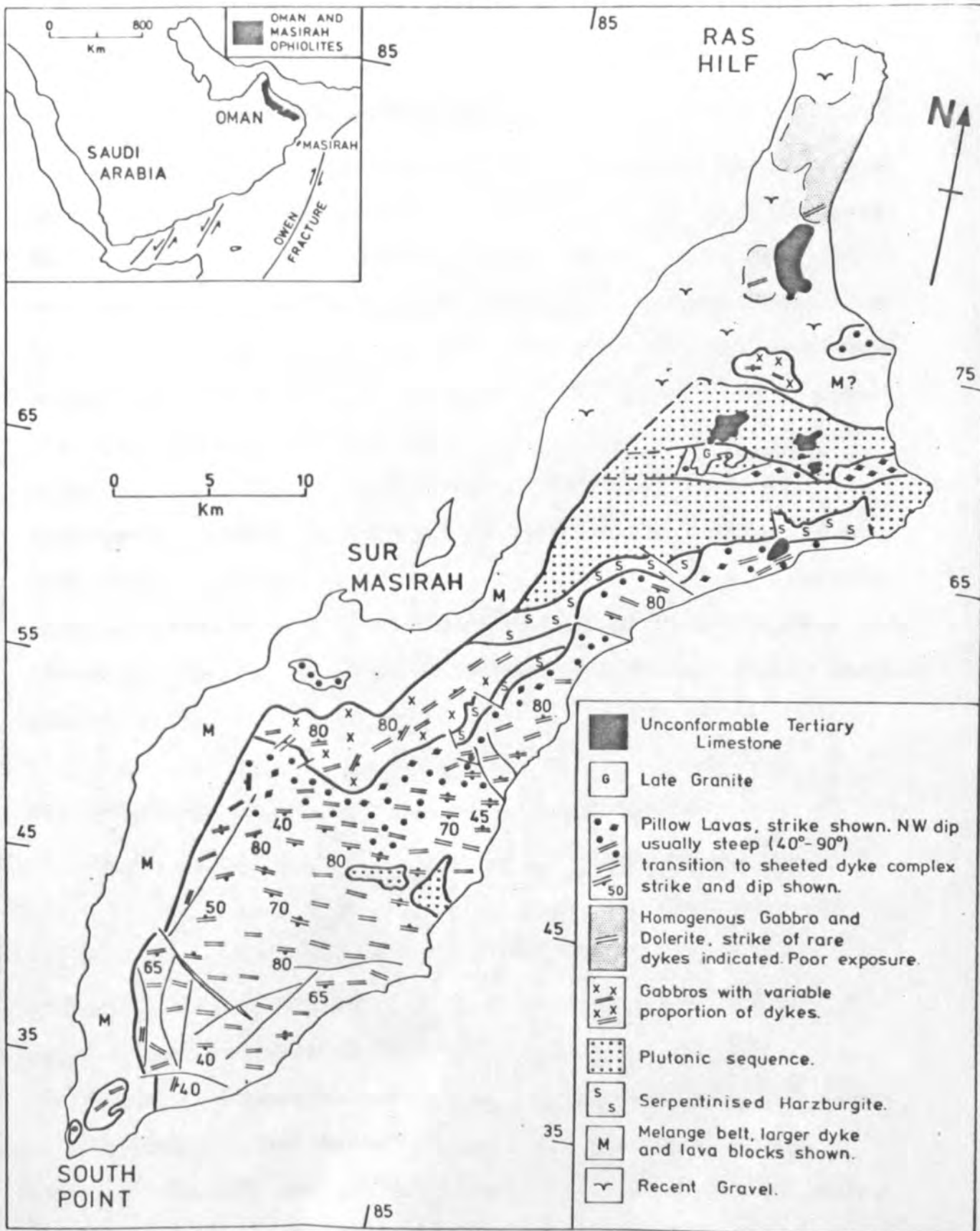
FIG.1. Geological map of Masirah Island showing the
disposition of the major lithological units. Gabbroic
rocks occur: (i) as minor intrusions of the serpentinized
harzburgites; (ii) as cumulates of the "plutonic sequence";
(iii) as massive gabbro screens between dykes of the sheeted
dyke complex; (iv) as intrusions of the sheeted dyke complex.

2. FIELD RELATIONS OF THE GABBROS

Approximately 38 per cent, or 250 sq.km., of the exposure on Masirah Island is composed of coarse-grained magmatic rocks. These vary from plagioclase-dunite, with 90 modal per cent cumulus olivine, to trondhjemitic differentiates with 33 per cent modal quartz. As a rather arbitrary division these rocks have four main types of occurrence (Fig.1). These are (a) minor intrusions, dominantly gabbroic, of mantle serpentinites. (b) Ultramafic-mafic cumulates which are frequently layered and intruded by rare dolerite dykes. They form high relief in the north of the island. (c) More massive gabbros intruded by a variable proportion of dolerite dykes (Abbotts, 1978b). (d) Ultramafic-mafic intrusions of the sheeted dyke complex.

2A. Minor intrusions in the mantle serpentinites

These minor intrusions form an integral part of the limited mantle-rock exposures on Masirah and their field-relations are described in detail with that of their host (Abbotts, 1978e). Briefly, they occur as complex systems of veins, dykes and pods of coarse to pegmatitic clinopyroxene-gabbro and leucogabbro, some virtually anorthositic, and rarer dolerites. All intrusions have sharp, cross-cutting contacts with the host serpentinite, whose harzburgitic nature is evident even in the field. The intrusions form 1-70 per cent of the outcrops, averaging 20 per cent, and their extent varies from 2-60 cm wide dykes and veins, which can be followed for 20-30 m before pinching out, to more irregular pods or bosses of 20-30 sq.m. outcrop.

2B. Ultramafic-mafic cumulates

(i) Magma chamber base.

Most cumulate exposures are delimited by steep faulting (Figs.1 and 2) but in two areas their stratigraphic base is exposed. At Turtle Beach (Fig.2) brown, low-lying, deeply-weathered, serpentinites which represent depleted spinel-harzburgite mantle (Abbotts, 1978e) are overlain by black-grey, crudely-layered, ultramafic cumulates (Fig.2). The cumulates vary in type from plagioclase-dunite to olivine-anorthosite and their layering has a $30-40^{O}$ dip to the NNW. The actual contact, the petrological Moho, is clearly conformable with the cumulate dip. South west and east of Jabal Hamra (Fig.2) the same boundary is much obscured by minor shearing and by subsequent gabbro-gabbro pegmatite-dolerite intrusion.
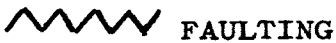
(ii) Cumulate crystallisation sequence

The crystallisation sequence followed by the cumulate rocks was (a) Cr + Ol, (b) Ol, (c) Ol + Pl, (d) Ol + Pl + Di, (e) Pl + Di, (f) Pl + Di + Hb + Mt. Table 1 sets out schematically the petrological and petrographical details of both the cumulate rocks and the massive gabbro unit.

(iii) Lower ultramafic cumulates

Basal chromite deposits equivalent to those present at the base of the Troodos sequence (Greenbaum, 1972) were not located. Small (< 0.5 mm) chrome spinel grains are frequently contained within, and therefore preceded, the cumulus olivine phase and it is possible that more detailed mapping might reveal

Table 1 : Main petrological details and deduced vertical sequence of the Masirah plutonic rocks

Lithologic unit	Type locations	Cumulus phases	Intercumulus phases	Percentages of dykes	Development of layering*1	Uralitization (amph/cpx)	Approx. Th.
Upper Massive gabbro	3 km SE of Sur-Masirah (830560)	Not cumulate Pl-Cpx-Hb-Mt-Ap-Zr		Variable 5-95	Usually massive. Rare steep layering	64% (n=10)	? *2
∿∿∿ FAULTING		-					
Gabbro cumulates	Ras Al Ya (030690)	Pl+Cpx - Ol+Pl+Cpx -	Overgrowths		Massive sequences alternate with layered	23% (n=18)	0.9-*3 1.1 km
Ultramafic cumulates	N.of Jabal Hamra (960720) + Rassier (035700)	Ol+Pl - Cr+Ol	Di (En) - Pl, Di	0-10	Layered throughout originally sub-horizontal.	3% (n= 7)	1.2-*3 1.4 km

Note: *1 = always accompanied by igneous lamination, extremely irregular and discontinuous.

*2 = ophiolite dislocation prevents thickness estimation. At least 1 km of sheeted dykes with massive gabbro screens.

*3 = estimation from maximum exposed thickness and averaged layering dip.

FIG.2. Simplified geological map of the plutonic
outcrops in the north of Masirah Island.

FIG.2.
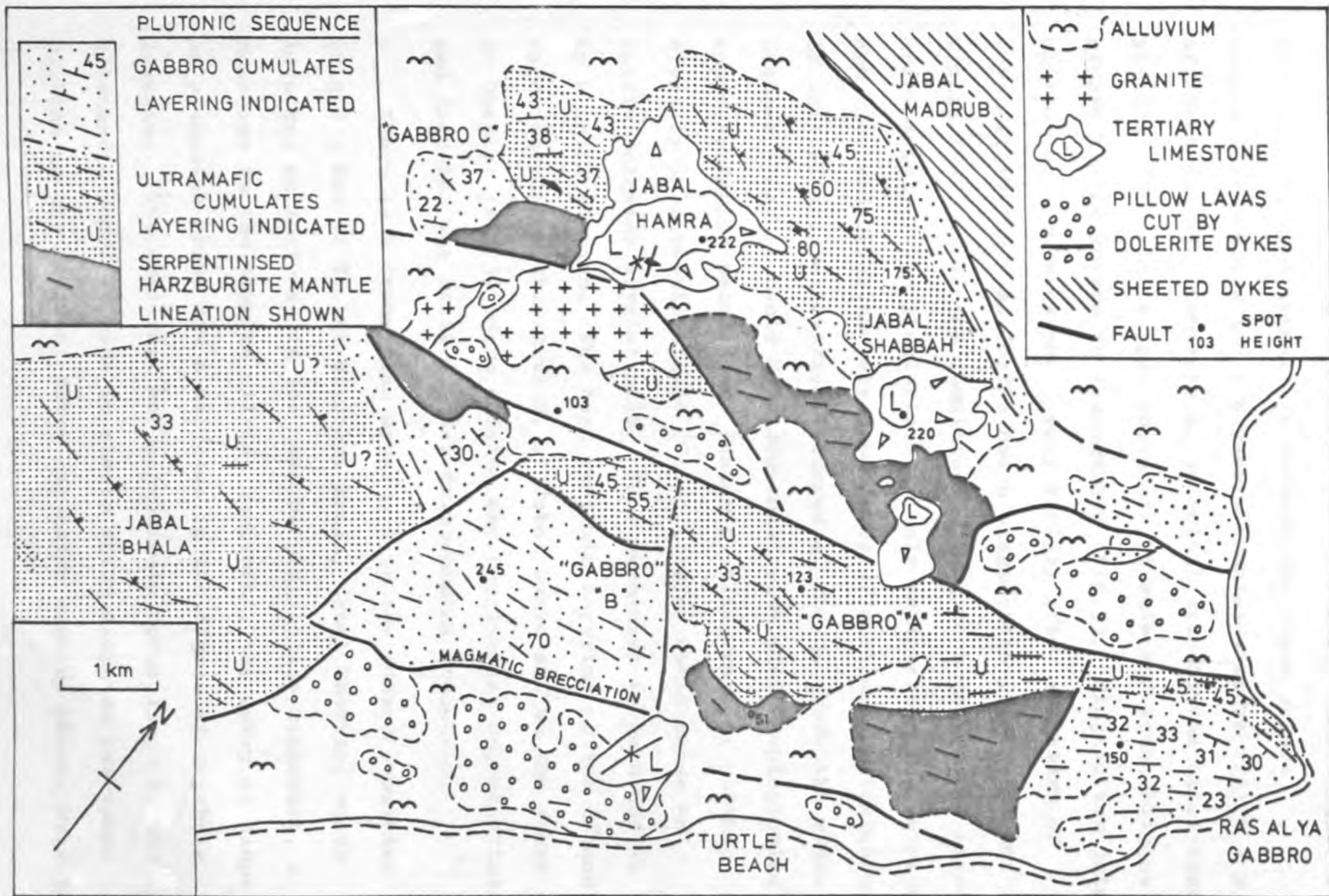
the presence of such deposits. The ultramafic cumulates form a crudely-layered transition between the non-cumulate serpentinites below and the gabbro cumulates above (Fig.2 : E. of Jabal Hamra). Complete lithological transitions exist from pl-(cpx) - dunite to cpx-troctolite to mela and leuco-olivine gabbro to cpx-gabbro to leucogabbro (Fig.5). Plagioclase joins olivine as a cumulus phase very rapidly after the start of crystallisation. At Turtle Beach plagioclase is present to within 10-20 m. of the cumulate-harzburgite boundary and elsewhere samples with plagioclase in only an intercumulus development are rare and unfortunately from areas of unclear relationships. If initial crystallisation occurred at 30-50m above the magma chamber floor it could have commenced with olivine-plagioclase coprecipitation because the faster settling-rate of olivine crystals in a basalt liquid (Good , 1976) would cause an initial olivine crystal pile. This mechanism is returned to in a later section. The best rhythmic layering on the island is developed in this unit N. of Jabal Hamra and on the coast at Rassier (Fig.3) where olivine and plagioclase coprecipitated and diopside was still a minor intercumulus component.

There is a transition upwards into the gabbro cumulates (Fig.2 : Ras Al Ya, NE of Jabal Bhala, Jabal Shabbah) which involves an increase in the cumulus plagioclase component, a decrease in the cumulus olivine component, the entry of diopside as a cumulus phase and a decrease in the degree of rhythmic layering. The arbitrary and approximate upper limit to the ultramafic cumulate zone is placed where diopside overtakes olivine as the dominant ferro-magnesian cumulus phase. Near to

Legend:

- ⌒∴ ALLUVIUM
- °₀° PILLOW LAVA
- GABBRO CUMULATES WITH DUNITE BLOCKS
- ULTRAMAFIC CUMULATES
- S S / S SERPENTINISED HARZBURGITE
- F / F FAULT
- 48 ⫻ STRIKE AND DIP OF DOLERITE DYKES
- 33 ⊣ STRIKE AND DIP OF IGNEOUS LAYERING

→ N

250m

RASSIER

RAS AL YA

50 48 35 45
22 21 35/45
33 25
30

A ———————————— B

100m
100m

A   B

SL
? F

GABBROIC CUMULATES

Pyroxene gabbro/leucogabbro;
olivine gabbro, dunite xenoliths
toward base. Common dolerite
dykes.

ULTRMAFIC CUMULATES

Base: pl-dunite,
ol-anorthosite passing
up into mela-leuco
olivine gabbro.

ARBITARY DIVISION

FIG. 3. Simplified geological map and section through the
Ras Al Ya gabbro. The ultramafic cumulate unit is shown
with a distinct ornament in the section to demonstrate
the irregular nature of the layering.

Jabal Shabbah (Fig.2) there are approximately 400 m of ol-pl cumulates before entry of cumulus diopside. There are 0.9-1.1 km vertical thickness of these ultramafic cumulates exposed NE of Jabal Hamra.

(iv) Gabbroic cumulates

These are predominantly clinopyroxene-plagioclase gabbros and leucogabbros in which plagioclase ranges from 50 to 90 per cent of the mode. Olivine continues as a cumulus phase but is usually resorbed and rarely forms more than 15-20 modal per cent. Rhythmic layering of mela to leuco olivine gabbro and clinopyroxene leucogabbro is best developed toward the base (e.g. Fig.2 : Gabbro "C"). In the clinopyroxene-gabbro rhythmic layering occurs spasmodically due to variation in the plagioclase: clinopyroxene ratio (e.g. N.of Jabal Madrub). Dunite-troctolitic xenoliths occur quite commonly: several examples of 6-60 sq.m. areal extent occur near the middle of the Ras Al Ya gabbro sequence (Fig.3) and larger blocks ($<$ 1000 sq.m), cut by gabbro veining, occur in the gabbros W. of Jabal Hamra.

(v) Cumulate textures

Both the cumulate units possess a fairly uniform grain-size with a range from 3-8 mm and an average of 5-6 mm. Most specimens, layered and unlayered, possess a primary igneous lamination caused by rough parallelism of the cumulus phases, particularly the tabular plagioclase crystals. Between early spinel and late magnetite precipitation a cumulus opaque phase

was not seen.

In the gabbro cumulates the olivine phase is often rounded and appears to have suffered resorbtion by the inter-cumulus liquid whilst rarely narrow orthopyroxene $(En'85)$ rims are occasionally developed. The olivine is always partially serpentinized (30-75 per cent) but never completely as in the mantle harzburgites. Serpentinization is clearly seen to be an expansive process, and therefore probably isochemical (Coleman and Keith, 1971), because it causes radial cracking of any surrounding plagioclase crystals. In the early ultra-mafic rocks serpentinization is frequently accompanied by rodingitization of the minor plagioclase component, whether in the form of individual anorthositic layers or the minor cumulus phase. Rodingitization in similar rocks has been described by Coleman (1967), Glennie et al (1974) and Honnorez and Kirst (1976). The combined alteration processes have produced the following assemblage, with the suggested elemental migrations from Glennie et al (1974).

OLIVINE | PLAGIOCLASE
                                           |
                SERPENTINE |
OLIVINE   +   AMPHIBOLE   CHLORITE | HYDROGARNET   Fibrous, near isotropic
                MAGNETITE | ZOISITE + ? MICA +
                                           | CHLORITE + QUARTZ
                                           |
                                           | CA, AL
                        ←——————————————————┼——————————————
                                    FE, MG
                         ——————————————————————————————→
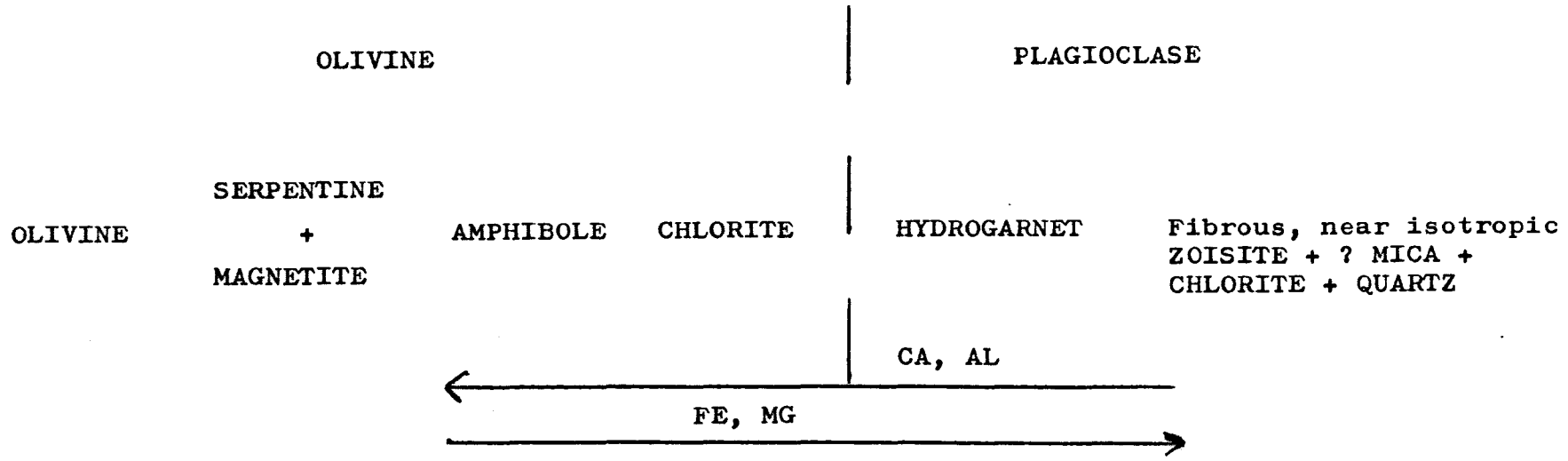
Plagioclase first appears as a rodingitised xenomorphic intercumulus phase, rapidly becoming cumulus and tabular. Diopside is a poikilitic intercumulus mineral, with an irregular distribution over the size of a slide, in most of the ultramafic cumulates. The distribution probably reflects the irregular pore space and nucleation of this final phase. Textures suggest dominantly adcumulate processes with lobate and irregular grain boundaries caused by unzoned mineral overgrowth, and only a limited intercumulus proportion.

(vi) Features of the cumulate layering

Lateral extent, layer boundaries and thickness.

Though only limited mineral chemistry studies have been made, no cyclic layering is apparent. Rhythmic layering is more widely developed in the lower ultramafic cumulates but occurs spasmodically throughout the gabbros. The irregular, discontinuous, nature of much of this layering must however be emphasized. If exposure allows, individual layers are seen to pinch out within 5-50 m and within these limits the layers commonly pinch or swell. In some areas repeated intrusion of leucogabbro, pegmatitic gabbro and occasionally dolerite lend further complexity. The result at Jabal Shabbah is exposures consisting of magmatic breccias with layered cumulate blocks in a more leucocratic matrix. Regular layering within the blocks varies widely in attitude from one to the next. The resulting impression is that of unstable conditions involving mobility of leucocratic magmas and continual intrusion of later magma.

Sharp and isomodal single layers are more common than mineral graded layers. Grain-size layering consisting of coarse, almost pegmatitic, and fine, almost doleritic, layers is not uncommon (e.g. N.of Turtle Beach or in isolated blocks 4 km N.of Jabal Madrub). Both mineral graded and grain-size layering possess sharp contacts.

Table 2 shows details from two, less deformed, areas of layering and illustrates the olivine-rich nature of the ultra-mafic unit and the plagioclase-rich nature of the gabbro unit. The thickness of individual layers usually varies from single crystal to 3.5 m. In contrast to the layering shown in Table 2 another common development is that of melanocratic and leucocratic layers of an equal (6-12 mm) thickness, such as on the beach at Rassier (034700).

Original attitude of the layering

Salient observations concerning the original attitude of the layering in the cumulate rocks include the following: (a) the layering and the igneous lamination appear to be always parallel; (b) there is little or no mineral lineation within the plane of lamination; (c) at Turtle Beach, the layering is parallel to the serpentinite-cumulate boundary, which represents the magma chamber base (Fig.2); (d) rare dolerite dykes intrude the cumulate rocks. North of Jabel Madrub the dip of the dykes (50/210) is approximately perpendicular to that of the layering (30/010). However layering in the Ras Al Ya gabbro dips at 30/145 while the dykes dip 50/195.

Table 2 : Details of two typical layered sequences

A. Ultramafic cumulates, N.of Jabal Hamra

Thickness (cm)	Dominant cumulus phase(s) and lithology	Lateral extent(m)	Layering boundaries
15	Pl > Ol Olivine anorthosite	10	
50	Ol > Pl > Cpx Clinopyroxene troctolite	> 30	
5	Pl ≫ Ol, Cpx Olivine anorthosite	15	Sharp isomodal
60	Ol ≫ Pl Plagioclase dunite	> 15	
15	Pl ≫ Ol Olivine anorthosite	15	
> 300	Ol ≫ Pl Plagioclase dunite	> 20	

⊥ = 50 cm

B. Gabbroic cumulates, SW of Jabal Hamra

Thickness (cm)	Dominant cumulus phase(s) and lithology	Lateral extent(m)	Layering boundaries
> 7	Pl > Cpx; gabbro		
1	Pl, Cpx, Ol; olivine gabbro		
12	Pl > Cpx; gabbro		
1	Pl, Cpx, Ol; olivine gabbro		
5	Pl > Cpx; gabbro	> 2	Sharp, isomodal
3	Pl, Cpx, Ol; olivine gabbro		
7	Pl > Cpx; gabbro		
2	Pl, Cpx, Ol; Olivine gabbro		
> 7	Pl > Cpx; gabbro		

⊥ = 5 cm

The widespread adcumulate textures, the lack of a mineral lineation and the common rhythmic layering composed of consistent mineral variation argue against a flow-layering origin. Instead the observations are best explained by crystal settling onto a sub-horizontal floor. The impersistent and irregular nature is discussed later but probably reflects the unstable conditions on the floor of a spreading centre magma chamber.

(vii) Ras Al Ya ultramafic-mafic cumulates.

The cumulate sequence at Ras Al Ya is probably the least disrupted on the island and is illustrated in Table 1 and Fig.3 to provide a summary of the features described above. The small but regular percentage of dolerite dykes indicate the availability of magma when almost the whole crustal section had solidified. A logical dyke-layering relationship cannot be achieved by gabbro or dyke reorientation to a horizontal or vertical attitude. Either this regularly layered body was tilted, with little internal disruption, prior to dyke injection, or the layering formed with an original dip. Reorientation of the dykes to the vertical suggests a steep dip for the layering of 60-75°.

(viii) Gabbro pegmatites.

Coarse to pegmatitic gabbros form common intrusions of the cumulate sequence to the W. of Jabal Hamra. They occur both as narrow (10-20 cm), cross-cutting, veins and as extensive developments of magmatic breccia with gabbroic blocks contained

in a pegmatitic matrix. Similar breccias occur south of Jabal
Hamra, where they are partly obscured by later granite intrusion
(Abbotts, 1978a), and along the SE margin of Gabbro "B" (Fig.2).

Within all magmatic breccias the matrix always appears to be
more leucocratic than the blocks e.g. dunite-troctolite in
olivine gabbro, the latter in gabbro, and gabbro in anorthositic
or pegmatitic gabbro.

3. UPPER MASSIVE GABBRO UNIT

An ENE-WSW striking sheeted dyke complex is well exposed
over 225 sq.km. of southern Masirah (Fig.1). Between the dykes
are common screens of a massive, uralitized, clinopyroxene-
gabbro with a 2-6 mm grain size. Olivine and an opaque phase
are rare within these gabbros and an average modal composition
is 65% plagioclase, 15% clinopyroxene and 20% uralitic
amphibole. A comparable average dyke consists of 45% plagioclase,
5% clinopyroxene, 50% uralitic amphibole and 5% Fe-Ti oxides.
The screens form an integral part of the sheeted dyke complex
and consequently their field relationships are described else-
where (Abbotts, 1978b), where the following interpretations were
made.

(a) A continuous sequence from 100% gabbro to 100% dykes
is nowhere exposed because of faulting. There are, however,
sequences varying from 95% cumulate gabbro to gabbro with 20-30%
dykes and from dykes with 40% gabbro screens to 100% sheeted dykes.
The evidence suggests a gradual though irregular transition from
cumulate gabbro, through massive gabbro cut by common dykes, to

sheeted dyke complex. This transition occurs over at least 1.0 km vertical thickness. The nature of the cumulate gabbro-massive gabbro junction is obscured by the breaks in sequence here but because the upper cumulates are poorly layered pyroxene gabbros the junction is, in any case, difficult to study in the field.

(b) The massive screens are believed to represent roof crystallisation in high axial magma chamber(s). They are exposed to within 1.3-1.5 km of the first pillow lava screens at both Haql and S. of Al Quarin. In both areas there appears to be no significant faulting in the sequences. The steep southerly dyke dip thus suggests gabbro crystallisation to within ∼ 300 m, vertically, of the dyke-lava contact.

(c) Gabbro underplating of early axial dykes is initially contemporaneous with dyke injection but progressively thickens and hinders it as the crust accelerates to its steady spreading rate. This model provides an explanation of a sequence which appears to be a gradual transition from 100% dykes to 100% gabbro. Though, similar, it was developed separately from the model of Kidd et al (1977), which was recently produced to explain comparable features in the Mings Bight Ophiolite.

3A. Local pegmatitic and silicic differentiates

The gabbro exposures within the sheeted dykes vary from screens 3cm, in width to areas, without dykes, 750 m across (Fig.4). Most pre-date dyke injection but the main gabbro X-Z in Fig.4 is clearly intrusive into the dykes (Abbotts 1978b, Chapter 4). The gabbro screens are locally transitional into a

FIG.4. (overleaf) Complex dyke-gabbro relationships toward the base of the sheeted dykes.

Legend:

70 ⊥ — MEASURED DYKE TREND AND DIP

⟋⟋⟍ — INTERPRETED TREND AND DIP

70 ⊥ · — GABBRO WITH LOCALLY DEVELOPED MINERAL LAYERING

✳ — COPPER MINERALISATION

M — MELANGE

Y — ALLUVIUM

⟋⟋ — FAULTS

500 METRES

N

EXTENSIVE BRECCIATION AND IRREGULAR DYKE TRENDS
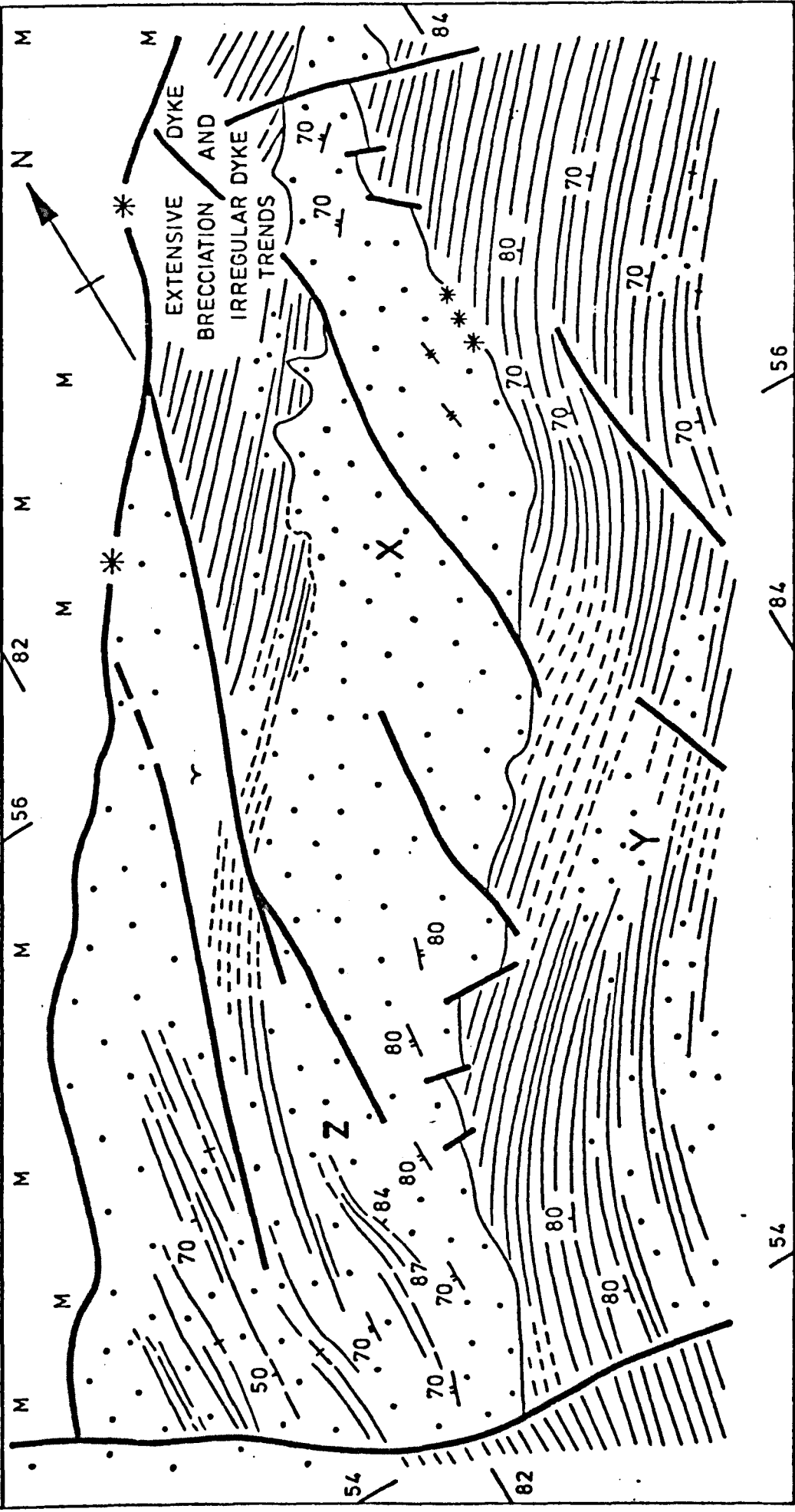
pegmatitic facies, although the pegmatites also occur as late cross-cutting veins. The pegmatite usually pre-dates dyke intrusion. Both the pegmatites and occasionally the massive gabbro contain a primary brown titaniferous hornblende phase which is distinct petrographically and chemically (Table 3) from the secondary uralitic amphiboles. The hornblende is not a liquidus phase but crystallises late and grows out from clinopyroxene.

Table 3 : Amphibole species in the massive gabbro unit

	Brown amphibole Hornblende	Green uralitic amphiboles Actinolite	Hornblende
SiO_2	43.71	54.31	47.29
TiO_2	3.31	0.19	0.37
Al_2O_3	12.35	2.98	10.81
Cr_2O_3	0.20	0.12	-
FeO	8.03	6.70	11.26
MnO	0.11	0.13	0.10
MgO	15.47	20.05	14.61
CaO	12.25	12.42	12.06
Na_2O	2.31	0.59	2.60
K_2O	0.65	0.08	0.11
TOTAL	98.39	97.57	99.22
MG	53.8	61.3	49.4
FE	15.6	11.4	21.3
CA	30.6	27.3	29.3

Silicic differentiates occur extremely rarely, forming less than 1% of the massive gabbro exposure. East of Sur-Masirah, within sheeted dyke complex with 90% dykes, a single meta-tonalite screen composed of plagioclase-amphibole-epidote was

found.   In addition narrow (2-3 cm) trondhjemite veins, with a quartz-plagioclase-epidote mineralogy cut cumulate gabbros W. of Turtle Beach (Fig.2).   These veins continue the pattern noted above of later liquids being more leucocratic.   This latter occurrence is cut by dolerite dykes which form 10-15% of the outcrop and post-date the trondhjemite.

3B.   Rare layering in the massive gabbro unit

Igneous layering or lamination is extremely rare in the massive gabbro unit and the usual texture is xenomorphic granular to sub-ophitic.   Rare layering in the unit is described elsewhere (Abbotts, 1978b) and because of its steep attitude and strong mineral lineation within the plane of layering is attributed to local magma turbulence.   The lack of cumulate textures, the dyke-gabbro relationships and the indications of increased PH_2O in the stabilised hornblende phase are all in keeping with a roof crystallisation environment.

3C.   Metamorphism of the massive gabbro unit

Metamorphism of the ophiolite has been reviewed elsewhere (Abbotts, 1978b) and is ascribed to hydrothermal circulation at the original constructive margin.   Whole rock metamorphism seems to be effectively limited to the depth of the dolerite dykes but local uralitization is common into the cumulate gabbro unit.   The stabilisation of primary brown hornblende in the massive gabbros suggests that water plays an important role in both magmatic and metamorphic processes.

3D. Magma chamber roof

The rare gabbro screens in sheeted dyke complex of 90-99% dykes seem to represent gabbro crystallisation to within 300-400 m, vertically, of the first pillow lava screens. However any vestiges of the actual roof to the gabbros has been obscured by subsequent intrusion of the larger proportion of dykes. These must have been intruded as the crust accelerated from the spreading axis, in order to isolate the rare screens. It must be emphasized in support of this interpretation that the dykes and gabbro screens have distinct modal compositions, distinct whole rock chemistries and that the gabbros, similar whether occurring as 3 cm screens or 100 m wide areas, are not coarse-grained dykes.

4. INTRUSIONS INTO THE SHEETED DYKE COMPLEX

Gabbroic intrusion into the sheeted-dykes is reviewed elsewhere (Abbotts, 1978b) and the gabbro shown in Fig.4 is reproduced from there. This clinopyroxene-gabbro is dominantly unlayered, although it occasionally exhibits the steep layering noted in the massive gabbro unit, and is similar to the massive screens in the adjacent dyke swarm. The gabbro is itself locally cut by dykes which follow the regional trend. The parallelism of the sheeted dykes, the gabbro intrusion and these later dykes suggests that all the intrusive activity probably occurred in the axial tensional regime.

Another gabbroic intrusive complex is that of the Ras Kaida pluton (Abbotts, 1978b; Fig.1). Here ultramafic and gabbroic cumulates have intruded with clear discordance over

an area of 4 sq.km into sheeted dyke complex with 70 per cent dykes. The ultramafic component occurs largely as blocks, up to 400 m diameter, contained in gabbros. The gabbros are frequently layered but there is no consistency in the attitude of this from area to area. It seems possible that the area represents upward intrusion of a partially consolidated crystal mush and not of liquid.

5. MULTIPLE MAGMA CHAMBERS OR A STEADY-STATE MODEL?

Allen (1975) suggests that the Troodos spreading centre was underlain by discrete magma chambers, in each of which the magma followed a slightly different evolutionary path, resulting in some lateral discontinuity in the gabbros. In contrast Cann (1970, 1974) and Dewey and Kidd (1977) have proposed steady-state models for plate accretion involving a spatially and temporally continuous axial magma chamber.

Table 1 suggests a cumulate thickness of 2.2-2.3 km. There is at least 1.3-1.4 km of dykes with massive gabbro screens and the products of magma chamber crystallisation appear to total 3.5-4.0 km vertical thickness. The evidence for discrete magma chambers, and their lateral dimensions, is partially obscured by faulting but the following areas show features relevant to the problem.

(a) The Ras Kaida intrusive complex (Fig.1) is clear evidence of a high-level gabbro pluton.

(b) The Sur-Masirah gabbro (Fig.4) indicates intrusion of the sheeted dyke complex before termination of dyke intrusion.

(c) The fault-bounded Ras Al Ya cumulate gabbro (Fig.2) contains several individual features including (1) a small ($\sim$ 5%) but regular proportion of dolerite dykes, which are rare to absent in other cumulates; (2) an absence of the usual gabbro-gabbro pegmatite intrusions; (3) largely undeformed rhythmic layering throughout; (4) an horizon of dunitic xenoliths toward the base of the gabbro cumulates.

(d) Gabbro "B" (Fig.2) is a fault-bounded gabbro giving rise to the highest relief in the ENE-WSW gabbro belt. Only the E and S contacts were examined and these largely consist of magmatic gabbro breccias. Layering is present but only in isolated blocks of gabbro, $0.5-30m^2$ in area, which are contained in a more leucocratic gabbro or gabbro pegmatite matrix. The breccia was examined for 200-300 m into the gabbro and appears to represent unstable conditions in which the accumulating crystal pile was continually intruded by more leucocratic (? remobilised) magma. Locally the intrusive magma reaches a trondhjemitic composition.

(e) The remaining areas around Jabal Hamra, Jabal Bhala and Gabbro "A" (Fig.2) appear to have similar cumulate successions, much intruded by gabbro and gabbro pegmatite. However without more extensive mineral chemistry studies their similarity could not be confirmed in detail.

In conclusion the Ras Kaida and Sur Masirah gabbros represent individual intrusions and the contrasting sequences of Ras Al Ya, Gabbro "B" and the Jabal Hamra group argue against a uniform steady-state model. The rhythmically layered Ras Al Ya intrusion appears to represent accumulation during

a period of relative quiescence. A significantly later magma

batch is indicated by the dykes which then intruded the gabbro.

In contrast Gabbro "B" formed under extremely unstable

conditions at an approximately similar level in the crust.

Multiple magmas are indicated by the complex gabbro-dyke

relationships and the contrasting cumulate sequences may be best

explained by invoking individual chambers.

It may be that there is some truth in both the steady-

state and the multiple chamber models. If the spreading rate

and the supply of magma are in equilibrium a steady-state

situation under at least segments of the spreading axis might

occur. If either spreading rate or magma supply is more

irregular, as is likely in nature, the steady state will

probably break down.

6. CONCLUSIONS CONCERNING THE FORMATION OF LAYERING

It has been suggested that the cumulate layering is formed

largely by crystal settling though the affects of deformation,

intrusion and flowage in the crystal pile may all play a part

in producing the discontinuous layering now visible. Goode

(1976) has used Stokesian particle behaviour to explain the

formation of layering in the Kalka basic intrusion of Australia.

Although this is a deep closed-system intrusion the internal

field descriptions are reminiscent of the less deformed and

intruded portions of the Masirah cumulates. Both sequences

contain small-scale px/ol-pl rhythmic layering, paralleled by a

primary lamination, somewhat irregular in extent and occurring

in zones alternating with laminated but unlayered sequences.

Goode (1976) suggests that crystallisation occurs near the floor of the intrusion because of the development of super-saturation at higher pressures. Crystallisation is then followed by gravitational settling with the variable crystal densities producing differential settling patterns.

Table 4 : Crystal settling times in a basaltic magma (from Goode, 1976)

Crystal phase	Density (gm/cm^3) c.f.basalt = 2.8	Settling time (yrs) 200 metres	1000 metres
Plagioclase	2.7 - 2.75	0.67	2.86
Clinopyroxene/Olivine	3.2 - 3.5	0.04	0.21

Some tendency for bottom crystallisation and/or settling explains the olivine-rich cumulates at the base of the Masirah sequence. The preponderance of plagioclase as the dyke-lava phenocryst phase (Abbotts, 1978c) is probably largely a result of the bouyancy of that phase.

Goode (1976) further notes that continuous nucleation and crystal settling will produce unlayered laminated sequences whereas discontinuous nucleation will lead to layered and laminated sequences. The latter is favoured in a slow cooling environment when the small degree of supersaturation is continuously interrupted by release of the heat of crystallisation.

Using these ideas, within the framework of the more dynamic spreading centre environment indicated by the Masirah exposures,

leads to the following interpretation of the Masirah cumulate
sequence. Initial bottom crystallisation occurs over a hot
harzburgite-mantle floor which will cause extremely discontinuous
nucleation and formation of the strongly banded ultramafic
cumulates. The crystal pile will be continuously penetrated
by ascending batches of magma, particularly during early axial
crystallisation before an extensive cumulus pile has developed.
Some of the magma batches may be trapped in the crystal pile,
some may be diverted and intrude along the lamination to
produce the grain-size layering, some areas may be so continuously
intruded that magmatic breccias with cumulate blocks result.
The hot environment and slow crystallisation will encourage
diffusion from the intercumulus liquid and produce the adcum-
ulate growth suggested later by the lack of mineral zoning and
low whole-rock incompatible element levels. The intrusion of
gabbros in dykes 8 cm wide and adjacent dolerites in dykes
30 cm wide confirm the occurrence of repeated intrusion through
the cumulates as they cool. As crystallisation continues the
cumulus pile builds up and begins to cool and become more
rigid. More continuous nucleation should occur and less melt
penetration from below will occur. The more massive laminated
clinopyroxene gabbros of the cumulate gabbro unit will thus form.

7. MINERAL CHEMISTRY

7A. Olivine

Five samples range from FO87.7, in a mela-olivine gabbro
from the ultramafic cumulates at Jabal Madrub, to FO79.5 in a
leuco-olivine gabbro from the Ras Kaida pluton. The range gives

evidence of significant fractionation subsequent to the mantle partial melting event but would undoubtedly be increased by a larger sampling population. The whole rock Fe (total iron)/Mg values correlate with the olivine compositions, varying from 0.26 (FO87.7) to 0.49 (FO79.5). Olivines from ophiolite mantle exposures usually range over FO94.5 to FO88.5 (Coleman, 1977) whilst ranges in ophiolite cumulates include FO89.6-78.3 (Papua: England and Davies, 1973), FO91.6-69.6 (Bay of Islands: Irvine and Findlay, 1972) and FO90.6-69.8 (Troodos: Allen, 1975). Cumulus plagioclase accompanies the FO87.7 olivine and cumulus plagioclase-diopside occurs with FO86.6. Nickel content varies from 1570-2350 ppm and whole rock values of 309-914 ppm are probably largely contained in the olivine phase ($K_D^{OL/L}{}_{Ni} \gg 1$; Leeman, 1976).

7B. Orthopyroxene

Olivine of composition FO87.7-85.3 shows minor liquid reaction to produce orthopyroxene (En85) reaction rims. This is the only form in which orthopyroxene definitely occurs in the Masirah gabbro sequence and the phase was identified only 5 times in 115 sections. It is not clear however whether rare actinolite pseudomorphs, in rocks where clinopyroxene remains unaltered, replace orthopyroxene or olivine. Approximately 95% of the "gabbros" contain minor normative Ne (Fig.16), not unexpectedly in view of the orthopyroxene scarcity. Similar observations have also been made in the Bay of Islands Ophiolite (Irvine and Findlay, 1972). In complete contrast serpentinised harzburgites from Masirah contain 4.3-17.3 per cent modal

orthopyroxene (mean = 12.3). Fig.5 illustrates the modal range and the plagioclase-dominated, orthopyroxene-free nature of the Masirah rocks.

7C. Plagioclase

Fig.6 sets out the variation in plagioclase composition throughout the gabbros, most of which are dominated by unzoned plagioclase with a composition of An85-80. Only in the upper gabbro unit do core compositions of An80-67 occur. Saussuritization prevented analysis of the tonalites-trondhjemites but these have normative compositions of An25-5 and would probably extend the range dramatically to low An values. Rim zoning of normal type is prevalent in the massive gabbros but also occurs in the Ras Al Ya cumulate gabbros (Fig.6: MA54, 67).

It is evident on Fig.6 that the dyke-lava phenocrysts have similar primitive core compositions (An86-81) to those of the cumulate rocks. Fig.7 plots plagioclase compositions against co-existing olivine in a comparison with other ophiolites and with the Skaergaard basic intrusion. The resulting Masirah trend, though based on only a limited sampling population appears very similar to that of early Skaergaard crystallisation and it is also apparent that Masirah, (Skaergaard, and Othris) precipitated a less anorthite rich plagioclase at equivalent FO levels to Troodos. The FO value is probably an accurate indication of the liquid Fe/Mg ratio (Roeder and Emslie, 1970).
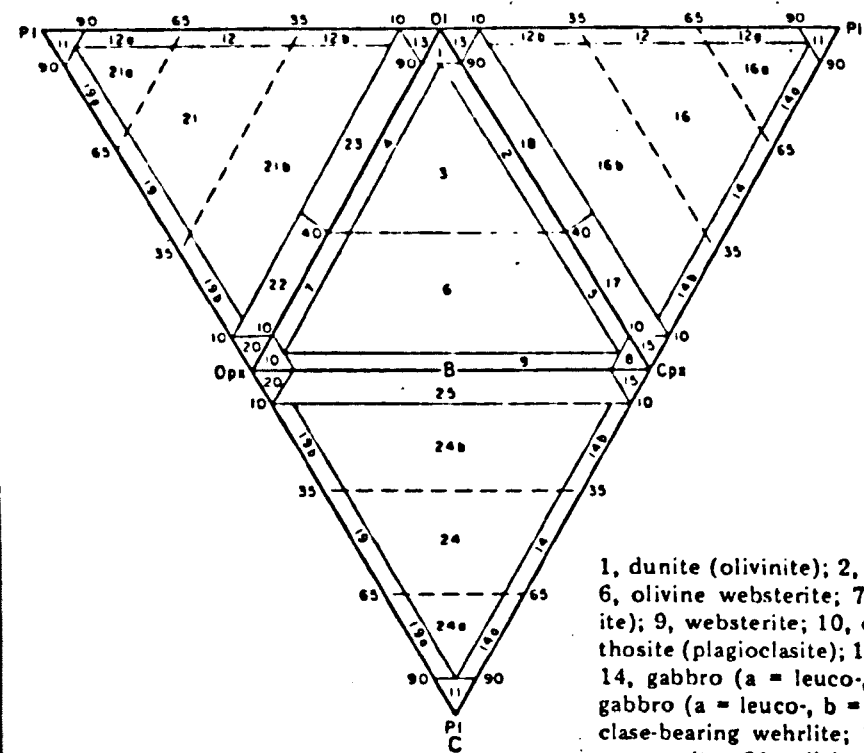
1, dunite (olivinite); 2, wehrlite; 3, lherzolite; 4, harzburgite; 5, olivine clinopyroxenite; 6, olivine websterite; 7, olivine orthopyroxenite; 8, clinopyroxenite (diopsidite, diallag- ite); 9, websterite; 10, orthopyroxenite (enstatitite, bronzitite, hypersthenite); 11, anor- thosite (plagioclasite); 12, troctolite (a = leuco-, b = mela-); 13, plagioclase-bearing dunite; 14, gabbro (a = leuco-, b = mela-); 15, plagioclase-bearing clinopyroxenite; 16, olivine gabbro (a = leuco-, b = mela-); 17, plagioclase-bearing olivine clinopyroxenite; 18, plagio- clase-bearing wehrlite; 19, norite (a = leuco-, b = mela-); 20, plagioclase-bearing ortho- pyroxenite; 21, olivine norite (a = leuco-, b = mela-); 22, plagioclase-bearing olivine orthopyroxenite; 23, plagioclase-bearing harzburgite; 24, gabbronorite (a = leuco-, b = mela-); 25, plagioclase-bearing websterite; 26, olivine gabbronorite (a = leuco-, b = mela-); 27, plagioclase-bearing olivine websterite; 28, plagioclase-bearing lherzolite.
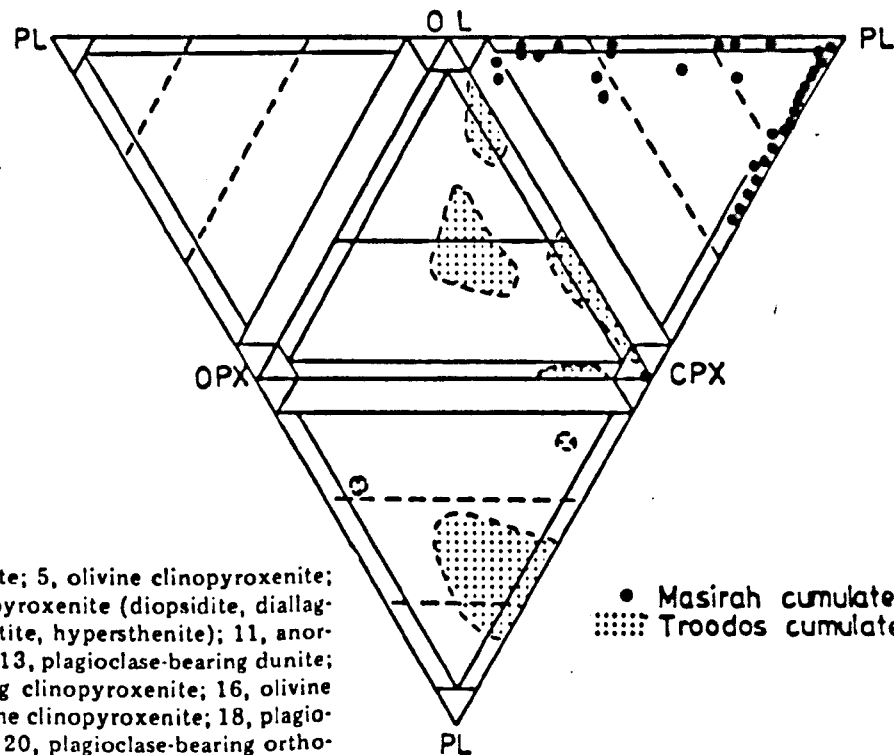
● Masirah cumulates
:::::: Troodos cumulates

FIG. 5.   Representative Masirah cumulate rocks plotted on the tetrahedral modal classification diagram of ultramafic and gabbroic rocks of Streckeisen (Fig. 4, 1976). For comparison Troodos cumulate rocks from Allen (1975) are also plotted. The diagram illustrates (1) the plagioclase domination of the Masirah sequence after the early olivine cumulates; and (2) the contrast between the orthopyroxene-free, plagioclase-rich, Masirah cumulates and the orthopyroxene-containing Troodos sequence. For the Masirah samples, accessories not accounted for are: (a) opaques, which are only important in the early olivine cumulates (cr ≤ 8%); (b) ortho-pyroxene, which only occurs in 5 rocks (≤ 3%); (c) amphibole, which is almost completely uralitic after clinopyroxene and is assigned to that phase.
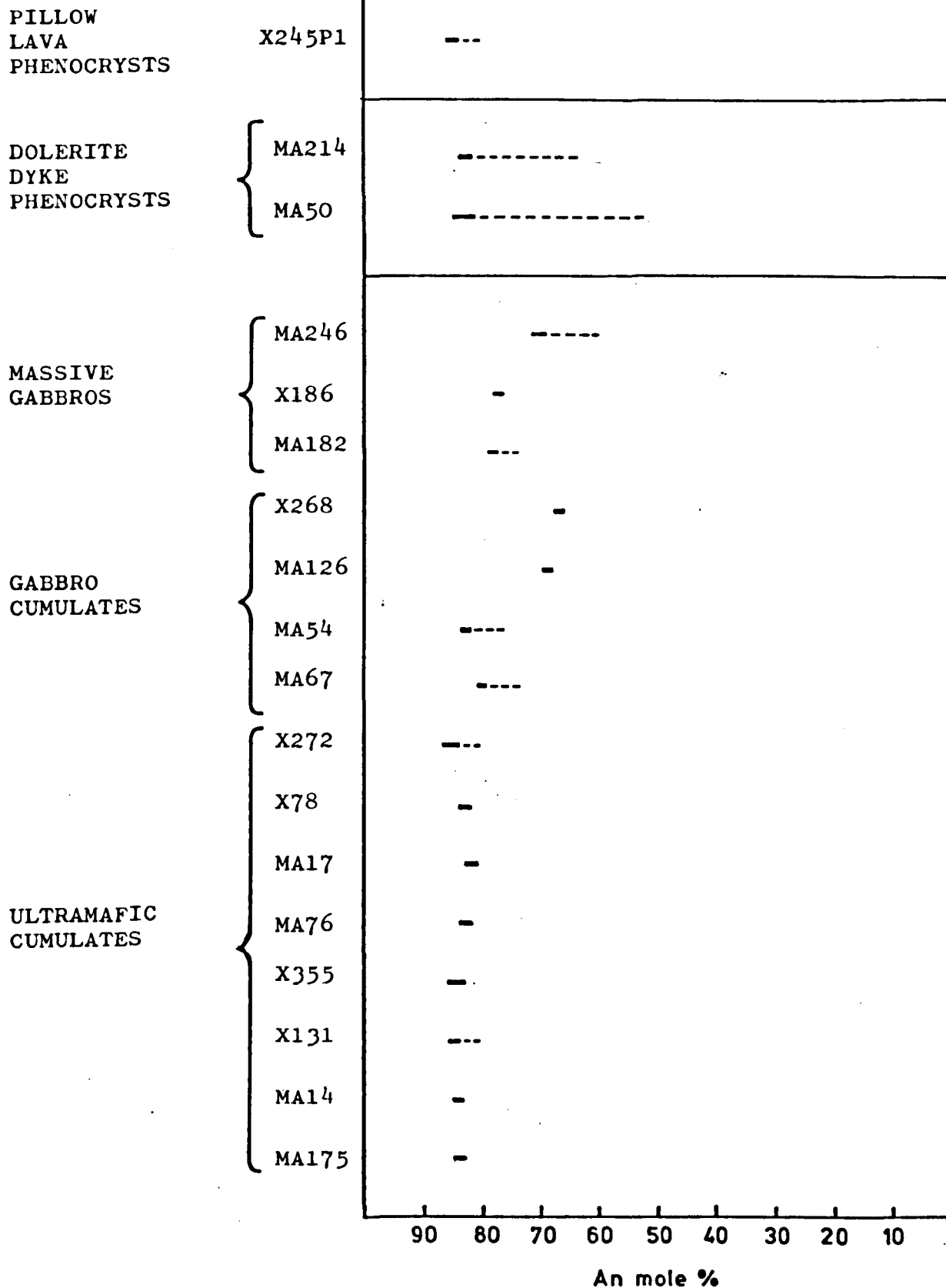
FIG.6. Plagioclase compositions and zoning plotted against lithologic unit. (Within the units the samples are ordered by increasing upward Fe*/Mg and not by strict stratigraphic height.) Solid lines show core compositions, dotted lines show extent of zoning. The Or component is negligible throughout.
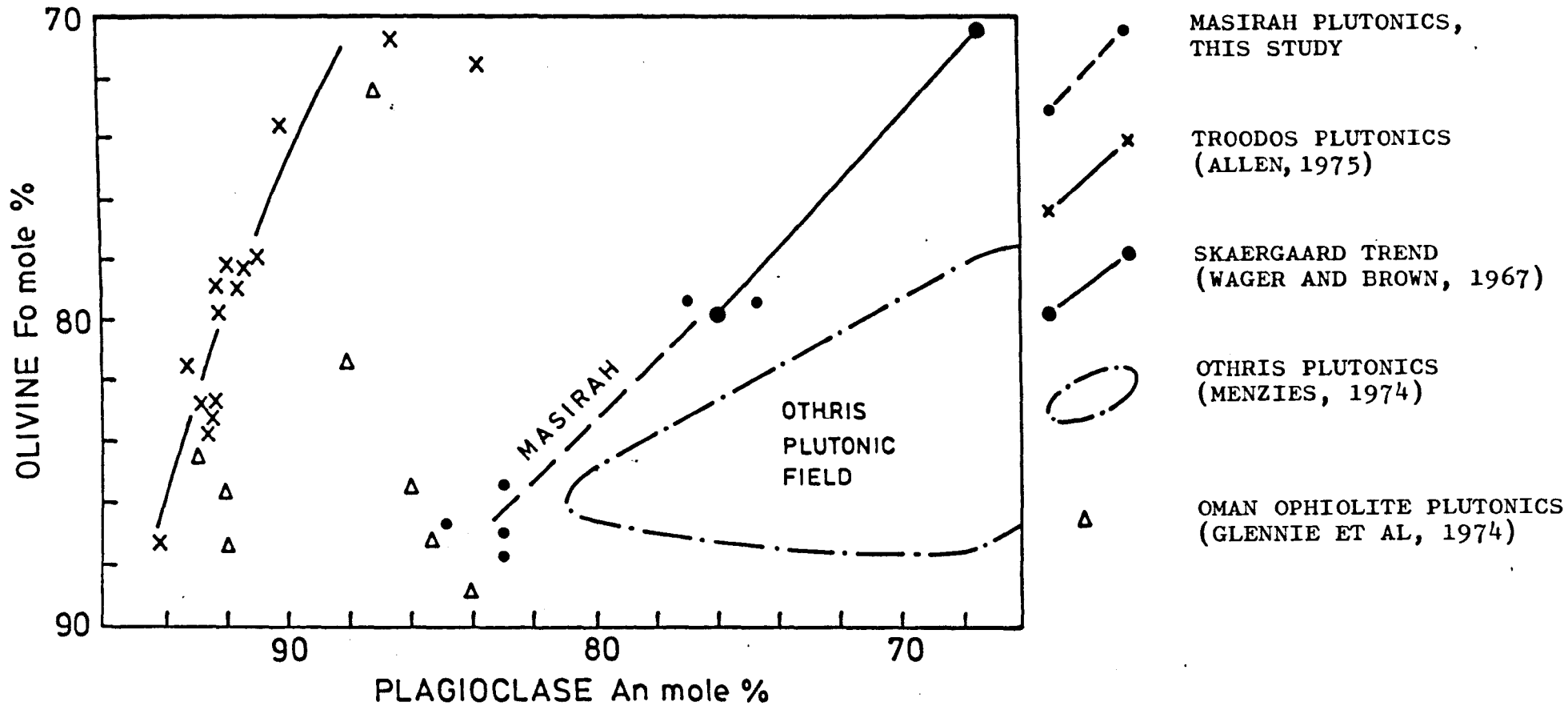
FIG.7.   Plot of coexisting olivine and plagioclase from the Masirah Ophiolite plutonics compared with those of other ophiolites and the Skaergaard layered intrusion.

7D. Clinopyroxene

The diopsidic nature throughout the "gabbros" is obvious on a pyroxene quadrilateral plot (Fig.8). This plot shows (i) moderate fractionation from the ultramafic cumulates (Fs5.1-8.0) through the gabbro cumulates (Fs6.1-10.3) to the massive gabbros (Fs8.3-12.9); (ii) the primitive nature of the rare clinopyroxene phenocrysts in the dykes which are equivalent to the clinopyroxene in the early cumulates.

Fig.9 plots Cr_2O_3 and TiO_2 in the clinopyroxene against the fractionation index of whole rock Fe (total iron)/Mg. The diagram shows (i) the primitive high Cr_2O_3 - low TiO_2 nature of the early intercumulus-cumulus diopside phase; (ii) the effect of Cr extraction from the liquid by the early clinopyroxenes causing lower levels in the higher rocks; (iii) the steady increase with fractionation of TiO_2 which probably enters the phase as $Ca\,Ti\,Si_2O_6$ (Yagis, 1967). Na_2O similarly increases from 0.27 in the early cumulates to 0.50 in the massive gabbros. The highest Cr_2O_3 value comes from a leuco olivine-gabbro layer in the olivine-dominated cumulates W. of Jabal Hamra. Adjacent layers with modal ol:pl:di varying from 10:70:20 to 70:25:5 have similar whole rock Fe/Mg values of 0.25-0.26 but very different Cr (690-1930 ppm) and Ni (190-900 ppm) contents reflecting the variable ol $(K_{D_{Ni}}^{OL/L} \gg 1)$: cpx $(K_{D_{CR}}^{CPX/L} \gg 1)$ ratio. The evidence argues for precipitation from a similar liquid and subsequent accumulation processes to explain the layering.
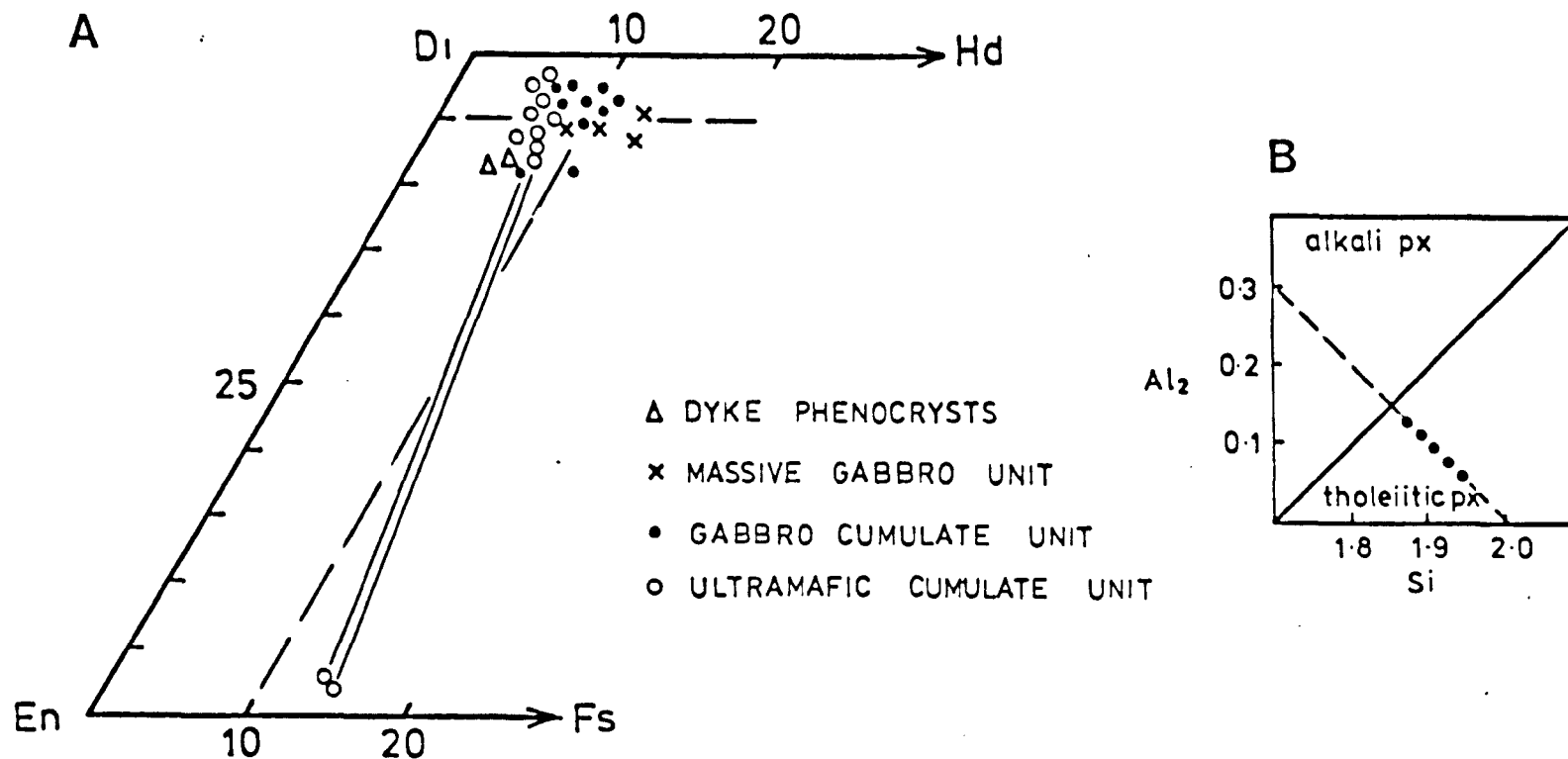
FIG.8.A Pyroxene compositions of Masirah ultramafic-mafic cumulates, massive gabbros and dyke phenocrysts in pyroxene quadrilateral. Solid lines join co-existing pyroxenes.

B Plot of Si-Al substitution in the clinopyroxene tetrahedral site. Alkali-tholeiitic discrimination line from Malpas (1978). The 5 samples plotted cover the full range of the Masirah plutonic samples.
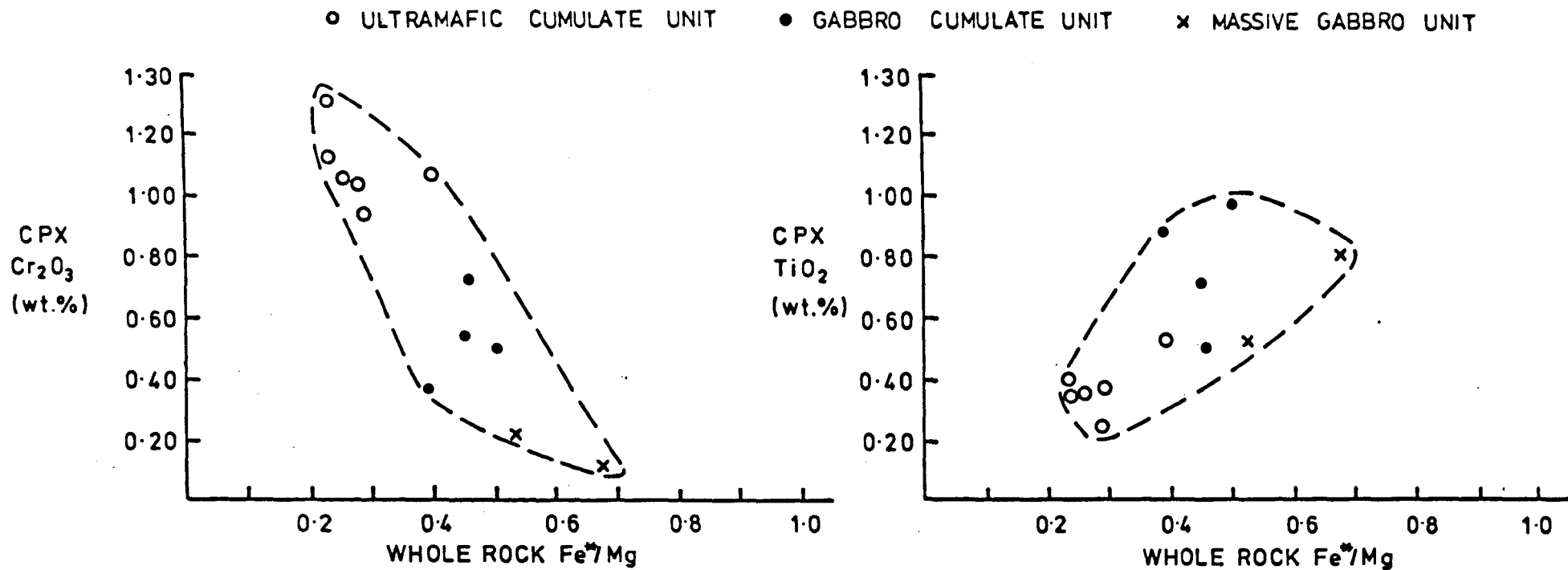
FIG.9. Clinopyroxene Cr_2O_3 and TiO_2 contents plotted against whole-rock Fe*/Mg for the Masirah gabbros.

Tholeiitic nature of the clinopyroxene phase

As clinopyroxene is the last phase to crystallise it will reflect the composition of the residual liquid in the early cumulates. Alumina variation throughout the clinopyroxenes of 2.11-3.62% results in an Al [4]/Al [6] ratio of 2-6 and limited Al [4] substitution (0.06-0.11) which indicates their tholeiitic nature (Fig.8 inset). Fig.10 plots TiO_2 against Al_2O_3 in the clinopyroxenes which then show a clear similarity to those in depleted ocean floor tholeiites.

A visual summary of all microprobe data on the 3 main mineral phases of the Masirah plutonic sequence is presented in Fig.11.

7D. Opaque Minerals

Except for the chromite phase in the early cumulates, opaques are rare throughout the gabbros. Approximately 20 per cent of samples contain accessory levels ($<$ 1 per cent) and only in the massive gabbro unit do rare samples provide evidence of significant Fe-Ti ore precipitation ($\leqslant$ 12%). Analysis of 2 adjacent grains in a uralitized gabbro screen with differentiated clinopyroxene (Fs = 12.9) were of chromiferous magnetite (Cr_2O_3 = 2.93%) and ilmenite.

7E. Thermometry-barometry of the plutonic rocks

Scarcity of the orthopyroxene phase and the problems of serpentinization hindered application of the various ultramafic geothermometers. Two-pyroxene pairs from a mela-olivine gabbro
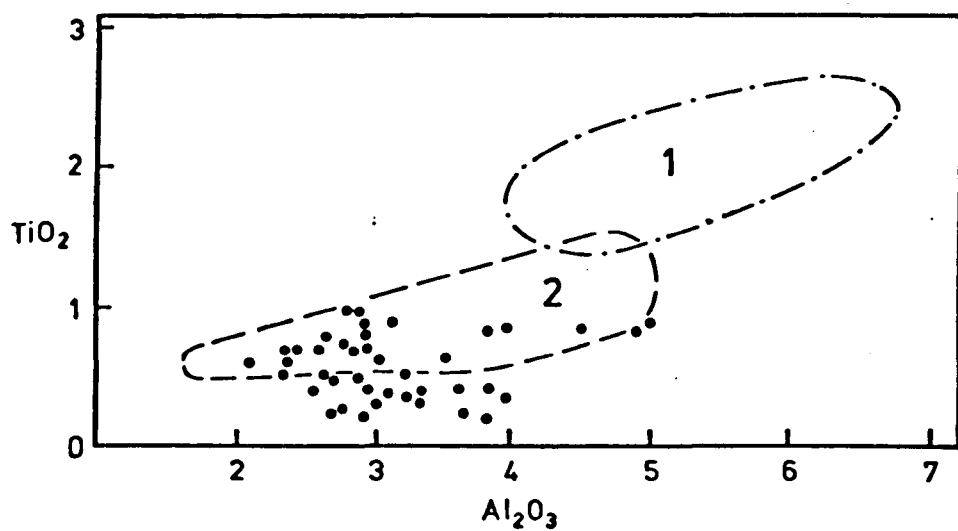
FIG.10. TiO_2 versus Al_2O_3 for Masirah plutonic clinopyroxene analyses. Fields from Frey et al (1974): 1 = LIL enriched ocean floor tholeiite with alkaline affinities, 2 = LIL depleted ocean floor tholeiite.
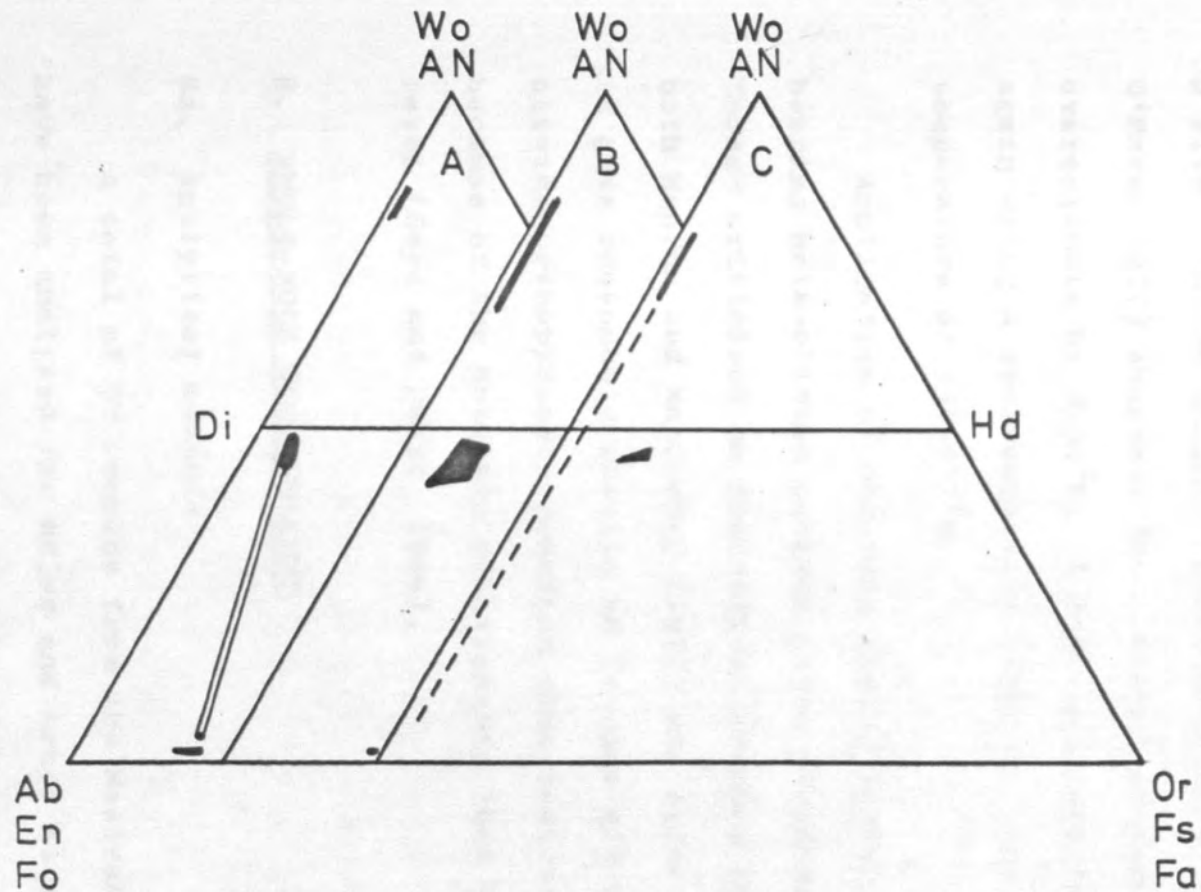
FIG.11. Summary of electron-microprobe data on Masirah plutonic rocks plotted on composite felspar-pyroxene-olivine ternary diagrams. Compositional fields are indicated in black; solid lines are tie-lines; the dashed line indicates the predicted plagioclase extension of the saussuritized plagiogranites (normative An = 25-5%). A = Ultramafic cumulate unit; B = Gabbro cumulate unit; C = Massive gabbro unit.

gave a crystallisation temperature of 1008-1012°C using the 2-pyroxene geothermometer of Wood and Banno (1975). This thermometer is semi-empirically formulated on the Fe-Mg exchange relation between the pyroxenes and assumes ideal 2 site solution mixing. Subsequent work (Hewins, 1975; O'Hara, 1977) suggests that, though precise, the method may overestimate by < 50°C. A reformulation by Wells (1977), again using a semi-empirical simple-mixing modal, gives a temperature of 936-941°C.

Application of O'Hara's (1967) pyroxene grid to spinel-bearing mela-olivine gabbros gives pressures of 1-2 Kb (3-6 km). Though criticised on theoretical grounds (MacGregor, 1974), both Moores and MacGregor (1972) and Allen (1975) declared that it gave reasonable results on Troodos ultramafic samples. The olivine-orthopyroxene reaction rims indicate pressure < 6 Kb because of the cotectic relationship that develops above this level (Boyd and Davis, 1964).

8. WHOLE-ROCK GEOCHEMISTRY

8A. Analytical methods

A total of 98 samples from the Masirah plutonic sequence have been analysed for major and trace elements using the University of Birmingham Phillips PW145D automatic X-ray fluorescence spectrometer. All elements were determined on 46mm pressed powder pellets using Cr, W and Mo tubes. To correct for major element problems of absorption and mineralogical effect, 16 samples were determined in duplicate using a fusion

bead technique. Calibrations were based on international and laboratory standards and spiked rock powders. Trace element results were corrected for mass absorption effects using WLB and MoKα Compton scatter lines. Details of spectrometer conditions, calibration methods, machine precision and accuracy can be found in Tarney et al (1978).

The REE analyses were determined by Instrumental Neutron Activation Analysis following the methods of Hertogen and Gjibels (1971) and using a low energy photon detector with the ocean basalt BOB-1 as a reference standard.

8B. Major element chemistry

Chemical analyses of representative cumulate plutonics, the massive gabbro unit and the minor intrusions of the mantle serpentinites are shown in Tables 5, 6 and 7 respectively. In the tables and various plots the pegmatitic gabbros are included in the massive gabbro unit because of their similar, slightly enriched, nature. They do in fact intrude all of the gabbro units as a late phase.

(i) Fe-Mg relationships in the gabbros.

On the A $(Na_2O + K_2O)$ - F (FeO_T) - M (MgO) diagram (Fig.12) the Masirah plutonics and dykes are compared with the trends for Skaergaard, Troodos and the Semail Ophiolite. Many of the Masirah plutonics fall in the ophiolite cumulate field of Coleman (1977); the residual scatter is caused by the cumulate leucogabbros which are enriched in plagioclase (75-95 modal per cent) and plot on the calc-alkaline side of the

Table 5 : Representative analyses of the Masirah cumulate
              plutonic rocks

| Sample | 1 | 2 | 3 | 4 | 5 |
No.	X355	MA76A	X69	MA122	X288
SiO_2	44.08	42.23	41.37	46.03	42.90
TiO_2	0.08	0.10	0.04	0.11	0.07
Al_2O_3	12.90	6.89	9.27	14.79	24.65
Fe_2O_3*	0.62	0.92	1.01	0.58	0.13
FeO	4.09	6.09	6.68	3.82	0.86
MnO	n.d.	n.d.	n.d.	n.d.	0.02
MgO	21.72	30.83	28.84	17.81	6.85
CaO	12.43	8.52	8.14	13.80	22.22
Na_2O	1.04	0.58	0.76	1.04	0.49
K_2O	0.02	0.02	0.02	0.02	0.03
P_2O_5	0.00	0.01	0.01	0.00	0.00
TOTAL	96.98	96.19	96.14	98.00	98.22
Ni	546	914	808	394	91
Cr	1729	2644	1145	1452	265
Zn	21	27	30	18	15
Ga	8	7	9	9	8
Rb	1	-1	-1	-1	-1
Sr	65	186	138	88	116
Y	-2	-2	-2	-2	-2
Zr	2	6	4	6	8
Nb	1	-1	-1	-1	-1
Ba	4	4	-4	5	7
La	-2	-2	2	2	2
Ce	-3	3	4	3	3
Pb	-3	14	-3	-3	-3

Note: *Iron allocated so that FE2O3/FEO = 0.15
       -2 = below lower limit of detection.
     n.d = not determined.

1 Mela-olivine gabbro (cumulus ol > pl; intercumulus di)
2 Plagioclase dunite   (cumulus ol ≫ sp; intercumulus pl, di)
3 Mela-olivine gabbro (cumulus ol > pl; intercumulus di)
4 Olivine gabbro   (cumulus pl > ol = di)
5 Leuco olivine gabbro (cumulus pl ≫ ol = di).

Table 5 (Continued)

Sample No.	6 MA168	7 X268	8 MA65	9 X265	10 MA47
SiO_2	48.41	50.07	46.37	49.33	47.05
TiO_2	0.20	0.16	0.18	0.30	0.21
Al_2O_3	14.41	28.22	17.18	18.15	16.51
Fe_2O_3*	0.48	0.20	0.59	0.48	0.52
FeO	3.18	1.34	3.89	3.15	3.44
MnO	n.d.	0.03	n.d.	n.d.	0.09
MgO	13.91	3.02	13.89	9.17	15.08
CaO	16.24	12.79	13.62	14.93	15.09
Na_2O	1.61	4.08	1.61	2.72	1.16
K_2O	0.03	0.22	0.09	0.18	0.06
P_2O_5	0.01	0.01	0.01	0.01	0.01
TOTAL	98.48	100.14	97.43	98.42	99.22
Ni	191	41	237	102	283
Cr	692	42	705	691	1063
Zn	18	7	24	19	13
Ga	13	23	14	16	12
Rb	-1	1	-1	1	-1
Sr	333	360	175	356	124
Y	5	2	3	5	4
Zr	12	25	8	12	18
Nb	-1	-1	-1	-1	3
Ba	17	42	16	33	12
La	-2	3	-2	-2	2
Ce	-3	3	-3	3	4
Pb	3	-3	-3	3	-3

Note: * Iron allocated so that FE2O3/FEO = 0.15

    -2 = below lower limit of detection.

    n.d = not determined.

6 Clinopyroxene gabbro   (pl, di)

7 Clinopyroxene leucogabbro   (pl ≫ di)

8 Clinopyroxene gabbro   (pl, di)

9 Clinopyroxene gabbro   (pl, di)

10 Clinopyroxene gabbro   (pl, di).

Table 6 : Representative analyses of the Masirah "upper massive gabbro" unit

Sample No.	1 MA238	2 MA47	3 MA205	4 X186	5 MA164
SiO_2	48.53	47.05	49.09	47.39	50.39
TiO_2	0.22	0.21	0.25	0.41	0.45
Al_2O_3	16.82	16.51	20.90	16.99	20.16
Fe_2O_3	0.45	0.52	0.52	0.65	0.53
FeO	2.94	3.44	3.43	4.31	3.52
MnO	0.07	0.09	0.00	0.10	0.07
MgO	12.19	15.08	7.24	11.31	5.68
CaO	15.56	15.09	11.14	14.69	12.45
Na_2O	1.89	1.16	3.89	1.65	3.80
K_2O	0.08	0.06	0.28	0.11	0.08
P_2O_5	0.01	0.01	0.02	0.01	0.02
TOTAL	98.76	99.22	96.76	97.72	97.15
Ni	180	283	70	123	40
Cr	909	1063	355	242	51
Zn	21	13	9	27	20
Ga	15	12	15	14	20
Rb	1	-1	2	1	-1
Sr	169	124	213	275	294
Y	5	4	3	7	4
Zr	14	18	19	32	28
Nb	-1	3	4	6	5
Ba	24	12	41	65	33
La	2	2	-2	2	2
Ce	3	4	-3	4	4
Pb	-3	-3	-3	3	-3
Th	-3	-3	-3	-3	-3

1-4 Clinopyroxene gabbros; screens to dolerite dykes.

5 Pegmatitic clinopyroxene gabbro.

Table 6 (Continued)

Sample No.	6 MA323	7 MA124	8 X106A	9 MA417	10 X308
SiO_2	48.86	45.83	57.13	59.01	72.12
TiO_2	0.66	5.68	0.16	0.55	0.20
Al_2O_3	18.80	11.41	22.91	18.77	14.82
Fe_2O_3	0.81	1.25	0.99	2.87	0.91
FeO	5.31	8.23	0.00	0.00	0.00
MnO	0.12	0.00	0.02	0.00	0.00
MgO	8.46	8.11	3.03	1.80	10.54
CaO	13.34	16.61	5.44	4.04	2.25
Na_2O	2.07	0.99	7.44	9.97	7.10
K_2O	0.13	0.05	1.11	0.05	0.80
P_2O_5	0.05	0.02	0.02	0.10	0.03
TOTAL	98.61	98.18	98.25	97.46	98.77
Ni	80	36	14	5	1
Cr	268	18	8	-1	2
Zn	20	29	69	4	3
Ga	17	18	26	24	14
Rb	-1	-1	1	-1	14
Sr	119	243	408	183	139
Y	16	28	57	57	54
Zr	42	56	745	711	88
Nb	3	18	118	52	34
Ba	21	93	316	87	281
La	3	5	29	44	53
Ce	6	6	68	88	86
Pb	4	6	-3	-3	-3
Th	-3	-3	-3	17	27

6 Pegmatitic clinopyroxene gabbro.

7 Clinopyroxene gabbro (with Fe - Ti ore $\sim$ 10 modal %).

8 Clinopyroxene gabbro; screen to dolerite dykes.

9 Plagioclase - epidote, meta-tonalite, screen to dolerite dykes.

10 Quartz-plagioclase-amphibole trondhjemite, screen to dolerite dykes.

Table 7 : **Representative analyses of minor intrusions of the mantle serpentinites (1-4) and of the ultramafic cumulates.**

	1 MA132	2 MA127	3 X217	-3 X205	4 MA413	5 MA75
SiO_2	45.54	49.09	46.91	44.50	44.28	43.56
TiO_2	0.10	0.41	1.83	2.83	0.90	0.89
Al_2O_3	26.92	13.27	15.52	13.03	14.47	11.32
Fe_2O_3	1.54	6.03	5.92	12.22	8.37	11.96
MnO	0.04	0.12	n.d.	n.d.	n.d.	n.d.
MgO	5.90	12.57	11.26	8.15	13.85	13.42
CaO	14.25	13.62	11.30	9.92	13.28	13.74
Na_2O	2.82	2.24	3.80	4.28	1.19	1.15
K_2O	0.06	0.09	0.16	0.39	0.11	0.04
P_2O_5	0.00	0.01	0.54	1.44	0.13	0.05
TOTAL	97.17	97.45	97.23	96.77	95.81	96.13
Cr	57	152	70	8	576	414
Ni	102	728	166	77	266	365
Zr	17	17	31	82	50	66
Ga	18	14	27	25	15	13
Rb	-1	-1	-1	4	-1	-1
Sr	261	213	328	244	291	94
Y	-2	10	100	117	18	22
Zr	15	27	100	172	82	51
Nb	1	2	25	68	8	2
Ba	19	32	100	244	38	25
La	-2	2	11	49	3	2
Ce	-3	3	40	117	11	5
Pb	-3	-3	3	6	3	4
Th	-3	-3	-3	-3	-3	-3

Note: n.d. = not determined; -3 = below lower limit of detection (= 3 ppm)

1 Coarse anorthositic gabbro
2 Pyroxene gabbro
3 Pegmatitic pyroxene gabbro
4 Dolerite dyke
5 Dolerite dyke cutting ultramafic cumulates.
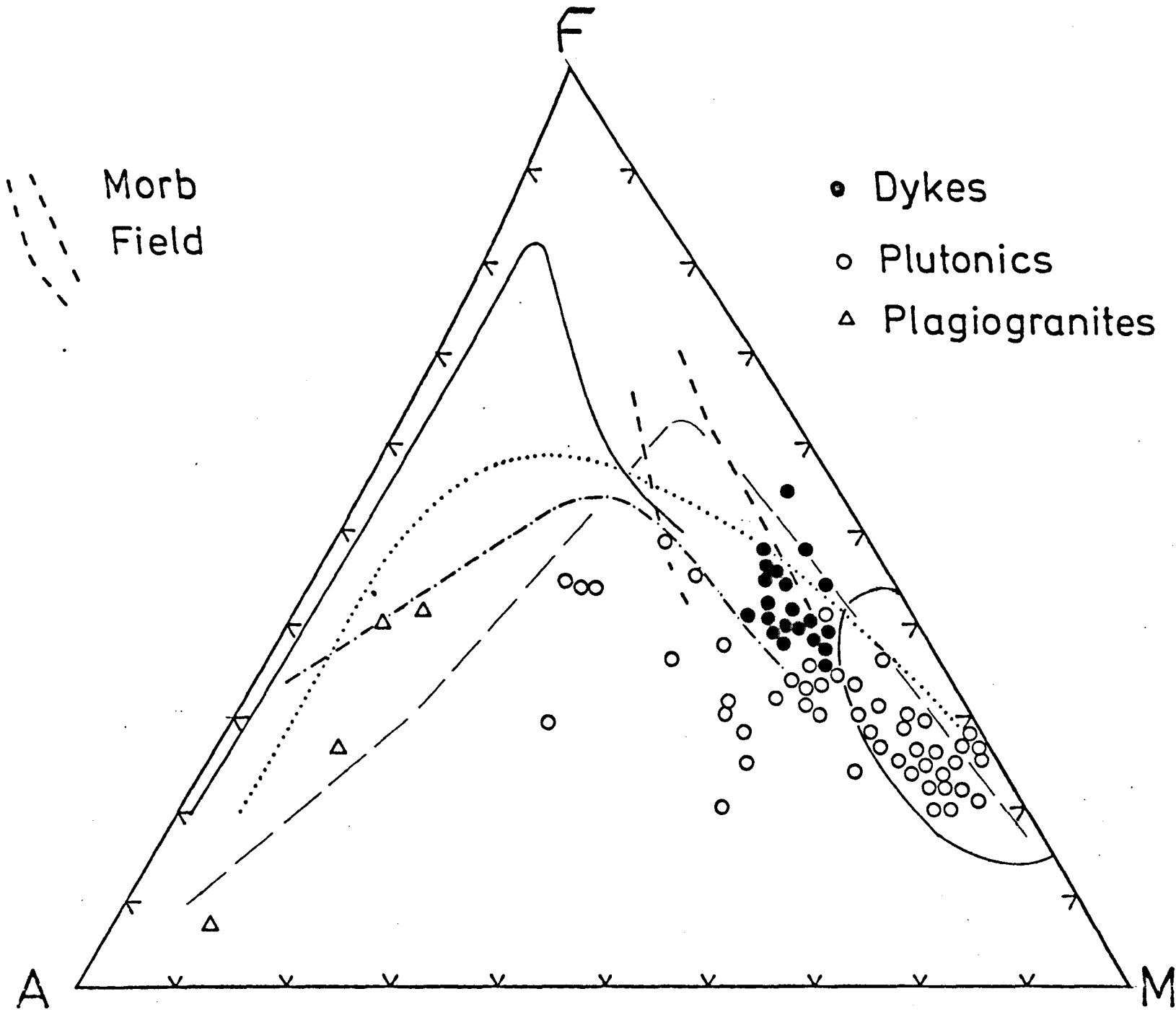
FIG.12. A (NA$_2$O + K$_2$O) - F(FEOT) - M(MGO) diagram for Masirah plutonic rocks. Dashed-dotted line separates the tholeiitic and calc-alkaline fields of Irvine and Baragar (1971). Solid line is the Skaergaard trend (Wager and Brown, 1967). Dotted line is the Troodos plutonic trend (Allen, 1975). Dashed line is a visual best fit for limited Semail data (Allemann and Peters, 1972). Dashed field = ocean tholeiites (Saunders et al, 1978). Solid field = ophiolite cumulates (Coleman, 1977).

dividing line of Irvine and Baragar (1971). The dykes appear to represent the more Fe-rich liquids from which the plutonics crystallised (Abbotts, 1978b) and dominantly fall in the ocean tholeiite field. Together with most of the cumulates they define a mild tholeiitic trend of Fe-enrichment. However it is apparent that the differentiated tonalites and trondhjemites have calc-alkaline affinities. The Troodos trend is somewhat similar to that of Masirah, though showing more Fe-enrichment. This again reflects the plagioclase-rich nature of the Masirah gabbros.

Church and Riccio (1977) used cumulus phase compositions and their known $K_D^{sol/liq}$ values to calculate features of the magma chamber liquids from which the gabbros crystallised. This procedure was followed elsewhere for the Masirah samples (Abbotts, 1978b). The results are summarized in Fig.13 which plots olivine and clinopyroxene FeO/MgO ratios against their liquid FeO/MgO ratio derived using the partition coefficients of Roeder and Emslie (1970). The main conclusion is that the dykes (FeO/MgO = 0.73-1.28) are roughly equivalent to the liquids from which the earlier cumulates crystallised. The validity of the data seems confirmed when the FeO/MgO ratio derived from the dyke clinopyroxene phenocrysts agrees with the whole-rock values (Fig.13). The complete separation of the plutonics and dykes on the AFM diagram is thus partly explained by the plutonics comprising cumulate minerals with lower FeO/MgO ratios than their liquids.

FIG.13. Diagram reproduced from Abbotts (1978b) and after Church and Riccio (1977). The figure illustrates the range in FeO/MgO weight ratio of the liquids from which the Masirah plutonic rocks crystallised, compared with the FeO/MgO range of the Masirah dykes. Note: (1) the FeO/MgO liquid ratios were calculated assuming K_D ol-liq = 0.3 (Roeder and Emslie, 1970);

(2) K_D cpx-liq value of 0.24 is estimated using the FeO/MgO ratio of the liquids calculated from the composition of the coexisting olivine and shows good agreement with the work of Church and Riccio (op.cit); (3) the iron to magnesium ratio in the dykes is given as FeO (total iron)/MgO and is therefore a maximum value.
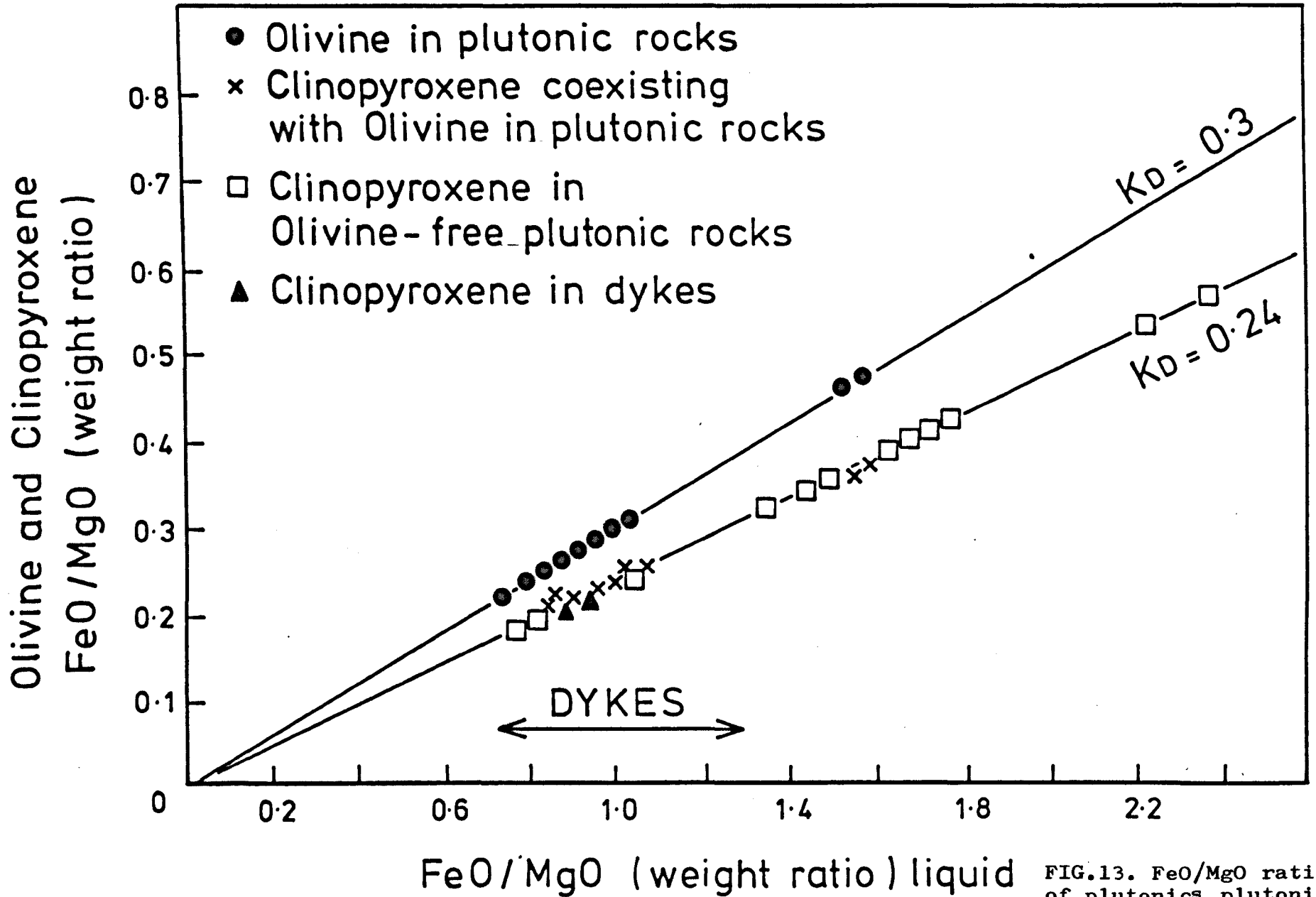
FIG.13. FeO/MgO ratios of plutonics, plutonic liquids, and dykes.

(ii) Major element variation with fractionation

Major element oxide variation is illustrated in Fig.14 by plotting against the Fe (total iron)/Mg index. This index is preferred for these cumulate rocks because (i) the K_D MG-FE sol/liq is somewhat similar for both olivine and clinopyroxene, and (ii) an incompatible trace element would measure the amount of trapped intercumulus liquid.

The plots of MgO, Fe_2O_3, Al_2O_3, CaO and SiO_2 show extensive scatter at low Fe/Mg levels because of the extreme ol:pl modal variability in the early layered cumulates. Within the massive gabbro unit the more fractionated samples are the pegmatites, tonalites and trondhjemites; the less fractionated are the gabbro screens to the sheeted dykes.

SiO_2 increases only slowly with fractionation and the rocks plot largely in the tholeiitic field of Miyashiro (1973), though close to the calc-alkali-tholeiite boundary. Over 90% of the Masirah plutonics fall in the SiO_2 range of 48-51% indicating a typical tholeiitic trait of limited SiO_2 enrichment. There is then extreme scatter in the more fractionated samples with SiO_2 ranging over 44-72%.

TiO_2 shows a linear correlation to Fe/Mg $\sim$ 1.25 but then shows a sharp increase followed by an even more pronounced decrease to the trondhjemite. Total iron $\left(Fe_2O_3\right)$ shows similar though less pronounced behaviour, after the initial scatter is passed. These characteristics suggest that precipitation of an Fe-Ti oxide caused the trend of SiO_2 enrichment. The Fe-Ti effect and the limited proportion of rocks involved are evident
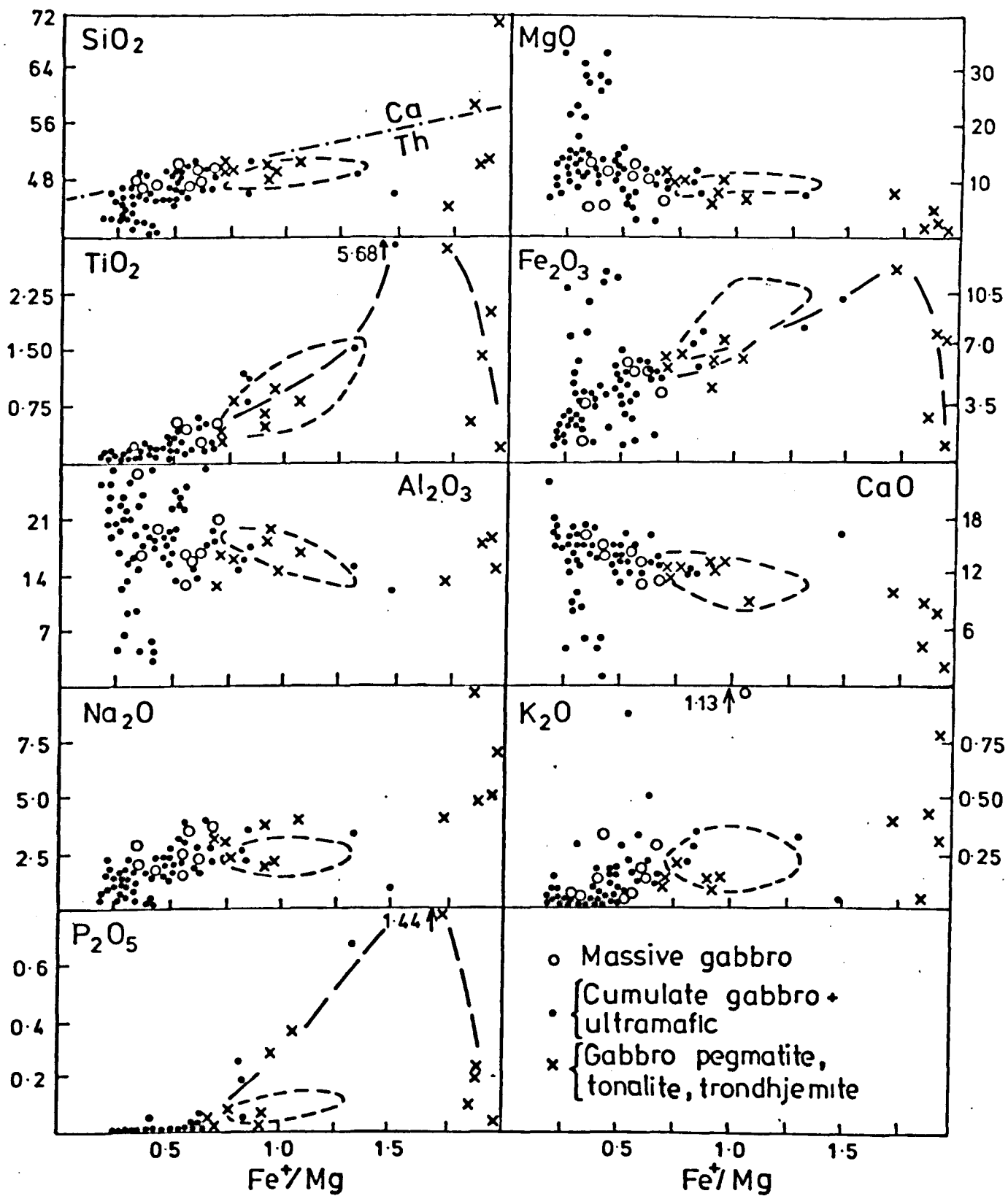
FIG.14. Major oxide variation against Fe*(total iron)/Mg.
Dotted-dashed line on SiO_2 plot from Miyashiro (1973).
Dashed fields enclose Masirah dykes. Dashed lines on TiO_2,
t Fe_2O_3(total iron) and P_2O_5 are visual best-fit trends.

in Fig.15B. Here TiO_2 is seen to correlate more convincingly with tFe_2O_3, than it did with Fe/Mg, reflecting their co-precipitation. The initial gradual increase in TiO_2 reflects increasing incorporation in the clinopyroxene phase (Fig.9). The extremely rapid increase of Ti as the opaque phase precipitates is obvious. The TiO_2-Y plot (Fig.15A.) shows good positive correlation except in the exceptionally high TiO_2 rock. This probably reflects their similar degree of incompatibility before and after opaque precipitation.

Al_2O_3 shows little variation after the initial scatter. The late decrease in CaO and concomitant increase in Na_2O, in rocks with a fairly constant proportion of normative felspar (60-75%), reflects the more sodic plagioclase in the late tonalite-trondhjemites. For a liquid crystallising olivine in the system Fo-An-Di, if plagioclase is to precede clino- pyroxene a liquid CaO/CaO + Al_2O_3 < 0.5 is required (Osborn and Tait, 1952). The comparable value for An60 is < 0.43 (Irvine, 1970). The Masirah plutonics followed an ol-pl-cpx crystallisation sequence; the dykes-lavas suggest the same in their phenocryst relationships. In contrast in the Troodos plutonics clinopyroxene preceded plagioclase (Allen, 1975). Major element mobility in the dykes-lavas precludes knowledge of the original liquid Ca-Al values but the Ca:Al ratio appears to have been lower in the Masirah liquid, relative to Troodos.

MgO varies widely in the initial stages but then remains relatively constant before a rapid decrease to the trondhjemite. Fe_2O_3 shows a tholeiitic trend of enrichment until ore mineral precipitation. The higher dyke levels reflect both their
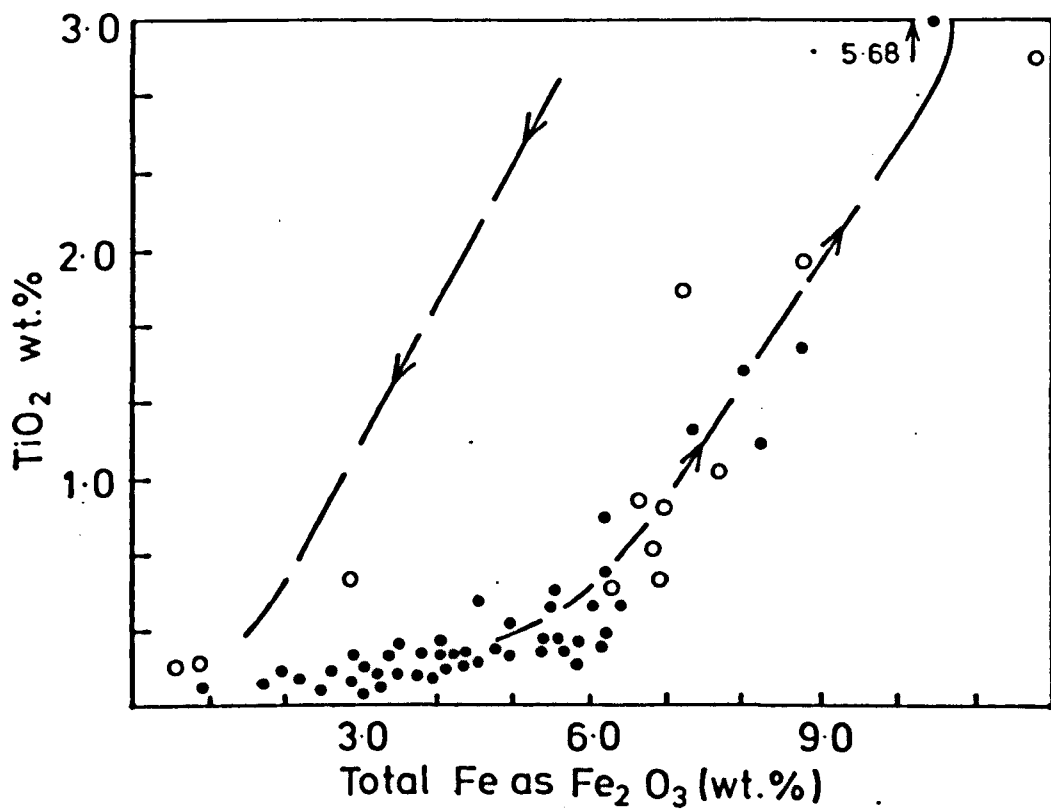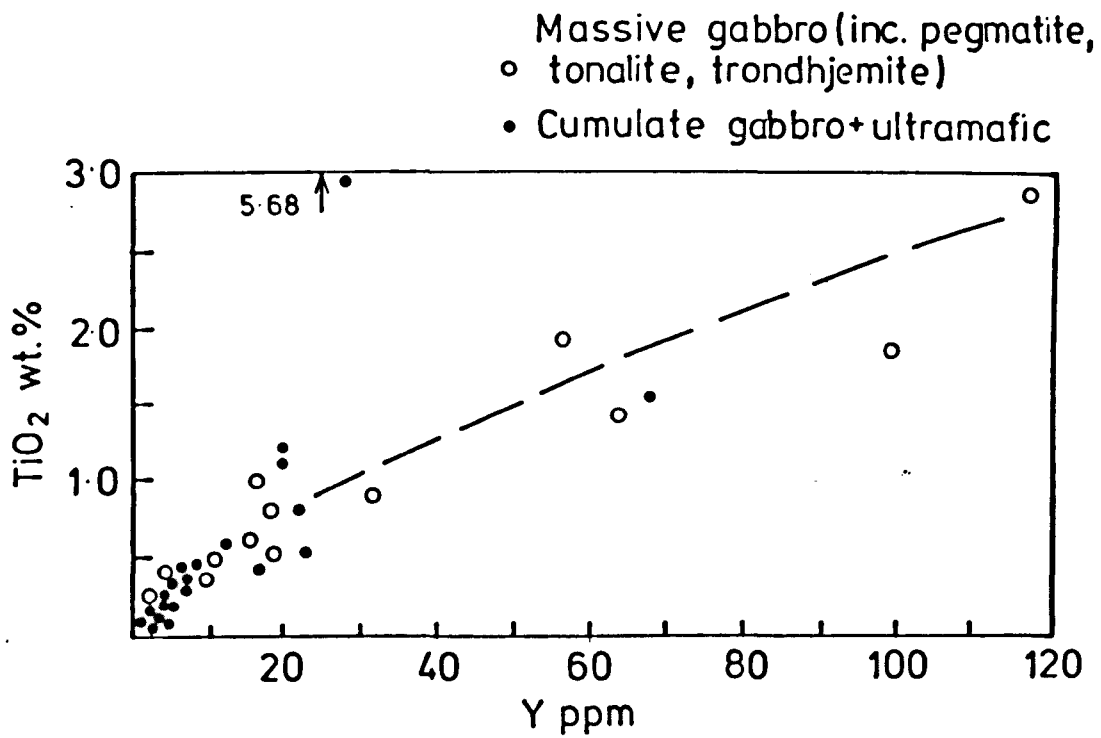
FIG.15. TiO$_2$ behaviour in the Masirah plutonic rocks shown by plotting against Y and against total iron. The dashed lines are visual best-fits for the differentiation trends.

higher cpx:pl content and their non-cumulate nature.

Fractional crystallisation involves strong K_2O enrichment from 0.01-0.02% to 0.80% in the trondhjemite. Although there is significant scatter, suggesting both hydrothermal enrichment and depletion, the suite is largely characterised by the low K_2O (< 0.25%) and high Na/K of ocean floor tholeiites. P_2O_5 behaves similarly to TiO_2. Most cumulates contain < 0.02% but rapid enrichment to 1.44% then occurs and apatite precipitates. Subsequent to this event the concentration falls even more rapidly to low trondhjemite levels.

(iii) Normative characteristics

Normative characteristics of the plutonics are illustrated in the Ne-Ol-Di-En-Q_3 diagram (Fig.16) and the normative felspar plot (Fig.17). In Fig.16 most of the cumulates contain minor normative Ne and plot near the Di-Ol join. Scatter along the join is due to modal variability. High Ne contents correspond to anorthositic gabbros (e.g. Table 5 : X268) and the Ne-normative character reflects the plagioclase dominance of the sequence (Fig.4). The more fractionated rocks show a trend of olivine depletion through the field of silica-saturation and then of increasing over saturation toward the Q_3 apex. The felspar diagram illustrates the low K_2O contents and the trend from pyroxene gabbros, with calcic plagioclase, to sodium-rich trondhjemites.
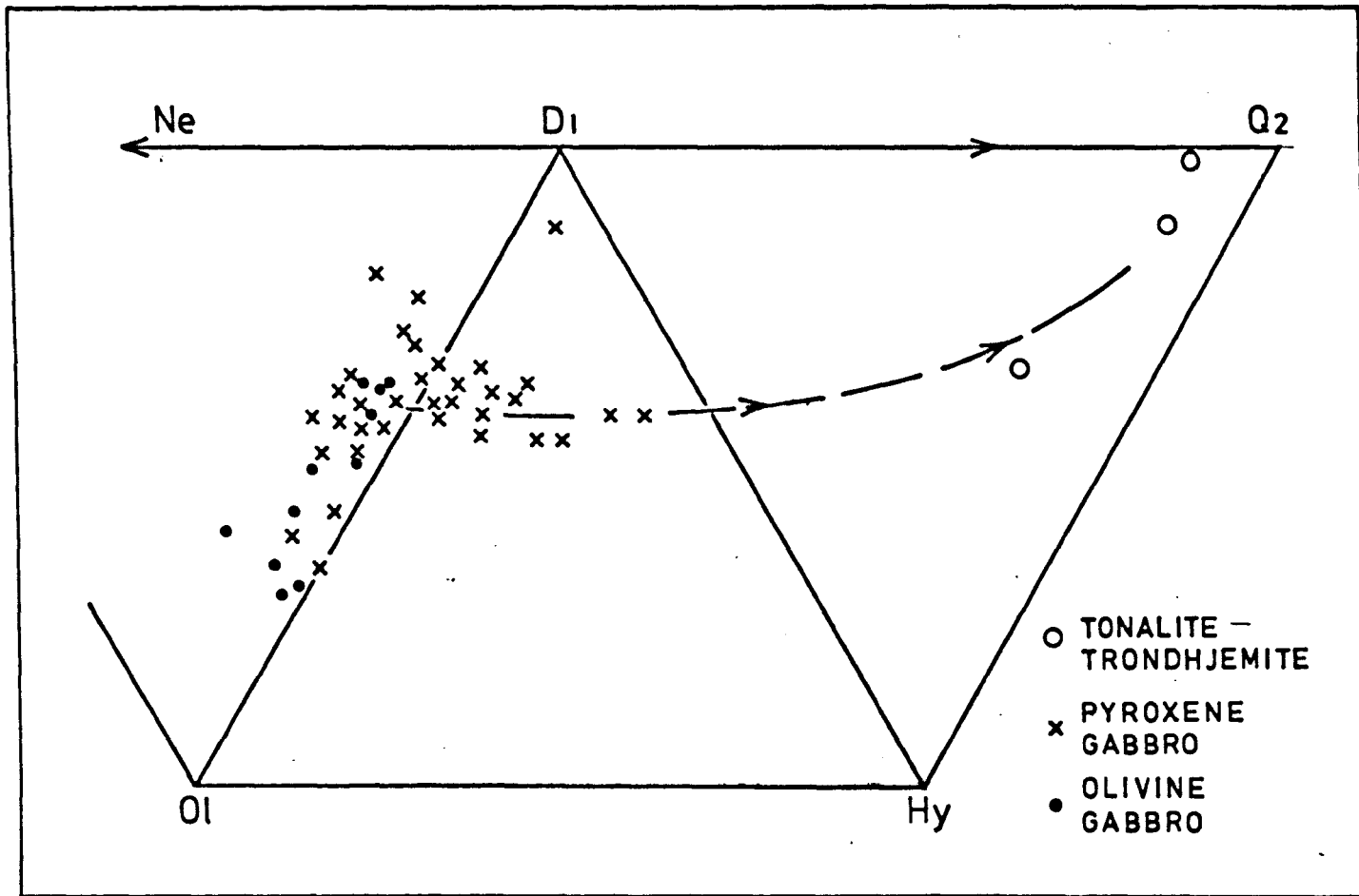
FIG.16. Normative Ne-Di-Ol-H_y-Q_z plot for Masirah gabbros. The dashed line indicates the trend to the tonalite-trondhjemite rocks.

An

- PYROXENE GABBRO
- GABBRO PEGMATITE } <52%
+ DIFFERENTIATED .PLUTONIC >52%

SiO2

Tonalite
Adamellite

Trondhjemite

Granite

Ab

Or
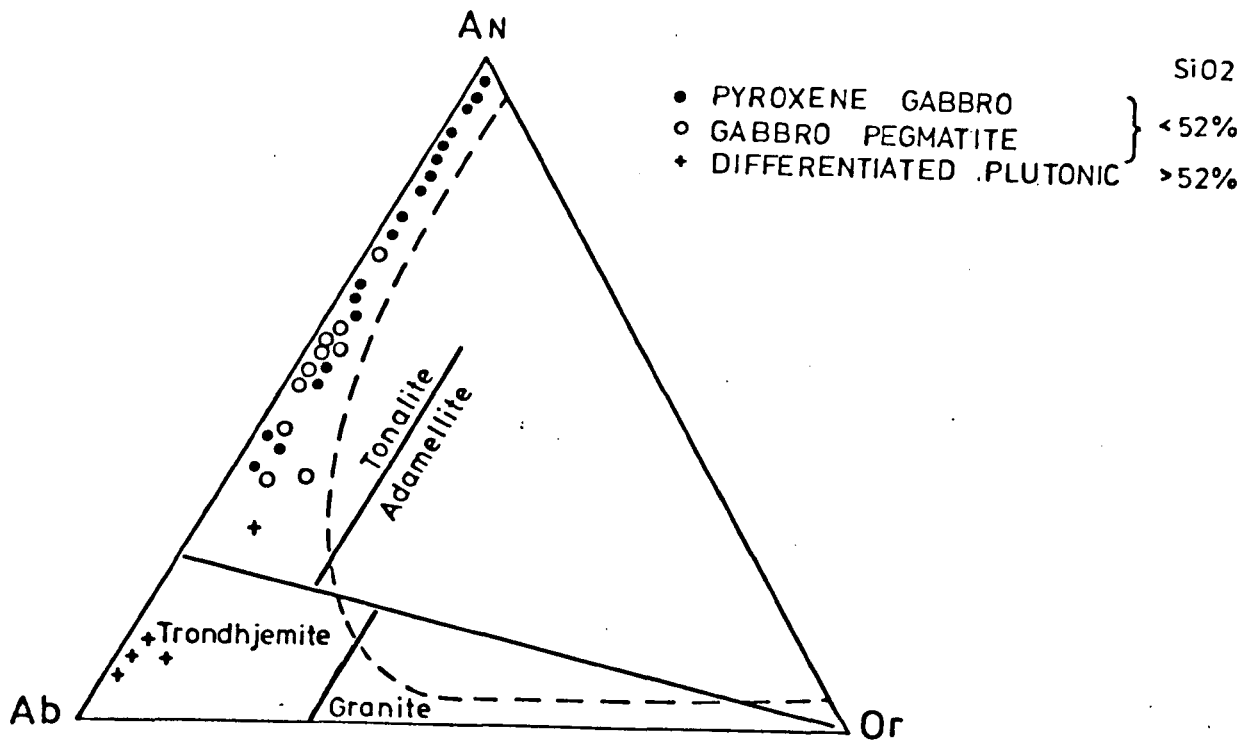
FIG.17. Triangular diagram of normative Ab-An-Or for
various Masirah gabbros. Below and to the left of the
dashed line is the low pressure felspar field (< 5 kbar).
The continuous lines separating various rock types are
taken from O'Connor (1965).

8C. Trace element chemistry

The more informative trace elements in the Masirah

sequence are plotted against Fe/Mg in Fig.18. Sr, Ni and Cr

show a wide variation in abundance in the early cumulates

because of their respective compatibilities for the plagioclase

$(K_{D_{SR}}^{PL/LIQ} > 1)$, olivine $(K_{D_{Ni}}^{OL/LIQ} \gg 1)$ and clinopyroxene

$(K_{D_{Cr}}^{CPX/LIQ} \gg 1)$ phases.

Zr shows a trend of strong enrichment to 700-800 ppm

after initial low levels (< 25 ppm) in most of the cumulates.

The element has a very low bulk distribution coefficient in

basaltic systems (Weaver et al, 1978) and consequently its

abundance in cumulate rocks is largely dictated by the amount

of trapped intercumulus liquid. The low levels of Zr, and

similarly of Ce, Y and Nb suggest only small amounts of
                                   and
trapped intercumulus liquid/give further indication of

adcumulate crystal growth. The extreme Zr enrichment into the

tonalites suggests concentration by near complete magma

crystallisation and these rocks probably approximate to residual

liquids in the manner that Wager and Brown (1967) treated the

Skaergaard melagranophyres. The trondhjemite which represents

the terminal stage of differentiation (Table 5 : X308) has a

Zr content of only 88 ppm. This value suggests zircon

precipitation at 700-800 ppm to deplete the final liquids.

Cumulus zircon was, in fact, seen in one tonalite which was

unfortunately not analysed.

FIG.18. (overleaf) Trace element variation
against Fe*(total iron)/Mg. Dashed fields
enclose Masirah dykes. Dotted-dashed lines on
Zr, Y, are visual best-fit trends.
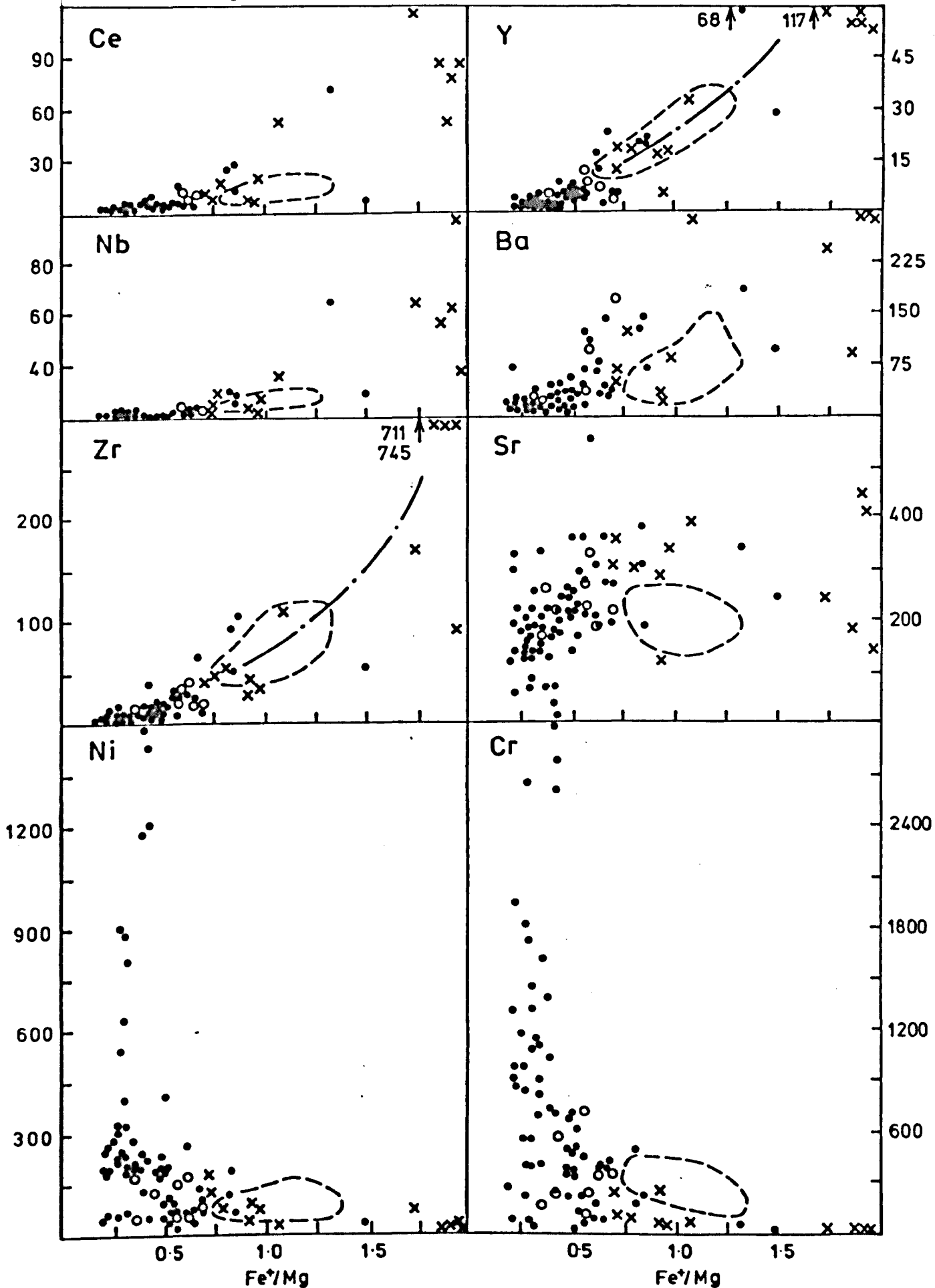
FIG. 18. Trace element variation in the Masirah gabbros.

Y shows a good linear positive correlation except for two high Y rocks which were found to contain cumulus apatite (P_2O_5 0.68-1.44%). The Y-apatite link is explained by the strong HREE (+Y) partitioning of the apatite phase.

Ba shows a weak positive correlation but with significant scatter. This incompatible element is commonly mobile at moderate grades of metamorphism (Tarney et al, 1978). The scatter appears to reflect mobility in the upper cumulate and massive gabbros into which the hydrothermal system penetrated.

Subject to the modal control noted before, Sr increases initially to ~ 400 ppm (Fe/Mg = 1.0) but then decreases smoothly into the late differentiates. This behaviour probably reflects preferential Sr entry into the more sodic plagioclase compositions causing melt depletion.

Ni and Cr show rapid early depletion of the melt by the olivine-chromite-chrome diopside phases. The olivine domination of the early cumulates is reflected in the more rapid Ni depletion. The Ni v Cr plot of Fig.19 illustrates the strong mineralogical control of the olivine and diopside cumulus phases on the elemental levels. The inset figure, taken from Abbotts (1978e), incorporates the "alpine peridotite" (= depleted mantle) - "stratiform complex" (≡ cumulates) discriminator of Irvine and Findlay (1972). The separation of the Masirah mantle serpentinites and the cumulus sequence reflects Ni-Cr retention in the mantle.

The stratigraphic section in Fig.20 illustrates in schematic fashion many of the geochemical characteristics of
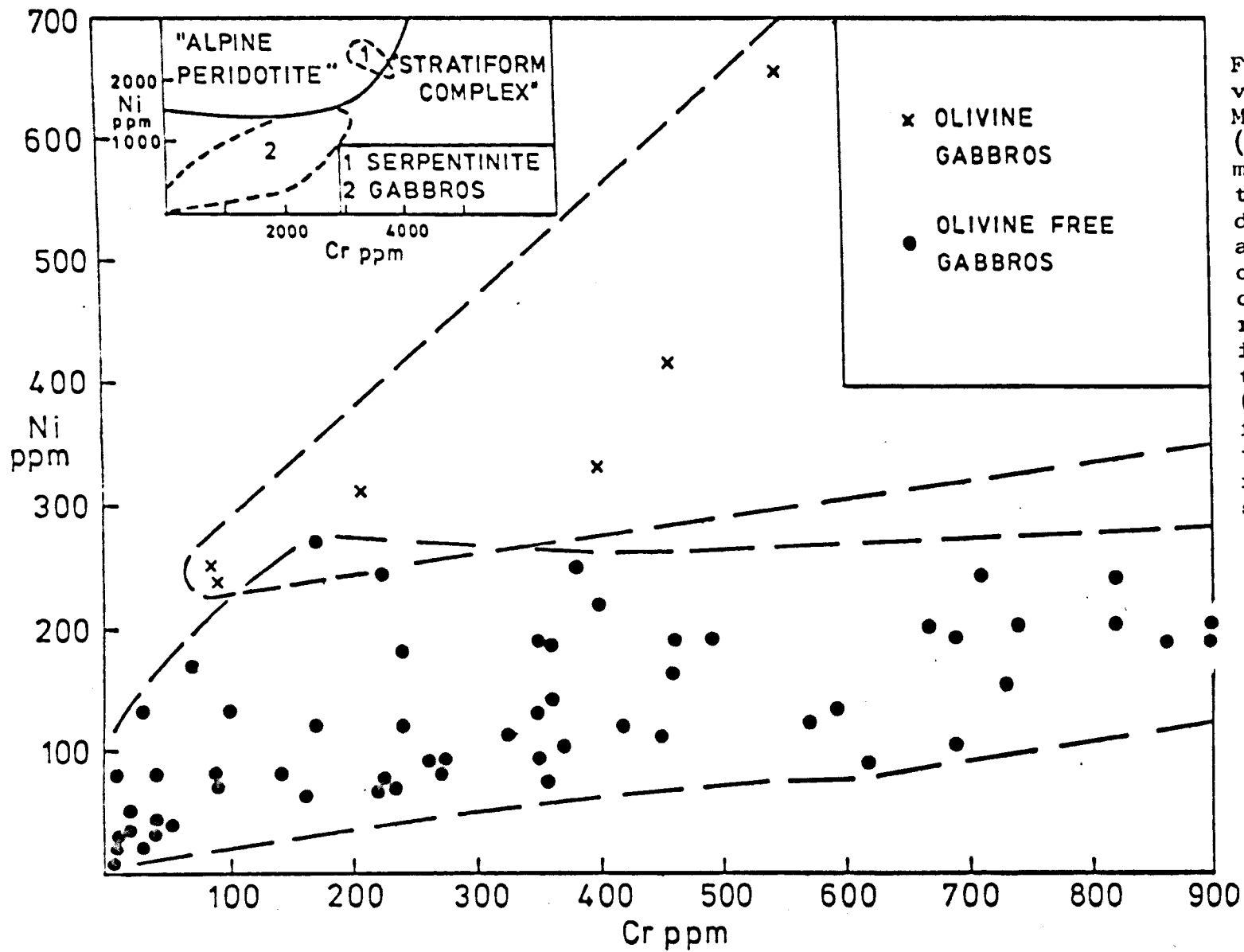
FIG.19. Ni v Cr variation in the Masirah gabbros (excluding the ultramafic dunites and troctolites). The dashed fields enclose all analyses of olivine gabbros and olivine-free gabbros respectively. The inset figure is taken from Abbotts (1978e) and shows the fields of (1) all of the Masirah plutonic rocks, (2) the Masirah serpentinites.

FIG.20. (overleaf) A schematic illustration of
the geochemical variation through the Masirah
Ophiolite. Within the rock-units the samples
are ordered by increasing upward Fe*/Mg. The
schematic nature of the diagram takes no account
of the extensive overlap of some units (e.g. dykes
and massive gabbros) and does not show that the
tonalites-trondhjemites are found at different
levels in the massive gabbro unit.
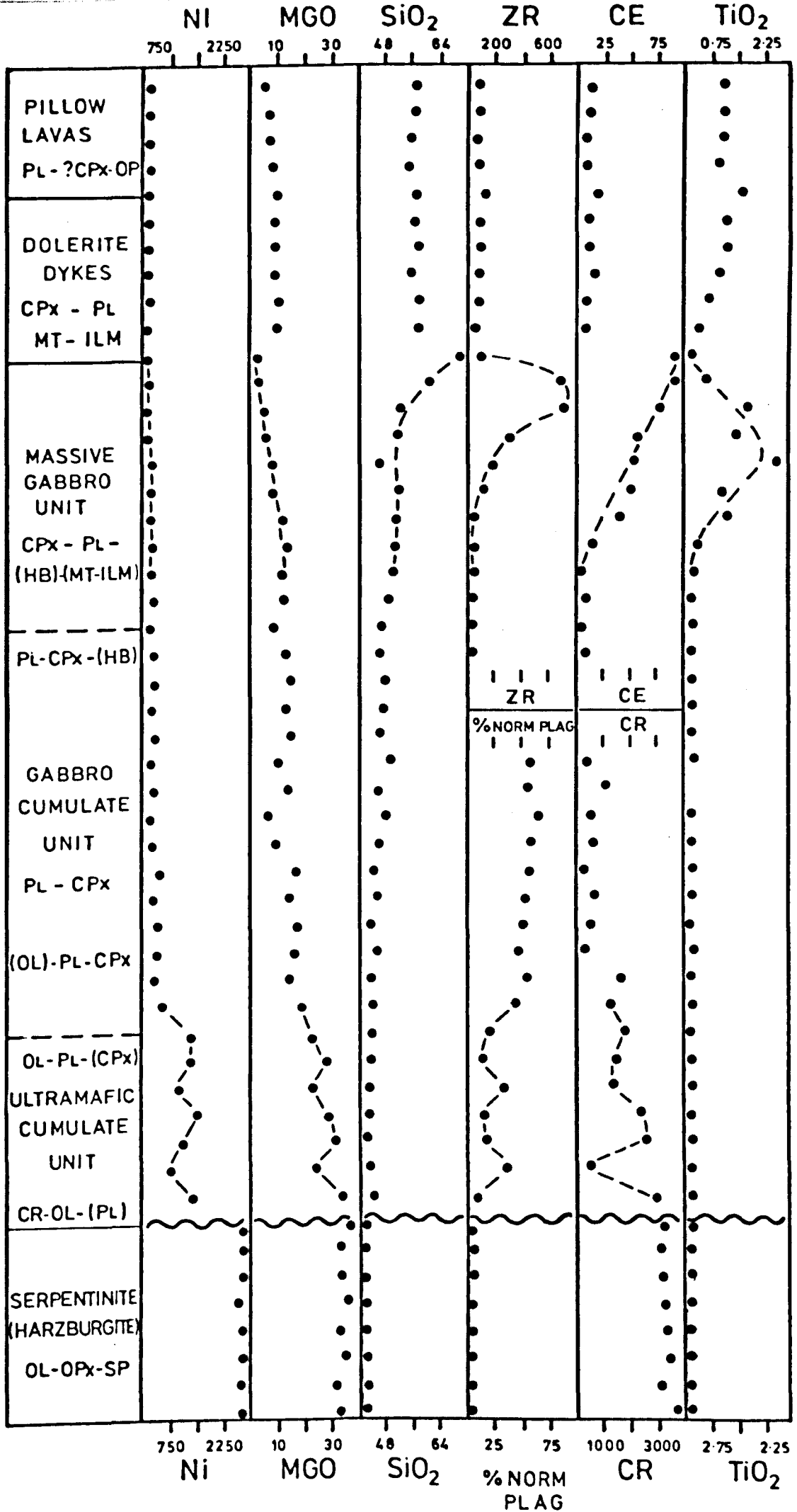
FIG.20. Geochemical variation through the Masirah Ophiolite.

these rocks. Points to note include: (i) the clear discontinuity of the serpentinites and the overlying ultramafic unit. The serpentinites are shown elsewhere to represent mantle harzburgite depleted by basalt extraction (Abbotts, 1978e); (ii) the wide chemical variability in the early ultramafic cumulates caused by the strong layering in these rocks; (iii) the increasing homogeneity of the cumulate gabbros, as layering becomes less important; (iv) the extreme differentiation achieved within the massive gabbro unit and the precipitation of an Fe-Ti opaque phase and then zircon, when Ti and Zr reach saturation levels.

8D. Rare-earth element chemistry

REE data for three Masirah plutonic rocks and one metadolerite dyke are presented in Table 8 and Fig.21. The plutonics have Fe/Mg ratios of 0.56 (X186), 0.77 (X11) and 1.93 (X106) and represent the middle to late stages of fraction-ation. The sub-parallel patterns of plutonics and dyke support the field evidence of origin in the same magma chamber(s). They demonstrate simple characteristics of (i) moderate LREE enrichment (CeN/YbN = 2.2-3.6) and (ii) increasing total REE's and LREE enrichment with increasing Fe/Mg or Zr (Table 8).

In a qualitative manner the development of these characteristics during gabbro fractional crystallisation is simple to explain. The fractionating phases in the middle-late stages of crystallisation were pl, cpx and minor hb. The LREE's are preferentially incorporated into plagioclase, though

Table 8 : REE data on selected Masirah plutonics (P) and dykes (D)

Sample No.	La*	Ce	Nd	Sm	Eu	Tb	Yb	Lu	Y*	CeN/YbN	Fe/Mg	Zr
X186 (P)	2.1	6.22	2.84	1.04	0.27	0.18	0.73	0.18	7	2.2	0.56	11
X11 (P)	6.4	17.1	11.8	2.99	1.13	0.51	1.80	0.32	18	2.4	0.77	53
MA183 (D)	7.2	17.2	12.6	3.52	1.23	0.54	1.92	0.34	25	2.3	0.87	115
X106 (P)	-	67.5	39.6	8.42	3.41	1.76	4.96	1.19	57	3.6	1.93	745
X219 (D)	-	146.4	73.6	12.5	4.17	2.46	8.13	0.80	59	4.7	4.45	784
BOB1[1]	-	18.3	12.4	3.1	1.16	0.66	2.62	0.41				
BOB1[2]	5.8	18.5	11.1	3.3	1.25	0.60	2.87	0.38				

Concentrations in ppm

BOB1[1] calculated as unknown

* XRF analysis, all others INAA

BOB1[2] standard analysis.
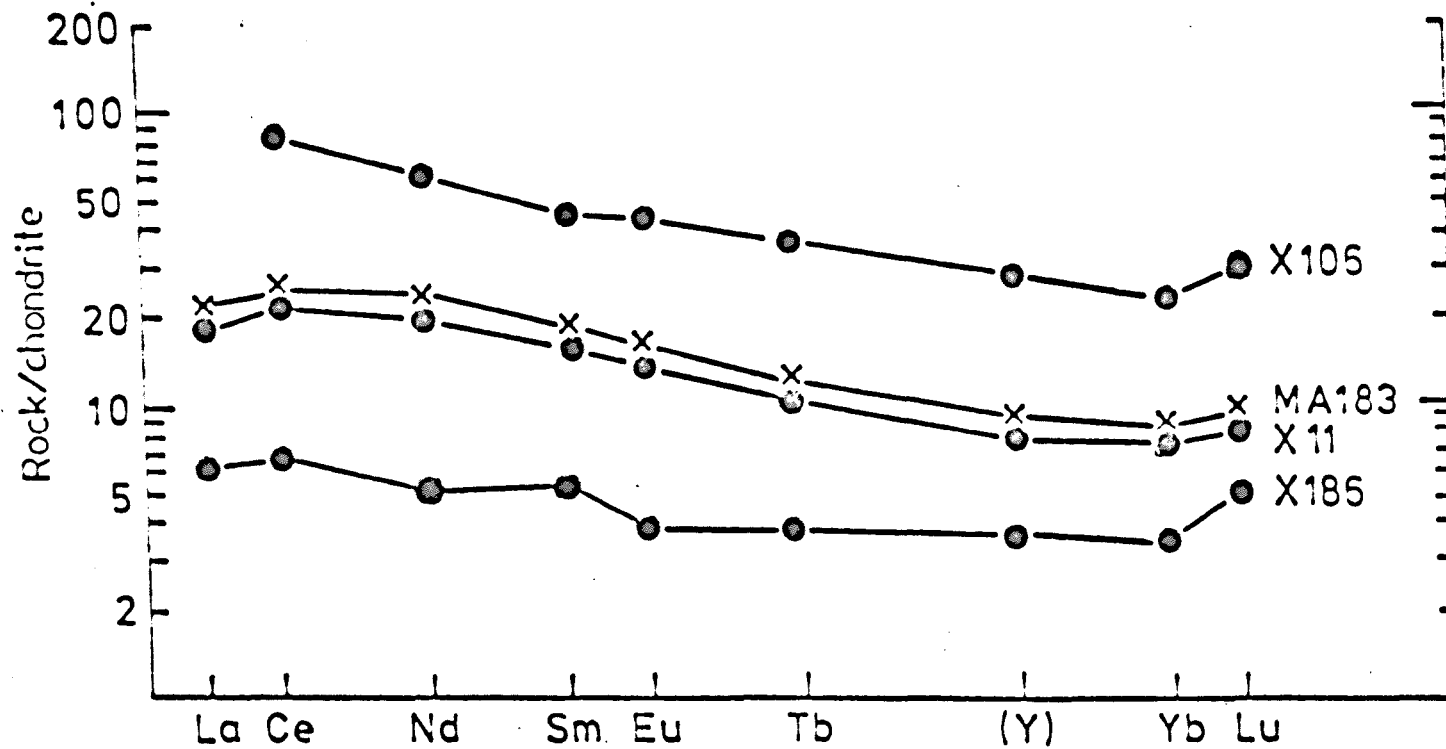
FIG.21. Chondrite-normalised REE patterns of Masirah plutonic rocks compared with the dyke MA183 (Zr = 115 ppm). The plutonic samples represent various stages of fractionation: X186 (Zr = 11 ppm), X11 (Zr = 53 ppm); X106 (Zr = 745 ppm);

all partition coefficients are $\ll 1$, whereas clinopyroxene and hornblende more effectively partition the HREE's (e.g. $K_D{}^{CPX/LIQ}{}_{Yb} = 0.28$). Thus crystallisation of the 3 phases will enrich the liquid in all REE's while the more effective cpx-hb fractionation of the HREE's will lead to an increasing LREE enrichment.

To test this hypothesis semi-quantitative modelling of the fractional crystallisation patterns has been attempted (Table 9, Fig.22) assuming Raleigh fractionation (surface equilibrium crystallisation). The model requires a LREE-enriched initial melt because the type, and proportions, of the crystallising phases could not produce the patterns from a flat or LREE-depleted magma. An initial melt was chosen (Table 9) with comparable characteristics to the most primitive (high Ni and Cr, low Zr) dyke which possessed LREE enrichment. The latter was assessed using the CeN/YN ratios of the dykes (c.f. Saunders et al, 1978). It is evident from the reasonable success of the modelling in Fig.22 that the observed REE patterns can be produced by fractionation of the phases present in the Masirah cumulates from a liquid of comparable composition to the more primitive, but LREE-enriched, Masirah dykes.

The initial melt required by the model and in evidence in dykes of the sheeted dyke complex has a pattern of LREE enrichment (CeN/YN $\sim$ 1.5) at rather low REE levels (CeN $\sim$ 14). Constraint of the source, and degree of melting, involved in production of this melt is hampered by (i) the lack of exposure of undepleted mantle and (ii) poor control of the REE levels in the undepleted mantle beneath spreading centres.

Table 9 : REE fractional crystallisation model for Masirah plutonic samples

Sample No.	X186			X11			X106		
Modal composition (Pl:Cpx)	60:40			55:45			70:30		
Estimated bulk composition of total preceding crystallisation (OL:PL:CPX:HB)	30:40:30:0			25:40:32.5:2.5			15:40:40:5		
Fraction of liquid remaining F(%)	28			8.5			2.0		
Measured REE	Ce	Sm	Yb	Ce	Sm	Yb	Ce	Sm	Yb
levels - Cs	7.8	5.6	3.5	21.4	16.1	8.8	84.6	45.3	23.8
Model REE levels - Cs[1]	7.9	5.6	3.1	21.4	16.2	9.5	83.6	46.9	23.1

All values chondrite-normalised. Model uses initial melt of Ce 14.5 Sm 11.0 Yb 7.5 (see text). Partition coefficients from Hanson (1977), supplemented by Leeman (1976) and Drake and Weill (1975).
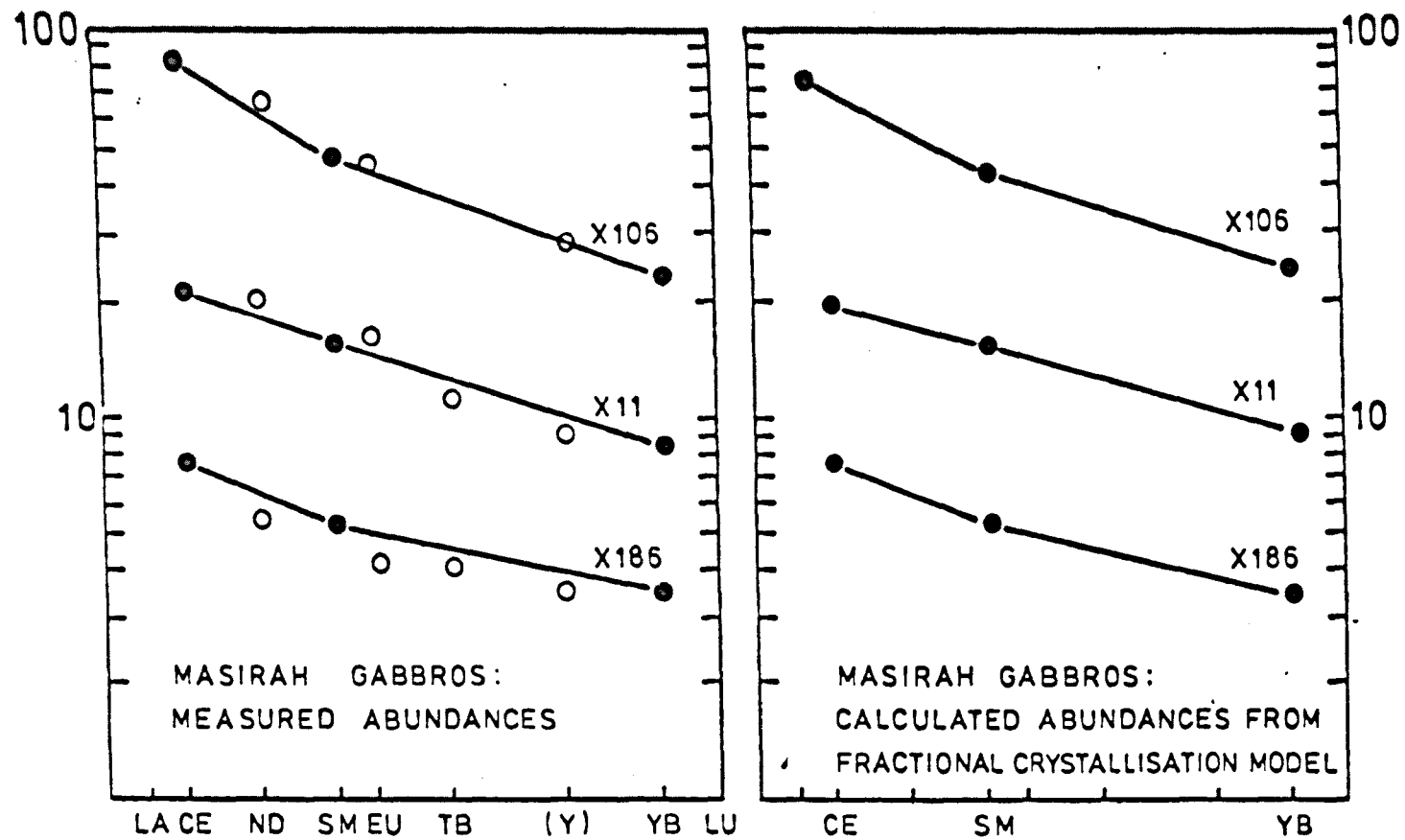
FIG.22. Measured Ce, Sm and Yb concentrations in the Masirah gabbros compared with concentrations calculated by the fractional crystallisation model described in the text.

Estimates vary from 0.6 to 2.5 x chondrite and from slightly depleted to slightly enriched patterns (Menzies et al, 1977; Malpas, 1978). If a flat or slightly LREE enriched, 2 x chondrite, source is assumed the Masirah "primary melt" can be modelled by moderate (10-15%) degrees of melting of (i) plagioclase lherzolite, provided largely plagioclase is melted (~ 70%); (ii) spinel lherzolite with approximately 25% clinopyroxene; (iii) garnet peridotite, provided the residue contains 1-2% garnet. The degree of melting reduces with the assumed source content: for example if the source is chondritic, 5-7% melting is required. Discrimination of these alternatives is difficult. Mass balance calculations assuming 5-6 km for the magmatic fraction and 15% partial melting suggest at least 28-35 km of depleted mantle. This may then suggest melting around the plagioclase lherzolite-spinel lherzolite boundary (~ 33 km).

Within the sheeted dyke complex there occur more primitive dykes than the assumed "primary melt". The "primary melt" is termed type A and the primitive dykes, type B, have characteristics of : Zr 34-51 ppm, CeN/YN 0.8-1.0, CeN~10. Additionally there are rare dykes, type C, which cut the complete cumulate sequence. These indicate late intrusion and have strongly depleted characteristics : Zr 40-50 ppm, CeN/YN 0.5-0.6, CeN ~ 6.5, Ni 300-360 ppm. The LREE enriched gabbros could not be cumulate, with the cumulus phases present, from depleted liquids such as B-C. Type B can be modelled from a 2 x chondrite, spinel lherzolite by a 20% batch melt, leaving the ol-opx residue represented by the Masirah

serpentinites. However, if the residue of partial melting
is harzburgitic the bulk $K_D^{REE/LIQ}$ of the residue is so low
that the source must have a pattern parallel to the melt.
Thus if type C was a batch melt of pristine mantle, that mantle
would have the depleted REE pattern of C. All evidence suggests
that primary lherzolite does not have such depleted patterns
(e.g. Menzies et al, 1977). Instead it is suggested that types
A, B, C are more likely to represent continued incremental
melting of a progressively more depleted mantle, as suggested in
the Troodos model of Smewing and Potts (1976). In this
explanation type C would be a later, possibly off-axis, melt
which is precisely what its field relations suggest. The main
distinction of this and the Troodos model is the smaller degree
of initial melting in evidence on Masirah to produce the LREE-
enriched "primary liquids". These contrast with the depleted
volcanics of Troodos.

9. GEOCHEMICAL IMPLICATIONS

9A. Open-system fractionation

Geochemical studies of the Masirah dykes and lavas have
revealed the low TiO_2, P_2O_5, and Zr, the high Y/Nb, and the lack
of SiO_2 enrichment, typical of tholeiitic magma. The plutonic
crystallisation sequence (Cr-Ol-Pl-Cpx) and the absence of an
increase in SiO_2 through most of the gabbros (Fig.12) suggest
that they form by low P fractionation of a tholeiite liquid.
The low incompatible levels, exemplified by Zr which is
< 25 ppm in most of the plutonics, suggests that general

fractionation does not progress very far. It is suggested that this is due to the open nature of the fractionation system. Beneath the spreading axis there will be a continual supply to the base of the system of new primitive magmas and a balancing withdrawal of magma from the top to feed the dykes and lavas. This open nature will continually set back the differentiation process and thus differ markedly from the Skaergaard type closed system crystallisation of a single magma. Consequently the bulk of the Masirah gabbros have Fe/Mg ratios which show only limited overlap with the early Skaergaard products. The phases involved on Masirah are olivine, calcic plagioclase and diopsidic clinopyroxene which are also those suggested to be important in the development of the ocean tholeiites (e.g. Miyashiro, Shido and Ewing, 1970; Hart, 1971; Cann, 1971).

It seems likely that the partial melt batches supplied to the base of the system will show more chemical variation than those drawn from the top because of the homogenisation as the melts mix with the magma chamber liquid. This in fact appears to be in evidence. Eight mantle minor intrusions (Table 7) show a wider chemical range than that of 40 combined dykes and lavas (Abbotts, 1978c). As an illustration, Zr ranges over 15-172 ppm in the minor intrusions and 34-161 in the dykes and lavas. The former range suggests variable degrees of mantle melting (Abbotts 1978e) and some crystal fractionation to explain Zr levels of 15 ppm which can only represent a cumulate origin.

9B.   Differentiation to tonalite-trondhjemite

The presence within the massive gabbro unit of igneous hornblende, followed by stabilisation of an Fe-Ti oxide phase, suggests an increasing PH_2O (c.f. Allen, 1975). Hydrothermal circulation clearly penetrated to this level because of the metamorphic mineral assemblages present. Following Allen (1975) it is suggested that water saturation occurs in the magma, possibly through both hydrothermal and juvenile contributions. An increased PH_2O would cause a FO_2 increase at constant temperature and prompt Fe-Ti oxide precipitation. This event immediately directs the magma on a calc-alkaline trend of increasing SiO_2 toward the granite minimum. The low K nature of the magma results in tonalites-trondhjemites. There is evidence of precipitation of hornblende-Fe-Ti oxide-apatite-zircon during the fractionation. The low AFM trend thus appears to result from two processes: (i) the predominant open fractionation and (ii) local calc-alkaline differentiation probably related to local increases in PH_2O. Similar high SiO_2, low K rocks ("plagiogranites": Coleman and Peterman, 1975) to the Masirah tonalite-trondhjemites have been described from the Indian Ocean (Engel and Fisher, 1975), the Sarmiento Ophiolite (Saunders et al, 1978) and the ophiolites of Troodos, Cyprus; Semail, Oman; and Point Sal, California (Aldiss, 1978). The rarity of these silicic differentiates on Masirah may suggest that suitable conditions of oxide precipitation occurred only spasmodically, possibly in local closures of the fractionation system. Tonalites-trondhjemites were found as screens to 90% dykes and as veins cutting

cumulate gabbro breccias, suggesting that formation occurred at variable heights within the crust. It is, in fact, difficult to judge if the rarity of the rocks is original or whether the faulting at the upper gabbro cumulate-massive gabbro level has "hidden" them.

9C.   Consequences of "Massive Gabbro" underplating

The trondhjemites represent local extreme differentiation but it is evident (e.g. Figs, 14, 18) that the whole massive gabbro unit is rather more fractionated than the lower gabbros. The depleted nature of the latter reflects their cumulate origin.   Rock textures and screen : dyke relationships have been interpreted as indicating an underplated origin for the massive gabbros, caused by the hydrothermal cooling of the overlying crust.   Such an origin would more closely reflect liquid composition than cumulate settling and may explain the more enriched nature.

The variability within the "massive gabbro" unit, from microgabbroic to pegmatitic grain-size, from massive and ophitic to laminated and banded, from gabbro to trondhjemite, must reflect the complex situation near the roof of the spreading centre magma chamber(s).   Local water penetration and periodic magma escape into dykes will both be contributory causes.   The pegmatites which intrude the whole gabbro sequence may represent water enriched residual fluids.

9D.   Degree of mantle melting

The LREE enriched characteristics of the Masirah sequence/ suggest moderate degrees of mantle melting; a 2 x chondrite lherzolite source would involve 10-15% melting.   In contrast the Troodos sequence contains LREE depleted patterns and is believed to represent higher degrees of melting (25-30% : Allen, 1975). The two ophiolites contain different crystallisation sequences; on Masirah plagioclase precedes clinopyroxene, on Troodos the reverse occurs.   Additionally the early plagioclase on Masirah is ~ An85 whereas Troodos is more calcic ~An94 (Fig.7). These relationships have been interpreted above as indicating lower CaO/Al_2O_3 and CaO/Na_2O ratios in the Masirah liquid.

The work of Allen (1975), and that discussed above, suggests that melting at both spreading centres may in part have occurred in the plagioclase-lherzolite stability field. The smaller degree of melting at Masirah could involve a higher pl $\rangle$ cpx + opx + ol contribution to the produced melt. This would explain the low CaO/Al_2O_3 and CaO/Na_2O, the LREE enrichment, the plagioclase-rich sequence and the absence of orthopyroxene in the Masirah gabbros.   However it should be noted that the Masirah serpentinites possess a low CaO/Al_2O_3 characteristic.   This may be an effect of advanced serpentinization or it may suggest that a mantle characteristic has affected the magmatic sequence.

9E. Fractional crystallisation effects on dyke-lava chemistry

The effect of gabbro crystallisation on dyke-lava chemistry has been reviewed elsewhere but Fig.23 provides a useful summary of the relationships. In this figure the crystallisation vectors cover the main cumulus phases in the Masirah gabbros, their origin is placed at the composition of the dykes used as the "primary liquid" of REE modelling, and their length represents 50% crystallisation. It can be seen that the variation in Masirah dyke-lava chemistry can be explained by extensive crystallisation of plagioclase-rich gabbros, as present on Masirah. The TiO_2 levels ($>$ .7%) suggests that the Masirah Ophiolite represents the high TiO_2 suite of Sun and Nesbitt (1978); the "primary liquid" dykes have the chondritic Al_2O_3/TiO_2 ratio ($\sim$20) and the TiO_2 content (0.7-0.8%) which Sun and Nesbitt (1978) quote for the least-fractionated magma of the high TiO_2 suite. The more primitive dykes which are not enclosed within the crystallisation vectors are the late depleted dykes which intrude the cumulate gabbros. These were interpreted as late melts in a process of incremental mantle melting and their high Al_2O_3/TiO_2 ratios (20-40) are in agreement with this model.
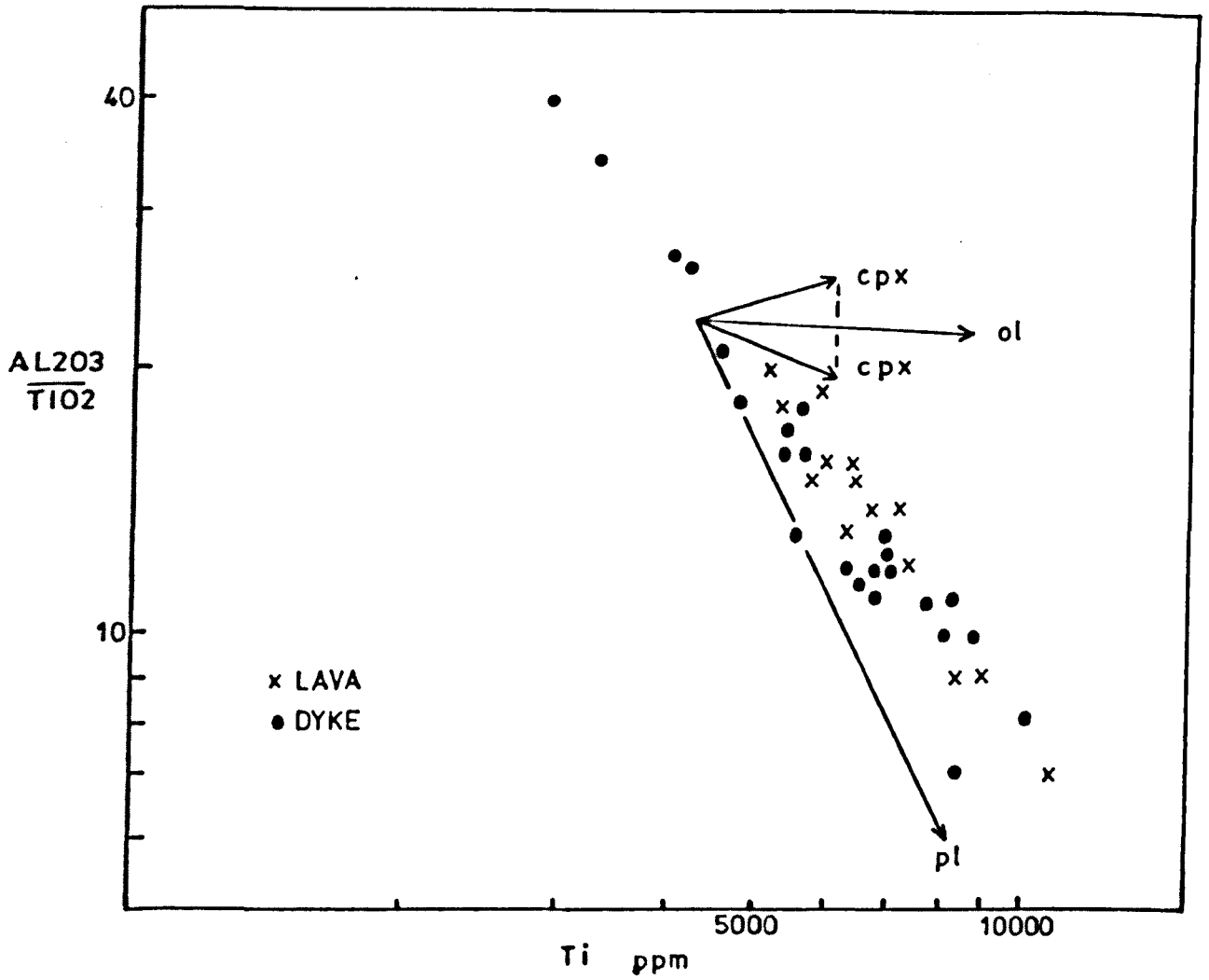
FIG.23. Al_2O_3/TiO_2 v Ti for the Masirah dykes and lavas. The fractionation vectors and their lengths are 50% crystallisation (taken from Pearce and Flower, 1978).

Plate 3. 1

(a) Layered gabbros composed of clinopyroxene
troctolite (dark) and olivine-clinopyroxene
anorthosite (pale) from the ultramafic
cumulate unit (p. 45)

Jabal Madrub FT962730

(b) Layered gabbros composed of anorthositic gabbro
(pale, at top), olivine gabbro and plagioclase-
bearing dunite (dark, in centre). The fold shown
by the dunite layer is a rare example. The hammer
is 60 cm long.

Humer FT972675

Plate 3.2

(a)   Layering caused by variation in olivine : plagioclase modal
      ratio.   The irregularity is typical of most of the cumulates.
      Rassier   GT015690.

(b)   Sharp contact of a gabbro pegmatite pod in massive
      clinopyroxene gabbro. These pegmatites are seen as
      late intrusions in all of the plutonic areas (P. 51a and54).
      Jabal Bhala   FT915640

Plate 3.3

(a)   Isomodal layering of mela and leuco-olivine gabbro in the
       ultramafic cumulates at Rassier (see P.51a). GT034706
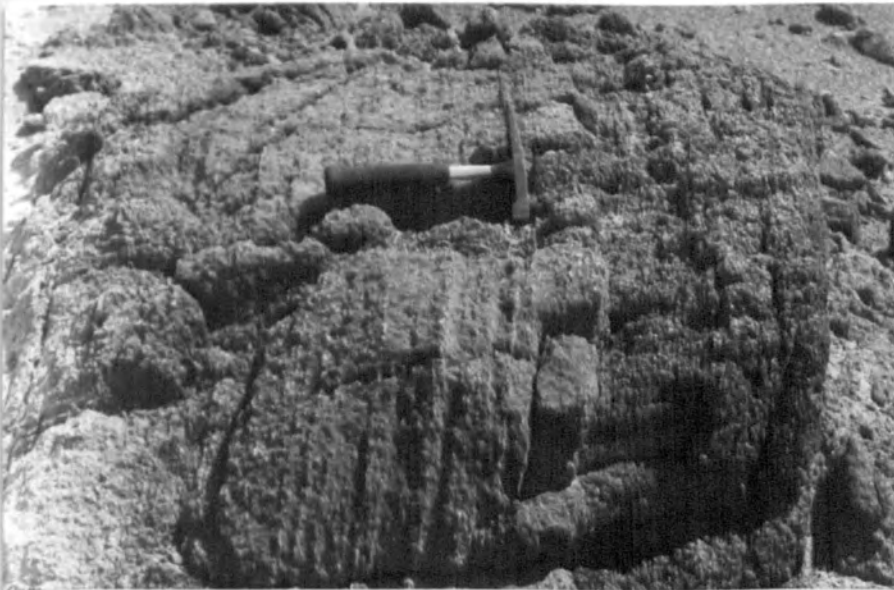
(b)   Block showing small-scale rhythmic layering of mela and
       leuco-olivine gabbro (P. 50).
       Rassier   GT034700

CHAPTER 4

INTRUSIVE PROCESSES AT OCEAN RIDGES: EVIDENCE FROM THE SHEETED DYKE
COMPLEX OF MASIRAH, OMAN.

I.L. ABBOTTS

Dept. of Geological Sciences, University of Birmingham, Birmingham,
B15 2TT, U.K.

ABSTRACT

Masirah Island largely consists of a late Mesozoic ophiolite
which includes extensive areas of near-vertical, ENE-WSW striking,
sheeted dykes. Previously the possibility has been suggested of a
correlation between the similarly-aged ophiolites of Masirah and
the Semail Complex of the Oman Mts. However the Masirah ENE-WSW
trend contrasts with N-S dyke trends from the Wadi Jizi area of the
Semail, possibly suggesting two unrelated spreading centres. The
dykes pass up into a pillow lava - minor sediment sequence, down
into both layered and unlayered gabbros and are bounded to the west
by a major N-S melange zone which may have originated as a ridge
transform fault. Age relations of the dykes and the gabbros are
complex: the dykes contain a variable proportion of gabbro screens
representing earlier crystallisation, but they are also intruded by
several small gabbro bodies which are themselves cut by still later
dykes. The lava and dyke-gabbro screen sequence shows evidence of
metamorphism from zeolite to low amphibolite grade. This metamorphism
was caused by ridge hydrothermal activity which appears to have been
effective approximately to the lower levels of the dykes. The rapid
passage from low-amphibolite dykes to fresh gabbro suggests lithological
control of the metamorphism. A combination of structural, geochemical
and mineral phase studies may indicate generation in a slow spreading

ridge environment and near-ridge metamorphism caused by a geothermal gradient of approximately 200°C/km.

INTRODUCTION

The island of Masirah lies off the S.E. coast of Oman and is composed of a well-exposed and fully-developed ophiolite (Moseley, 1969; Glennie et al, 1974; Abbotts, 1978). Field investigations in 1976 and 1977 showed that serpentinised harzburgites, ultramafic and gabbroic plutonics, minor plagiogranite, a sheeted dyke complex and pillow lavas are all exposed, and of these one of the most impressive features is the sheeted dyke complex which outcrops over approximately 225 km^2.

The ophiolite has associated Lower to Mid-Cretaceous sediments (Glennie et al, op.cit.) and is unconformably overlain by Lower Tertiary limestone. It probably represents Mesozoic (? Cretaceous) ocean crust emplaced during Upper Cretaceous-Lower Tertiary times. The site of the former constructive margin is problematical. Previous correlation of the Masirah Ophiolite with the Semail Complex of Oman (Fig. 1, inset C) could suggest an origin in the ocean to the NE of Oman in which the Semail Complex is thought to have formed (Glennie et al, op.cit.). However recent work places some doubt on this Semail-Masirah correlation and may indicate a possible origin for the latter to the SE of Arabia as ocean crust formed during early Indian Ocean spreading. (Moseley and Abbotts, in press).

This paper examines the structural, intrusive and metamorphic history of the sheeted dykes and their associated rocks and provides information on the processes operative at the constructive margin at which the dykes were generated.

FIG.1. (overleaf) Geological map of the south
and centre of Masirah Island showing the outcrop
of the sheeted dyke complex and adjacent
lithologies.

AN AREA OF THE SHEETED DYKE COMPLEX
SHOWING RAPID VARIATION IN THE PROPORTION
OF DYKES (▨) TO GABBRO SCREENS (▨)

A

30   44
30   40
40   70
30   52   45
47   45
80
85

QTZ VEINING
BRECCIATION

250m

N

50

45

KALBAN   M   M

AL QUARIN   M

70   Area shown
in Fig. 2

C
OMAN AND
MASIRAH
OPHIOLITES

0   800
Km

SAUDI
ARABIA

OMAN   MASIRAH

OWEN FRACTURE

55   75

SHEETED DYKE COMPLEX-
PILLOW LAVA RELATIONSHIPS

40

B

50

80

500 m

80

M

SOUTH
POINT   M

70
30

M

65
50   50   80   80
60   80   80   50
80   40   70
70   30   70   40
40   40   70   70
40   70   70   80
70   70   70   50
80   80   50   70

70

80

40   40
45   40

80

45   65
65
55   65

URF

70   70   70
70   50
70   80   40   80
70   81
45   88   85   80
80

80   80   80

M
S S S S S
S S S S
S S S S S
S S S S S
S S S S S S

80

S S
S S
S S

HAQL   MACULA   60

30 80   35   40   45   50   55 90

RAS
KAIDA

THINLY BEDDED
MARLY LST

PURPLE ALTERED
PILLOW LAVA

GREEN FRESH
PILLOW LAVA

GREEN PILLOW
LAVA CUT BY DYKES

SHEETED DYKE
COMPLEX

GABBRO WITH VARIABLE
AMOUNTS OF DOLERITE DYKES

GABBRO SERPENTINISED
TROCTOLITE AND PICRITE

SSS
SS
SSS   SERPENTINISED HARZBURGITE
+ MINOR GABBRO VEINS

M   OPHIOLITE MELANGE

40   DYKE DIP
AND STRIKE

70   LIMESTONE DIP
AND STRIKE

Y   ALLUVIUM

FAULT

AREAS OF
COPPER
MINERALISATION

LITHOLOGICAL
BOUNDARY

STRUCTURE OF THE SHEETED DYKE COMPLEX AND ASSOCIATED ROCKS

Sheeted dykes form most of the southern third of Masirah Island. They trend ENE-WSW and are generally either vertical or dip steeply (70-85°) to the SSE (Fig. 1). There are further areas of sheeted dykes, of more north-easterly trend, in the "gabbro with dolerite dykes" unit of the centre of the island. The main southern sheeted dykes can be subdivided according to the types of screen present, whether pillow lava or gabbro, in a similar way to the subdivision of the Troodos by Moores and Vine (1971). Dykes with pillow lava screens are rare, restricted to a few outcrops along the NW boundary with the pillow lava belt, and form approximately 5 km^2 of the complex. The remaining 220 km^2 is largely composed of dykes with a variable proportion of gabbro screens.

Dyke complex-pillow lava relationships

Relationships along the NW boundary of the sheeted dykes are partially obscured by faulting which often results in an abrupt contact between dyke complex, with 100 percent dykes, and red pillow lavas. This causes a marked topographic feature due to the more erosion-resistant dykes. However detailed (1:10000) mapping at several localities has revealed sequences less disturbed by faulting. At Haql (Fig. 1, inset B) the sequence from SE to NW consists of dykes with gabbro screens, 100 percent dykes, dykes with green pillow lava screens, green pillow lavas cut by rare dykes, red pillow lavas and locally at the top of the sequence 20-30 metres of marls. The succession is then cut off by a NE-SW tectonic line. This whole sequence occurs over a distance, normal to strike, of 3300 metres and is believed to represent the original ocean crust stratigraphy because: (a) dykes are rare in the red pillow lavas but are commonly seen cutting outcrops of the green pillow lavas;

(b) the red pillow lavas, the green pillow lavas and the dykes show the effects of an ordered downward increase in metamorphic grade.

The dykes are either vertical or steeply-dipping to the SSE and thus minimum thicknesses of the pillow lava units can be estimated. The steep dyke dip suggests that even here the pillow lava outcrop may be determined by faulting. An anomoly is presented by the marls at the top of the sequence which are strongly folded and dip at 30-90° to the NW, rather steeper than expected. Their steep attitude and strong folding may however be the result of movement on the adjacent NE-SW tectonic line, which is probably a complex fault which places gabbros and serpentinites against the lava unit (Fig. 1).

Dyke complex with gabbro screens

As noted before most of the dyke area contains screens of gabbro, or very rarely diorite and quartz diorite. There are no ultramafic screens, though 5 km NW of Macula (8862), in the "gabbro, serpentinised troctolite" unit (Fig. 1), dolerite intrudes serpentinite both as dykes, forming up to 50 per cent of the outcrops, and as irregular plugs 40-50 metres in diameter. The gabbro screens are easily recognisable in the field by their coarser grain-size and abrupt contacts with the dykes (Plate 1). They also possess distinct petrographical and geochemical differences from the dykes (Table 1 and Abbotts, in press) confirming that they are not the coarser centres of dykes isolated by further intrusion. In common with other ophiolites (Kidd et al, 1978) the gabbro is generally plagioclase-rich and lacking in opaques. The screens are usually unlayered though near Urf (8139) and in the centre of the island (Fig. 2) a good mineralogical layering and accompanying strong mineral lineation is developed. The former is continuous only over 5-10 metres and consists of plagioclase or

FIG.2. (overleaf) Complex dyke-gabbro
relationships toward the base of the sheeted dykes.
See Fig.1. for location.

FAULTS

70 ⊥ MEASURED DYKE
      TREND AND DIP

70 ⊥ INTERPRETED
      TREND AND DIP

70 ⊥ GABBRO WITH
. . . LOCALLY DEVELOPED
       MINERAL LAYERING

✳ COPPER
   MINERALISATION

M MELANGE

Y ALLUVIUM

500 METRES

N

EXTENSIVE
DYKE
BRECCIATION
AND
IRREGULAR DYKE
TRENDS

PAGE NUMBERING AS

ORIGINAL

measurements of the dyke proportion yielded means of 86 percent dykes in the northern area, 73 percent in the central and 59 percent in the southern. The corresponding mean dips were $85°$, $82°$ and $81.5°$, all to the SSE, though it should be noted that dykes occur occasionally throughout dipping steeply to the NNW. Ophiolite studies (e.g. Dewey and Kidd, 1977) suggest a gradually decreasing proportion of dykes around the dyke base. On Masirah the southward dip of the dykes, though steep, implies exposure of lower crust in a southerly direction and probably explains the decreasing dyke proportion. A complete passage into gabbros without dykes is not seen in the main southern outcrop. However the "gabbro with dolerite dykes" outcrops in the centre of the island contain an average of 30-40% dykes and include large areas of 90-100 percent gabbro (Fig. 2) whilst higher ground in the north of the island is composed of layered gabbros and ultra-basics with 0-5 percent dykes. These outcrops which cannot be strictly related because of tectonic disruption probably represent progressively deeper levels with decreasing dyke proportions.

The 160 measured localities throughout the main dyke complex yield a mean dyke percent of 76 implying at least 11.4 km extension in the 15 km of exposure. This is a minimum value because these localities include the southern end of the main complex which it is suggested above represents deeper dyke levels; 100 percent extension is indicated by the outcrops with 100 percent dykes immediately south of the pillow lavas. As suggested for the Troodos Ophiolite (Gass and Smewing, 1973) and for the Semail complex (Glennie et al, 1973) the only known mechanism for such levels of extension would seem to be spreading at a constructive margin.

Dyke trends

Figure 1 summarizes the dyke trends throughout the complex and shows the consistent ENE-WSW strike and vertical to steep SSE dip. This suggests a phase of smooth sea-floor spreading and an original ENE-WSW constructive magin, assuming no subsequent tectonic rotation. The generally consistent dip and strike of the dykes indicates that the easiest ascent is usually defined by the tensional regime and the pre-existing vertical dykes.

Along the western margin of the dyke complex dykes locally occur with a N-S trend, at obvious variance with the regional strike (Fig. 1: 7437, 7443, 7649). These all occur close to the contact with the N-S melange zone, which cross cuts the ophiolite to the west, though in one instance (7649) dykes of a normal trend intervene between the melange and those of N-S strike. This vertical melange zone is up to 5 km wide and contains blocks from all crustal levels, including troctolite, gabbro, dolerite, lava and chert. These are commonly contained in a serpentinite matrix. Sampling of present-day transforms exposes a similar variety of rocks and similarly extensive serpentinite, the occurrence of which is commonly attributed to extensive ocean crust diapirism. (e.g. Melson and Thompson, 1971; Bonatti and Honnorez, 1976; Bonatti, 1978). It has been suggested elsewhere (Moseley and Abbotts, op.cit.) that this melange may have originated as a ridge transform fault, along which there has been extensive serpentinite diapirism triggered by water penetration along the fault. The melange is almost perpendicular to the dykes in classic transform - spreading axis relationship.

The dykes with a normal trend at 7649 appear to rule out the mechanical rotation of whole blocks by any tectonic processes which

might have operated along the melange zone. Instead it seems likely that the N-S dykes represent intrusion parallel to the postulated transform, similar to that noted in the Troodos (Moores and Vine, 1971).

Dyke dips

Irregularities of dip occur only rarely. South of Haql in a sequence of normal near-vertical dykes, which strike NE-SW, are found occasional dykes which dip at 40-45° to the NW. Cann (1974) has described how late off-axis dykes may cut the existing sequence, which dips away from the spreading axis because of a process of isostatic compensation for lava extrusion. However at Haql the dominance of the vertical dykes is the reverse of the situation expected in that theoretical model. The majority of dykes are between 15-100 cm wide (total range 3-400 cm) and a simpler explanation for the rare discordant examples might be diversion of normal vertical magma ascent by faults in the young ocean crust. East of Kalban (7544), again near the western edge of the complex, is a small area of narrow intrusions with irregular dips (10-90°) and strikes (E-W to N-S). This area may be further evidence of irregular intrusive activity caused by interference of the postulated transform on the normal tensional stress field. The shallower dips could represent the presence of thin sills of similar dimensions to the dykes. Sills are commonly described in the ophiolitic literature & have been noted from ocean-floor drilling (e.g. Bass et al., 1973; Marsh, pers comm: evidence from Leg 58).

Gabbro intrusions of the sheeted dykes

At Ras Kaida there are two irregularly-shaped intrusions, amounting together to approximately 4 km^2. (Fig. 1). They are composed of olivine-gabbro, pyroxene gabbro and gabbroic anorthosite, which contain abundant blocks, up to 400 metres in diameter, of serpentinised picrite

and troctolite. The intrusions are clearly discordant to the surrounding dyke swarm, which here contains 70-80 percent dykes. The ultramafic blocks probably represent lower level plutonics caught up by the magma as it rose and could be either early remobilized cumulates of the Ras Kaida gabbro itself or pre-existing lower oceanic crust. Both intrusions are cut by rare dolerite dykes which form less than 1 percent of the outcrops and appear to have a trend (WNW-ESE) at variance with that of the main dyke swarm (ENE-WSW). The rarity of these dykes and possibly their oblique trend may suggest off-axis gabbro intrusion outside the zone of active spreading tension.

Part of the "gabbro with dykes unit", of the centre of the island, is illustrated in Fig. 2. This shows both the presence of another gabbro intrusion and the complex relations in these lower dyke levels. Dyke complex, with 10 percent gabbro screens representing earlier crystallisation (at Y), is intruded by an obviously discordant gabbro (X), which possesses the steep mineral-layering noted before. This gabbro appears to pass laterally into outcrops where it is intruded by 20-30 percent dykes. (near Z) The near-parallelism of all the dykes of this region suggests that all this intrusive activity took place within the near-axial, active-tension, regime.

SUB-SEA FLOOR METAMORPHISM

Within the ophiolite the pillow lavas and the sheeted dyke complex have been subjected to an ordered zeolite-greenschist-low amphibolite metamorphism, the cause and affects of which are broadly similar to those adequately described in the literature both on the ophiolites of Cyprus (Gass and Smewing, 1973), E. Liguria (Spooner and Fyfe, 1973), Newfoundland (Coish, 1976) and Chile (Saunders et al., 1978) and on samples drilled from active ridge crests (Bonatti et al,

1975; Bonatti, 1976). Thus the important features of the metamorphism are summarized in Table 1 and only those aspects unique to Masirah will be considered here.

The metamorphism is ascribed, as are those above, to the sub-sea floor hydrothermal circulation and high geothermal gradients prevalent at and near to the active spreading ridge at which the Masirah ophiolite was (almost certainly) generated. Metamorphism in this environment explains (a) the oxidised calcite-haematite assemblages at the top of the ophiolite sequence in the red pillow lavas; (b) the lack of any recrystallisation fabrics which are so typical of dynamothermal green-schist-amphibolite metamorphism; (c) the metamorphic peak in the sheeted dykes with fresh plutonics below, which suggests a circulation base near the base of the dykes; (d) the appearance/disappearance of metamorphic minerals which approximately parallels the different lithologic units and thus also the original rock-water interface.

The dykes often show preferential saussuritization of the calcic cores of their metamorphically-zoned plagioclase which may indicate a retrogressive element in the metamorphism as the crust moves away from the spreading centre. Similarly the prescence together of both green hornblende and actinolite in some of the gabbro screens suggests metamorphic complexity with amphibole growth responding to differing metamorphic conditions (c.f. Grapes, 1975).

Problem of the red pillow lavas

The presence of red-purple pillow lavas at the top of the succession on Masirah is interesting since such lavas do not appear to be sampled from present-day ocean-floors. This may suggest that the coloration was acquired after ophiolite emplacement by weathering in those upper levels in which iron was not fixed in stable phases

Table 1   Petrography and metamorphic assemblages in the Masirah Ophiolite

Lithologic unit	Metamorphic mineral assemblage	Metamorphic mineral appearance	Metamorphic mineral disappearance	Original igneous minerals and textures versus recrystallisation
Metamorphosed red pillow lavas	Zeolite-?Smectite-haematite-calcite-(chlorite)	Zeolite-?Smectite-haematite Chlorite	Zeolite (?smectite, haematite, calcite, decrease to accessory levels)	Plagiophyric (An86); rare olivine, opaque, and clinopyroxene phenocrysts. Matrix: perfectly preserved vitrophyric, variolitic, sub-ophitic pillow zones. (Rare dykes as below except finer-grain, fresher clinopyroxene, less recrystallisation).
Metamorphosed green pillow (and rare metadolerite dykes).	(Haematite)- chlorite- (actinolite)	Actinolite Actinolitic hornblende	Chlorite decreases to accessory level.	
Metadolerite dykes (and gabbro screens)	(Chlorite)- actinolite- actinolitic hornblende- sodic plagioclase- sphene	Brown hornblende*		Dykes = aphyric-plagiophyric, only rare olivine, clinopyroxene, phenocrysts. Matrix of plagioclase (An70)-endiopside-ilmenite-titanomagnetite. Uralitization destroys sub-ophitic texture. Screens = plagioclase (An81-86)-diopside-very minor ilmenite-titanomagnetite. Coarse parallel texture. Minor to extensive uralitization.
Plutonic sequence — Rare metagabbro	Actinolite-hornblende (green)-sodic plagioclase			Igneous mineralogy and texture as for screen gabbro. Minor uralitization.
Plutonic sequence — Fresh gabbro				Igneous mineralogy and texture as for screen gabbro.

99

Note: * Difficult to decide if brown hornblende is of late igneous or metamorphic origin.
     Mineral identification and composition determinations by optical and electron microprobe methods.

(e.g. green lava chlorite?). They form approximately 80 percent of the lava outcrops on Masirah although this figure is probably increased by faulting-out of the green pillow lavas. This contrasts with the situation in the Oman Mts where Smewing et al (1977) describe red hematitic lavas as of very limited extent compared to green lavas.

Lithological control of metamorphism

The passage from low-amphibolite facies dykes to fresh gabbros is rapid in both vertical and lateral directions at the base of the dykes. Labradorite-diopside gabbros with only minor uralitization and unzoned, or slightly zoned (An81-77), plagioclase grade over 80-100 metres into dyke-rich areas in which the clinopyroxene phase of the dykes is extensively uralitized, the plagioclase has acquired a metamorphic zoning from An80 to An27, and use of the Fe-Ti oxide geothermometer of Buddington and Lindsley (1964) suggests that the ore minerals have re-equilibrated to temperatures of 320-340°C. It seems that there is a lithological control on the hydrothermal metamorphism probably caused by a permeability decrease from a unit of narrow, vertical, dykes which would permit water passage along dyke boundaries to one of massive, homogenous, gabbro. It is also possible that increasing temperature, and fault closure with depth, help to prevent further water penetration. Thus the base of the dykes approximately coincides with the base of hydrothermal circulation and of metamorphism.

Geothermal gradient of metamorphism

The appearance of actinolite near the base of the green pillow lavas is indicative of a temperature of at least 320°C (Keith et al., 1968), a value which seems to be corroborated by dyke Ti-ore geothermometry which gives reequilibration temperatures of 320-340°C. The passage from a smectite to chlorite around the red-green pillow lava

junction, though blurred by the occasional occurrence of both together, suggests a temperature around $210\pm20^\circ C$ (Spooner and Fyfe, 1973). In the unfaulted sequence at Haql a maximum of 1 km of red pillow lavas and 0.75 km of green pillow lavas outcrop. These vertical thicknesses are calculated assuming (1) a lava dip of 37.5°, which is an average of that indicated by the marls above and the dykes below and (2) that the marls represent the top of the lava succession. These thicknesses, combined with the temperatures above, indicate a geothermal gradient of approximately $170-200^\circ C$. It is possible that the dykes give a better indication of lava thickness than the folded marls in which case the estimated gradient is on the low side. This value compares with $160^\circ C$/km for the Troodos ophiolite (Gass and Smewing, 1973) and $300^\circ C$/km for the Betts Cove ophiolite (Coish, 1976).

CONCLUSIONS CONCERNING THE TECTONIC ENVIRONMENT OF DYKE INTRUSION

Ocean ridge, marginal basin, or island arc?

There is now wide acceptance by most earth scientists of an ocean crust origin for fully-developed ophiolites but it is often less clear whether individual ophiolites represent the products of (a) mid-ocean ridge spreading (b) marginal basin spreading or (c) early island arc volcanic activity (e.g. Saunders et al., 1978). Origin of the Masirah ophiolite at a spreading ridge is suggested by the outcrop of 225 km^2 of parallel sheeted dykes, by the lack of evidence of subduction and island arc volcanism in the late Mesozoic-early Tertiary on this passive Arabian continental margin, and by geochemical studies of the dykes (Abbotts, in press). These latter clearly indicate both the tholeiitic nature of the dykes and their strong ridge affinities in levels of MgO, Ni, Cr and probably TiO_2 (Table 2 and Fig. 3).

Table 2   Masirah Ophiolite: mean dyke analysis compared with mean mid-ocean ridge and island arc basalt analyses

	Mean Dyke[1]	Mean Mid-Ocean Ridge Basalt[2]	Island-arc tholeiite basalt[3]
SiO_2	47.84	49.21	51.38
TiO_2	1.08	1.39	0.57
Al_2O_3	14.73	15.81	18.25
tFe_2O_3	9.57	10.20	10.13
MgO	10.20	8.53	6.13
CaO	11.85	11.14	11.81
Nc_2O	2.21	2.71	1.81
K_2O	0.26	0.26	0.26
P_2O_5	0.11	0.15	0.02
Trace elements in ppm			
Cr	336	296	43
Ni	131	123	24
Zn	42	122	n.d.
Ga	16	18	18
Rb	2	5	5
Sr	211	123	105
Y	22	43	n.d.
Zr	79	100	55
Nb	8	5	n.d.
Ba	72	12	28
La	4	n.d.	n.d.
Ce	12	n.d.	n.d.

Note: n.d. = not determined.

1   = mean of 22 dyke samples

2   = Average MOR-basalt value (Engel et al, 1965; Melson and Thompson, 1971; Erlank and Kable, 1976)

3   = Sample SSV9.1, porphyritic basalt from the S. Sandwich Is. (Baker, 1978)

From Saunders et al (in press)
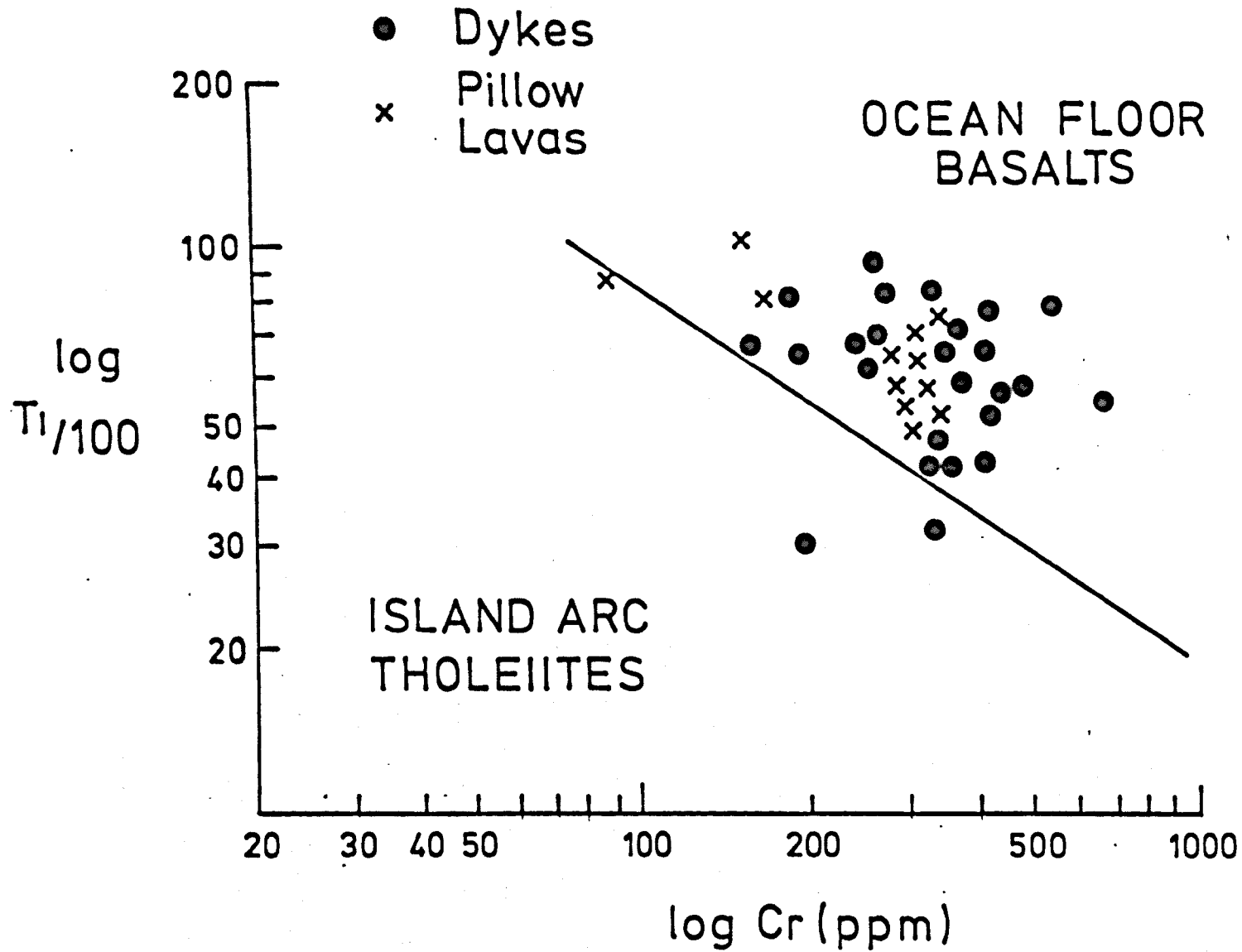
FIG.3. Figure taken from Abbotts (in press) showing Masirah dyke and lava samples plotted on a log Ti - log Cr discrimination diagram (Pearce, 1975). Note the clear ocean floor basalt affinity.

It is more difficult to discriminate between mid-ocean and marginal basin environments, particularly as all gradations may well exist between the two. A small marginal basin seems to present advantages as the site of ophiolite generation because: (1) the sandwiched position of the ocean-crust between blocks of continental crust, (2) the shallower sea and (3) the more bouyant mantle (Hawkins, 1976) beneath the back-arc basin may all help in emplacement of the ophiolite. Previously the correlation has been made between Masirah and the Semail Ophiolite of the Oman Mts, which is believed to have been derived from the NE of Oman in the late Cretaceous (Glennie et al, 1973). Arguments have however recently been presented which cast doubts on the correlation (Moseley and Abbotts in press), one being the contrasting dyke trends of N-S in at least the Wadi Jizi area of the Semail (Smewing et al, 1977) to ENE-WSW on Masirah. It seems possible that Masirah may instead represent ocean floor generated during initial Cretaceous spreading at an early NE-SW mid-Indian Ocean ridge. The north-eastwards movement of the Arabian continental plate in the Tertiary (Gass and Gibson, 1969) could have caused oblique compression at the plate boundary with the north-western Indian Ocean plate and may have led to ophiolite uplift or upthrust along the weak melange (? transform) line. There are two arguments which support this hypothesis: (1) the evidence of D.S.D.P. drilling which penetrated Palaeocene basement 250 km SE of Masirah, and that of Upper Cretaceous-Lower Tertiary magnetic anomolies to the E of Masirah suggest adjacent Cretaceous crust (2) the orientation of the dykes (ENE-WSW) is similar to that of the early E-W Indian Ocean ridge. This ridge was abandoned approximately 50 m. yrs ago (McKenzie and Sclater, 1977; op.cit., Gealey, 1977). Planned palaeomagnetic work on oriented dyke samples may add further constraints here.

Geochemical studies of the Masirah rocks do not help to discriminate between this possible mid-ocean origin and a marginal basin environment because (a) the elements K, Rb, Ba and Sr which are possibly enriched in marginal basin basalts (Saunders et al, in press) have been subjected to secondary mobility during their metamorphism (Abbotts, in press), and (b) because of problems caused by the large chemical variation within fresh MOR-basalts and their extensive chemical overlap with marginal basin basalts.

Timing of dyke intrusion and gabbro crystallisation

Cann (1974) and Dewey and Kidd (1977) both suggest in theoretical models that a ridge magma chamber will develop normal floor cumulates and because of hydrothermal cooling of the thin (2-3 km) crust above should freeze from the top downward as homogenous unlayered gabbro. They both suggest that the depth of the dyke-gabbro transition zone may be controlled by the lower limit of hydrothermal circulation. On Masirah homogenous unlayered gabbro appears to form 80-90 percent of both the dyke screens and the gabbro component of the "gabbro with dykes" unit of the centre of the island, which is thought to represent the lower levels of the dyke complex. These unlayered gabbros are probably the products of the roof crystallisation suggested by the above models. Layered gabbros make up the other 10-20 percent. The layering is always steeply dipping, usually sub-parallel to the dykes, occurs in areas with 10 to 60 percent dykes and is rather irregular in extent and scale. There is no indication that it is either cumulate in origin or part of wide, coarse dykes and it seems more likely that it may indicate vertical flowage at or near the top of the magma chamber(s). Frequently the elongate plagioclase plates and diopide prisms define a good lineation suggestive of such directional flow. It seems possible that this occasional sub-vertical flowage of magma may have been the

feeders of the slightly higher dykes. Its relation to the dykes contrasts with the layering in the gabbros and ultrabasics of the north of the island. There the much rarer dykes cut the gabbro layering at high angles, the layering is rather more regular, and the gabbros possess foliated and cumulate textures. The lack of a mineral lineation combined with these observations, suggests cumulate layering here.

A model of the intrusive processes at the Masirah spreading centre must explain the vertical variation from 90-100 percent dykes found in the main sheeted dyke complex to 95-100 percent gabbro found in these northern outcrops of the island.

As the newly formed ocean crust began to accelerate away from the Masirah ridge axis it would probably have consisted of early lava flows and dykes above a magma chamber which had only undergone limited crystallisation. This situation is suggested both by theoretical cooling models (Cann, op.cit.; Dewey & Kidd, op.cit.) and geochemical work referred to below. Continued acceleration would have caused further tensional dyke injection while contemporaneous crystallisation of diopside-plagioclase roof gabbros should occur, gradually underplating the early dykes. As gabbro underplating continued and the crust accelerated up to its steady spreading rate, ending active tension, the two factors would have combined to make dyke intrusion progressively more difficult. All variations from 100 percent dykes to 100 percent gabbros could be generated by the increasing importance of the gabbro underplating process relative to that of dyke injection. The model is similar to that recently used to explain the Mings Bight Ophiolite, Newfoundland (Kidd et al, 1978). Dewey and Kidd (1977) suggest a half width for the axial zone of dyke intrusion, based on ARCYANA observations, of 1.25 km.

Geochemical study (Abbotts, in press) has shown a complete range
of dykes from primitive members with low Zr (34-51 ppm), Ti, P, Y and
REE's, whose chemistry is virtually unaffected by gabbroic fractional
crystallisation and reflects the mantle partial melting process, to
more enriched dykes with higher Zr (130-135 ppm), Ti, P, Y and REE's.
It has also shown that the enrichment in these dykes was probably
caused by fractional crystallisation of olivine, plagioclase and
diopside, the phenocryst phases found in the dykes, and also the
phases forming the gabbro sequence. These observations suggest that
gabbro crystallisation caused the progressive enrichment of the
escaping dykes, which fits well with the explanation above of gabbro
underplating, contemporaneous with dyke escape and intrusion. The
gabbro screens, representing early roof crystallisation, are usually
plagioclase rich gabbro anorthosites and anorthositic gabbros with
diopside and only very rare olivine. In contrast the lower level
plutonics are cumulus olivine and then olivine-plagioclase rocks,
with only intercumulus diopside. The contrasting mineralogy is
probably explained by the cumulate nature of the lower plutonics
whereas the screens may largely represent mafic liquid frozen on
the roof of the magma chamber.

Origin of the local variation in the dyke: screen ratio

There are obvious complications to this simplified picture in
the form of the abrupt changes and lateral transitions from 80-90 percent
dykes to 80-90 percent gabbros. These are particularly common in the
south of the main complex and in the "gabbro with dykes" unit, both
believed to represent the lower levels of the sheeted dykes. These
variations are rather similar to those described by Kidd et al (1978)
in the Mings Bight Ophiolite Newfoundland though here they are both
of larger scale and more diverse in origin. Gabbro-rich areas within

levels of dominant-dykes occur up to 750 m across, an example being
the intrusive gabbro X in Fig. 2. It is possible that faulting and/or
roof-stoping might encourage such intrusion parallel to the strike
of the dykes but no supporting evidence for this process has been seen
in the way of dyke-blocks sunk into the gabbros. The transgressive
Rai Kaida pluton is also evidence of late gabbro intrusion into the
sheeted dykes. Here the irregular transgressive shape and lack of
dykes cutting the pluton suggest off-axis intrusion. In other cases
there is simply a rapid but transitional increase in the screen
proportion, an example being the gabbro rich area, 400 m across, N of
South Point (Fig. 1, centre of inset A). These areas cannot be
ascribed to gabbro intrusion and Kidd et al (1978) simply suggest
alternating zones of preferred (and excluded) dyke injection. Another
possibility might be that a gabbro-rich area could indicate a period of
increased spreading rate which would cause an upward movement of the
crustal isotherms. This would cause a nearer-surface development of
the magma chamber roof leading to a thinner dyke unit and a thicker
gabbro unit, as suggested by Cann (1974).

Spreading rate

The vertical thickness of the sheeted dykes on Masirah is difficult
to estimate because an unfaulted vertical transition into the cumulates
of the north of the island is not seen. In the main complex an average
dyke dip of 83° and a minimum width perpendicular to strike of 15 km
suggests a minimum thickness of 1.8 km down to a level where there is
still 59 percent dykes. This is thicker than the Semail dyke unit (1 km),
which may again suggest two different ridge systems, but comparable to
that on Troodos ($\sim$2 km), which is suggested to have been generated
at a slow-spreading ridge (Smewing, et al., 1975). The combined dyke-
lava thickness of approximately 3.5 km is again similar to Troodos,

thicker than the Bay of Islands, Newfoundland, and similar to the
Semail because of thicker lavas there (Christenson and Salisbury,
1975). Cann (1974) suggested on theoretical grounds that slower
spreading would encourage a thicker dyke unit and a wider zone of
intrusion. On Masirah, the vertically thick dyke unit, the common
plutonic screens within it, the lack of dyke one-way chilling
(Moores and Vine, 1971), extensive serpentinite intrusion along major
faults in the ophiolite and the evidence of plutonic fractionation
before intrusion of the more enriched dykes all may qualitatively
indicate either a wide zone of intrusion and/or a slow spreading
rate. It is argued elsewhere (Abbotts, in press) that the low TiO_2
contents (0.46 - 1.60 percent) of these dykes are the result of the
nature, extent and timing of fractional crystallisation and not
necessarily indicative of the former spreading rate (c.f. Nisbet
and Pearce, 1973). The average dyke thickness is approximately 50 cm
and if a slow half spreading rate of 1-2 cm/yr is assumed, an average
intrusion rate of 1 dyke every 12.5 - 25 years is indicated. Though
obviously simplistic the figure gives some impression of the geologically
rapid rates of magma supply at ocean-ridge systems.

Correlation with sonobouy studies of modern ocean crust

Correlation with the sonobouy model 2 of Christensen & Salisbury
(1975, 1978) suggests that the basal high velocity part of layer 3
corresponds to the picrites, troctolites and olivine gabbros on
Masirah, the lower velocity part of layer 3 to the combined olivine-
free gabbros and overlying dykes, and the lavas to layer 2. The
estimated lava thickness of 1.75 km compares well with the model.
The vertical thickness of gabbro, troctolites and picrites cannot be
measured accurately though there is a minimum of 2 km present in the
north. Using this value the minimum dyke and gabbro thickness is
3.8 km which compares with the model layer 3 value of about 5.5 km.

Plate 4. 1

(a)   Lower levels of the sheeted dyke complex with dark
      metadolerite dykes intrusive into pale coarse uralitized
      gabbro. Part of the transition from sheeted dykes to
      gabbro (P.   94   ).
      South Point   FT720330.

(b)   Thick metadolerite dyke between two screens of uralitized
      gabbro in the sheeted dyke complex.
      NE of South Point FT745350

Plate 4.2

(a) Upper levels of the sheeted dyke complex with 100%
     metadolerite dykes. The absence of screens makes
     individual dykes difficult to distinguish. They are
     here sub-vertical and strike perpendicular to the
     plane of the photograph.
     N. of Haql   FT885540

(b) Sheeted dyke complex. Dark metadolerite dykes alternate
     with pale screens of gabbro.
     Ras Kaydah   FT450830

Plate 5. 1

(a)   Rassier   GT015710

(b)   SE of Al Quarin   FT500775

Details of pillowed flows in the red pillow lava unit.
Individual pillows are 30-120cm in diameter (P 126   ).

Plate 5.2

Vertical thinly-bedded marls.
These are intercalated with
pillowed flows at the top of
lava unit (see description on
p 91).

Rassier   GT015710

CHAPTER 5

MASIRAH OPHIOLITE SHEETED DYKES AND PILLOW LAVAS: GEOCHEMICAL EVIDENCE OF THE FORMER OCEAN RIDGE ENVIRONMENT

I. Abbotts

Department of Geological Sciences, University of Birmingham, Birmingham. B15 2TT

Abstract

The island of Masirah is composed of a fully-developed, late-Mesozoic, ophioli— in which are exposed extensive tracts of regularly-trending, sheeted-dyke complex and associated pillow lavas. These upper ocean-crust rocks have been subject to a hydrothermal constructive-margin metamorphism, which has had profound effects on their major and alkaline-trace element geochemistry. Minor, trace and rare-earth element characteristics suggest: (1) the involvement of extensive magma-chamber fractional crystallisation in the development of their chemistry (2) their origin at a former spreading centre, though whether mid-ocean or marginal basin cannot be constrained by their geochemistry alone.

Introduction

Most earth scientists now accept that the more complete ophiolite suites represent fragments of oceanic lithosphere. Problems remain however in assigning individual ophiolites to a mid-ocean ridge, small marginal basin or early island arc environment of generation. A geochemical study of sheeted dyke·rocks and pillow lavas from Masirah Island has been made to attempt to define their tectonic environment of generation and the intrusive processes involved.

GEOLOGICAL SETTING OF THE MASIRAH SHEETED DYKE-PILLOW LAVA SEQUENCE

Masirah Island is largely comprised of an ophiolite complex, probably of Upper Cretaceous age (Glennie et al, 1974), composed of serpentinized harzburgites, ultra mafic, mafic, and local plagiogranite plutonics, extensive sheeted dyke complex outcrops and pillow lava-sediment sequences (Abbotts, 1978a). Unconformable

Tertiary (Eocene?) limestone, locally overlying the ophiolite, and one area of later granite intrusion (Abbotts, 1978b), complete the geology of this dominantly ophiolitic island. To the W the ophiolite complex is bounded by a 5 Km wide vertical melange belt, of N-S trend, which has been interpreted as a transform fault in origin and which aided ophiolite emplacement by providing a weak suture in the oceanic lithosphere (Moseley and Abbotts, 1978). Some disruption of the plutonic levels, which outcrop in the N of the island, occurred during emplacement but the original upper ocean crust stratigraphy is largely preserved in the centre and south (Abbotts 1978a). There is exposed a sequence of red pillow lava-sediment passing down into green pillow lava with rare dykes, into metadolerite dykes with green pillow lava screens, into 90-100 per cent dykes and finally into dykes with increasing proportions of plutonic screens (Fig. 1). Near-vertical red pillow lava-sediment occurs in a narrow ENE-WSW belt which cuts the northern plutonics. These were almost certainly tectonically incorporated.

The plutonic sequence comprises dunites, mela to leuco-olivine gabbros, diopsidic gabbros and leucogabbros, a late pegmatitic gabbro-facies and rare tonalites and trondhjemites. The fractional crystallisation sequence was chromite + olivine, olivine, olivine + plagioclase, olivine + plagioclase + diopside and then plagioclase + diopside. Ore minerals made an insignificant contribution throughout and only in the late stages were Fe-Ti ores and hornblende precipitated. The plutonic-dyke transition shows complex structural and age relationships interpreted by Abbotts (1978a) as gabbro underplating at the roof of the magma chamber(s), contemporaneous with dyke escape and upward injection, this latter decreasing in frequency in proportion to the thickening gabbro unit (c.f. Dewey and Kidd, 1977). Serpentinised harzburgite occurs along the length of the melange, where it is probably diapiric in origin (Moseley and Abbotts, 1978), and along major tectonic lines through the ophiolite. Only at Ras Al Ya (Fig. 1) does it occur as a conformable floor to the cumulate succession.
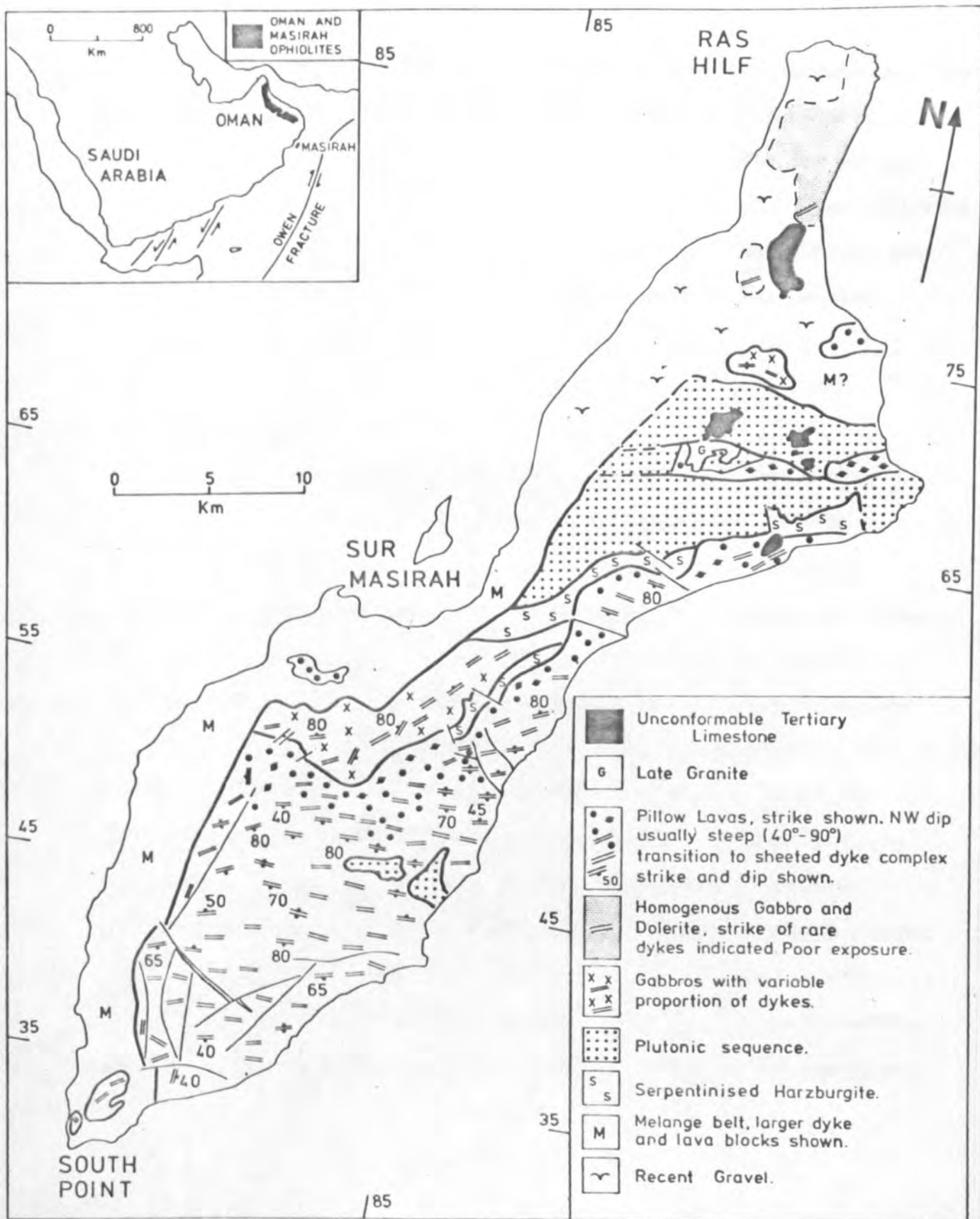
FIG. 1. Geological map of Masirah Island showing the distribution of the main lithologies. Most of the dyke and lava samples came from the southern sheeted dyke complex and central pillow lava belt.

Sheeted dyke complex outcrops with a regular ENE-WSW trend and steep southward dip over 225 Km^2 of the island (Abbotts 1978b). It has a minimum vertical thickness of 1.8 Km while the overlying lava sequence adds a further 1.5 Km. Dyke samples come largely from the main southern and central exposures (Fig. 1) though 4 were collected from large blocks incorporated in the western transform melange. Lava samples were taken predominantly from the main central lava belt but also from the northern tectonic belt and again from melange blocks.

PETROGRAPHY AND METAMORPHISM

The lavas, dykes and upper gabbros show evidence of zeolite - greenschist - low amphibolite metamorphism effective approximately to the base of the dykes, below which occur fresh plutonics. This has been interpreted as constructive margin metamorphism induced by the high geothermal gradient and hydrothermal circulation (Abbotts 1978a). The dykes show evidence of the highest grade of metamorphism and their uniform mineralogy consists of plagioclase with strong metamorphic zoning (An70 - An20), clinopyroxene relicts within ubiquitous secondary amphibole (actinolite + actinolitic hornblende), reequilibrated Fe-Ti oxides and occasional sphene. Both they and the lavas are commonly either aphyric or plagiophyric but olivine or diopside occasionally accompany plagioclase as phenocryst phases. The lava groundmass usually consists of relatively fresh plagioclase laths in either a chlorite-(actinolite)-ore matrix (green pillow lavas) or a zeolite-haematite-calcite-smectite matrix (red pillow lavas). Details of the metamorphism presented elsewhere (Abbotts, 1978a) suggest a geothermal gradient of approximately $170-200^{\circ}\text{C/Km}$.

DYKE AND LAVA CHEMISTRY

1. ANALYTICAL TECHNIQUES

44 dyke and pillow lava samples were analysed for 21 major and trace elements, one dyke was included in 6 samples selected from the ophiolite for REE analysis and

the mineral chemistry of the modally important dyke mineral phases were determined

by electron microprobe. The major and trace element analyses were carried out on

a Philips PW 1450 automatic X-ray fluorescence spectrometer using 46mm diameter

powder pellets. In addition a selection of samples were analysed using a fusion

bead technique to overcome major element problems of absorption and mineralogical

effect. Details of spectrometer conditions, calibration methods, machine precision

and accuracy can be found in Tarney et al (1978 in press). REE analyses were carried

out by INAA following the methods of Hertogen and Gijbels (1971) and using a low

energy photon detector with the ocean basalt BOB-1 as a reference standard. Agree-

ment of La and Ce results with those of X-ray fluorescence were good. Mineral phases

were analysed on a Cambridge Microscan 5 electron probe microanalyser at Leicester

University. The X-ray intensities were converted to oxide percentages using a

modified version of the Magic IV programme (Beaman and Isasi, 1970) which corrects

for dead-time, atomic number, absorption and fluorescence. Representative whole

rock analyses are presented in Table 1, selected to cover the full Zr range of the

rocks and set out in order of increasing Zr. 98 plutonic samples were also analysed

and Table 2 shows representative plutonic analyses compared with the means of the

lavas and dykes and with 4 basalts from different tectonic environments.

2. MAJOR AND TRACE ELEMENT MOBILITY DURING OCEAN RIDGE METAMORPHISM

The Masirah ophiolite has been subject to a zeolite - greenschist - low amphi-

bolite metamorphism, at or near the former ocean ridge, with the metamorphic peak

in the dyke unit (Abbotts 1978b). It is important to appreciate the affects of

this metamorphism before considering the genetic implications of the rock chemistry.

An additional complication is the original large variation in the plagioclase:

clinopyroxene modal ratio. The affect of this is illustrated by the chemistry of

dyke MA 424 which contains 50 per cent plagioclase phenocrysts and has high Al, Ca

and Sr and low Fe, Mg and Y levels. For reasons adequately stated elsewhere (e.g.

Weaver et al, 1972; Tarney et al, 1977) Zr has been shown to be useful as an index

MASIRAH OPHIOLITE : REPRESENTATIVE DYKE AND LAVA ANALYSES

Table 1.

Sample	METADOLERITE DYKES							GREEN PILLOW LAVAS		RED PILLOW LAVAS		
	MA248	MA424[1]	MA366[2]	MA206[3]	MA236	MA183	X176*	X330[5]	X326[4]	MA400[6]	X245PII[7]	MA422[8]
SiO_2	48.91	48.12	46.52	47.62	49.07	48.52	50.51	49.41	47.79	47.30	47.38	47.66
TiO_2	0.46	0.50	0.69	0.91	1.15	1.34	1.40	1.05	1.08	0.83	1.04	1.74
Al_2O_3	13.58	19.92	18.45	16.10	13.64	14.28	13.85	13.71	15.51	14.38	16.34	12.10
tFe_2O_3	9.55	6.59	7.97	9.20	9.47	9.39	9.25	9.59	9.72	8.26	9.22	9.44
MgO	9.98	7.62	8.68	9.43	10.09	11.52	10.17	9.18	8.59	7.04	4.48	7.78
CaO	13.42	14.51	13.25	11.92	12.64	11.40	8.34	10.44	10.12	15.34	12.73	9.83
Na_2O	2.39	2.10	2.18	2.19	2.48	2.29	2.34	3.42	3.62	3.11	4.12	3.67
K_2O	0.12	0.26	0.07	0.08	0.11	0.11	1.88	0.25	0.86	0.36	0.92	1.57
P_2O_5	0.09	0.05	0.08	0.09	0.14	0.16	0.17	0.09	0.01	0.08	0.11	0.26
TOTAL	99.38	99.66	97.88	97.68	98.91	99.17	98.04	97.10	97.34	96.68	96.53	94.06
Trace elements in ppm												
Cr	274	195	323	332	409	426	188	405	364	344	321	170
Ni	83	67	119	192	98	169	80	139	129	102	52	82
Zn	22	16	25	62	22	36	20	131	53	56	54	68
Ga	17	16	14	15	16	16	17	14	17	16	14	18
Rb	-	2	-	-	2	-	21	12	12	14	12	15
Sr	135	254	120	211	193	202	369	172	273	181	132	148
Y	19	11	18	22	22	25	24	26	25	20	24	27
Zr	34	45	51	70	87	115	133	63	74	57	67	161
Nb	5	7	3	6	9	13	12	-	4	4	6	27
Ba	29	37	29	160	29	80	268	68	146	40	31	20
La	2	-	2	3	3	6	7	3	4	4	5	16
Ce	7	4	6	15	13	17	22	7	9	8	13	34

Note: tFe_2O_3 = total iron as Fe_2O_3;   - = below lower limit of detection;   * = dyke outcrop in melange belt

1 = plagiophyroc, phenocrysts = 50%;   2,3 = plagiophyric (2,(3) phenocrysts = 15(5)%); remainder of dykes aphyric

4 = plagioclase (9%)> olivine (1.2%)+clinopyroxene (1.7%) phenocrysts; 5 aphyric

6,7,8 = plagiophyric (6 = 21.5% phenocrysts)

Table 2.

Sample	PLUTONICS X335	MA238	X247	MEAN DYKE(22*)	MEAN GREEN PILLOW LAVA(3)	MEAN RED PILLOW LAVA(19)	MEAN OCEAN[1] RIDGE BASALT	ISLAND ARC[2] THOLEIITIC BASALT	MARGINAL BASIN BASALTS LAU BASIN[3]	SOUTH SANDWICH[4]
SiO_2	44.07	48.53	47.36	47.84	48.50	47.38	49.21	51.38	48.8	50.24
TiO_2	0.08	0.22	0.24	1.08	1.04	1.09	1.39	0.57	1.2	1.64
Al_2O_3	12.90	16.82	21.59	14.73	15.19	15.66	15.81	18.25	16.4	14.41
tFe_2O_3	6.47	5.23	5.29	9.57	9.34	8.87	10.20	10.13	9.7	9.74
MgO	21.72	12.19	8.63	10.20	8.88	5.81	8.53	6.13	8.6	7.99
CaO	12.43	15.56	14.72	11.85	9.81	12.78	11.14	11.81	12.6	11.01
Na_2O	1.04	1.89	2.31	2.21	3.27	3.67	2.71	1.81	2.4	3.44
K_2O	0.02	0.08	0.06	0.26	0.97	1.03	0.26	0.26	0.18	0.42
P_2O_5	-	0.01	0.01	0.11	0.03	0.11	0.15	0.02	0.08	0.17

Trace elements in ppm

Cr	1729	909	371	313	361	282	296	43	387	269
Ni	546	180	97	102	122	73	123	24	173	67
Zn	21	21	20	40	226	54	122	nd	68	69
Ca	8	15	19	16	16	16	18	18	nd	16
Rb	1	1	-	2	13	14	5	5	2	6
Sr	65	169	255	197	219	219	123	105	118	214
Y	-	5	4	22	25	23	43	nd	nd	30
Zr	2	14	21	79	68	81	100	55	nd	129
Nb	1	-	-	8	3	8	5	nd	nd	8
Ba	4	24	25	72	180	79	12	28	34	77
La	1	2	3	4	3	6	nd	nd	nd	9
Ce	2	3	1	12	7.7	19	nd	nd	nd	18
Th	-	-	-	-	-	-	2	nd	nd	1

Note: * = number of samples used in mean
- = below lower limit of detection
nd = not determined
X335 = mela-olivine gabbro
MA 238 = pyroxene gabbro
X247 = pyroxene leucogabbro

Taken from Saunders et al (1978) in press {

1 = Average MOR-basalt value (Engel et al 1965, Melson and Thompson 1971, Erlank and Kable 1976).
2 = Sample SSV9.1, porphyritic basalt from the South Sandwich Islands (Baker, 1978).
3 = Average of 11 least altered basalts, Lau Basin (Hawkins, 1976).
4 = Average of dredge 23, South Sandwich spreading centre (Saunders and Tarney, 1977).

of fractionation and thus indirectly of element mobility. Zr shows a range from 34 to 161 ppm in the combined dykes and lavas and has a similar range and mean value in all three lithological units of dykes, green pillow lavas and red pillow lavas. (Tables 1 and 2). This similarity of Zr and other incompatible element levels support the field evidence presented elsewhere (Abbotts 1978a) that the dykes and lavas are comagmatic. In view of this the levels of the incompatible alkaline elements K and Rb (Tables 1 and 2) are informative. These suggest leaching from the dykes, where Rb is frequently below the lower limit of detection, and/or addition in the upper crustal levels represented by the red pillow lavas. The affect is probably due to the circulating hydrothermal fluids near the ocean ridge and a similar cause and affect are noted in the Chilean Sarmiento Ophiolite by Saunders et al (in press 1978). Sodium shows similar evidence of mobility with mean values of 2.21 per cent, 3.27 per cent and 3.67 per cent in the dykes, green pillow lavas and red pillow lavas respectively. The "normal" ocean basalt levels in the dykes suggests a process largely of sea-water - induced enrichment in the upper crustal levels. Ba, and to an even greater degree Sr, show weak positive correlations with Zr indicating increasing metamorphic stability, as noted by Tarney et al (in press 1978). However occasional anomolously high Ba levels do occur. The Sr correlation is obscured by a modal affect whereby strongly plagiophyric rocks have higher Sr levels. The stability of Sr is probably due to its location in the metamorphism-resistant calcic plagioclase though the resulting modal control causes some scatter in the correlation.

The major elements Al, Ca, Fe and Mg and the minor compatible elements Ni and Cr scatter widely against Zr, partly as a result of modal variations and partly due to secondary mobility. Mg shows a progressive and substantial decrease in the green and red pillow lavas suggesting loss from the higher crustal levels. These affects, in conjunction with the evidence of alkali mobility, suggest extreme care with the use of Fe/Mg ratios, AFM diagrams and normative plots in the study of

ophiolitic rocks. Fe^{3+}/Fe^{2+} was not determined because of the susceptibility to alteration and for CIPW norm calculation an artificial ratio of $Fe^{3+}/Fe^{2+} + Fe^{3+} =$ 0.15 was assumed. Even with this standardization the scatter on Fig. 2., particularly in the lavas, shows the considerable affect of major element mobility. The lavas all appear undersaturated and plot as far as the Ne-Di boundary. This is believed to represent not a primary characteristic but to reflect their secondary enrichment in alkalies and loss of Mg. The 3 green pillow lavas, which occupy an intermediate dyke-lava position in the crust, are the least undersaturated of the lavas and just plot into the ridge-basalt field, confirming this conclusion. A similar affect is obvious in the AFM diagram (Fig. 3) where the dykes plot largely into the ridge-basalt field but the lavas are displaced significantly towards the alkali apex. The fresh plutonics, plotted for comparison, show a wide scatter due to large variations in the plagioclase : clinopyroxene modal ratio. These two affects, of modal variation and secondary mobility, cause a low-lying AFM trend and only limited evidence, predominantly within the dykes, of tholeiitic iron-enrichment. SiO_2 varies from 44 to 51 per cent in the dykes and lavas and shows no correlation with Zr or evidence of increase by differentiation. In addition there is none of the extensive SiO_2 metasomatism seen in the Troodos ophiolite and the mean SiO_2 value of 47.7 is low, even for ocean tholeiites. The elements Ti, P, Nb, Ce, La and, to a lesser extent, Y exhibit good positive linear correlations with Zr (Figs. 4-9) largely confirming the findings of previous workers (e.g. Pearce and Cann, 1973; Floyd and Winchester, 1976; Tarney et al, 1977) that they are stable during metamorphism to amphibolite grade.

MINOR, TRACE AND RARE-EARTH ELEMENTS

A plot of TiO_2 v Zr (Fig. 4) shows a good positive correlation with the development of a curvilinear relationship, a feature noted in other basalt suites (Tarney et al, 1978 in press). The Masirah dykes and lavas show a strong curvature and thus reach lower TiO_2 levels than many basalts (Fig. 4, inset). The discrimination
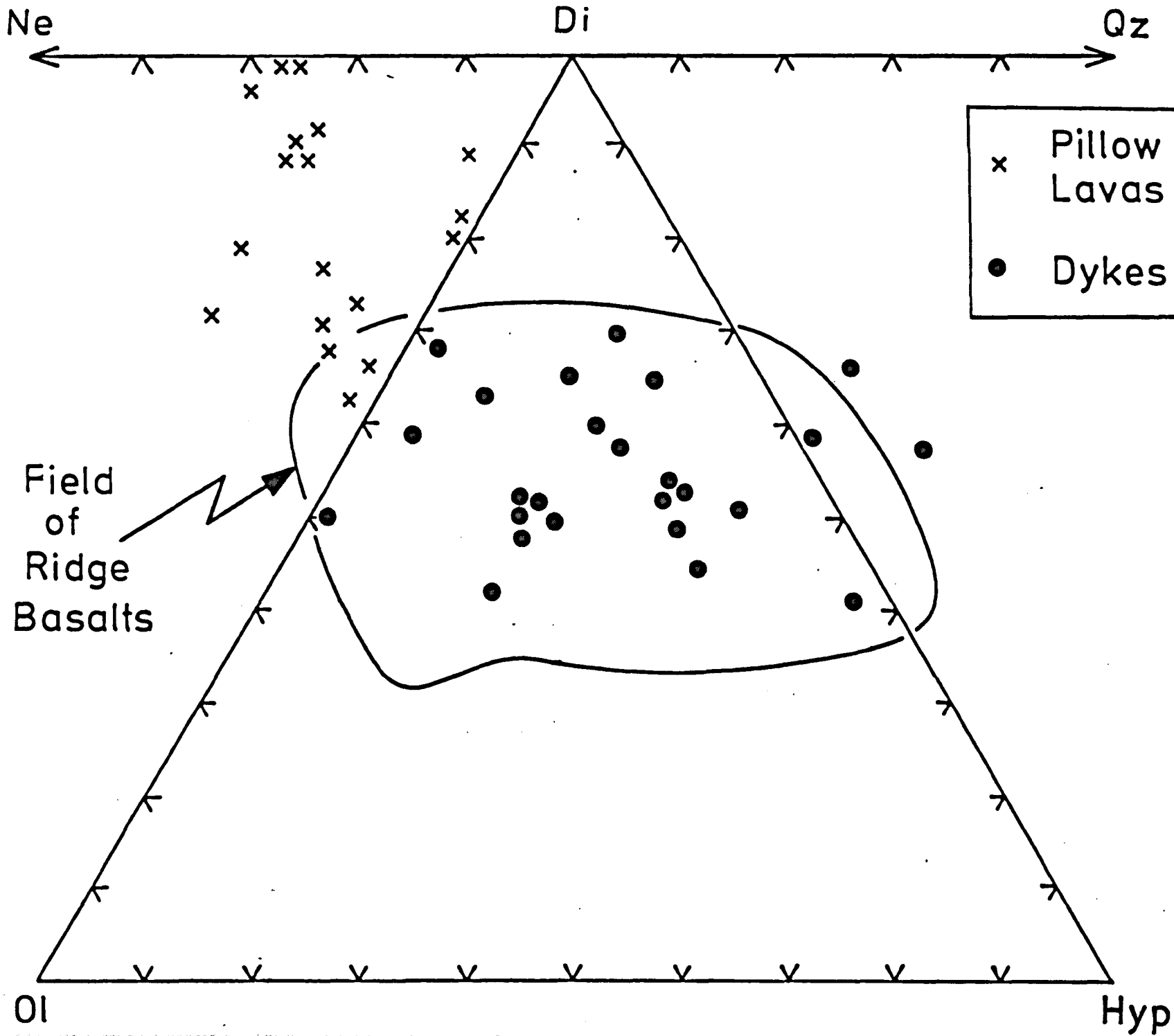
FIG.2. Normative compositions of the Masirah dykes and lavas plotted in the Ol-Di-Hy-Ne-Q_3 system. C.l.P.W. norms calculated assuming $Fe^{3+}/Fe^{2+} + Fe^{3+} = 0.15$. Field for ocean-floor basalts from Saunders et al (1978 in press).
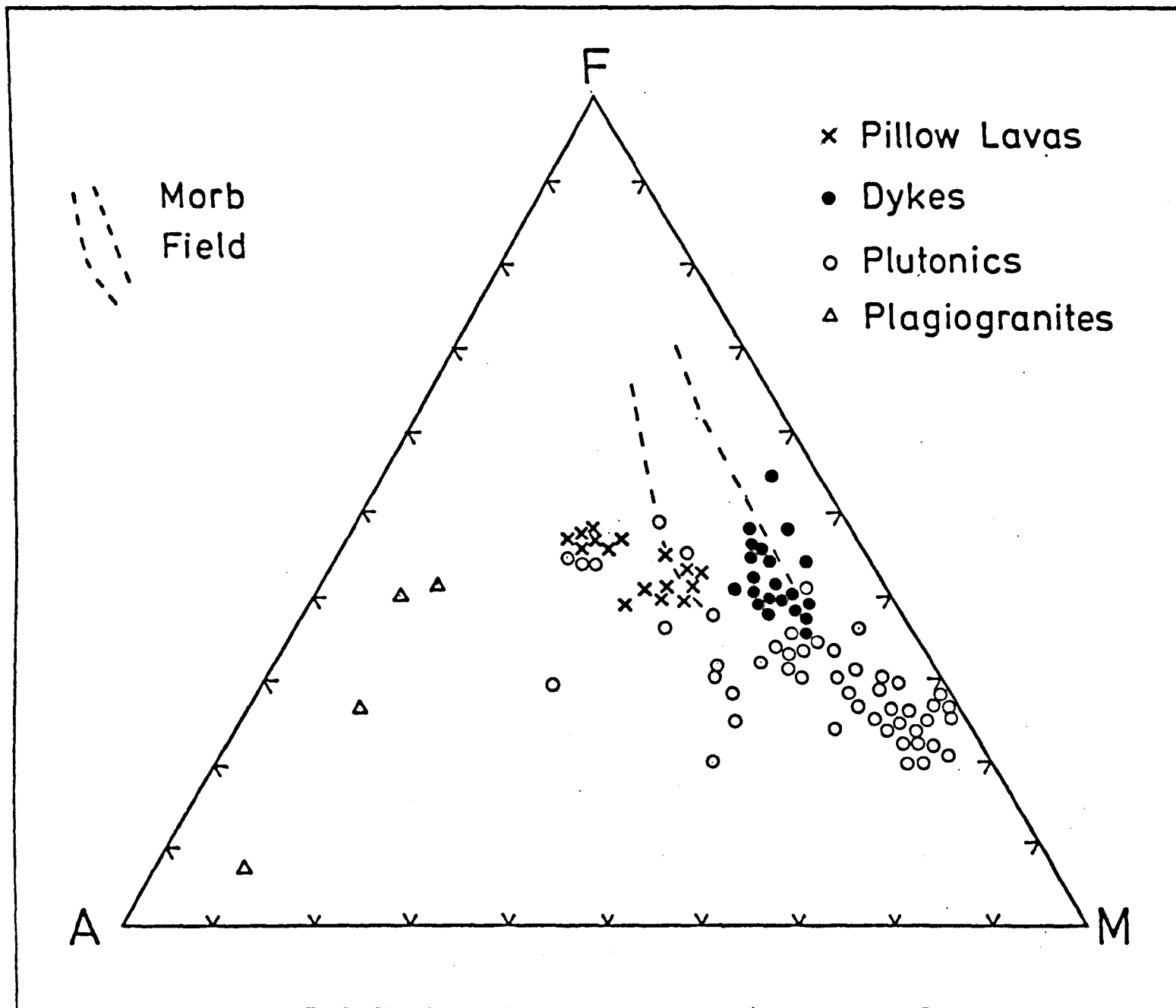
FIG.3. AFM diagram for Masirah Island lavas, dykes and plutonics. The transverse scatter in the plutonics is due to wide variations in the modal plagioclase: olivine-pyroxene ratio. The lavas show the effect of alkali enrichment and Mg loss.

FIG.4.   TiO$_2$ v Zr for Masirah dykes and lavas.
Inset shows comparison of Masirah TiO$_2$ v Zr
curvature with those of various ocean basalts
(data from Tarney et al, 1978 in press).
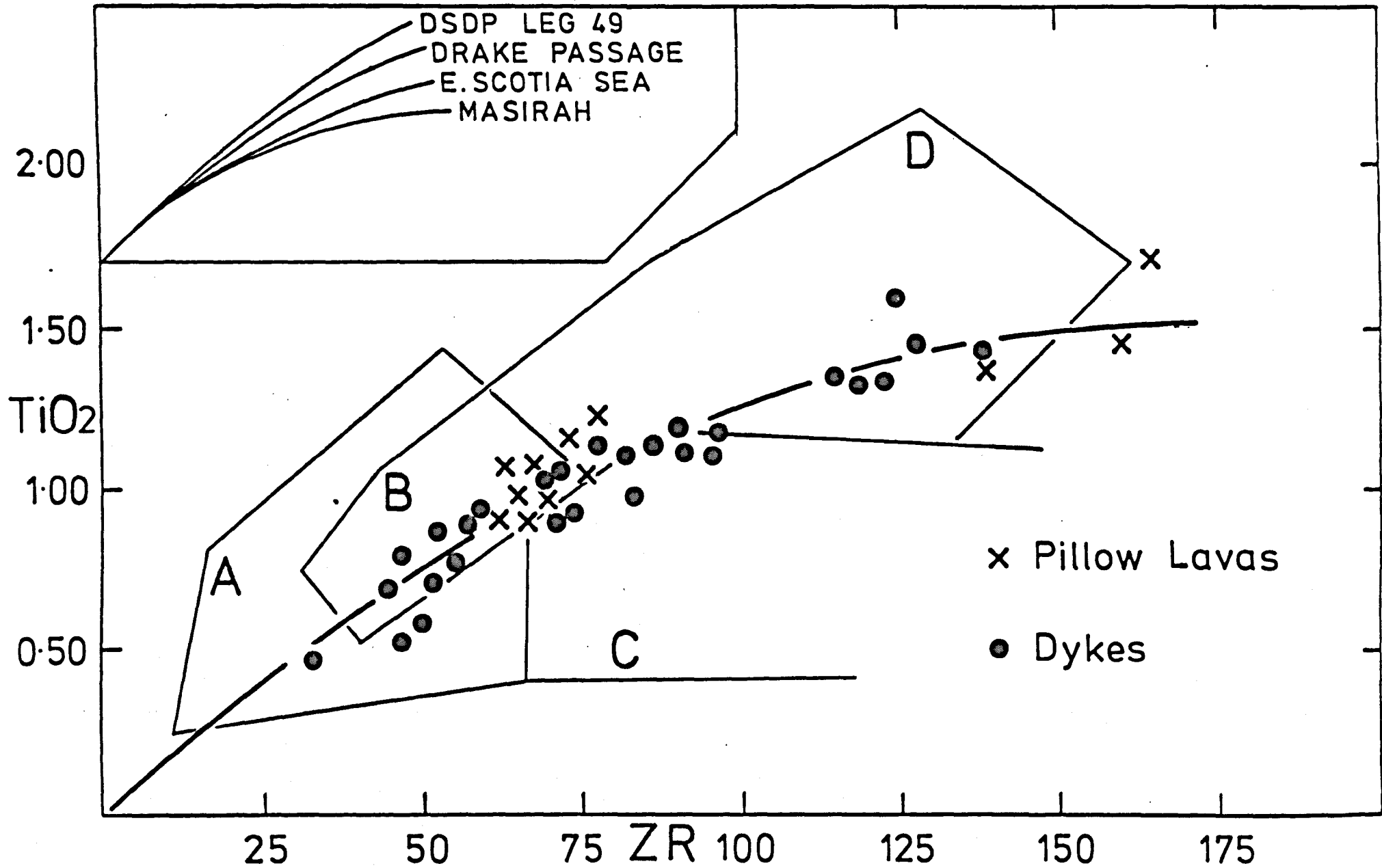
fields of Pearce and Cann (1973) have been placed on Fig. 4 and slightly favour an ocean floor origin.

Y levels are low in the dykes and lavas and show no significant correlation with Zr contents (Fig. 5A). Fig. 5B shows that Y correlates slightly better with Al_2O_3 than with Zr. This suggests that Y-Zr scatter is largely due to variations in the original plagioclase: clinopyroxene modal ratio, caused by the variable plagioclase phenocryst content (0-50 per cent). The appropriate Y partition coefficients, interpolated from Schnetzler and Philpotts (1970) and assuming $KD^Y = KD^{DY}$, are plagioclase = 0.06, diopside = 0.21, augite = 0.68. The variation from the aphyric MA 248 to MA 424 with 50% plagioclase phenocrysts, causing a clinopyroxene decrease from 50 per cent to 30 per cent of the mode, is sufficient to explain the decrease from 19 to 11 ppm Y (Table 1).

The original dyke mineralogy consisted of plagioclase + clinopyroxene + Fe-Ti ore $\pm$ olivine. In contrast to Y, which would be largely accommodated in clinopyroxene TiO_2 is found mainly in the ore phase (31-62% TiO_2) which is always present as a small percentage of the mode (2-3%) and less significantly in the clinopyroxene phase (0.3 - 0.9% TiO_2). Thus while Y is dependant on the modal plagioclase: clino-pyroxene variation, TiO_2 is also determined by the more constant ore phase and correlates well with Zr. The lavas, fine-grained and extensively altered, were not probed and it can only be suggested, because of co-geneity, similar liquidus phases, etc, that they might similarly be explained. The dykes and lavas plot largely in the ocean floor basalt field of Pearce and Cann (1973) in Fig. 6. Phosphorous and Niobium exhibit a good positive correlation with Zr and P v Zr is plotted in Fig. 7. The good correlations follow previous conclusions that these elements behave in-compatibly during fractionation in basalt systems and are immobile in metamorphism to amphibolite grade. The tholeiitic nature of the rocks is indicated on Fig. 7 using the discrimination lines of Floyd and Winchester (1975).
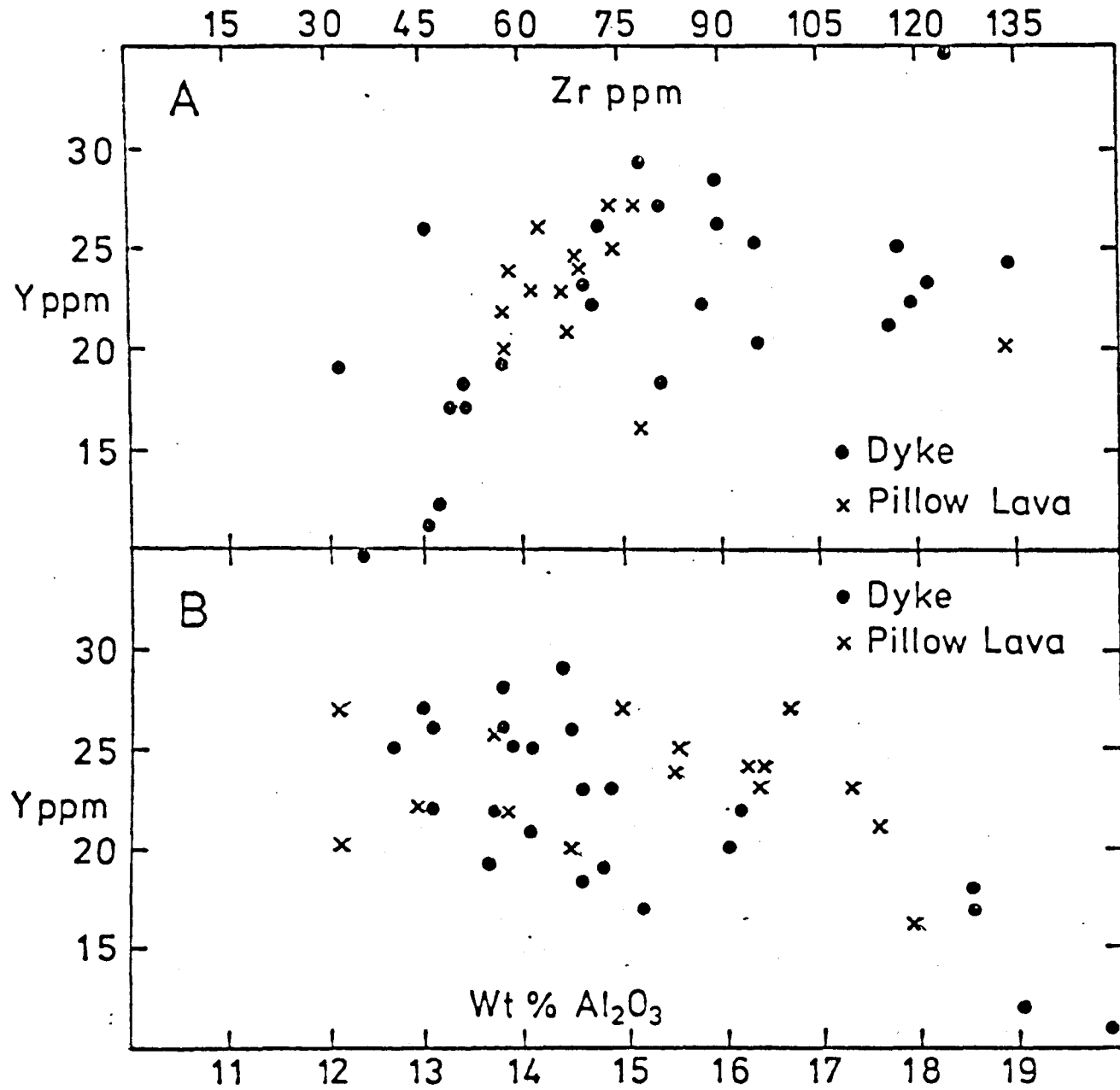
FIG.5. Plots of Y v Zr and Y v Al₂O₃ for Masirah dykes and lavas.
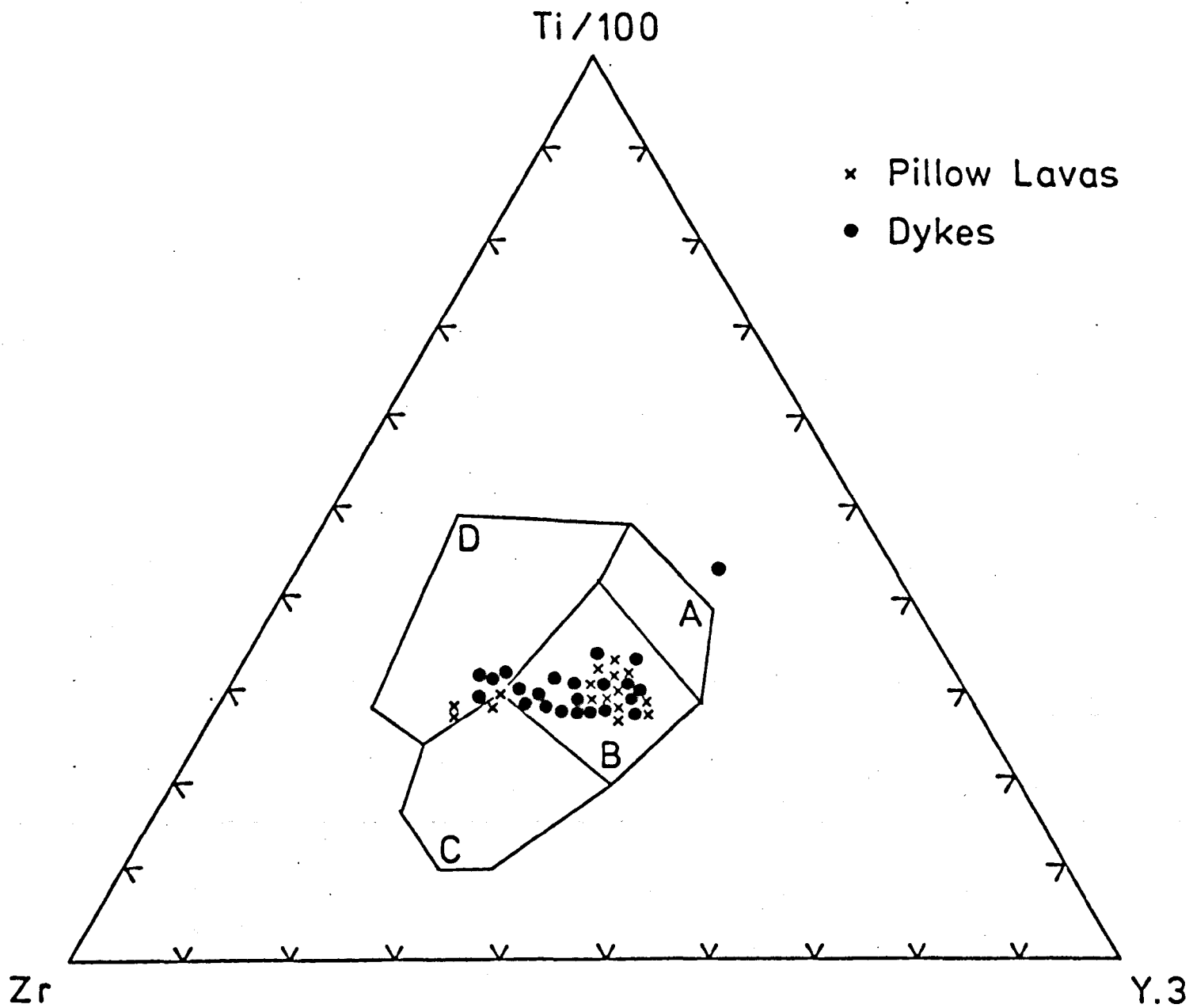
FIG.6. Masirah dykes and lavas plotted on the Ti v Zr v Y discrimination diagram of Pearce and Cann (1973). Field A, island arc tholeiites; Field B, mid-ocean ridge basalts; Field C, calc-alkaline basalts; Field D, within-plate basalts.
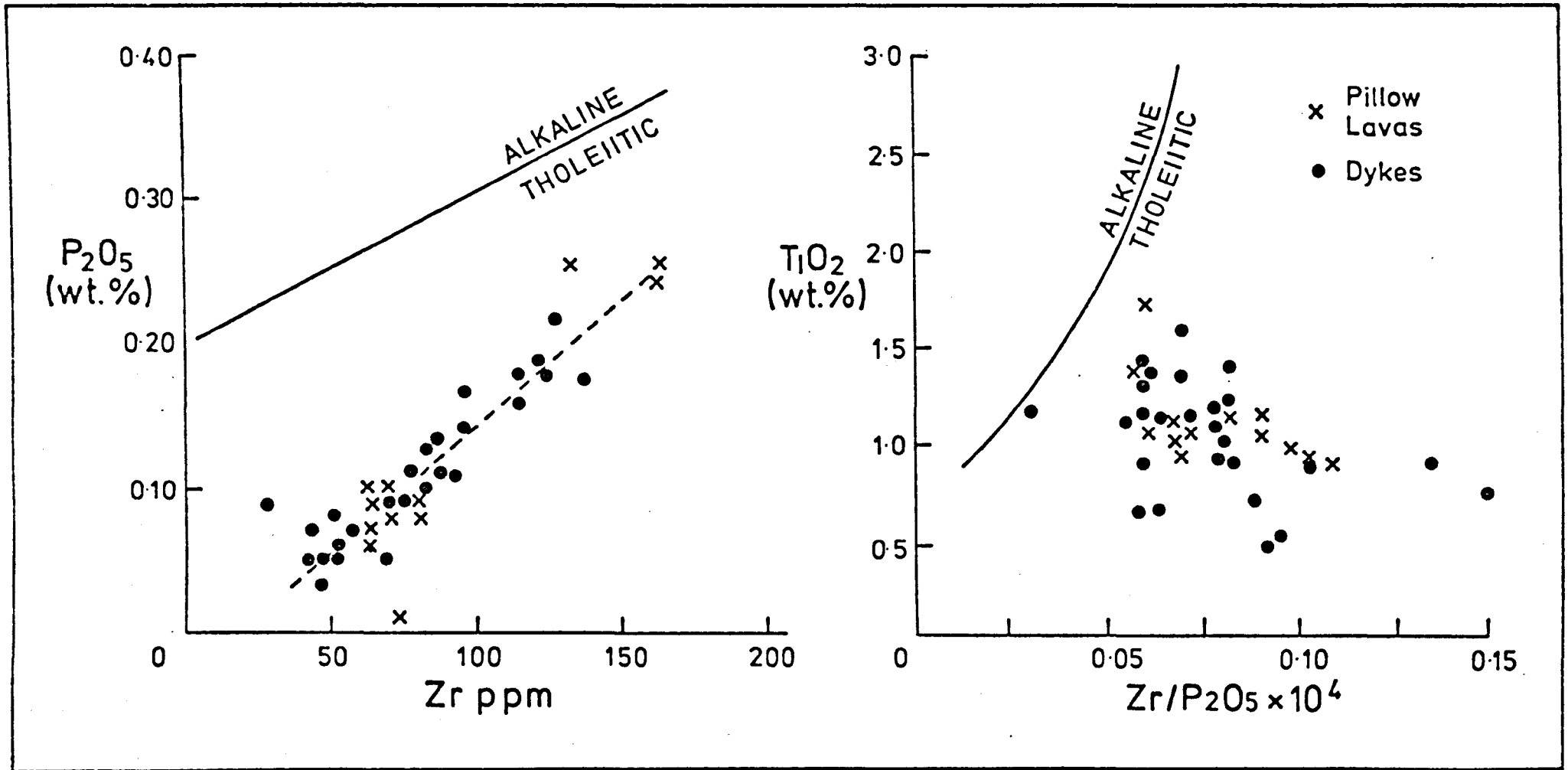
FIG.7. Discrimination plots of P_2O_5 v Zr and TiO_2 v Zr/P_2O_5 x 10^4 (after Floyd and Winchester, 1975) for Masirah dykes and lavas.

The light rare earths Ce and La show positive linear correlations with Zr, and Ce v Zr is shown in Fig. 8. This shows substantially less scatter than the corresponding Y plot (Fig. 5) probably because the LREE will be located in both the clinopyroxene and the fresher plagioclase phase and thus modal plagioclase: clinopyroxene variation will not affect its abundance. Consideration of Ce and Y abundances can give an insight into REE behaviour (e.g. Tarney et al, 1977; Saunders et al, in press) However the Y scatter does suggest care in this approach. The more primitive dykes and lavas (Zr = 34 - 51 ppm), excluding those highly plagiophyric dykes such as MA 424, have Ce_N/Y_N ratios of 0.5 - 0.9 at Y levels of 9 - 12 x chondrite while the more enriched rocks (Zr 114 - 161 ppm) have ratios of 1.3-3.0 at Y 10 - 14 x chondrite Though the broad ranges may be due to modal (? and mobility) effects, a positive correlation of Zr content and LREE enrichment is evident.

The chondrite-normalised REE patterns of dyke MA 183 (Zr = 119 ppm) and 4 gabbros of varying Zr content are shown in Fig. 9. All show approximately parallel and smooth patterns suggesting derivation from a similar source and there is a trend within the gabbros of increasing LREE enrichment with increasing overall REE abundance. Thus Ce_N/Yb_N values are 2.22, 2.43, 3.55 and 4.71 respectively.

DISCUSSION

The curvilinear relationship between TiO_2 and Zr suggests either that TiO_2 was retained in the mantle at lower levels of partial melting of the upwelling asthenosphere or that plutonic fractional crystallisation progressively removed TiO_2 from the melt which was periodically tapped to form the dykes and lavas. The gabbros show a trend of increasing LREE enrichment with increasing Zr and total REE levels. These two observations suggest the involvement of clinopyroxene in the fractionation history of these rocks because of the affinity of that phase for both the HREE and TiO_2 and because it is believed to occur as an early-melting mantle phase and is important in the Masirah fractional crystallisation sequence. This presents the problem of whether the fractionation occured during the partial melting or fractional
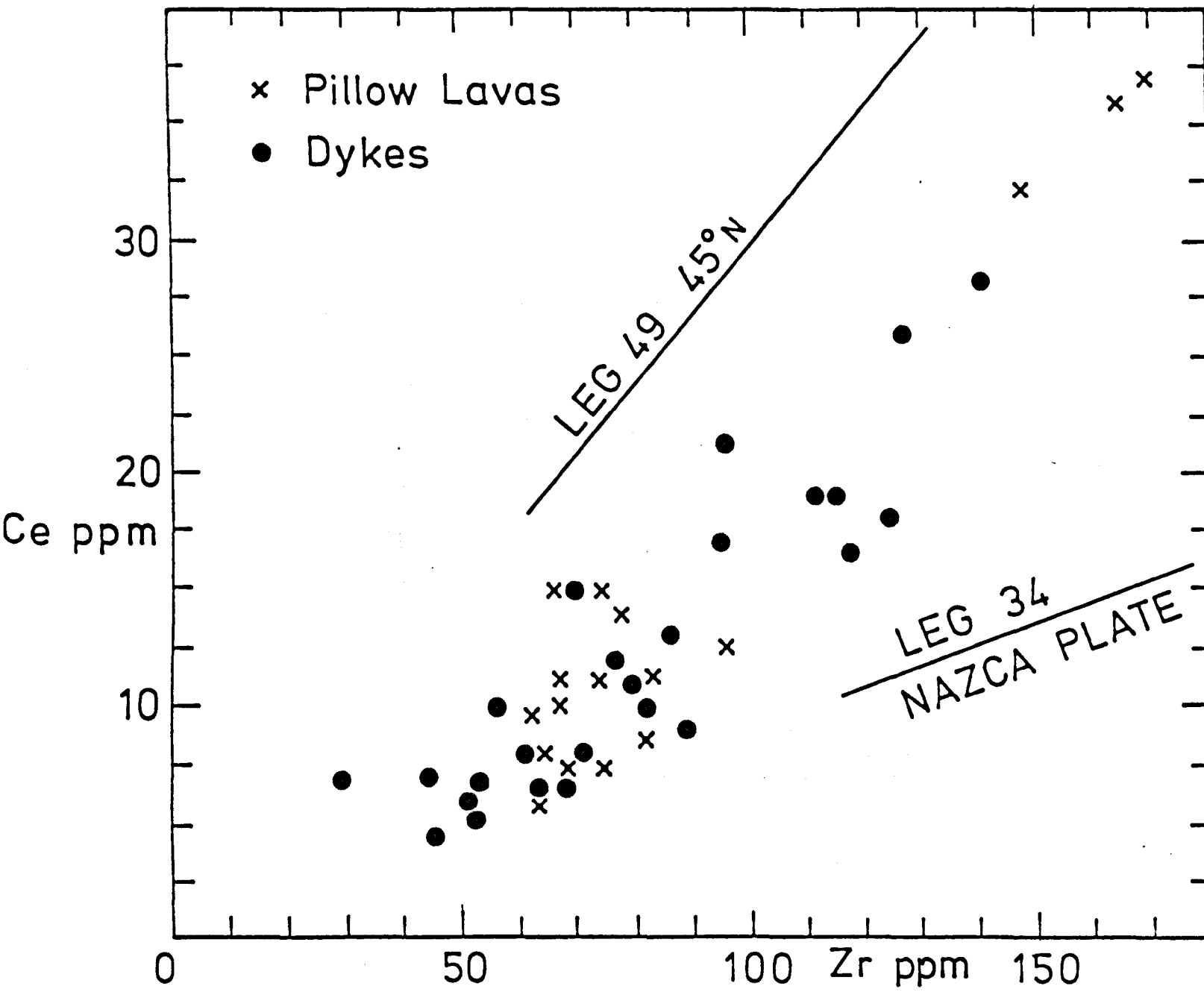
FIG.8. Ce v Zr for Masirah dykes and lavas. Shown for comparison are trends for the Nazca Plate (Rhodes et al, 1976; Thompson et al, 1976) and 45°N (Tarney et al, 1978 in press).
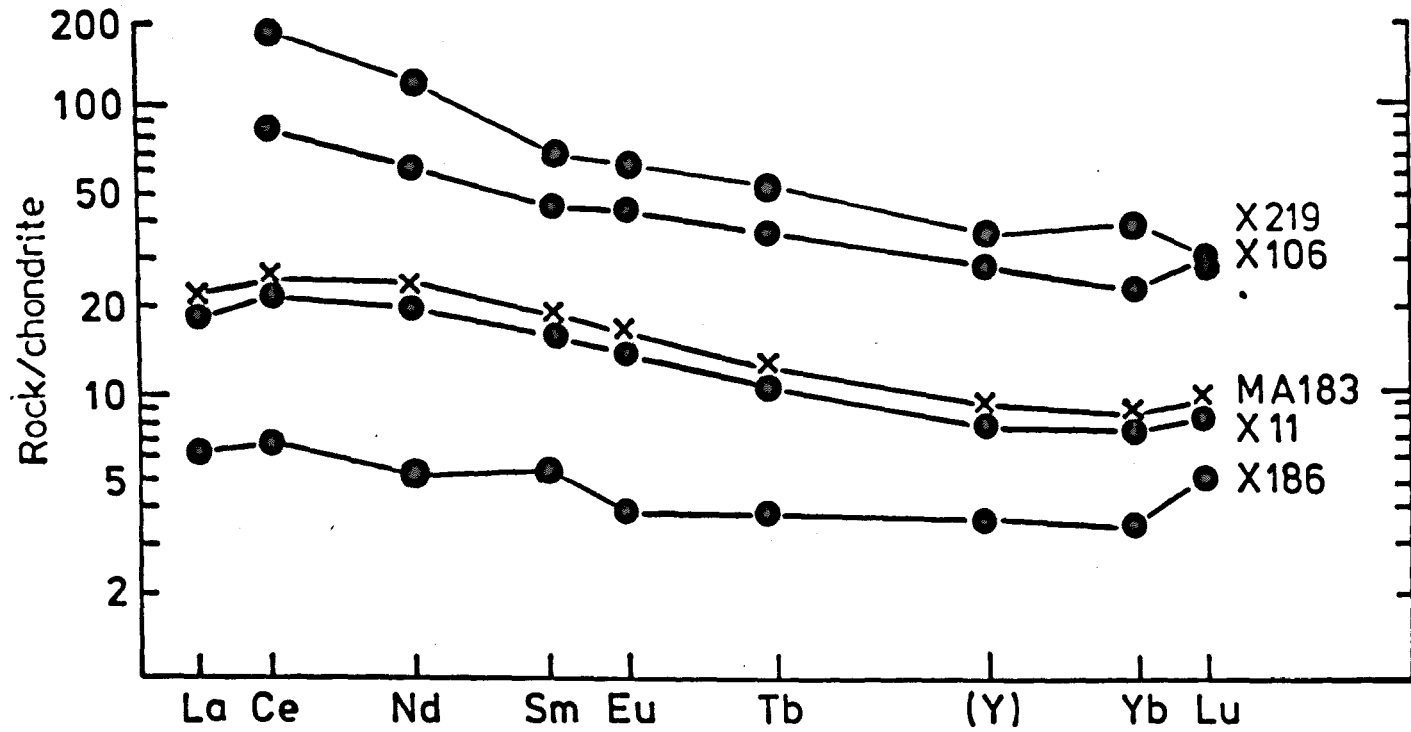
FIG.9. Chondrite normalised REE pattern of Masirah dyke MA183 (Zr = 115 ppm) compared with 4 plutonic samples showing variable stages of fractionation: X186 (Zr = 11 ppm), X11 (Zr = 53 ppm), X106 (Zr = 745 ppm) and X219 (Zr = 784 ppm).

crystallisation processes. Field and petrographic observations provide some support for the latter alternative. The occurrence of plutonic screens within the dyke unit, more common in their lower levels, and a minimum of 2 Km of plutonic rocks below the dykes suggests both the presence of ridge magma chamber(s) and crystallisation of roof gabbros in the manner of Dewey and Kidd (1977). It has been suggested elsewhere (Abbotts 1978a) that dyke intrusion occurred contemporaneous with such gabbro 'underplating' until the thickness of roof gabbros inhibited the intrusion of further dykes and the outer limit of active dyke intrusion was reached. Such a process provides the only satisfactory explanation of outcrops with dyke: screen ratios which vary from 100:0 to 0:100 in a downward direction.

Microprobe studies have been made of the important mineral phases of the dykes and the plutonic sequence. The plutonic phases, diopside (Fs 5.1 - 13.9) + calcic plagioclase (An 83-85) $\pm$ forsteritic olivine (Fo 80-87), and the low incompatible element levels of these rocks (e.g. Table 2: X355, MA 238), confirms their cumulate origin. Church and Riccio (1977) in the Bay of Islands ophiolite used cumulus phase compositions and known solid-liquid K_D values to calculate features of the magma chambers liquids from which the gabbros crystallised. A similar procedure was followed with the Masirah rocks and is illustrated in Fig. 10 where the determined clinopyroxene-liquid K_D of 0.24 compares favourably with a value of 0.237 determined by the above authors. The common problems with this work, of unjustified assumption of equilibrium crystallisation or accuracy of K_D values (in this case K_D olivine-liquid = 0.3) are minimized because (1) phase compositions are being used to determine the liquids from which they crystallised and not in conjunction with their present whole rock compositions and (2) for the broad conclusions made here, small errors in the assumed K_D are not significant. From Figure 11 it can be seen that the dyke FeO/MgO ratios (0.59 - 1.28) are encompassed within, and fall at the lower end of, the deduced FeO/MgO range of the liquids from which the plutonics crystallised (0.69 - 2.29). Thus the AFM diagram (Fig. 3) shows only limited overlap of

FIG.10. Diagram after Church and Riccio (1977), illustrating the range in FeO/MgO weight ratio of the liquids from which the Masirah plutonic rocks crystallised compared with the FeO/MgO range of the Masirah'dykes. Note: (1) the FeO/MgO liquid ratios were calculated assuming K_D ol-liq = 0.3 (Roeder and Emslie, 1970);

(2) K_D cpx-liq value of 0.24 is estimated using the FeO/MgO ratio of the liquids calculated from the composition of the coexisting olivine and shows good agreement with the work of Church and Riccio (op.cit); (3) the iron to magnesium ratio in the dykes is given as FeO (total iron)/MgO and is therefore a maximum value.
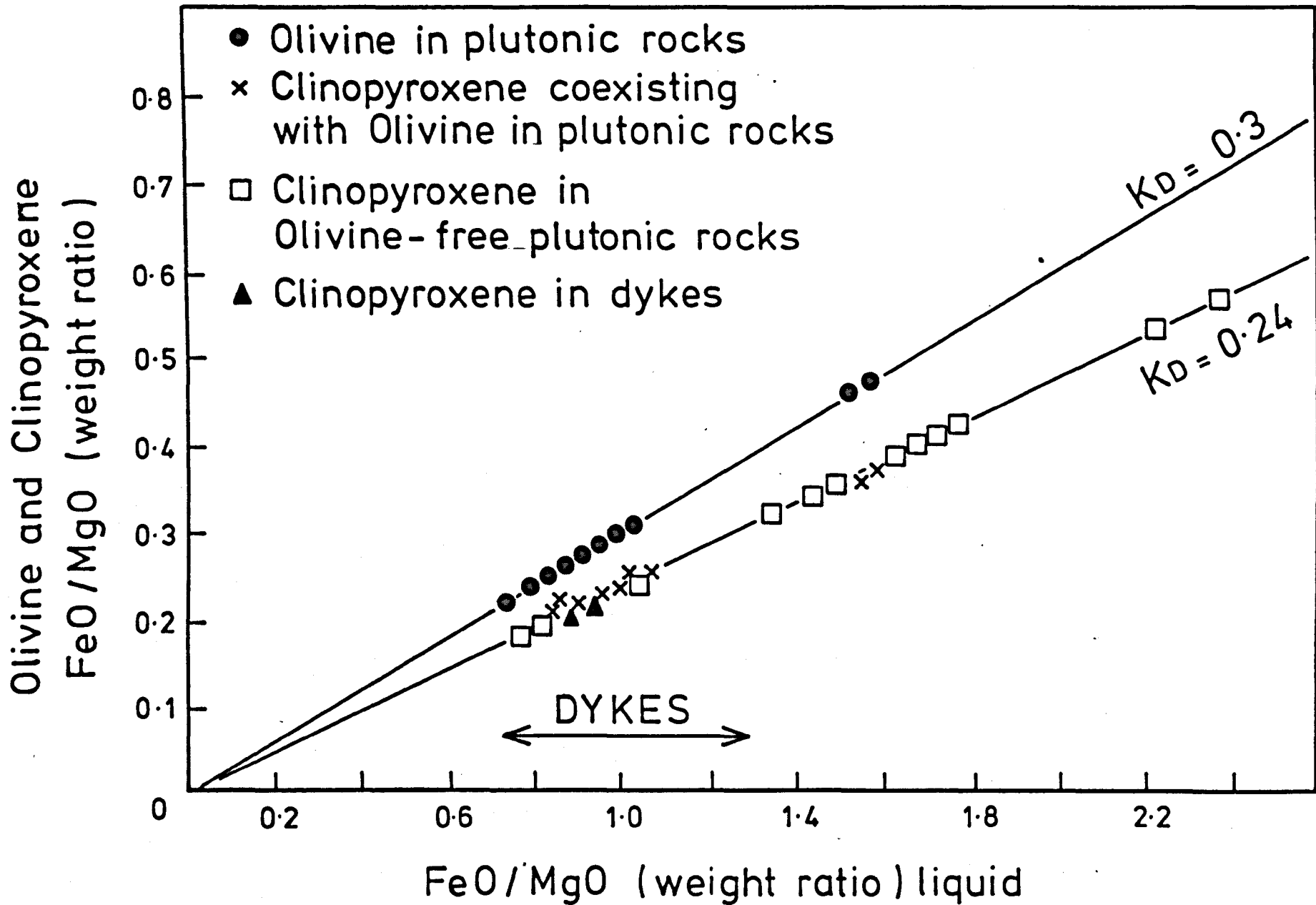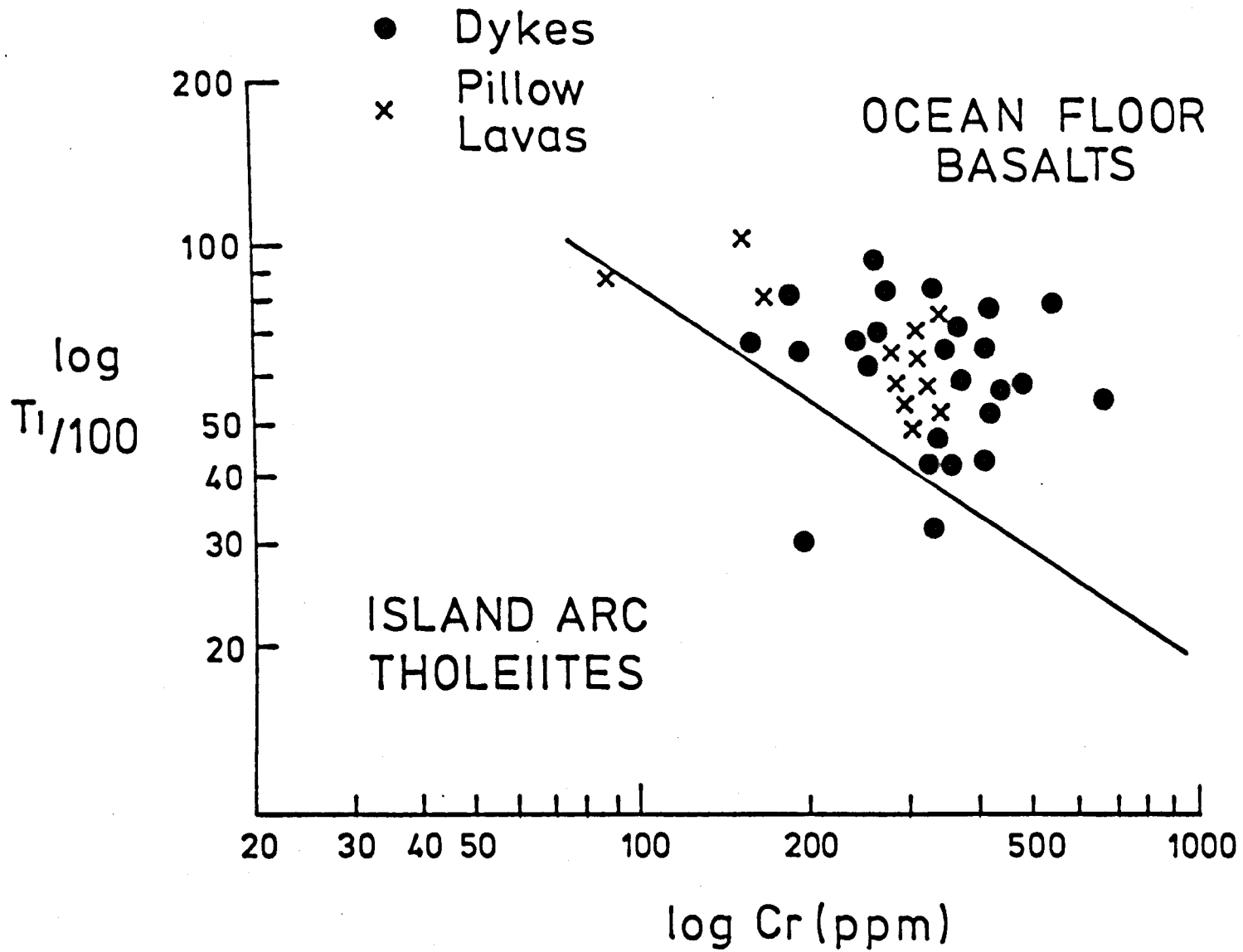
FIG.11.
Discrimination plot
of log Ti v log Cr
(after Pearce, 1975).
for Masirah dykes
and lavas.

dykes and plutonics not because the dykes are more differentiated but because the plutonics comprise minerals with FeO/MgO ratios lower than the liquids from which they crystallised. Low TiO_2 (0.2 - 0.4%) and high Cr_2O_3 (0.75 - 1.00%) levels in the clinopyroxene phenocrysts from the dykes and the clinopyroxene phase in the olivine-bearing-plutonics is further support for: (I) the equivalence of the dykes and the liquids from which the more primitive plutonics crystallised and (II) the earlier conclusions of dyke escape and roof gabbro crystallisation initially contemporaneous at the top of the magma chambers. These conclusions suggest that the chemistry of the more primitive dykes cannot be much affected by fractional crystallisation and will reflect the partial melting process. A similar deduction is obvious from their low Zr levels (34 - 51 ppm).

As noted before the plutonic fractional crystallisation sequence on Masirah comprised: chromite + olivine, olivine + plagioclase, olivine + plagioclase + diopside, plagioclase + diopside, plagioclase + diopside (+ minor Ti-ore). The mean TiO_2 content of 14 gabbro diopsides was 0.5% with a range of 0.2-1.0%, of which the lower values occur in earlier olivine dominated plutonics. In the absence of a Ti-ore phase in the gabbros,diopside contains virtually all of the TiO_2. Thus during fractional crystallisation Zr is incompatible with respect to all crystallising phases but TiO_2 is incorporated in the diopside phase, forming approximately 0.2-0.3% of the early diopside but increasing to 0.6-0.8% of the later. Though more compatible than Zr, $KD_{Ti}^{cpx/L}$ is well below unity (0.3-0.4). (Pearce 1978). The more compatible Ti behaviour, which may increase as the pyroxene becomes more fractionated (Fs_5 to $Fs_{13.9}$), probably explains the curvilinear TiO_2-Zr relationship (Fig. 4). Tarney et al (in press) suggest, that for Leg 49 basalts, such curvilinear relations are caused by compatible behaviour during the partial melting process. The evidence from Masirah, where there is control of the plutonic processes, suggests that fractional crystallisation can achieve the same result.

Nisbet and Pearce (1973) recorded a positive correlation of spreading rate and

basalt TiO_2 content but Tarney et al (in press) note a wide TiO_2 range from one drilling station (Site 407) which, at least in part, negates the correlation. Applying the correlation to these Masirah rocks would suggest, because of their low TiO_2 content, a slow spreading environment. This suggests the possible correlation of extensive fractional crystallisation with slower spreading but, in all likelihood, the attained TiO_2 level is dependent on several factors which may include: (i) the degree and relative importance of partial melting and fractional crystallisation processes (ii) the type, order of appearance and proportions of cummulate phases and (iii) the relative timing of dyke intrusion and plutonic fractional crystallisation. It is interesting to note that several geological parameters, including the thick dyke unit, the common plutonic screens and the lack of dyke one-way chilling all suggest a wide zone of intrusion and slow spreading (Abbotts 1978a).

The observation was made that there is increasing LREE enrichment with increasing Zr content. The plutonic phases olivine, plagioclase and diopside all have low partition coefficients for Zr and Ce (and the other LREE's) but diopside will fractionate the (HREE's (and Y)). Thus the patterns can be qualitatively explained by the plagioclase-diopside crystallisation.

This fractional crystallisation model for Masirah is reminiscent of the fractionation model developed for some ocean ridge basalts by Shido et al (1971), where initial olivine or plagioclase crystallisation leads to cotectic crystallisation of those two phases, which are then joined by clinopyroxene.

The Zr/Ce and Zr/La ratios of approximately 4.7 and 11.5 are lower than the chondritic ratios of 7 and 20 possibly suggesting LREE enrichment over Zr of the Masirah mantle source which is a similar conclusion to that drawn by Tarney et al (in press) for MAR basalts.

The tholeiitic nature of the Masirah lavas and dykes is shown by their low levels of TiO_2 (<1.74%), P_2O_5 (<0.26%) and Zr (<161 ppm), by their high Y/Nb ratios (1.0 -

11.0), their position in the discrimination plots of Floyd and Winchester (Fig. 6A and B) and their lack of SiO_2 enrichment with increasing FeO/MgO.

The question has been raised (e.g. Miyashiro, 1973) that some ophiolites might represent former island arcs and not products of ocean ridge spreading centres. Several lines of evidence negate this possibility on Masirah. Comparison of the mean Masirah dyke and lava analyses with an island arc tholeiite (Table 3) shows significantly higher levels of MgO, Cr, Ni and possibly of TiO_2 in the Masirah rocks, though substantial MgO and Ni loss from the red pillow lavas render that group some superficial similarity. The mean Al levels are also lower than in the island arc basalt but the more plagiophyric dykes do range up to, and include, the latter. The Masirah rocks compare more favourably with the mean MORB analysis. This point is illustrated in the Ti v Cr discrimination plot of Fig. 11 which demonstrates their ocean floor affinity. In addition, the presence of the regular, extensive, parallel, sheeted dykes seem more compatible with the spreading ridge mechanism. Finally there appears to be no geological evidence of subduction and associated island arc activity on this relatively passive Arabian continental margin in the late Cretaceous-early Tertiary.

Accepting their tholeiitic nature and spreading centre origin, one obvious question to be raised is the possibility of assigning a mid-ocean or marginal basin environment to the dykes. A small marginal basin seems to present advantages as the site of any ophiolite generation: a shallow marginal sea, the sandwiched position of the oceanic crust between block of continental crust, and the possibility of more bouyant mantle beneath back-arc marginal basins (Hawkins, 1976) should aid ophiolite preservation. Alternatively it has been suggested that Masirah may represent Cretaceous ocean floor generated during initial Indian Ocean opening i.e. at a mid-ocean ridge (Moseley and Abbotts, 1978; Abbotts, 1978a). Table 2 contains mean analyses of both mid-ocean ridge and marginal basin basalts. Saunders et al (in press) suggest that marginal basin basalts, particularly if representative of

early spreading, may have higher K, Rb, Ba, Ba/Sr and lower K/Rb than those from mid-ocean ridges. However they note that the Lau marginal basin (Hawkins, 1976) contains MORB-type levels of these elements whilst the enriched nature of some mid-ocean ridge basalts (e.g. 45°N) adds further problems to the discrimination.

Unfortunately in the Masirah dykes and lavas, and most other ophiolites, the elements K, Rb, Ba and probably Sr have been too mobile for use in classification. The dyke X 176 is representative of 4 dykes which contain higher levels of K, Rb, Sr and Ba than the other samples with compatable incompatible element levels. They were all collected from large sheeted dyke outcrops at the southern end of the ophiolite melange and not from the sheeted dyke complex itself. Similar to the other dykes in other chemical aspects, including Cr, Ni and incompatible levels, they cannot simply represent smaller degrees of partial melting. It is possible that they represent melting over a short period of an enriched (? deeper) source, perhaps tapped by the oceanic transform along which the melange is believed to form (Moseley and Abbotts, 1978). Alternatively a simple explanation might be secondary enrichment of these extreme mobile elements along a major weakness in the ocean crust which would encourage, and concentrate fluid movement.

The LREE enriched nature of the Masirah magma (Fig. 9) can be modelled by low ($\sim$ 10%) degrees of melting of a plagioclase peridotite source and the more primitive dykes, with low total REE levels, low Zr and low Ce_N/Y_N, by incremental melting of that peridotite (Abbotts, 1978d). The LREE characteristic is found in basalts of both mid-ocean ridge origin (MAR 45°N: Tarney et al, 1978) and marginal basin setting (Sarmiento Ophiolite of Chile: Saunders et al, 1978).

In the present state of knowledge and considering the alkali mobility in these Masirah samples, the large chemical variation within fresh MOR basalts and their extensive overlap with more enriched basin basalts, it seems impossible on chemical grounds, to assign Masirah to either ridge environment.

CHAPTER 6

EVIDENCE FOR BOTH AXIAL AND OFF-AXIS VOLCANISM IN THE MASIRAH OPHIOLITE

1. INTRODUCTION

Extensive studies have shown that the dominant rock-type extruded at mid-ocean ridges is an "oceanic-tholeiite" characterized by low incompatible element levels (e.g. Engel et al, 1965; Erlank and Kable, 1976). In contrast, many of the oceanic islands situated on the flanks of these ridges comprise central volcanoes extruding a more enriched alkali olivine basalt to trachyte series (e.g. Baker, 1969; Bonatti et al, 1977).

The Masirah Ophiolite contains three volcanic groups, each with distinctive field-relations, petrography and geochemistry. The first group consists of pillow lavas which are clearly comagmatic with the extensive sheeted dyke complex (Abbotts, 1978b and c). These are volumetrically much the most important and are termed the Axis Sequence pillow lavas, following the terminology used in the Troodos Complex (Gass and Smewing, 1973). The second group is here called the Melange Lavas and occurs only as tectonically-isolated blocks within the major melange zone which runs the length of the islands west coast (Fig.1). This structure may represent an on-land exposure of a major transform fault (Moseley and Abbotts, 1978). Finally, the Shinzi Volcanic Group forms a fault-bounded inlier within the tectonically disrupted lower crustal levels of the ophiolite (Fig.1).
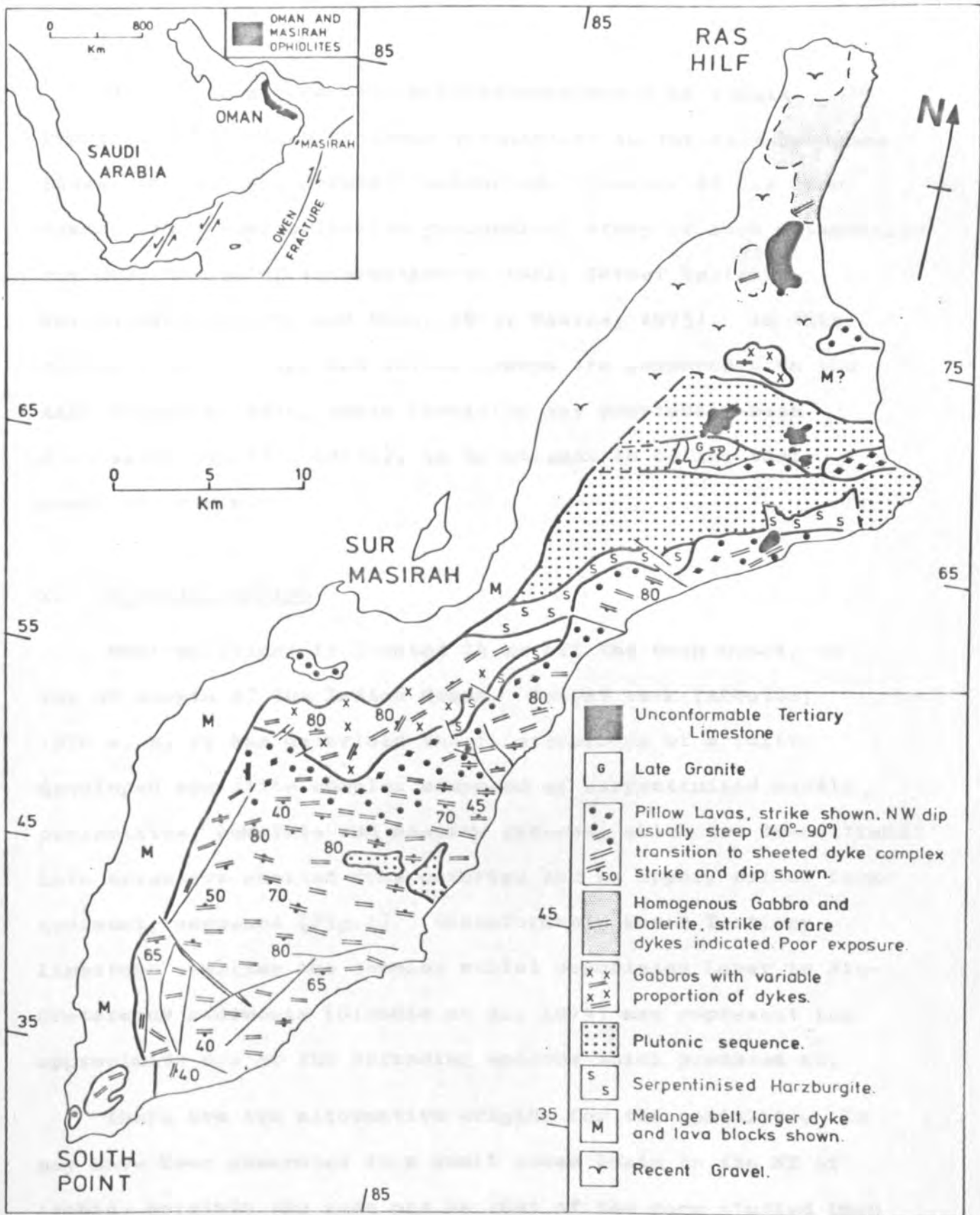
FIG.1. Geological map of Masirah Island showing the
disposition of the major lithological units.

All three groups have been metamorphosed at zeolite grade, locally reaching lower greenschist in the Axis Sequence lavas, and all are strongly weathered. However it has been demonstrated that selective geochemical study of such metabasalts can provide useful information on their former tectonic environment (Pearce and Cann, 1973; Pearce, 1975). In this context, the Melange and Shinzi groups are compared with the Axis Sequence lavas, whose chemistry has previously been discussed (Abbotts, 1978c), in an attempt to define their place of origin.

2. TECTONIC SETTING

Masirah Island is located 24 km off the Oman coast, on the NW margin of the Indian Ocean. Recent work (Abbotts, 1978 a, b, c) has described the relationships of a fully-developed ophiolite complex composed of serpentinised mantle peridotites, cumulate and massive gabbros, which are transitional into extensive sheeted dyke outcrops and an upper, pillow lava-sediment, sequence (Fig.1). Unconformable Lower Tertiary limestone overlies the complex whilst associated Lower to Mid-Cretaceous sediments (Glennie et al, 1974) may represent the approximate age of the spreading episode which produced it.

There are two alternative origins for the ophiolite. It may have been generated in a small ocean basin to the NE of Arabia, possibly the same one as that of the more studied Oman Ophiolite (Carney and Welland, 1974; Allemann and Peters, 1972), or it could have formed during spreading at an early Indian Ocean Ridge (see Abbotts, 1978b).

3. GEOLOGY OF THE VOLCANIC GROUPS

3.1. Axis Sequence Pillow Lavas

These are everywhere pillowed, no massive flows or evidence for sills was seen. There is a transitional downward sequence from red pillow lavas to green pillow lavas cut by occasional dykes to sheeted dyke complex. This correlates with a downward increase in metamorphic grade from zeolite facies in the red pillow lavas to low greenschist in the green lavas and is described elsewhere (Abbotts, 1978b). Toward their top the red pillow lavas are intercalated with, and then appear to be covered by, up to 20 m. of thinly-bedded marls and marly limestones.

Pillows, and rarer bolster shapes, have diameters ranging from 30-180 cm, averaging 70 cm, which seems typical for tholeiitic lava erupted into water (Dimroth et al, 1977). Occasionally brecciated hyaloclastic developments are seen. It is difficult to assess flow dimensions but N. of Macula (Fig.1) erosion has produced a series of steps in the pillow lavas, on an 8-10 m scale, which may reflect individual flow thickness there. Previous work (Abbotts, 1978b) estimated an approximate total lava thickness of 1.5 km, which compares with an average of 1 km, and range of 0.3-6.0 km, for recorded ophiolites (Coleman, 1977).

3.2. Melange Lavas

The ophiolite is bounded to the west by a major melange zone which has a minimum width of 5 km and is composed of a chaotic mixture of blocks of all of the ophiolitic lithologies,

often set in a serpentinite matrix (Moseley and Abbotts, 1978).
The zone cross-cuts all the ophiolite units, with a trend
which is almost perpendicular to that of the sheeted dykes, and
the actual steep contact is marked by extensive shearing.
Along the length of the melange there occur blocks of shallow-
water marine limestone, dated as Mid-Cretaceous (Glennie et al,
1974), which are not seen outside the zone. These are
particularly common in the south where they range up to 2 km
in length, with an elevation of 100 m. Occasionally primary
bedding is visible, but usually the blocks are extensively
brecciated and recrystallised, having a "marble"-like appearance.

The limestone blocks frequently sit on the basaltic
substrate of the Melange Lavas. These are often sheared or
brecciated but infrequently pillows are visible on a 30-60 cm
scale. Occasionally low-lying areas of red radiolarian cherts
outcrop in close proximity to the limestone-lava association.

In the south of the melange there are blocks both of red
pillow lavas and of sheeted dykes which are very similar in
field appearance to those of the Axis-Sequence, except for an
increased degree of internal brecciation.

3.3. Shinzi Volcanic Group
The volcanics at Shinzi occupy an area of 2.5 sq.km. They
include (1) pillowed basalt flows, which are cut by narrow
(< 50 cm) basaltic dykes; (2) structureless fine-grained
exposures which may represent thicker massive flow-units;
(3) areas composed of 2-6 m. thick basaltic sheets, which
possess dips of 40-50° in various directions, and may be parts

of an irregular dyke swarm. Occasionally these are more felsitic in appearance. The complexity of the area contrasts markedly with the simpler pillow lava-sheeted dyke relationships of the Axis sequence, perhaps suggesting an origin at other than the tensional spreading axis.

4. PETROGRAPHICAL CHARACTERISTICS

4.1. Axis sequence pillow lavas

These basalts are always plagiophyric, plagioclase phenocrysts forming 5-30% of the rock mode, whilst approximately 30% also contain olivine ($\pm$ chromite) phenocrysts and 10% clinopyroxene. The plagioclase is quite calcic (An85), with minor rim zoning (An85-80), suggesting equilibrium growth and rapid extrusion. Olivine is always pseudomorphed by calcite-serpentine or chlorite-actinolite combinations. It has been suggested that plagioclase dominance amongst the phenocryst phases, when olivine and/or clinopyroxene were coexisting liquidus phases in the magma chamber, may reflect the relative bouyancy in a basaltic liquid of that phase (Abbotts, 1978d). The pillows show a clear zonation from dark devitrified glassy-margin through an outer zone with quenched plagioclase microlites to a holocrystalline, frequently sub-ophitic, core. An original plagioclase-pyroxene-ore groundmass is largely replaced by the assemblages of zeolite-haematite-calcite-smectite (red pillow lava) or chlorite + ore $\pm$ actinolite (green pillow lava). The plagioclase laths however are relatively fresh. The lavas are frequently veined by calcite,

less commonly by quartz, epidote and chlorite. Occasional small (< 0.75 mm) vesicles form up to 5% of the lavas and are infilled by calcite, zeolite or smectite. Previous studies (Abbotts, 1978b) suggest that the metamorphic assemblages were probably developed during spreading centre hydrothermal circulation under a geothermal gradient of 170-200°C/Km.

4.2. Melange Lavas

These lavas are either aphyric or contain occasional (< 5%) plagioclase microphenocrysts; clinopyroxene occurs as a very rare liquidus phase. Groundmass textures are either vitrophyric, with quench microlites, or dominated by a fluidal alignment of fine plagioclase laths. In addition to plagioclase, oxidised opaque grains and an altered ?mesostasis complete the groundmass. Calcite and zeolite-infilled versicles are more common and of larger size than in the Axis sequence; they form up to 30% of the rocks and have diameters $\leqslant$ 4 mm. This suggests relatively shallow water and/or a greater volatile content. The occurrence of the lava, as substrate of shallow marine limestone, may indicate the former. The lavas frequently show evidence of brecciation in the late stages of solidification.

4.3. Shinzi Volcanic Group

These are dominantly metabasalts with similar fluidal textures to those of the Melange Lavas. Occasional trachytic varieties are pale orange-brown rocks with a groundmass of plagioclase laths and minor interstitial quartz. The lavas are

only rarely porphyritic with plagioclase, of a peculiar pinkish hue in hand-specimen, and rare clinopyroxene, forming up to 5% of the rock. Frequently the plagioclase phenocrysts are replaced by a quartz-epidote-calcite assemblage. Vesicularity varies from 0 to 25% with an infilling of calcite or zeolite. Both these, and the Melange lavas have suffered zeolite facies metamorphism.

5. GEOCHEMISTRY OF THE VOLCANIC GROUPS

5.1. Analytical techniques

34 lavas from these 3 volcanic groups have been analysed for major and trace elements using the University of Birmingham Philips PW1450 automatic X-ray fluorescence spectrometer. The methods employed are as set out in Abbotts (1978c) and Tarney et al (1978). Representative analyses of the Axis sequence pillow lavas and analyses of the Melange and Shinzi lavas are set out in Tables 1 and 2. Both tables are set out in order of increasing Zr.

5.2. Major and trace element mobility

It has been demonstrated elsewhere (Abbotts, 1978c) that the combined effects of low grade metamorphism and extensive weathering of the axis sequence pillow lavas has resulted in extensive mobility of many of the major and trace elements. In line with earlier work (e.g. Pearce and Cann, 1973; Floyd and Winchester, 1975), it was found that Ti, P, Zr, Nb, Y and the REE remained relatively stable and Al, Cr and Sr were only

Table 1 : Representative analyses of the Axis Sequence pillow lavas

Table 1	GREEN PILLOW LAVAS			RED PILLOW LAVAS												
Sample	X330	MA401	X326	MA400	X249	X323	MA391	MA139	MA142	X245PII	X245	MA448	MA440	MA437	MA439	MA422
SiO_2	49.41	48.27	47.79	47.30	47.87	48.29	47.90	48.96	48.29	47.38	48.64	47.30	45.61	43.98	45.44	47.66
TiO_2	1.05	0.99	1.08	0.83	0.94	0.89	0.91	0.91	0.94	1.04	1.05	1.21	0.95	1.35	1.48	1.74
Al_2O_3	13.71	16.35	15.51	14.38	13.76	16.35	17.28	17.10	17.46	16.34	17.06	15.00	17.85	12.06	12.85	12.10
tFe_2O_3	9.59	8.71	9.72	8.26	8.82	8.79	8.81	8.31	8.39	9.22	9.19	9.93	7.99	8.12	6.59	9.44
MgO	9.18	8.87	8.59	7.04	7.11	7.20	6.85	6.49	7.06	4.48	6.24	5.42	6.96	4.55	5.43	7.78
CaO	10.44	8.86	10.12	15.34	13.34	12.21	12.59	12.55	12.25	12.73	12.51	11.46	10.84	17.58	16.80	9.83
Na_2O	3.42	2.76	3.62	3.11	3.35	3.14	2.88	3.25	2.76	4.12	3.23	4.79	4.40	2.68	3.19	3.67
K_2O	0.25	1.81	0.86	0.36	1.06	0.89	0.87	1.07	1.01	0.92	0.51	1.02	0.56	2.30	1.97	1.57
P_2O_5	0.09	-	0.01	0.08	0.07	0.06	0.06	0.07	0.07	0.11	0.08	0.13	0.09	0.25	0.07	0.26
	99.10	96.70	97.34	96.68	96.41	98.36	98.29	98.85	98.42	96.53	98.75	96.27	95.23	92.90	94.03	94.06

Trace elements in p.p.m.

	X330	MA401	X326	MA400	X249	X323	MA391	MA139	MA142	X245PII	X245	MA448	MA440	MA437	MA439	MA422
Cr	405	314	364	344	391	347	314	316	312	321	292	185	205	189	86	170
Ni	139	99	129	102	112	95	83	98	90	52	67	53	44	77	81	82
Zn	131	493	53	56	60	58	34	35	39	54	50	67	50	53	57	68
Ga	14	16	17	16	18	19	17	16	15	14	17	17	19	16	18	18
Rb	2	26	12	4	13	11	11	16	15	12	7	16	9	46	18	16
Sr	172	211	273	181	168	153	206	227	199	132	208	225	608	462	388	148
Y	26	23	25	20	22	24	23	22	21	24	24	27	16	20	22	27
Zr	63	66	74	57	57	58	63	67	67	67	72	77	78	134	159	161
Nb	-	4	4	4	2	3	3	5	6	6	5	5	7	27	33	27
Ba	68	257	146	40	41	22	49	36	63	31	51	26	62	276	314	207
La	3	2	4	4	4	2	5	4	3	5	4	3	4	15	16	16
Ce	7	8	9	8	10	6	6	10	11	13	14	11	13	32	37	36
Pb	3	6	-	-	4	-	4	3	3	-	-	-	3	5	-	4
Th	-	-	-	-	-	-	-	-	-	-	-	-	-	3	6	3

Notes: tFe_2O_3 = total iron as Fe_2O_3; - = below lower limit of detection

Table 2 :
Whole-rock
analyses of the
Shinzi Volcanics
and the Melange
Lavas.

Table 2			SHINZI	VOLCANICS							MELANGE	LAVAS		
Sample	X220AI	X223	X222	MA425	X222A	X219A	MA427	X219I	MA246	X220A	X346	MA352	MA356	MA354
SiO_2	47.05	48.40	47.12	46.41	48.15	45.30	44.55	51.18	56.47	64.82	51.08	48.36	46.26	56.75
TiO_2	1.74	2.05	2.10	2.34	2.35	2.98	2.31	1.92	0.70	0.20	2.17	1.88	2.10	2.16
Al_2O_3	15.41	13.40	13.55	14.47	13.86	12.62	12.46	14.87	13.92	16.52	14.39	13.18	12.98	16.14
tFe_2O_3	9.22	9.36	8.14	10.12	8.93	10.17	8.84	10.85	8.78	3.60	8.61	5.98	7.55	5.61
MgO	5.26	9.02	5.91	10.42	6.17	7.43	5.70	3.77	5.31	0.14	6.30	3.82	5.36	2.01
CaO	13.87	8.41	11.92	6.88	9.75	9.73	14.96	7.81	3.24	0.61	5.48	11.92	13.33	8.35
Na_2O	2.25	3.56	3.49	3.38	4.36	2.30	2.46	3.31	5.18	7.23	6.35	3.46	3.39	3.96
K_2O	1.20	2.05	2.56	1.69	2.08	2.13	0.91	0.86	2.29	3.81	2.06	5.73	3.24	3.27
P_2O_5	0.29	0.32	0.45	0.72	0.48	0.57	0.79	0.72	0.13	0.02	0.28	0.43	0.57	0.76
	96.28	96.71	95.39	96.41	96.28	93.12	92.99	95.43	96.02	96.94	96.71	94.74	94.90	99.21

Trace elements in p.p.m.

	X220AI	X223	X222	MA425	X222A	X219A	MA427	X219I	MA246	X220A	X346	MA352	MA356	MA354
Cr	83	264	146	126	138	25	10	-	-	-	186	147	126	6
Ni	62	99	64	76	59	26	24	-	-	-	76	90	54	2
Zn	54	72	63	62	61	73	66	161	76	81	71	52	64	111
Ca	22	18	18	18	18	23	27	30	34	42	19	16	20	23
Rb	22	22	36	27	31	33	30	11	29	64	19	68	41	28
Sr	448	384	494	560	518	272	484	301	143	37	115	334	258	459
Y	23	27	26	31	31	37	33	67	71	98	25	26	24	50
Zr	163	209	240	248	273	293	331	480	633	1286	173	260	283	396
Nb	30	44	52	56	59	67	86	69	85	182	34	70	82	105
Ba	225	433	603	461	425	471	30	486	391	98	429	1303	513	457
La	18	16	16	38	31	40	54	37	55	101	21	39	36	37
Ce	40	44	54	77	67	82	111	89	120	196	41	77	72	106
Pb	4	5	4	-	4	-	13	-	-	5	5	4	7	8
Th	-	3	6	6	4	5	14	-	11	29	3	11	12	11

Note: tFe_2O_3 = total iron as Fe_2O_3; - = below lower limit of detection

Open circles = Melange lavas, triangles = Shinzi Volcanics

A : ophiolite dykes = filled circles, pillow lavas = crosses

B : ophiolite dykes and lavas = dotted field.
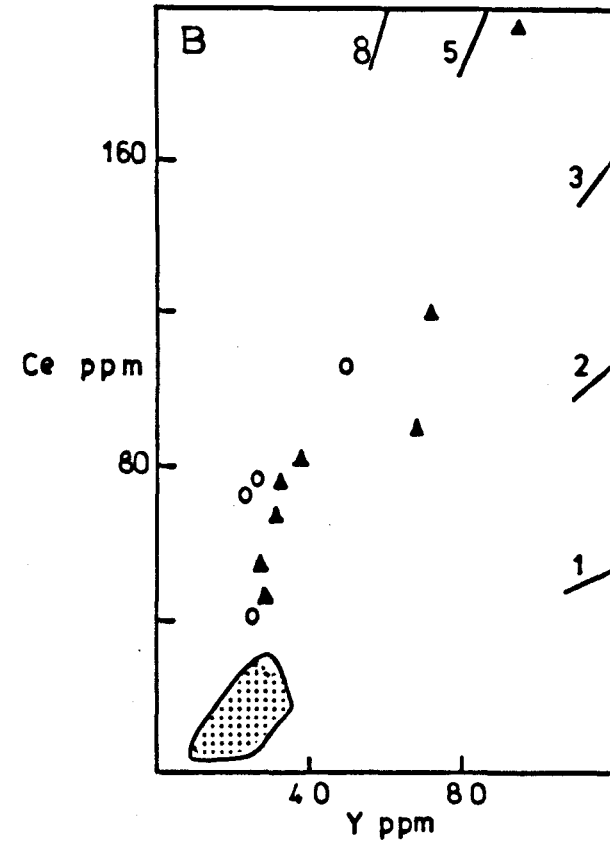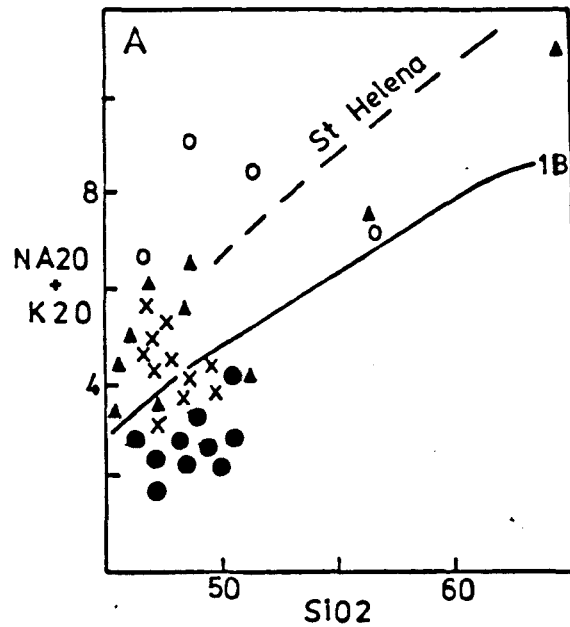
FIG.2A. Alkali -silica plot for the various volcanic groups of Masirah Island. 1B is the alkaline-subalkaline division of Irvine and Baragar (1971). The dashed line is the St. Helena trend (Baker, 1969).

FIG.2B. X-ray fluorescence Ce-Y data for the volcanic groups. Chondrite normalised Ce/Y ratios are indicated.
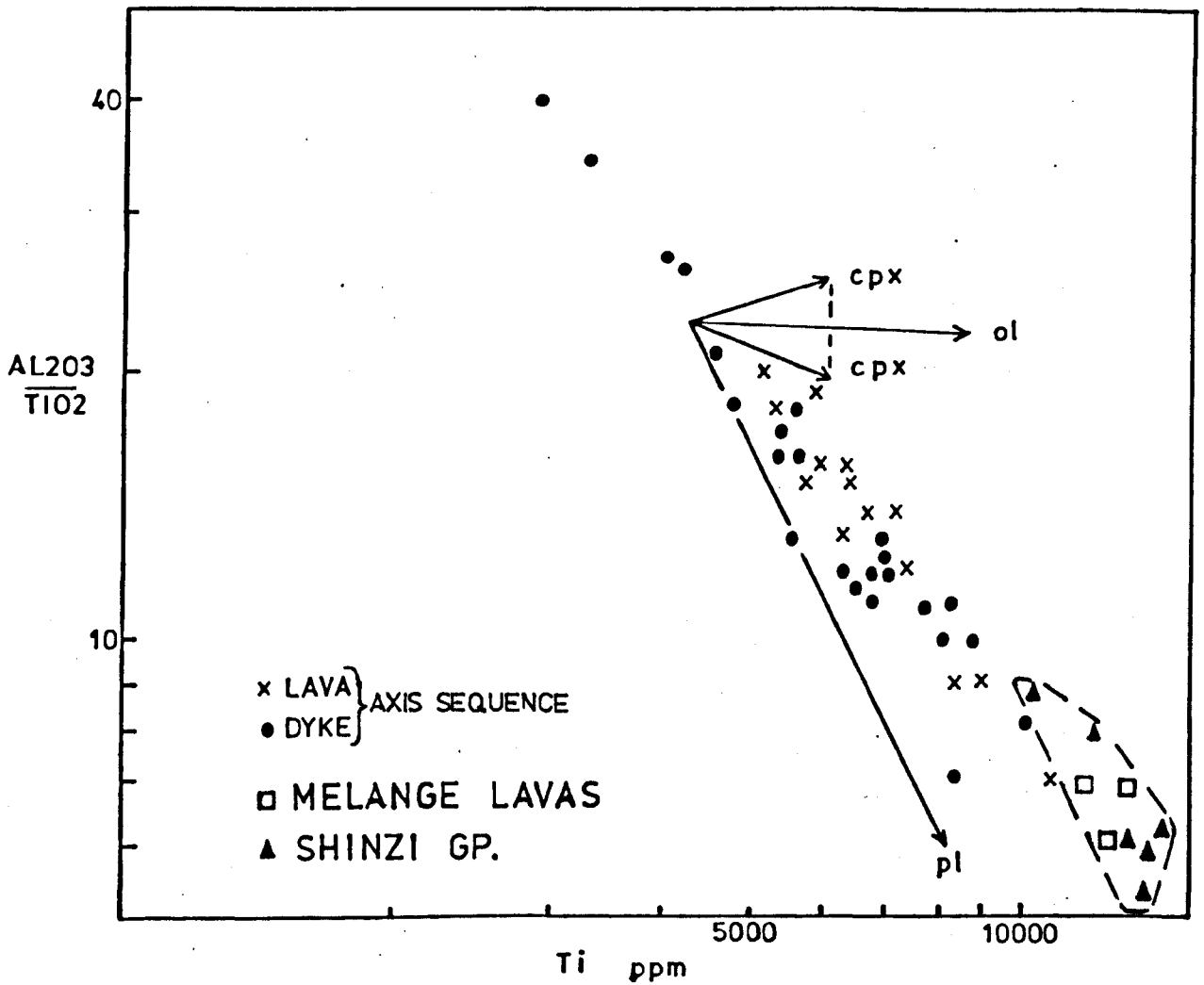
FIG.3. Al_2O_3/TiO_2 v Ti for the various volcanic groups on Masirah. The fractionation vectors and their lengths are 50% crystallisation (taken from Pearce and Flower, 1978).

moderately affected. Figure 2A. plots total alkalies v SiO_2 and illustrates the effects of elemental mobility. The axis sequence lavas are enriched in alkalies relative to the "ocean floor" levels in the dykes, to the extent that they plot into the alkaline field of Irvine and Baragar (1972). This is wholly attributed to secondary enrichment (Abbotts, 1978c), a process which makes it difficult to interpret the apparently higher alkali levels in the Melange lavas. Consequently geochemical study here is confined to the more immobile elements listed above.

5.3. Al_2O_3 / TiO_2 ratio of the basalts

The Al_2O_3 /TiO_2 ratio can be used to assess the degree of involvement of plagioclase in the fractionation history of a rock (Pearce and Flower, 1978). The Al_2O_3 /TiO_2 v Ti diagram (Fig.3) is taken from Abbotts (1978c), where the dyke-lava variation was shown to be caused largely by fractional crystallisation dominated by plagioclase.

The Shinzi and Melange basalts have been added to the diagram and can be seen to fall on the Axis-sequence trend but to possess higher Ti and lower Al_2O_3 /TiO_2. These effects can be caused either by extensive fractional crystallisation or smaller degrees of mantle partial melting. Extensive fractional crystallisation of the axis sequence liquids produced trondhjemites with 72% SiO_2 and Ce_N/Y_N ratios of $\leqslant$ 4 (Abbotts, 1978c). The Melange-Shinzi basalts have Ce_N/Y_N ratios of 4-8 (Fig.2.B) at SiO_2 44-50% which cannot be linked by fractional crystallisation with the axis-sequence.

The suggestion is that they represent smaller degrees of partial melting. The limited trend within the Shinzi basalts suggests some plagioclase fractional crystallisation controlling their internal chemical evolution. This is confirmed by the low Sr in the more fractionated lavas (Table 2).

5.4. Immobile minor and trace elements

Zr is extensively used as an index of fractionation. Fig.4 plots the incompatible elements Y, Nb and TiO_2 v Zr. The good correlations of these elements confirm previous conclusions of their stability in low grade metamorphism. The high levels of Zr, Nb and Ti in the Melange-Shinzi basalts involve only minimal overlap with the ocean-floor tholeiite levels in the axis sequence and are more typical of basalts of alkalic affinity (e.g. Floyd and Winchester, 1975). Y levels are similar in the basalts of all three groups and the element only reaches higher concentrations in the Shinzi intermediate volcanics. Nb is noticeably enriched in both Shinzi and Melange lavas so that the Zr/Nb and Y/Nb levels, of 4.0-5.0 and < 0.75 respectively, are typical alkali-basalt values (Pearce and Cann, 1973; Floyd and Winchester, 1975). High TiO_2 in these basalts (> 2.0%) is a further alkalic trait. The Shinzi Gp shows a marked inflexion at 2.5-3.0% TiO_2 and 250 ppm Zr which is probably caused by Fe-Ti ore precipitation (Fig.4). The same event in the tholeiitic axis sequence liquid occurred at 100-120 ppm Zr (Abbotts, 1978d). These early terminations of Fe-Ti enrichment probably reflect high H_2O content in the magmas (Saunders et al, 1978). The enriched nature of the

o MELANGE LAVAS   x SHINZI LAVAS
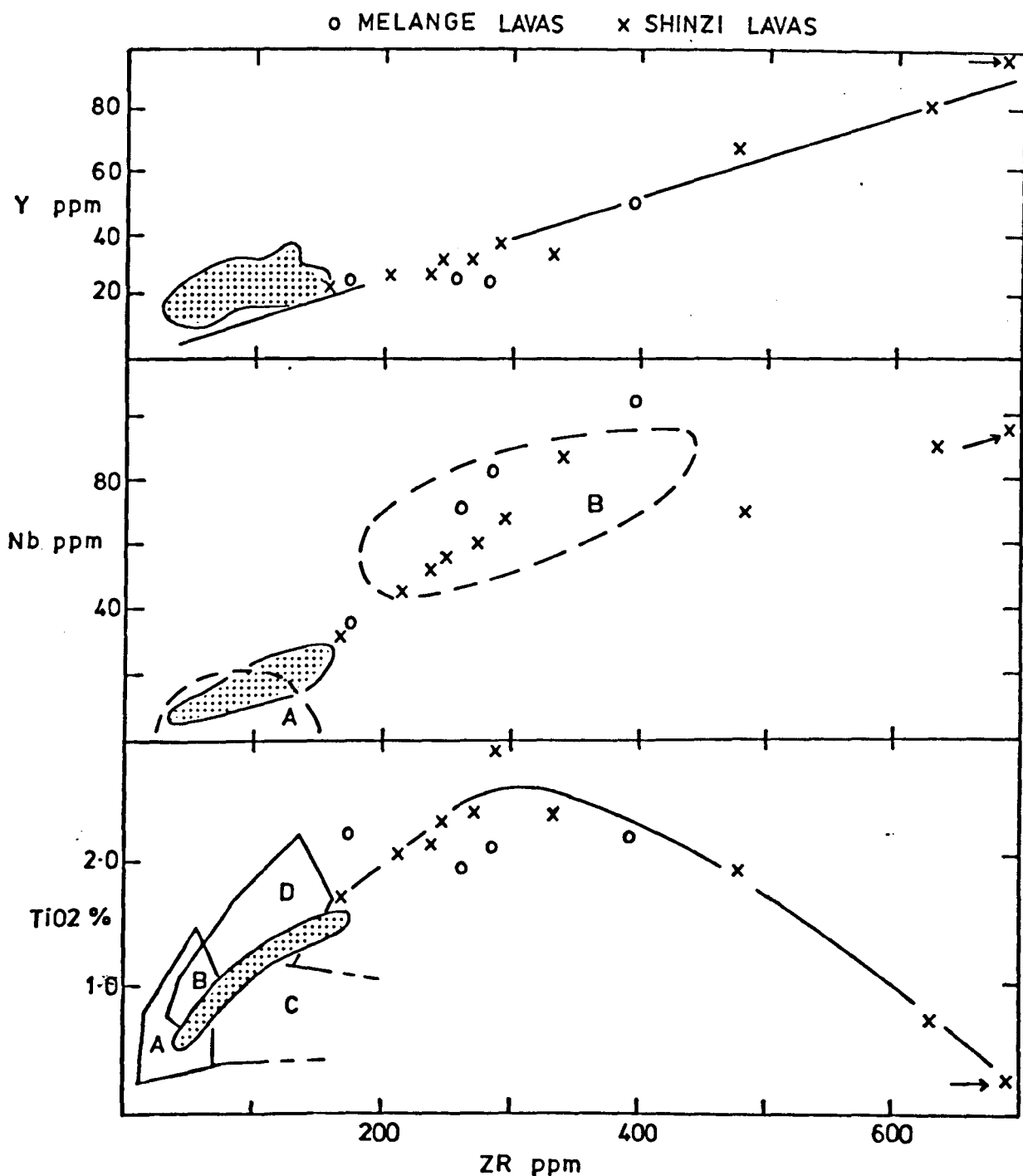
FIG.4. Plots of Y, Nb and TiO_2 v Zr for the various volcanic groups on Masirah. The dotted fields are the axis sequence dyke and lava compositions from Abbotts (1978c). The solid lines are visual best-fits for the Shinzi Volcanics. The fields on the Nb v Zr plot are from Bass et al, 1972 (A = ocean ridge tholeiites, B = oceanic island basalts). The fields on the TiO_2 v Zr plot are from Pearce and Cann (1973):

A + B = low potassium tholeiite
C + B = calc-alkaline basalt
D + B = ocean floor basalt.

Shinzi-Melange basalts means that neither group plot in the
Ti-Zr discrimination fields of Pearce and Cann (1973).

The three most enriched lavas in the Axis Sequence group
(Table 1 : MA422, 437, 439) have incompatible levels approaching
those of the Shinzi-Melange basalts. It is interesting to
note that these are all from the blocks which are tectonically
incorporated in the melange zone. In field appearance and
petrography these resemble the Axis Sequence, their tectonic
position is similar to the Melange Lavas, and their chemistry
is transitional between the two. A recent review of the
geochemistry of the sheeted dykes (Abbotts, 1978c) noted the
similarly-enriched nature of blocks incorporated in the melange.

In the Ti-Zr-Y discrimination diagram of Fig.5 the Melange
and Shinzi basalts plot in and around the "within-plate" basalt
field. This field includes basalts of the oceanic islands and
the continental rifts, both of which vary from being tholeiitic
to highly alkalic in character. The discrimination plots of
Floyd and Winchester (1975) shown in Fig.6. confirm the mildly
alkalic nature of the Melange-Shinzi lavas.

Fig. 2B. illustrates the Ce-Y relationships of these
volcanic rocks. This plot gives an impression of the REE
characteristics of a rock because Y behaves like an intermediate
to heavy REE (Saunders et al, 1978, Weaver et al, 1978). The
high Ce (= LREE) and Ce_N/Y_N (= LREE enrichment) levels of the
Shinzi-Melange lavas are evident on this plot. This degree of
LREE enrichment is common in alkalic ocean island basalts (e.g.
Guadalupe: Batiza, 1977; Easter Island: Bonatti et al, 1977).
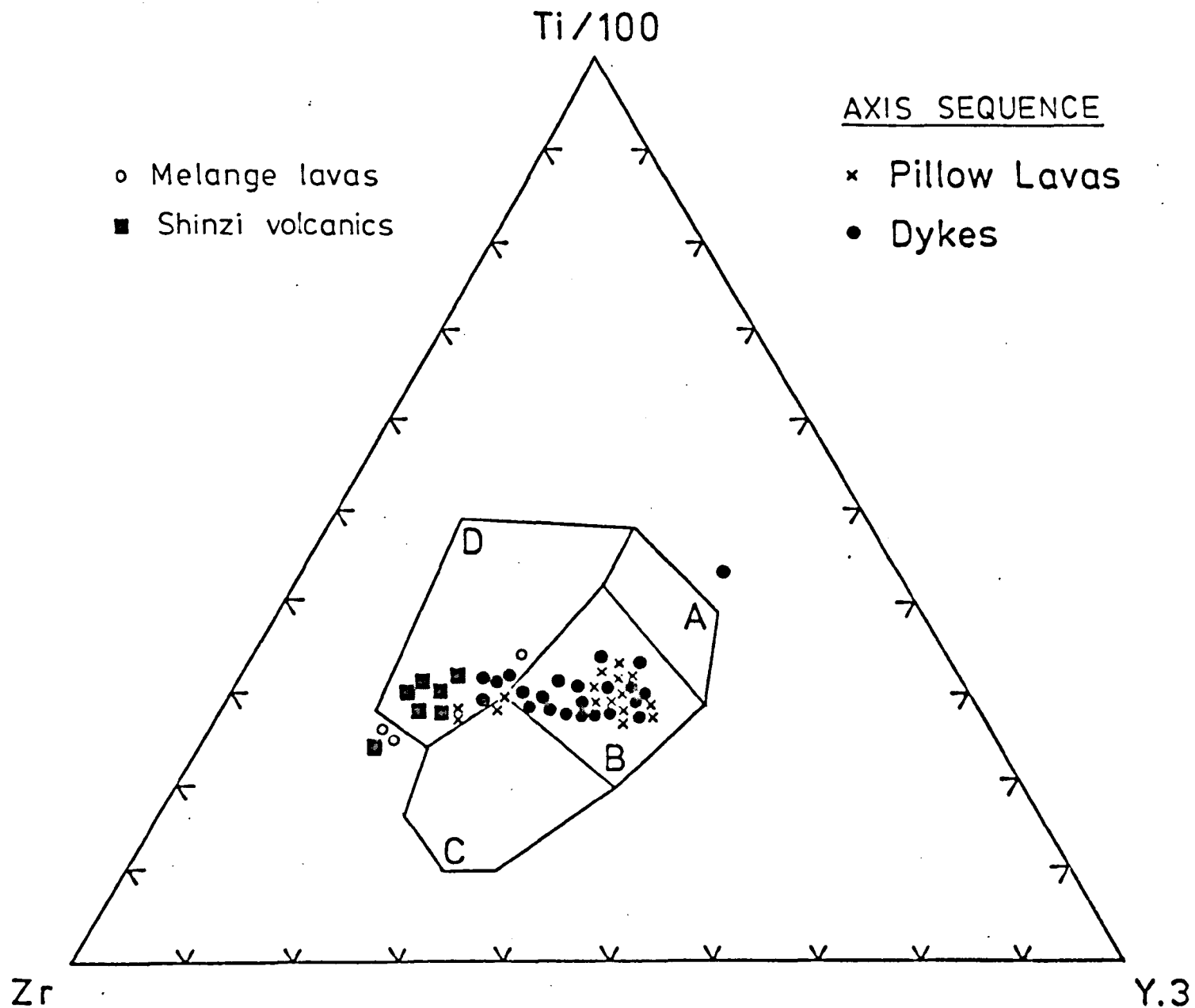
FIG.5. Basalts of the Shinzi and Melange groups added to the Ti - Zr-Y discrimination diagram from Abbotts, 1978c (after Pearce and Cann, 1973).

Field A = island arc tholeiites

Field B = mid-ocean ridge basalts

Field C = calc-alkaline basalts

Field D = within-plate basalts.
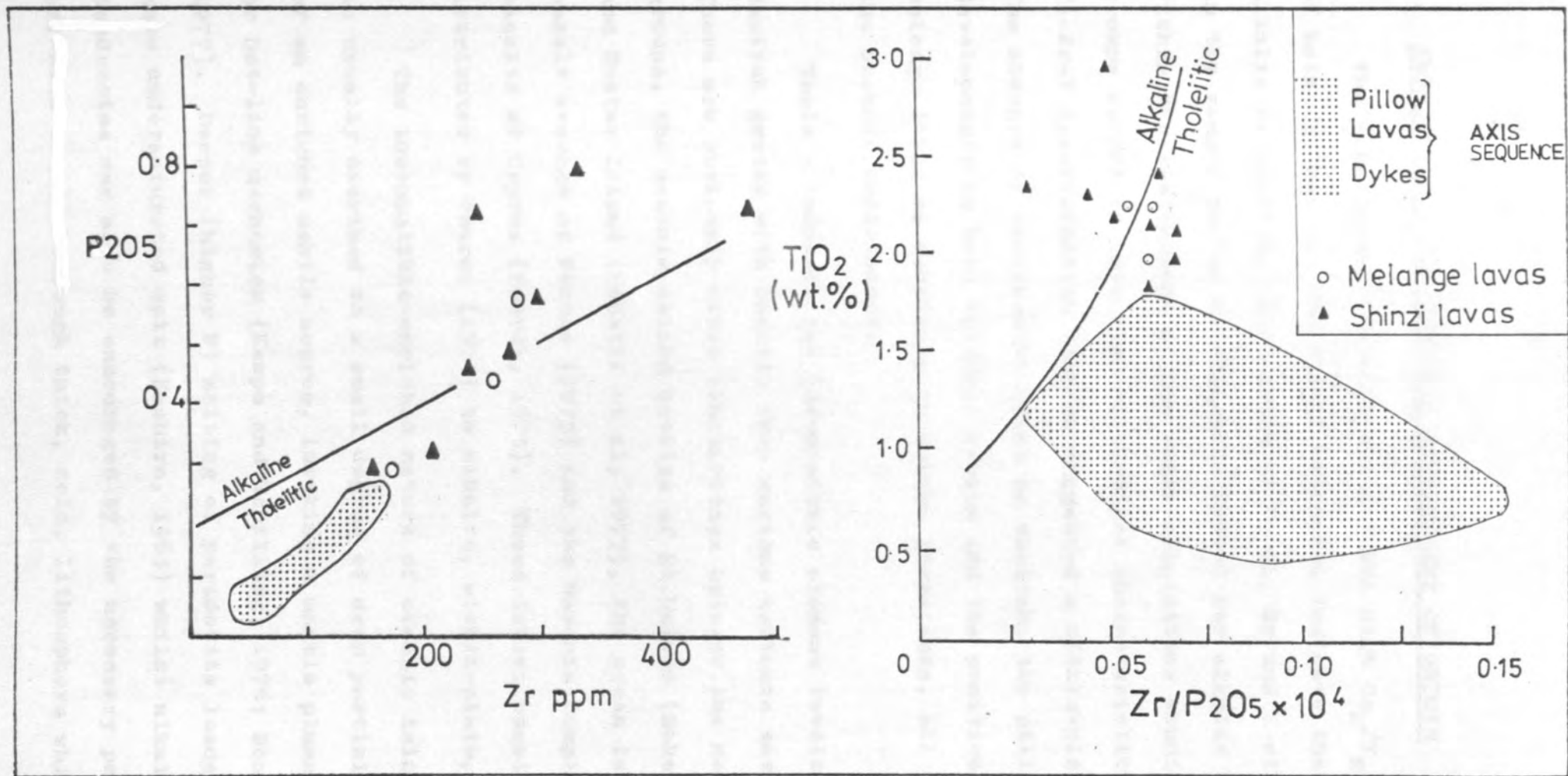
FIG.6. Discrimination plots of P_2O_5 v Zr and TiO_2 v Zr/P_2O_5 x 10^4 (after Floyd and Winchester, 1975) for the basalts of the various volcanic groups on Masirah.

6. IMPLICATIONS FOR TECTONIC ENVIRONMENT OF ORIGIN

The high incompatible levels and the high Ce_N/Y_N ratios of both the Melange and Shinzi volcanics indicate their alkalic affinities. The levels of P, Ti, Zr and Y all fall in the ranges quoted by Miyashiro (1978) for alkalic basalts. Within the limitations of the small populations studied, both groups appear to have similar chemical characteristics. The Ti-Zr-Y discrimination diagram suggested a within-plate origin. The absence of continental crust on Masirah, the pillowed developments in both volcanic groups and the position of the melange lavas as substrate to marine limestones, all indicate the oceanic environment.

Table 3 compares the incompatible element levels in the Masirah groups with basalts from various tectonic environments. There are obviously close similarities between the Melange-Shinzi groups, the oceanic island basalts of St.Helena (Baker, 1969) and Easter Island (Bonatti et al, 1977), the ocean island basalt average of Pearce (1975) and the Mamonia Complex basalts of Cyprus (Pearce, 1975). These latter basalts were attributed by Pearce (1975) to alkalic, within-plate, volcanism.

The incompatible-enriched nature of oceanic island basalts is usually ascribed to a small degree of deep partial melting of an enriched mantle source, invoking a mantle plume, hot-spot or hot-line mechanism (Kempe and Schilling, 1976; Bonatti et al 1977). Deeper (higher P) melting of peridotite leads to a more undersaturated melt (Kushiro, 1965) whilst alkalic tendencies may also be encouraged by the necessary passage of off-axis liquids through thick, cold, lithosphere which provides

Table 3 : <u>Mean values of selected minor and trace elements in the Masirah volcanic groups compared with other basalt types. Only basalts with 44-50% SiO_2 are included.</u>

	Masirah Ophiolite				Saint Helena (9)	Mamonia	O.I.B [1]	M.O.R.B. [2]	Easter Island (5)
	Axis—Sequence Dykes(22) Lavas(22)		Shinzi Gp.(3)	Melange Lavas(8)					
TiO_2	1.08	1.08	2.22	2.05	3.01	2.62	3.12	1.39	3.58
P_2O_5	0.11	0.10	0.54	0.43	0.64	-	-	0.15	0.54
Zr	79	77	280	239	262	282	215	100	260
Y	22	23	34	25	46	33	29	43	52
Nb	8	7	58	62	57	69	32	5	-
Ce_N/Y_N	1.3	1.9	5.1	6.2	-	-	-	-	2.8
					Baker (1969)	--------Pearce- (1975)		Saunders et al (1978)	Bonatti et al (1977)

Note: *1 Ocean island basalt compilation, Pearce (1975).

*2 Mid-ocean ridge basalt (Engel et al, 1965; Melson and Thompson, 1971; Erlank and Kable, 1976).

opportunity for high P crystal fractionation (Malpas, 1978).

The Melange-Shinzi basalts have both high absolute Ce levels (40-111 ppm) and the high Ce_N/Y_N ratios (4-8) which are found in the oceanic island basalts of Discovery Tablemount (6: Kempe and Schilling, 1976), Guadalupe (6-11 : Batiza, 1977) and Easter Island (3-8 : Bonatti et al, 1977). The high Ce_N/Y_N ratios and low Y abundances (23-33 ppm) suggest a residual mantle phase capable of retaining Y and the HREE. The obvious contender is a garnet peridotite source with some garnet amongst the melt residue.

Beneath the Oman Ophiolite in the Oman Mountains there occur exotic limestones which are frequently associated with a basalt substrate. Glennie et al (1974) attributed the association to either: (a) elevated ocean ridge volcanism to a depth which encouraged the growth of shallow later limestone or (b) volcanism on the shallow Arabian continental margin, which was subsequently covered by limestone growth. The broad environmental similarity to the Masirah Melange Lavas seems inescapable, although there seems no question of direct correlation: the Oman exotics are dated at Mid to Late Permian and Late Triassic whereas the Masirah limestones are Mid-Cretaceous (Glennie et al, 1974). Unfortunately published geochemical data on the Oman basalts is confined to major elements.

Previous work (Abbotts, 1978 b and c) has suggested that the axis sequence lavas and dykes were produced at an oceanic spreading centre by moderate degrees ($\sim$ 15%) of shallow

melting of plagioclase or spinel peridotite and subsequent low P magma chamber fractionation of the tholeiitic liquid. It is suggested in conclusion that the more enriched Shinzi-Melange lavas were extruded in an "off-axis" environment and probably reflect smaller degrees of melting of a deeper source. Their extensive vesicularity and the Melange association with shallow marine limestones suggests a shallow water environment. The tectonic incorporation of both groups obscures identification of their precise place of origin and its position relative to the constructive margin which produced the axis sequence. Though the melange is believed to have originated as an oceanic transform fault it has also been suggested (Moseley and Abbotts, 1978) that the resulting lithospheric weakness was utilized during ophiolite uplift and emplacement. It is not clear if the exotic limestones and their basalt substrate were developed along the transform or were simply "caught up" along that line during the emplacement processes. It may be significant that the pillow lava-sheeted dyke blocks, apparently of axis sequence type, which are also found within the melange are moderately enriched in incompatible elements. Unfortunately their occurrence as tectonic blocks again makes it difficult to assess if they were generated along the possible transform fault.

Plate 6.1

Two small exotic limestone blocks resting on basalts
of the Melange Lava Gp. (see P 127)

N of Al Quarin   FT770555

THE OPHIOLITE MELANGE OF MASIRAH, OMAN:

A CRETACEOUS INDIAN OCEAN TRANSFORM

F. MOSELEY and I. L. ABBOTTS

Department of Geological Sciences, University of Birmingham, Birmingham B15 2TT.
U.K.

SUMMARY

The Masirah Ophiolite consists of serpentinites, gabbroic intrusions, an extensive sheeted dyke complex, pillow lavas and sediments. It is truncated to the west by a N-S trending, 5 km wide vertical melange zone; a megabreccia with blocks up to 2 km long of all the above lithologies. The melange trend is perpendicular to that of the sheeted dyke complex, a common relationship between a transform fault and spreading centre. The variable lithologies in the melange can be explained by diapirism, but distribution of other reported ophiolites along the S.E. coast of Arabia and granite, which probably represents a partial melt of lower continental crust, intrusive into the Masirah Ophiolite, suggests upthrust of oceanic rocks onto the continent.

The Masirah Melange and the dyke trends are parallel respectively to the Owen Fracture (and other transforms) and to magnetic anomalies in the Indian Ocean, and it is suggested that both melange and ophiolite are related to the initial opening of the Indian Ocean, rather than to the Semail Ophiolite of the Oman Mountains as has been previously supposed.

1. INTRODUCTION

The Semail Ophiolite of mainland Oman, impressively exposed in mountainous desert with an outcrop exceeding 14000 km^2, is becoming increasingly well known following intensive work during the last ten years (Glennie et al, 1973, Glennie et al, 1974, Greenwood & Loney, 1968, Reinhardt, 1969 and Smewing et al, 1977). It represents oceanic crust of Upper Cretaceous age, emplaced as a nappe onto Arabian continental crust during the late Cretaceous.

The Masirah Ophiolite resembles the Semail Ophiolite in some details and is also likely to be of Cretaceous age, so that although it is more than 250 km from the nearest Semail outcrop, there has been an understandable belief that it could be part of the same unit, perhaps offset by dextral displacement along a Masirah Fault (Glennie et al op.cit., Morton, 1959, Moseley 1969, Stoneley, 1974). However, a more detailed survey of Masirah by the authors (1976 and 1977) revealed more structural complexity and differences from the Semail than had previously been supposed suggesting that this correlation was unlikely. For example the Semail is a thrust sheet whereas all the Masirah structures are high angle; no high K granite has been recorded from the Semail, whereas it is present on Masirah; the Semail sheeted dykes are N-S whereas those of Masirah are E.N.E. and finally the Masirah Melange, the subject of this paper, differs in both structure and composition from those associated with the Semail Ophiolite. It is therefore necessary to decide the place of Masirah in the late Cretaceous - early Tertiary tectonics of S.E.Arabia and the melange may well be a key to this understanding.

2. THE MASIRAH OPHIOLITE

The ophiolite is well exposed over the greater part of Masirah Island, and occupies about 1000 km^2. It includes serpentinised spinel-harzburgites and a plutonic sequence with dunites, troctolites, olivine diopside and hornblende gabbros and minor tonalitic and trondhjemitic differentiates. Sheeted dyke complexes occupy large areas, particularly in the south of the island (Abbotts, 1978a) whereas steeply inclined pillow lavas, with intercalated bedded limestone - marl sequences and associated red cherts are common, often within tectonic zones. Local copper mineralisation is associated with pillow lava and with major tectonic zones.

3. THE MASIRAH MELANGE

A zone of mega-breccia, which in places is more than 5 km wide, dominates the west coast of Masirah. It contains all the ophiolite components as blocks ranging from outcrops of more than 2 km^2 to fragments a few centimetres

in diameter. The larger blocks are themselves often internally brecciated. The junction between the melange and the rest of the ophiolite is tectonic and generally vertical, with a NNE trend approximately perpendicular to the trend of the sheeted dyke complex in the south of the island (Fig. 1). Some exposures of the junction are horizontally slickensided but this may be no more than a minor late stage effect. Lithologies common within the melange are as follows.

A. __Limestone blocks__ possibly of Middle Cretaceous age (Glennie et al, 1974) are the most obvious melange component. They are exotic blocks, there being no comparable limestone outside the melange, and they vary considerably in size, the largest, Jabal Suwayr (Grid ref. 73 33, figure 1 and figure 4), being 2 km long and rising more than 100 m above the surroundings, whereas the smallest are boulders a few metres in diameter. Their contacts are highly irregular, truncating bedding in the limestones and structures (dykes, gabbro layering etc) in the adjacent ophiolite. The majority of the limestone blocks have undergone partial or complete internal brecciation resulting in monogenetic limestone breccias with fragments ranging in size from a few metres to a few centimetres (figure5). This type of internal brecciation within blocks also commonly applies to the other lithologies referred to below.

B. __Chert blocks__ are found throughout the melange, though less abundantly than the limestones. They usually occur as thin interbeds of red chert with grey marly limestone, similar to outcrops in other parts of the ophiolite outside the melange. Bedding is almost always strongly deformed into minor folds, and there is lateral passage into breccia.

C. __Pillow lava__ blocks are often in contact with limestones and cherts and were probably their original substratum. They are also internally brecciated, although in this case a hyaloclastic origin is always a possibility. In the
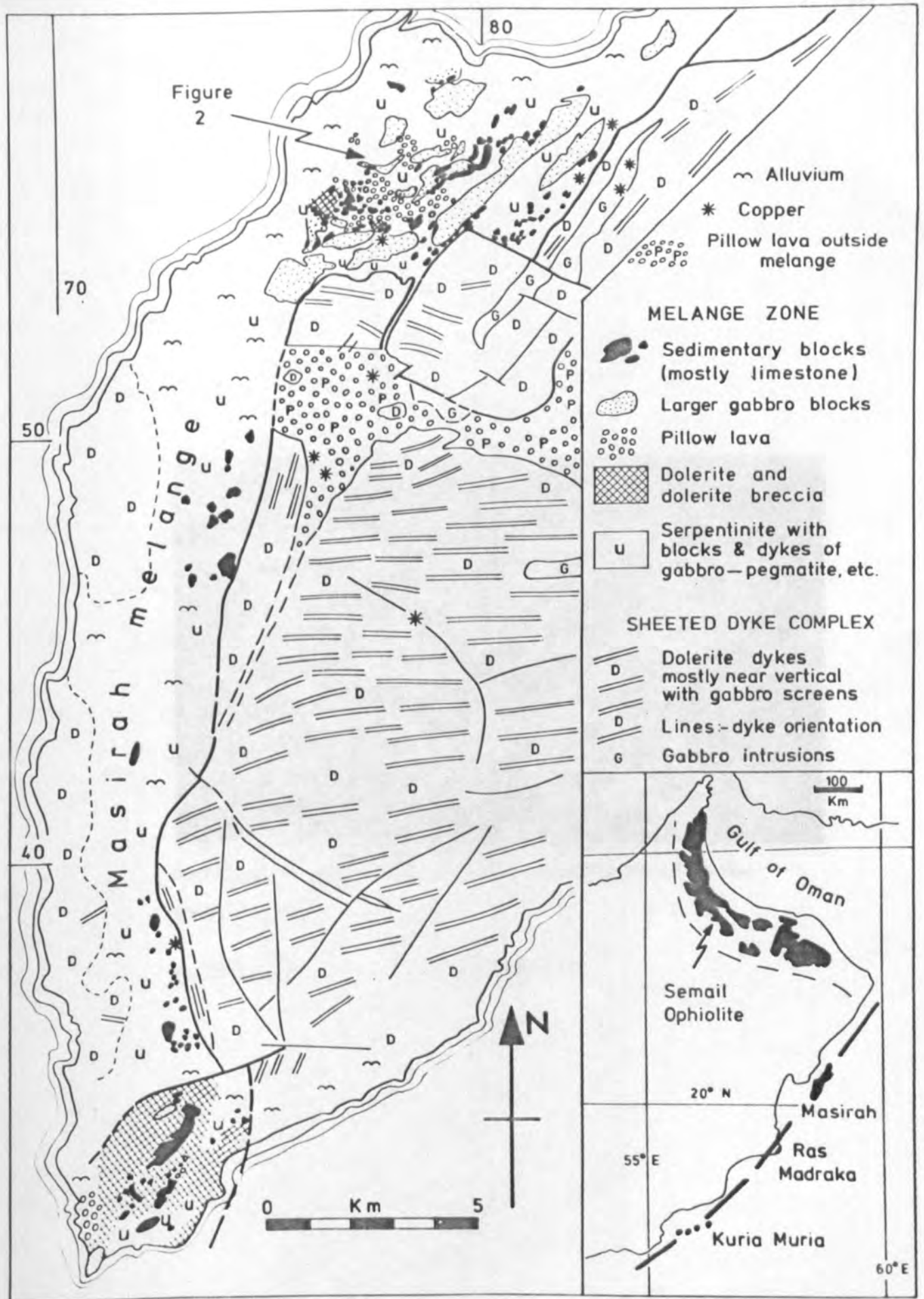
FIG.1. The principal outcrop of the Masirah Melange.

Fig. 4

Brecciated nature of an exotic limestone block in the melange zone

South Point   FT720315

Fig. 5
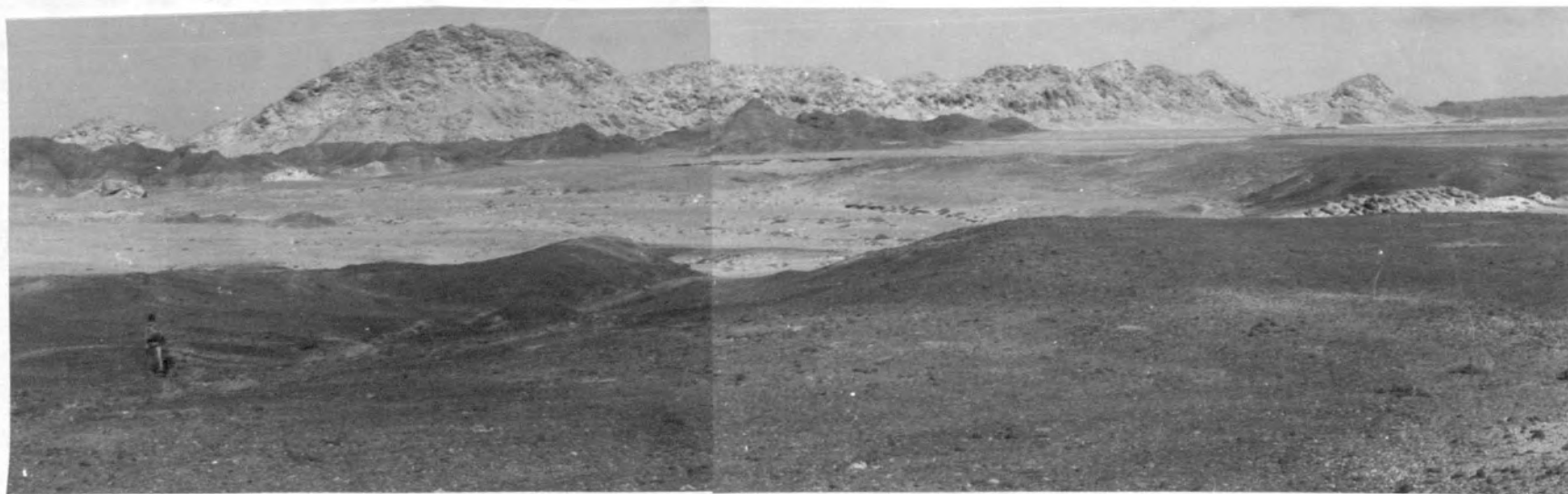
The large limestone exotic of Jabal Suwayr. The highest point rises 100m above the gravel plain. The dark outcrops are sheeted dyke blocks in the melange.

Jabal Suwayr   FT730330

melange there is considerable difficulty in distinguishing between tectonic and igneous breccia, but considering the internal brecciation of limestone, chert and dyke rock a tectonic origin seems to be the more likely, and this is supported by the fact that there are few hyaloclastites associated with pillow lavas in the main ophiolite region. The details of pillow lava geology and geochemistry are considered elsewhere (Abbotts 1978b) but it can be noted briefly that the melange basalts are more alkalic and incompatible element en-riched than those of the ophiolite axis-sequence (Table 1). It has been suggested (Abbotts, op.cit.) that this may reflect extrusion of the melange lavas in an "off-axis"environment.

D. <u>Sheeted dyke complex</u> occurs as brecciated and unbrecciated blocks. The former are in part so completely brecciated that the original dyke structures are no longer recognisable. These blocks occur either as monogenetic dolerite breccia or dolerite-gabbro breccia, depending on the original proportion of gabbro screen, whilst local transition into normal dyke complex indicates their former origin. Unbrecciated blocks, best seen in the south of the island, vary from 100% dolerite, where the dykes are in contact with each other, to dolerite with gabbro screens. The dyke orientation varies from place to place, as would be expected with allochthonous blocks.

The perpendicular relationship between the melange and sheeted dyke trends has already been noted, but there are exceptions, and attention is drawn to elongate outcrops along the eastern margin of the melange where the dykes are parallel to it (Fig. 1, 75 48 and 73 38).

E. <u>Gabbros</u> of varying types have extensive outcrops within the melange zone. The large units cover areas exceeding 2 km^2 (Fig. 2) and many are cut by dolerite dykes, which can form a substantial proportion of the outcrop suggesting origins as gabbro-rich lower levels of a sheeted dyke complex.(Abbotts, 1978a).
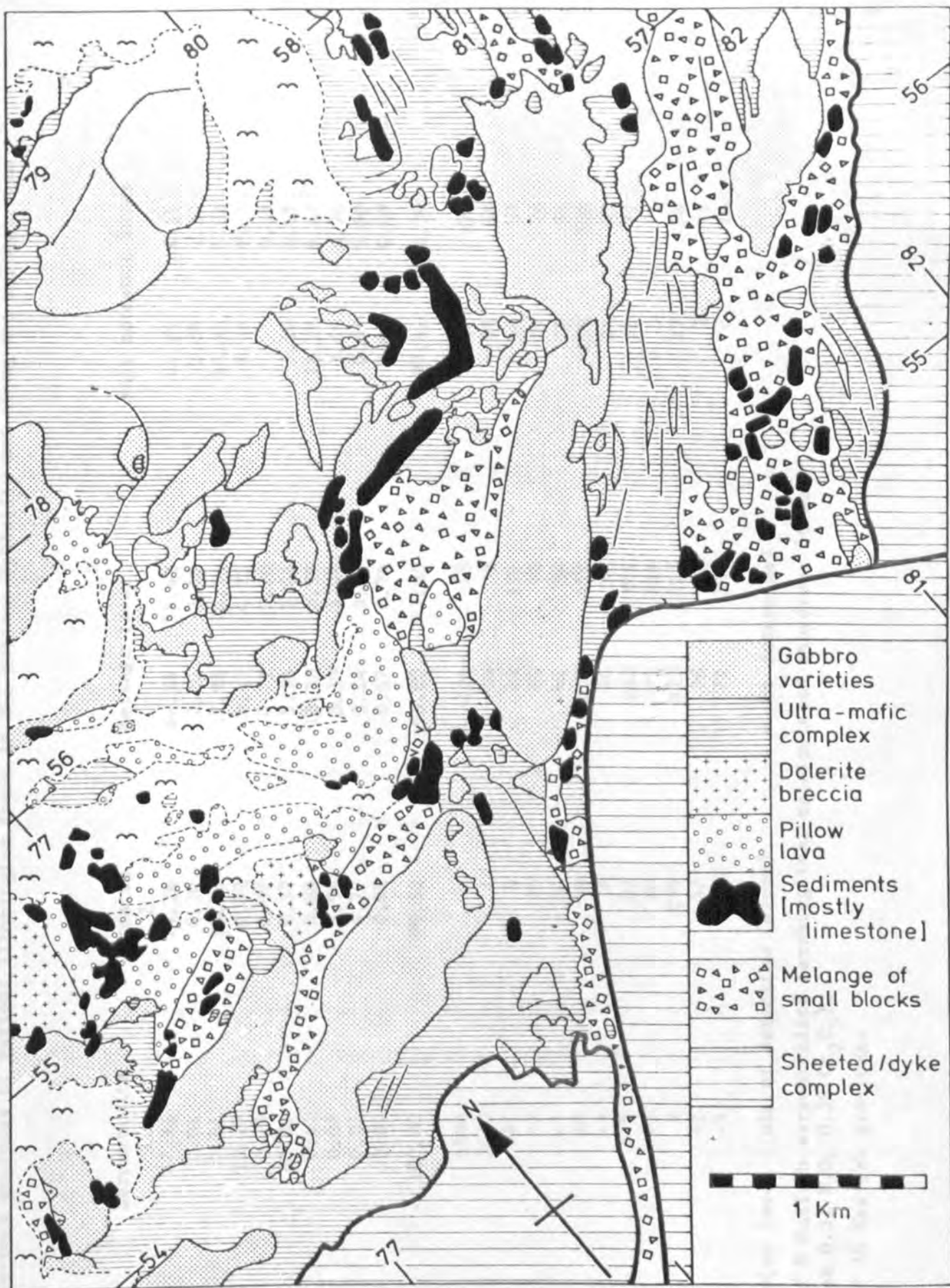
FIG.2. Detailed outcrop of part of the Masirah Melange.

Table 1 : Whole-rock analyses of various lithologies found in the Masirah Ophiolite and along the melange zone

	Serpentinite 1	Granite 2	Melange lavas		Axis sequence lavas	
SiO_2	47.31	74.26	46.26	58.42	48.29	48.35
TiO_2	0.01	0.10	2.10	2.16	0.89	1.22
Al_2O_3	0.81	13.78	12.98	16.14	16.35	17.08
Fe_2O_3	10.10	0.92	6.45	4.23	7.85	9.67
MnO	0.15	0.02	0.12	0.20	-	0.18
MgO	40.30	0.37	5.36	2.01	7.20	4.65
CaO	0.41	0.88	13.33	8.35	12.21	9.42
Na_2O	0.08	3.99	3.39	3.96	3.14	4.74
K_2O	0.01	4.77	3.24	3.27	0.89	0.90
P_2O_5	0.01	0.01	0.57	0.76	0.06	0.09
Total	100.00	99.52	93.80	97.83	97.42	96.30
Cr	3390	8	126	16	347	330
Ni	2412	1	54	2	95	59
Zn	41	6	64	111	58	57
Ga	-2	15	20	23	19	16
Rb	-1	81	41	28	11	11
Sr	18	59	258	459	153	150
Y	-2	8	24	50	24	27
Zr	5	82	283	396	58	77
Nb	-1	55	82	105	3	6
Ba	8	699	513	457	22	59
La	-2	37	36	37	2	6
Ce	-3	54	72	106	6	14

Note   -2 = below lower limit of detection (=2ppm)   - = not determined

1. Avg. of 8 Masirah serpentinised harzburgites, recalculated anhydrous (total includes 0.31 N.O, 0.50 Cr_2O_3).

2. Avg. of 10 Masirah granites.

More deeply-derived gabbros are associated with partially serpentinised dunites and troctolites. Internal brecciation is less common in these rocks, probably because they are more massive and stronger. Figure 2 shows that most outcrops occur as isolated islands in a sea of brecciated lava and serpentinite, but some have irregular sub-vertical contacts with limestone blocks while others seem scarcely detached from outcrops outside the melange zone (76 54, Fig. 1). The best interpretation of the gabbros is again that of blocks within the melange.

F. Serpentinites are the final important lithology of the melange. They are cut by and contain complex systems of dykes, veins and pockets of coarse to pegmatitic gabbro, leucogabbro and anorthosite and rarer fine-grain dolerites. There is much internal brecciation, and from the way in which serpentinite often surrounds the blocks of other lithologies (Fig.2), it seems to have acted as an incompetent matrix to the more resistant rocks.

4. POSSIBLE MECHANISMS OF FORMATION

The problem of the origin of the Masirah melange requires consideration of the plate tectonics of the whole of S.E.Arabia from the late Mesozoic to the present day. Of particular relevance are the Semail Ophiolite of the Oman Mountains to the north, a possibility that there may be ophiolites on the Kuria Muria Islands and at Ras Madraka to the S.E. and the results of research in the Indian Ocean where the older oceanic crust is late Cretaceous and there are transform faults and magnetic anomalies with N-S and E-W orientations respectively (Fig.3: McKenzie and Sclater, 1971; Whitmarsh et al, 1972). In this connection the melange itself exhibits a number of features some already outlined for which explanations are necessary.

(i) The melange, more than 5 km wide, has a general NNE trend, there is some NNE preferred orientation of the larger blocks, for example some of the lime-stones and gabbros on Fig.2 and there are near vertical NNE shear planes cutting through the matrix (shown as lines on Fig.2, e.g. 805555).

(ii) The melange sharply truncates structures in the remainder of the Masirah Ophiolite. In particular the main part of the sheeted dyke complex has a trend

perpendicular to the melange, although there are local areas where the dykes are parallel to it (Fig. 1, 75 48, 73 38).

(iii) The contact between the melange and the remainder of the ophiolite generally follows a NNE trend, but in detail this is irregular, and in places there are abrupt trend changes of up to 90° (Figs. 1 and 2). In some cases these variations are a result of later faulting but in others this explanation will not suffice, for example note the relationships at 8055, where the melange contact has an apparent 1 km dextral strike slip displacement, whereas an adjacent gabbro mass to the west is unaffected.

(iv) High K granites, intrusive into serpentinised harzburgites and gabbros, occur within 3.5 km of the line of the melange as sheets, veins and lenses which locally coalesce into larger masses. Their geochemistry (Table 1), particularly their high K, Rb and Nb, low Zr and highly fractionated REE patterns (Ce_n/Yb_n 39, Yb_n 3) rule out a co-genetic link with the ophiolite and suggest partial melting of continental crust (Abbotts, 1978c).

(v) Many of the large blocks of the melange are internally brecciated. They occur as monogenetic tectonic breccia (Plate 2), an évent which preceded emplacement of the blocks, thus suggesting polyphase tectonic activity.

All these features together with those described above, can be interpreted in several ways, as follows.

A. Diapirism

The melange incorporates rocks from all crustal levels, with serpentinite forming a substantial proportion, both as blocks and matrix. The harzburgitic nature of the serpentinite is evident even in hand specimen, with bronze bastites set in a black serpentine matrix. Table 1 includes an average analysis of 8 serpentinites which are extremely uniform modally and chemically. Their depleted chemistry and high Ni-Cr levels distinguish them from ultramafic cumulates in the plutonic sequence, and suggest an origin as mantle depleted by basalt extraction (Abbotts, 1978b). The serpentinites have a low density, are incompetent, and would be likely to rise diapirically, especially if subjected to tectonic stress.

Many examples of the disruptive effects of diapirism, caused by a variety of tectonic processes, are known from other parts of the world. For example structural complexes analogous to the Masirah Melange are found in the Alpine belt of Southern Spain, where Triassic gypsiferous mudstones have risen upwards along linear wrench zones, carrying with them exotic blocks of lime-stone and volcanics hundreds of metres in diameter (Moseley, 1973). The materials are different to those of the Masirah Melange, but the effects and principles are similar. It is undoubtedly possible to interpret the Masirah Melange as this type of diapiric structure, with rising serpentinites incorporating rocks from all higher crustal levels. Such diapirism would have required forces to set it in motion, and these could have been supplied by transform, wrench or thrust faulting, or some combination of these processes.

B. Transform Fault

Present day transform faults are known mostly from geophysical evidence supplemented by drilling and dredging of the ocean floor. A great variety of rocks have been collected from these zones including ultra-mafic, gabbroic, basaltic and sedimentary rocks, but the limitations of sampling mean that their detailed geological relationships are little known (Bonatti, 1978, Bonatti and Honnorez, 1976, Melson & Thompson, 1971). It is probable that the abundant serpentinised peridotites in the transform zones are mantle derived and tectonically emplaced, with diapirism as the most likely mechanism. It has been suggested (Bonatti and Honnorez, op.cit., Wenner & Taylor, 1971) that serpentinisation could have been caused by sea water penetration along transform fractures and that this alteration to a lower density rock would favour diapiric rise along the fault zone.

Few fossil transforms have been described, but Simonian and Gass (1978) have interpreted the Arakapas fault belt of Cyprus as such. This region has some similarities to the structure on Masirah, including (1) development within a basement sheeted dyke complex (2) some trend rotation of the dykes adjacent to the melange (3) serpentinite emplacement near and along the "transform".

However, important differences between the two occurrences are the greater degree of brecciation and diapirism in the Masirah example.

On Masirah the sheeted dyke complex (Fig. 1) has a trend almost perpendicular to the melange which is a common relationship between ridge and transform, and all the Masirah lithologies are known from modern oceanic transforms (Bonnatti & Honnorez, 1976). It therefore seems reasonable to suggest that many transforms, when they become known in more detail, may prove to be melange zones comparable with the Masirah Melange.

C. A major wrench zone

A correlation of the Masirah and Semail ophiolites would require a dextral strike slip fault parallel to the Arabian Coast with a displacement of 250 km. It could be a late Cretaceous transform fault as indicated above, a late Tertiary wrench fault along the line of an earlier transform, or simply a late Tertiary wrench with no transform movement involved. The last two interpretations would both satisfy Gass and Gibson's suggestion (1969) that late Tertiary north-easterly movement of Arabia relative to adjacent regions is reflected by dextral and sinistral displacement along the Masirah and Jordan faults, the tensional opening of the Red Sea and Gulf of Aden, and the compressional Zagros Thrust. It is possible for major wrench faults to give rise to structures like the Masirah Melange, especially when diapirism and incompetent rocks are involved, and the example from the orogenic zone of southern Spain, referred to above, is a case in point.

D. Upthrust onto Arabian continental crust.

The previous hypotheses would involve tectonic movement parallel to the S.E. Arabian coast, but there is also the possibility of movement perpendicular to that coast, with upthrust of the ophiolite from the south-east on to the continental margin. Since the melange contacts are vertical, the upthrust would have to be vertical or nearly so, but such structures are by no means uncommon. The Masirah Melange runs parallel to the Arabian coast and the reported, although

so far unconfirmed, ophiolites of Kuria Muria and Ras Madraka continue the same trend. An upthrust relationship would therefore satisfy these other occurrences whereas the previous hypotheses would not. An explanation is also required for the high potash granites within the ophiolite which have not been reported from the Semail Ophiolite (Aldiss pers. comm.). South-east Arabia seems likely to have been a passive margin throughout the late Mesozoic, and neither regional geology nor Masirah granite chemistry provides evidence for collision orogeny or appreciable calc-alkali vulcanicity. Nevertheless the granites seem to be of continental crust derivation and presumably indicate the presence of this type of crust beneath the Masirah ophiolite during the late Cretaceous. Such relations are most easily explained by upthrusting.

5. CONCLUSIONS

None of the above mechanisms taken singly adequately explains all the features of the melange, which seems more likely to have been the result of two or more processes, possibly operating at different periods of geological time. The presence of the sheeted dyke complex suggests proximity of a spreading centre at the time the rocks were formed. The date for this event seems likely to have been late Mesozoic, since although there is now considerable doubt about direct correlation with the late Mesozoic Semail Ophiolite of the Oman Mountains, observation of Cretaceous to Eocene sediments on the flanks of the Carlsberg Ridge (Le Pichon and Heirtzler, 1968) show that much of the western Indian Ocean could be of Cretaceous age, generated during the break up of Gondwanaland. The melange is a polyphase structure with brecciation of individual blocks preceding the formation of the large scale "mega-breccia", the former possibly a result of initial transform movement, and the latter more likely to be a diapiric effect as the transform developed. The sharp trend changes of the melange contact also suggest polyphase activity. For example the easiest way to explain the geology near 80 55, (Fig. 2) is (i) NNE strike slip (transform movement) along the present contact (ii) WNW strike slip displacing the transform fault boundary and (iii) diapirism along the whole zone, during which the gabbro and other blocks were emplaced.

Previous correlation of the Masirah and the Semail Ophiolites (Glennie et al, 1973, Morton, 1959, Moseley, 1969, Stoneley, 1974) made it necessary to invoke a large strike slip fault parallel to the Arabian coast. The objections to this correlation have been referred to in the introduction and it is unneccessary to detail them all again, but it is worth emphasising first that the ENE-WSW dyke trend on Masirah contrasts with the N-S trend recorded in parts of the Semail Ophiolite (Smewing et al 1977), suggesting that the spreading centre there may have been at right angles to that of Masirah, and second, that a strike slip fault solution cannot account satisfactorily for ophiolites on Ras Madraka and Kuria Muria assuming that these reports prove to be correct. Thus previous citations of strike slip faulting to explain the location of the Masirah ophiolite seem to be oversimplifications. It is possible that the melange developed in the following way.

(a) The most likely origin seems to have been as a transform fault parallel to other transforms in the Indian Ocean (Fig. 3; McKenzie and Sclater, 1971; Whitmarsh et al, 1972), which displaced a late Mesozoic spreading centre (represented by the dyke swarm). The initial small scale brecciation may have occured at this time. The texture of these breccias indicates that they are fault or tectonic breccias rather than sedimentary breccias.

(b) Diapirism is a plausible explanation for the megabreccia in which there are rocks from depths of up to several kilometres (serpentinites, troctolites, gabbros and dolerites), mixed with surface rocks (limestones, cherts and pillow lavas). This may have taken place as the transform developed into a major structure. The lithological range is paralleled by the transform zones of modern oceans, and large scale diapirism has been suggested for many of these structures (see above).

(c) Tertiary movements seem likely to have been as depicted by Gass and Gibson (1969) with Arabia moving north-eastwards relative to Africa and Iran. This movement is however unlikely to have been absolutely parallel to the

FIG.3. Map of the northern Arabian Sea. Data sources:
(a) magnetic anomalies and transform faults. (McKenzie and
Sclater, 1971; Whitmarsh and others, 1974), (b) D.S.D.P.
stations and results (Whitmarsh and others, op.cit),
(c) bathymetry, gravity anomalies and earthquake epicentres.
Geological and geophysical atlas of the Indian Ocean, 1975),
(d) seismic refraction studies and estimates of sediment
thickness (White and Klitgord, 1976; Farhoudi, 1977).
Dyke trends: Oman Mountains (Smewing et al, 1977; Smewing,
pers.comm.), Masirah (this study). Note the approximate
parallelism of the Masirah dykes and the melange with,
respectively, the Indian Ocean magnetic anomalies and transform
faults. Owen Basin magnetic anomalies : Whitmarsh (1978, in press).

already established SE coast of Arabia (a continental margin), and oblique movement could have resulted in oceanic crust riding upwards onto the continent from Kuria Muria to the easterly tip of Arabia at Ras al Hadd (Fig. 3). Ophiolite upthrust would have occurred at some stage during the late Cretaceous-early Tertiary period. If Masirah was subsequently displaced by dextral slip faulting this could be expected to posthumously follow an earlier transform or upthrust line.

High-potassium granites in the Masirah ophiolite of Oman

I. L. ABBOTTS

(Plates 1–2)

Summary. Masirah Island lies off the SE coast of Oman and comprises a fully developed, though tectonically disturbed ophiolite, unconformably overlain by early Tertiary limestone. The ophiolite consists of harzburgites and peridotites, cumulate gabbros, a sheeted dyke complex, and pillow lavas with sediment intercalations. Within the ophiolite occur granites the geochemistry of which, particularly their high K_2O and Rb, and low Zr and Zr/Nb, is more typical of a continental crust environment and suggests that at the time of their formation continental crust existed beneath or immediately W of the Masirah Ophiolite.

1. Introduction

Masirah is a desert island, 64 by 16 km, lying 24 km off the SE coast of Oman. It was geologically surveyed in 1976 and 1977, when the work was facilitated by the high degree of exposure, the good quality of aerial photographs (1:12000 and 1:60000) and the unfailing logistic support provided by the R.A.F. The Masirah Ophiolite is similar to the Semail Ophiolite of the Oman Mountains in containing all the typical ophiolitic components of harzburgites, peridotites, gabbros, a sheeted dyke complex, and pillow lavas (Fig. 1). However, Masirah lacks the undisturbed igneous stratigraphy of the Semail and the different lithologies usually have tectonic and not gradational contacts with each other. Tertiary limestone rests unconformably on the ophiolite. The only previous publications referring to the geology of Masirah are by Lees (1928), Moseley (1969), who recorded the granites referred to in this paper, and Glennie *et al.* (1974). The granites which outcrop over 4 km² within the ophiolite (Fig. 1) possess an unusual geochemistry ($K_2O \sim 5\%$, Rb 50–100 ppm) considering their environment.

2. The Masirah ophiolite

As host to the granites, a brief description of the ophiolite is necessary. The harzburgites and peridotites make up less than 10% of the total volume and are strongly serpentinized. Most of the gabbros are massive plagioclase–clinopyroxene rocks, though olivine and amphibole-bearing varieties are present and a late stage gabbro pegmatite phase is common. The sheeted dyke complex is continuously exposed for over 150 km² and is composed of 70–100% meta-dolerite dykes generally WSW trending with the remainder being well-defined screens of uralitized gabbro. The dykes are generally no more than 2 m wide and are quite uniform in their mineralogy (zoned plagioclase–amphibole–sphene–ore). At higher levels there is a transition zone of dykes with pillow lava screens and finally extensive spreads of basaltic pillow lavas. The internal stratigraphy of the ophiolite has been much disturbed by subsequent tectonic movements so that natural contacts, such as the dyke–lava transition, are rare.

3. Field relations and petrography of the granites

Figure 2 is a simplification of the area of granite intrusion into ophiolite, the latter being a complex magmatic breccia containing serpentinized peridotites, gabbro, gabbro-pegmatite and dolerite in blocks varying in diameter from 10 cm to 800 m. Within this breccia the order of intrusion is peridotite, then gabbro and dolerite and finally gabbro pegmatite. Thus the peridotite occurs as xenolithic blocks, the pegmatite as a breccia matrix, and the gabbro and dolerite occur in both roles. The mutual age-relationship of the gabbro and dolerite is not clear.

Granites of Masirah Island
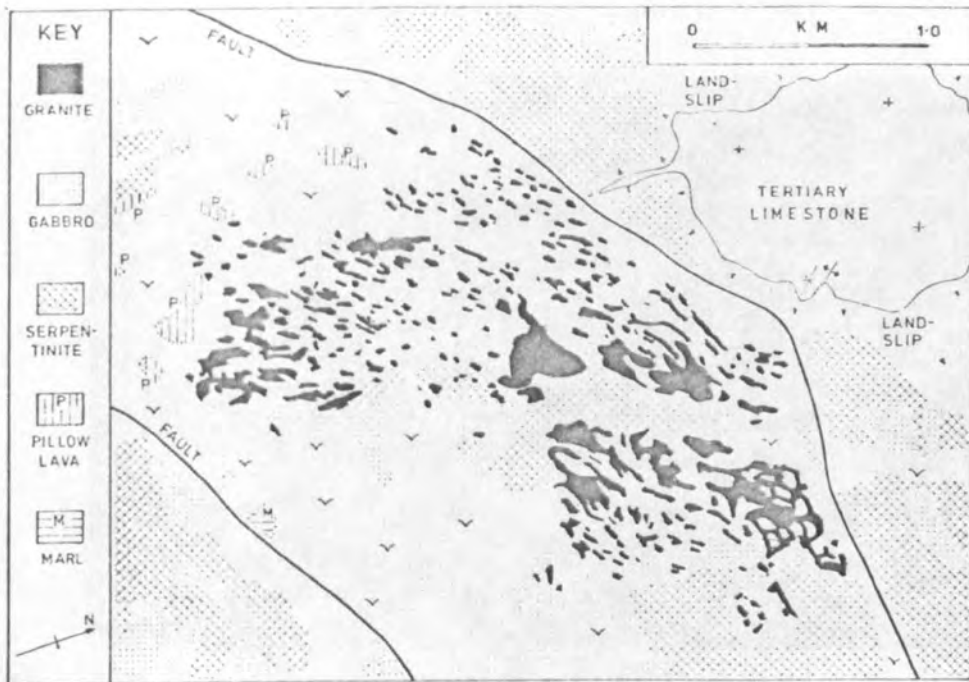
Figure 2. Geological map of the area of granite intrusion.

Complexity is further increased by the intrusion of the granites, which cut all the ophiolite components in the final magmatic event of the area. The granites occur as veins, sheets and irregular pods, ranging from a few cm to 40 m in width. Exposures vary from isolated thin granite veins forming 10% of the outcrop to coalesced veins and sheets containing only a few, partially absorbed, basic xenoliths (Plates 1A and B).

Table 1. Average modal composition of 9 granites, Masirah

Quartz	41.9
Orthoclase (perthitic)	34.5
Plagioclase (albite-oligoclase)	21.6
Biotite (chloritized)	2.0

The granite, cream to pink in colour, is extremely leucocratic with mafic minerals composing less than 3% of the mode (Table 1) and has cataclastic textures varying from a typically granular granite with only slight brecciation of crystal margins   to a protomylonite with felspar porphyroclasts in a sutured quartz matrix   The ophiolitic country rocks adjacent to the granite do not have cataclastic textures but instead are largely recrystallized. (This different reaction to stress of acid and basic rocks is described by Higgins, 1971.) The dolerites and gabbros have clinopyroxene retrogressed to amphibole and plagioclase partly albitized, the peridotites are completely serpentinized and the gabbro pegmatites have altered to albite-sericite–amphibole–quartz–epidote rocks. Similar but less advanced recrystallization is common on the island throughout the dyke complex and in some of the gabbros and may be evidence of a static metamorphism at the site of ophiolite generation, such as that described in the Sarmiento marginal basin ophiolitic complex of southern Chile (Saunders *et al.* 1978). The more advanced recrystallization around the granites is then ascribed to the added effects of granite intrusion and the subsequent localized P-T conditions which mylonized the granites.

Plate 1.

(a) Veins of pale granite cutting darker gabbro.
Jabal Hamra   FT940700

(b) Pale granite with darker gabbro xenoliths. The
xenoliths are 0.3-1.0m in width
Jabal Hamra   FT945700.
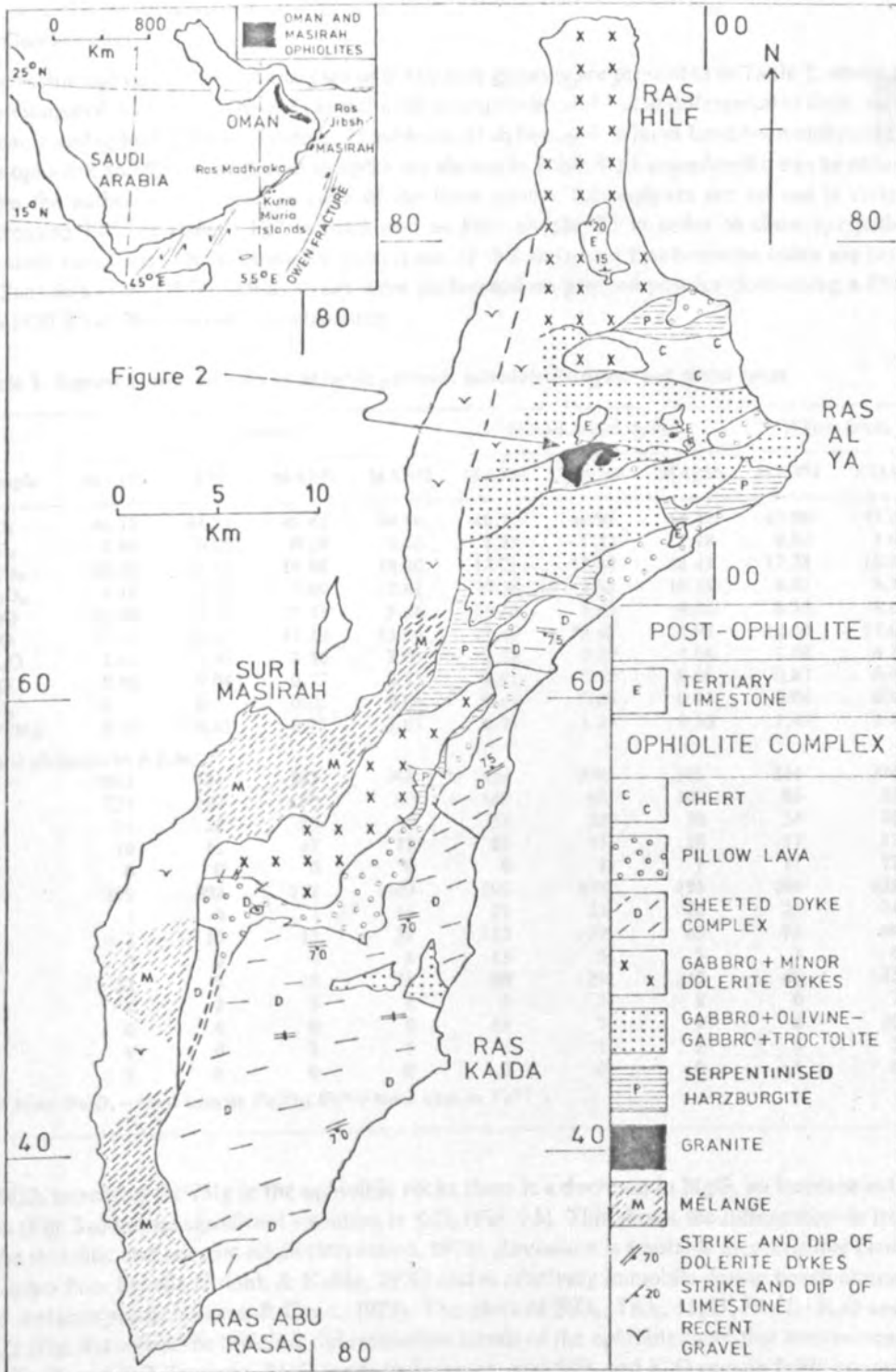
Figure 1. Geological map of Masirah Island showing the outcrop of the various ophiolite lithologies, the granites, and the later Tertiary limestone.

Granites of Masirah Island

4. Geochemistry

The major and trace element analyses of 9 Masirah granites are presented in Table 2, where they are compared with a continental crustal melt leucogranite and 3 acid differentiates from various oceanic and ophiolite areas. To date, 75 gabbros, 42 dykes, and 30 lavas have been analysed from the ophiolite and 9 representative samples are shown in Table 3. (A complete list can be obtained from the author on request.) In each of the three groups the analyses are set out in order of increasing Fe^*/Mg (where Fe^* is total iron as Fe^{2+} weight %) in order to show sympathetic element variations. The reasons for preference of this ratio as a fractionation index are set out in Saunders *et al.* (1978). All analyses were performed on pressed powder discs using a Philips PW1450 X-ray fluorescence spectrometer.

Table 3. Representative analyses of Masirah gabbros, metadolerite dykes and pillow lavas

Sample	Gabbro's				Metadolerite dykes			Pillow lavas	
	MA175	X71	MA272	MA323	MA183	MA248	MA286	MA391	X245PI
SiO_2	46.17	44.95	49.42	48.86	48.52	48.91	48.42	47.90	47.64
TiO_2	0.09	0.05	0.28	0.66	1.34	1.22	1.18	0.91	1.06
Al_2O_3	18.69	22.18	15.98	18.80	14.28	13.58	14.43	17.28	16.37
Fe_2O_3	4.18	4.74	7.09	7.81	9.39	9.55	10.19	8.81	9.34
MgO	13.98	12.22	10.47	8.46	11.52	9.98	9.44	6.85	4.65
CaO	15.57	13.63	13.19	13.34	11.40	13.42	11.98	12.59	12.66
Na_2O	1.49	1.50	2.36	2.07	2.29	2.39	2.06	2.88	4.17
K_2O	0.10	0.04	0.13	0.13	0.11	0.12	0.08	0.87	0.92
P_2O_5	0	0	0.01	0.05	0.11	0.09	0.11	0.06	0.10
Fe^*/Mg	0.35	0.45	0.79	1.07	0.95	1.11	1.26	1.49	2.33
Trace elements in p.p.m.									
Cr	1931	384	345	268	426	274	346	314	314
Ni	271	247	90	80	169	83	107	83	55
Zn	14	20	23	30	53	22	70	54	76
Ga	10	12	17	17	16	17	18	17	15
Rb	0	0	0	0	0	1	1	11	12
Sr	129	202	177	109	192	135	195	196	133
Y	1	0	7	16	25	23	26	23	24
Zr	7	10	13	37	115	29	89	63	68
Nb	0	0	1	3	13	5	5	3	4
Ba	22	7	28	21	80	29	45	49	42
La	4	2	3	4	9	2	8	6	7
Ce	0	0	0	6	19	7	9	6	10
Pb	1	0	2	4	0	1	2	4	3
Th	1	0	0	0	0	0	0	1	0

* Note Fe_2O_3 = total iron as Fe_2O_3; Fe^* = total iron as Fe^{2+}

With increasing Fe^*/Mg in the ophiolitic rocks there is a decrease in MgO, an increase in total iron (Fig. 3 *a*) but no significant variation in SiO_2 (Fig. 3 *b*). This shows the differentiation trends to be tholeiitic and not calc-alkali (Miyashiro, 1973). Zirconium is a notable incompatible element in ocean floor basalts (Erlank & Kable, 1976) and is relatively immobile during basalt alteration and metamorphism (Pearce & Cann, 1973). The plots of SiO_2, TiO_2, MgO, Fe_2O_3, K_2O and Sr *v.* Zr (Fig. 4) confirm the tholeiitic differentiation trends of the ophiolite (note that with increasing Zr, Fe_2O_3 and TiO_2 increase, MgO tends to decrease, and SiO_2 and K_2O remain fairly constant). More importantly the plots illustrate the clear chemical distinction of the more alkaline granites and their tholeiitic host rocks.

One possible origin of the granites is that of extreme differentiation of the tholeiitic magma

Table 2. Analyses of 9 Masirah granites, with 1 continental granite and 3 oceanic acid differentiates for comparison

Sample...	MA37	X37	X86	X35	MA120A	MA28	MA358	MA44	X33	11*	125.16†	PA23J‡	CY.55C§
SiO_2	74.97	74.13	74.66	74.95	75.98	75.05	73.61	74.70	73.31	75.10	76.37	74.21	69.4
TiO_2	0.10	0.21	0.07	0.05	0.10	0.15	0.10	0.06	0.17	0.10	0.42	0.27	0.33
Al_2O_3	13.50	13.82	14.01	13.91	13.16	13.57	14.30	13.63	13.77	13.85	12.78	12.28	14.0
Fe_2O_3‖	0.74	1.68	0.72	0.58	0.56	1.08	1.00	0.70	1.57	1.40	0.90	3.31	5.5
MnO	0.01	0.03	0.02	0.01	0.02	0.02	0.04	0.03	0.04	0.04	0.02	0.05	0.06
MgO	0.40	0.61	0.18	0.14	0.29	0.49	0.21	0.11	1.07	0.16	0.87	0.23	0.54
CaO	0.57	1.30	0.85	0.61	0.59	1.09	0.99	0.50	1.58	0.78	0.84	5.55	4.6
Na_2O	3.76	4.43	3.86	3.62	4.00	3.53	4.72	3.83	3.74	3.72	7.70	3.61	3.8
K_2O	5.20	3.35	4.95	5.75	4.58	4.49	4.33	5.34	4.49	4.46	0.07	0.01	0.07
P_2O_5	0.01	0.01	0.01	0	0.01	0.02	0.02	0	0.02	—	0.02	0.04	0.15
	99.26	99.57	99.33	99.63	99.28	99.49	99.29	99.89	99.75	99.46	100.22	99.56	100.00

Trace elements in p.p.m.

Cr	5	8	6	6	4	9	6	4	28	2.8	7	7	—
Ni	0	1	0	0	0	3	0	0	8	<1	29	6	15
Zn	10	23	10	5	6	12	8	8	15	—	—	15	—
Ga	13	17	17	14	13	14	19	16	16	12	—	15	20
Rb	77	56	101	102	67	60	60	85	95	260	—	1	<1
Sr	56	73	34	40	72	92	88	30	72	62	86	224	135
Y	3	8	11	10	6	6	9	9	9	23.5	180	114	30
Zr	49	103	98	72	26	102	146	92	72	117	550	575	70
Nb	27	93	73	53	23	53	56	48	81	—	25	17	—
Ba	798	218	183	137	2970	994	658	224	348	510	180	1	20
La	23	50	18	20	83	65	30	29	23	39	—	30	—
Ce	37	76	31	36	108	94	49	47	39	—	—	73	—
Pb	5	5	6	6	4	6	5	6	7	21	47	3	—
Th	17	50	43	42	50	46	20	39	34	21.1	—	12	—

* Leucogranite; Snowy Mountains, Australia (Kolbe & Taylor I, 1966).
† Alpite (trondhjemite); Indian Ocean (Engel & Fisher, 1975).
‡ Plagiogranite; Sarmiento ophiolite, Chile (Saunders et al. 1977).
§ Plagiogranite; Troodos ophiolite (Coleman & Peterman, 1975).
‖ Fe_2O_3 = total iron as Fe_2O_3.
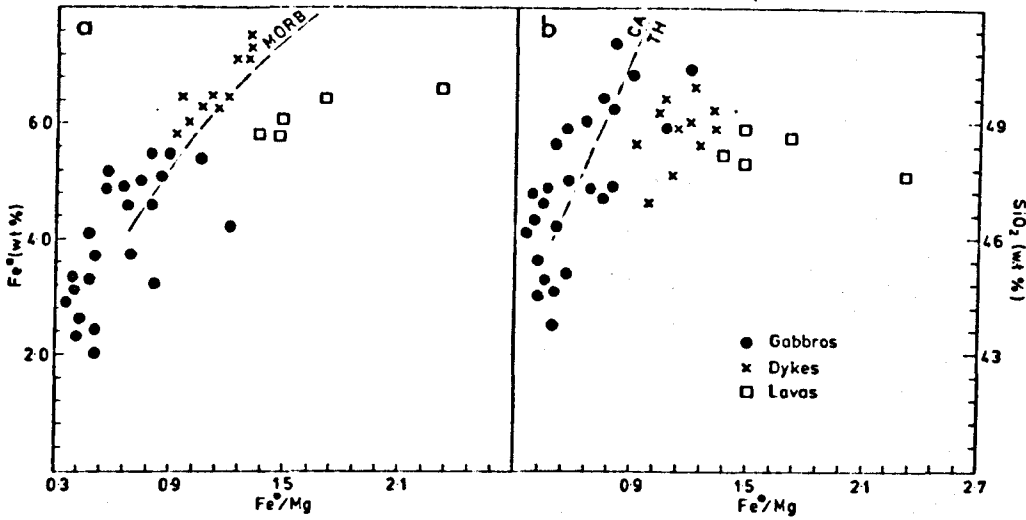
Figure 3. Plots of Fe* and SiO₂ v. Fe*/Mg for Masirah ophiolitic rocks. The fractionation trend for abyssal tholeiites is based on published data and the dashed line separating tholeiitic and calc-alkaline trends is from Miyashiro (1973). Fe* is total iron as Fe^{2+} weight %.

from which the Masirah ophiolitic rocks were derived. Such acid differentiates have been termed plagiogranites and have been described from the Troodos Ophiolite (Coleman & Peterman, 1975), the Sarmiento Ophiolite (Saunders *et al.* 1978), and the Argo Fracture Zone in the Western Indian Ocean (Engel & Fisher, 1975). The incompatible elements yttrium and zirconium are strongly concentrated by fractionation and a plot of log Y v. log Zr (Fig. 5) shows how the differentiation trend of the Masirah ophiolitic rocks, if continued, could produce the plagiogranites with their high incompatible levels but could not produce the Masirah granites whose Y levels are too low. There are other obvious differences between the Masirah granites and the plagiogranites: K_2O and Rb in the granites are respectively over 10 times, and 50-100 times, those of the plagiogranites (Table 2). Thus the evidence argues strongly against deriving the granites from the tholeiitic magma which produced the Masirah ophiolitic rocks.

Alternatively the granites might be derived from a continental crust melt. Fields for such crust-derived granites have been produced on Figure 4 and the Masirah granites are seen to fall largely within these. There is also a striking similarity in both the major and trace elements between the Masirah granites and the leucogranite of Kolbe & Taylor (1966, table 2-11). The leucogranite is thought to have formed by extreme fractionation of a melt derived from low-level continental crust (Price & Taylor, 1977). Thus evidence points towards an origin as a continental crust melt for the Masirah granites. However, Brown (1977) argued that many granites at destructive plate margins are probably formed from predominantly mantle-derived melts. These melts are produced in or above the subduction zone, are tonalitic in nature and fractionate at higher levels in the continental crust to produce intrusive granites. Evidence for the mantle source of these granites lies in their low initial strontium isotope ratios (0.703–0.708) and it might be noted here that the leucogranites of Kolbe and Taylor give a value of 0.704. Thus the possibility of a mantle source, as opposed to a continental crust-melt origin, for these Masirah granites cannot be ruled out in the absence of strontium isotope work. It is hoped that such work will be possible.

Granites of Masirah Island
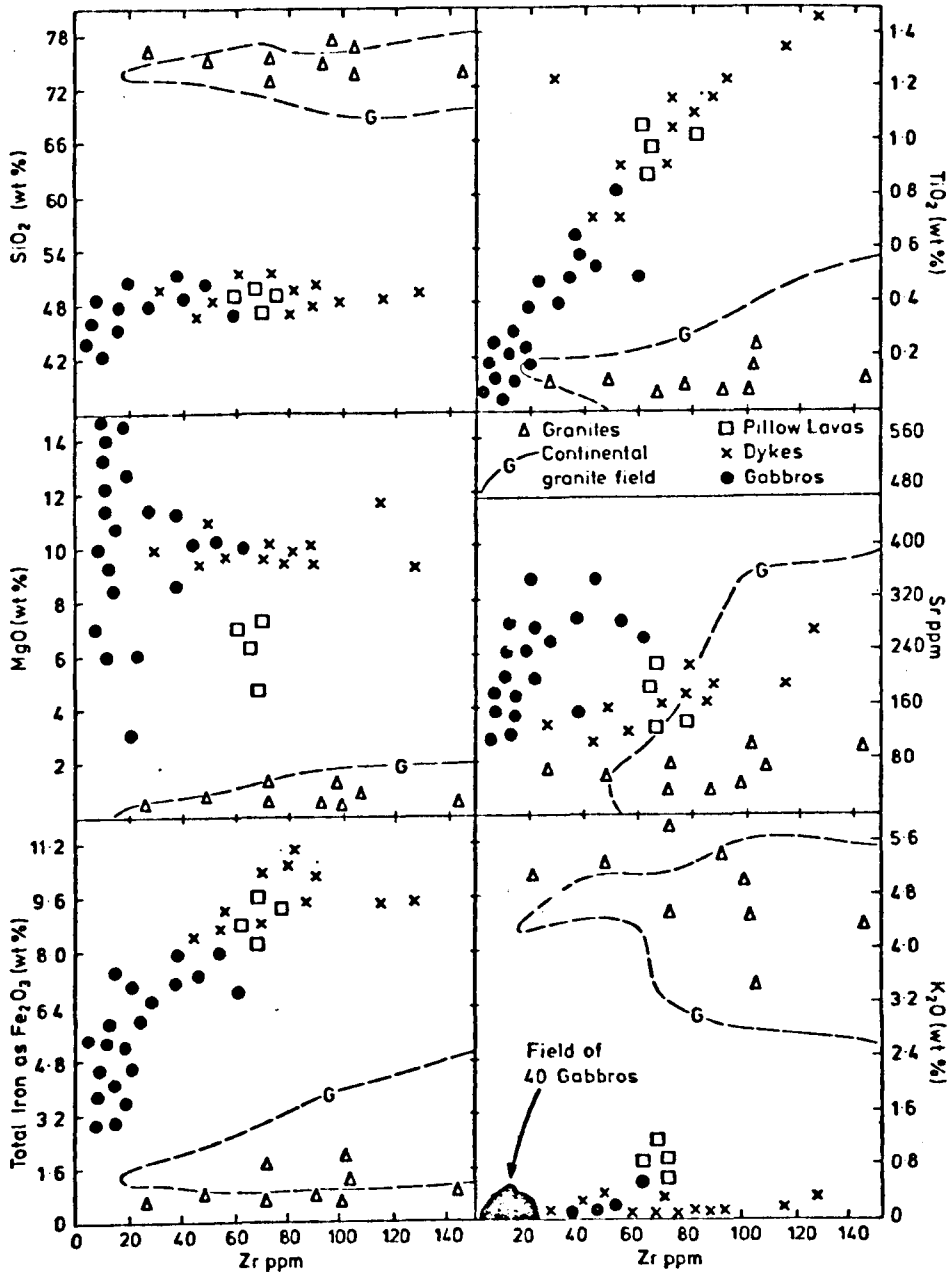
Figure 4. Plots of SiO₂, TiO₃, MgO, Sr, Fe₂O₃ and K₂O *v.* Zr for the Masirah mafic rocks and granites. Note the differentiation trends shown by the mafic rocks and the isolation of the granites. The continental granite fields are based on the following published sources: Alburquerque (1971, 1977), Beckinsale (1974), Clifford, Rooke & Allsopp (1967, 1969), Condie (1969), Hahn-Weinheimer & Ackerman (1967), Larsen (1948), Kolbe & Taylor (1966), MacDonald, Upton & Thomas (1973), McKenzie & Clarke (1975), Nagasawa (1970), Nockolds & Allen (1953), Smith (1974), Thompson (1968), West (1974).
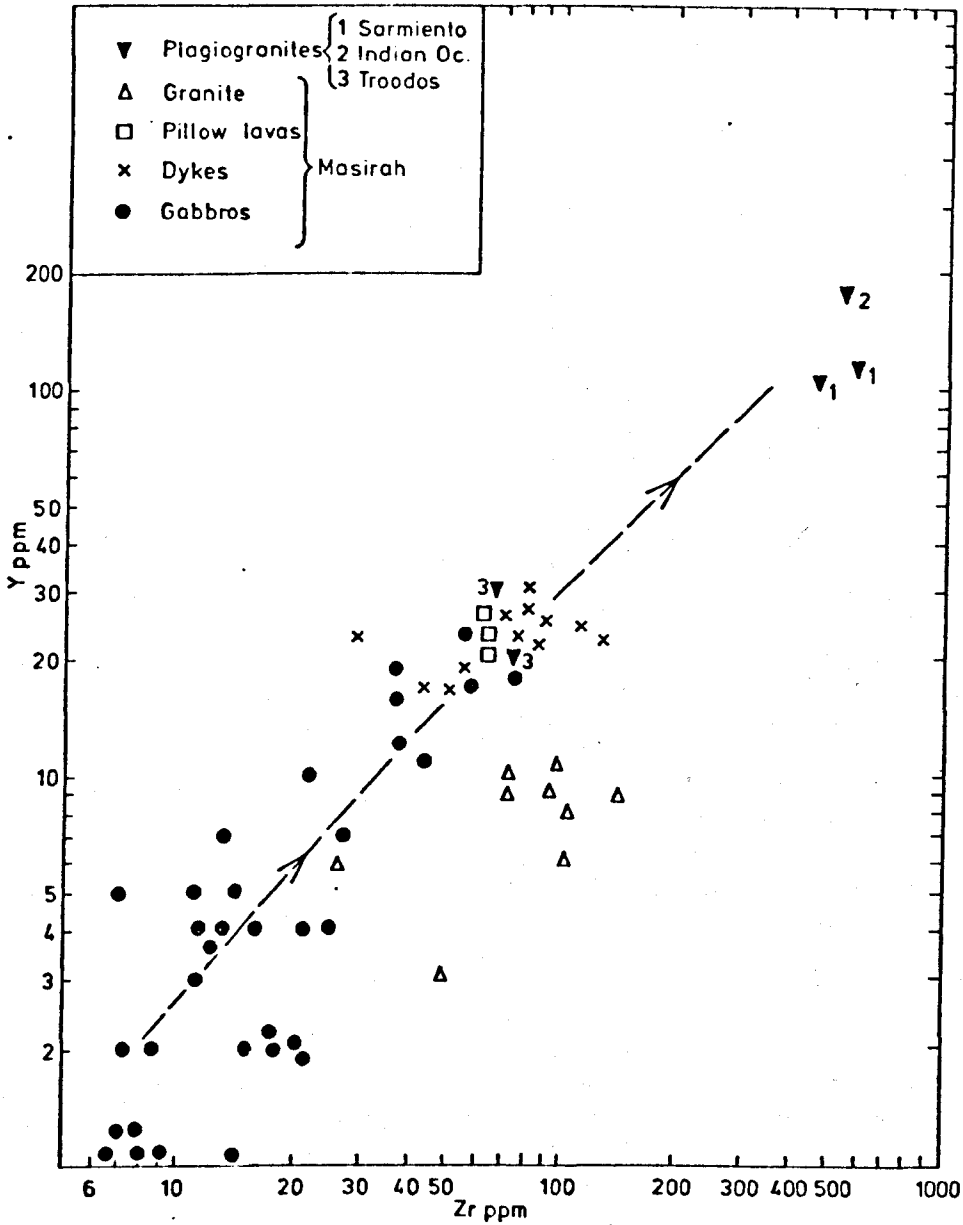
Figure 5. Plot of Y v. Zr for the Masirah mafic rocks, the Masirah granites, and for silicic differentiates of tholeiitic mafic rocks from the Sarmiento Ophiolite (Saunders *et al.* 1978), the Indian Ocean (Engel & Fisher, 1975) and the Troodos complex (Coleman & Peterman, 1975). Note how a continuation of the differentiation trend shown by the Masirah mafic rocks could produce the silicic differentiates but not the Masirah granites.

5. Ophiolite emplacement and granite origin

On geochemical grounds the Masirah granites, which occur on a completely ophiolitic island, are probably continental crust melts though a mantle source remains a possibility. Of relevance to their origin are the problems of the mechanism and timing of ophiolite emplacement. The Masirah ophiolite is demonstrably pre-Tertiary but can be assigned no lower age-limit as the base is never seen. The only dated rocks within the complex are early Cretaceous cherts and mid

Granites of Masirah Island

Cretaceous limestone blocks caught up in the western *mélange* (Glennie *et al.* 1974). Previous authors have correlated the ophiolite with the Semail Ophiolite of the Oman Mountains (Lees, 1928; Morton, 1959; Wilson, 1969), itself dated as Permian to Upper Cretaceous (Glennie *et al.* 1974); this correlation is based on lithological similarity and assumes the dextral displacement of Masirah along a postulated Masirah Fault (Fig. 1). Glennie *et al.* (1974) suggested the Semail was generated in a Mesozoic ocean to the NE of Oman and emplaced as a nappe south-westwards onto the Arabian continent in the Campanian. The Masirah–Semail correlation would involve the detachment of part of the ophiolite nappe (with some coupled continental crust beneath?) and its displacement 100 km SSW along the Masirah Fault, between the Campanian and the early Tertiary. The granites could then be partial melts of the continental crust beneath the ophiolite, and the major faults bounding the granites to the NE and SW (Fig. 2) could possibly be lines of structural weakness directing upward movement of the melts.

However, the reality of the Masirah Fault and the Semail–Masirah correlation is made less convincing by the reports of ophiolite at Ras Jibsh (Glennie *et al.* 1974), Ras Madhraka (Lees, 1928) and the Kuria Muria Islands (Reed, 1949; Mayer, pers. comm.), 100 km N, 150 km S and 400 km S, respectively of Masirah (Fig. 1). These occurrences, with Masirah, define an offshore ophiolite zone extending 500 km along the Arabian coast and geometrically inconsistent with a Masirah Fault displacing the Semail Ophiolite. The four ophiolite occurrences may define an ophiolite thrust front emplaced from the E or SE in the late Cretaceous and related to the northward movement of the Indian plate past the Afro-Arabian plate. As the ophiolite was emplaced either on to or against the Arabian continent, partial melting of the crust and upward granite intrusion into the ophiolite may have occurred. Here, as in the alternative origin above, the heat source for crustal fusion is conjectural. The absence of any evidence of subduction beneath the ophiolite argues against melting above a Benioff Zone. Perhaps relative motion at the plate boundary might have caused melting of the continental plate at depth? At the present time no more definite answer to the problem of crustal fusion beneath Masirah can be presented. As some support to this second hypothesis, granites of continental affinity are reported associated with the Kuria Muria ophiolite (Reed, 1949; Mayer, pers. comm.), whereas there are none reported in the Semail.

The other possible granite origin is that of a mantle source. Following Brown (1977), this would involve a destructive plate margin, subduction and mantle-melting at the subduction zone. Only the first hypothesis of ophiolite emplacement involving a Masirah–Semail correlations, could possibly involve this situation. However the lack of any end-Cretaceous island-arc or calc-alkali magmatism associated with the Semail seems to preclude such an explanation.

In conclusion the occurrence and geochemistry of the Masirah granites suggests an origin as continental crust melts probably produced at the time of ophiolite obduction, though in the absence of strontium isotope work a mantle source cannot entirely be ruled out.

ADDITIONAL NOTE CONCERNING THE ORIGIN OF THE HIGH-K GRANITE ON MASIRAH

Recent studies of granitic rocks have demonstrated the use that can be made of the REE in elucidating their petrogenesis (e. g. Alburquerque, 1978; Hanson, 1978). This note considers recently obtained REE data for the high-K granite which intrudes the Masirah Ophiolite and thus continues discussion of their origin begun in an earlier major-trace element study (Abbotts, 1978a).

The REE patterns of one of the granites and four plutonic rocks from the ophiolite are shown in Fig. 1. Fig. 2 compares the granite with selected silicic rocks from other areas. The sample used for REE determination (MA28) is one for which major and trace element data have been obtained (Table 2 : Abbotts, 1978a). Analyses were made by an INAA technique similar to that described by Randle et al (1968).

OPHIOLITE-GRANITE RELATIONSHIPS

The granite intrudes serpentinites and gabbros of the ophiolite. Throughout the 4 km^2 of intrusion there is little variation in either major or trace element levels and there are no associated basic-intermediate intrusives. Extreme fractionation within the ophiolite produces volumetrically insignificant tonalites and trondhjemites characterized by high Na/K, Zr, Nb and REE, low K and Rb, and $Cen/Ybn \sim 4$. These appear to be produced by ol-pl-cpx-hb-mt crystallisation from an initial tholeiitic liquid with $Zr \sim 50$ ppm and $Cen/Ybn \sim 1.5-1.7$ (Abbotts, 1978d; Chapter 3). Fig. 1 shows that the granite has an extremely fractionated pattern ($Ybn = 2.7$, $Yn = 3$, $Cen/Ybn = 39$) which cannot be derived by the crystallisation sequence in the ophiolite. A similar conclusion was reached earlier by trace-element studies (Abbotts, 1978a).

GRANITE SOURCE

There is no exposure on Masirah of any other possible source for these high-K granites. It is not clear if the pre-Permian calc-alkalic Arabian Shield (Greenwood et al, 1975) extends under Masirah from its nearest point 24 km distant on the Oman mainland. Consequently there can be no quantitative
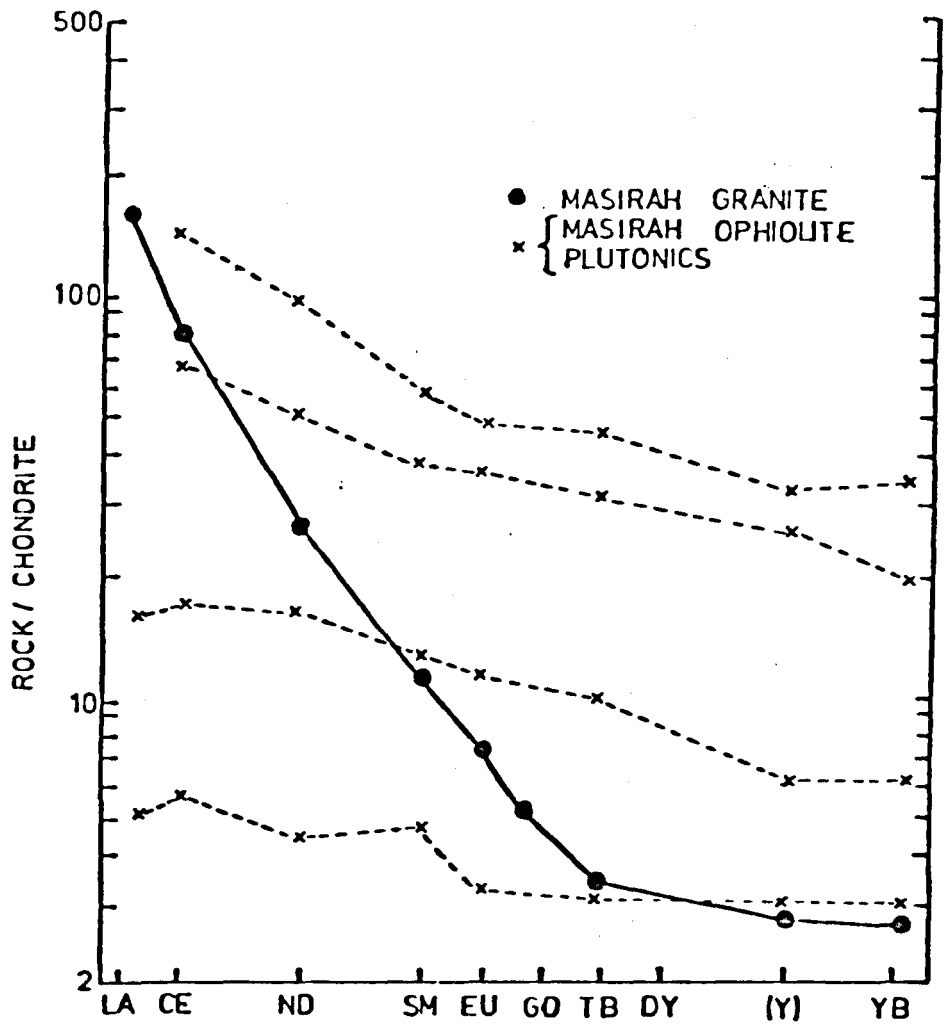
FIG.1. Chondrite-normalised REE patterns of the Masirah granite and four gabbros from the ophiolite. The gabbros are taken from Abbotts (1978d) and represent almost the complete range developed by fractional crystallisation. (Zr contents from bottom to top are 11, 58, 745 and 784 ppm).
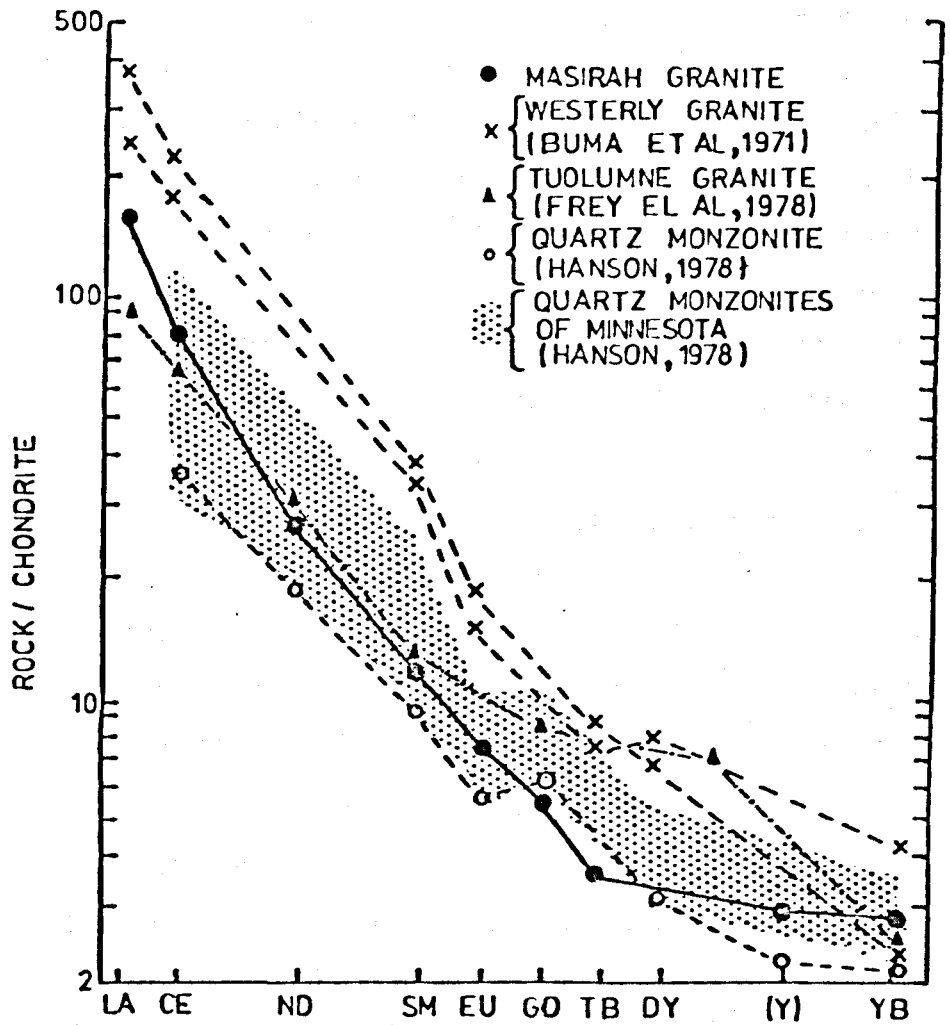
FIG.2. Chondrite normalised rare earth element patterns for the Masirah granite and other comparable granitic rocks.

petrological constraint of the source of these granites. Recent granite studies (e.g. Arth and Barker, 1976; Alburquerque, 1978, Frey et al, 1978; Hanson, 1978) suggest two possible origins for the extremely HREE depleted patterns of Fig. 2. These are (1) partial melting with residual garnet or hornblende or (2) fractional crystallisation of hornblende. In Fig. 2 the quartz monzonites (Hanson, 1978) and the Westerly granite (Buma et al, 1971) are believed to be derived by the former process. The very similar Tuolumne granite porphyry pattern was, however, produced by hornblende crystallisation in a concentrically-zoned granite pluton. Hanson (1978) suggests 20-50% melting of a greywacke-argill ite sequence with residual garnet-hornblende-plagioclase to produce the monzonites.

The homogeneity of the granites and the absence of associated basic-intermediate rocks may suggest partial melting of a rather uniform source with insignificant subsequent fractionation. The other possibility is that fractional crystallisation has taken place to produce the granites which then penetrated to a higher structural level by virtue of their greater buoyancy and volatile content.

The lack of an Eu anomaly in the granite suggests a balance either in the source residuum or during crystallisation between mineral phases with a positive anomaly (plagioclase, K-felspar) and those with a negative anomaly (garnet, amphibole, zircon, apatite, hypersthene). Hanson (1978) calculated that a residuum containing twice as much plagioclase as hornblende will generate a melt with no Eu anomaly. Involvement of plagioclase in formation of the granites is also indicated by their low Sr levels, which range 30 - 92 ppm, (Table 2 : Abbotts, 1978a).

The adjacent Arabian shield is an obvious possibility for a granite source. The shield is dominantly calc-alkalic and may possess the high Cen/Ybn ratios, and low Ybn levels, common in calc-alkaline rocks (e.g. Jakes and Gill, 1972; Bruhn et al, 1978). Both Hanson (1978) and Alburquerque (1978) suggest the melting of such a source in the lower crust to produce highly fractionated granites similar to Masirah.

GRANITE ZR AND NB LEVELS

The Masirah granites have low Zr (26-103 ppm, mean of 9 = 84 ppm) and relatively high Nb (23-93 ppm, mean of 9 = 57 ppm). The low Zr could indicate either (1) fractional crystallisation involving cumulus zircon or (2) partial melting with a residual zircon phase. Zircon fractionates the HREE (Hanson, 1978) and, whether cumulus or residual, will help slightly in producing the depleted HREE characteristic of these granites. Neary et al (1974) suggest that granites generated in and above subduction zones have lower Nb (0-10 ppm) than those of "within plate" granites (50-400 ppm). A Lower-Middle Cretaceous age for the ophiolite is suggested by associated sediments (Glennie et al, 1974). The absence of granites in the adjacent overlying Lower Tertiary limestone thus suggests granite intrusion in either Upper Gretaceous or early Tertiary. There is no evidence of subduction beneath Masirah during these, or later, times and therefore the Nb levels in these granites appear to agree with the observations of Neary et al (1974).

CONCLUSIONS

These granites possess fractionated REE patterns with high Cen/Ybn and low Ybn. Their REE chemistry can be explained by either fractional crystallisation or partial melting. Their very homogeneity and the absence of cogenetic basic-intermediate rock-types may favour the partial melting hypothesis. The low levels of Zr, Sr and HREE would then indicate a residual source containing plagioclase + zircon + (hornblende and/or garnet). Alternatively a fractional crystallisation model would involve plagioclase, hornblende and zircon as cumulus phases. The only evident source is the adjacent Arabian shield. The heat source for possible partial melting is unknown but the moderately high Nb levels may suggest dry melting which would agree with the lack of geological evidence for subduction involvement.

CHAPTER 9

A MODEL OF THE CONSTRUCTIVE MARGIN
AT WHICH THE MASIRAH OPHIOLITE WAS FORMED

Fig. 1 is an interpretive cross-section of the constructive margin at which the Masirah Ophiolite was formed, based on field, petrological and geochemical data. Disruption suffered during ophiolite emplacement precludes correlation of Fig. 1 with any one section through Masirah but all features, except for relationships in the crystallising magma chambers, are based on recorded evidence. Fig. 2 provides an index map for the various locations used in the model. Points to be noted on Fig. 1 are designated A - T, approximately ordered from left to right, and include:

A1-2 Sub-vertical faults, with significant displacements, have trends approximately parallel to the strike of the sheeted dykes and thus to the original ridge axis. Examples are found associated with the Gp. 3 serpentinite lenses (A1; Chapter 2) and also at Urf (A2), where sheeted dyke complex (90% dykes) is faulted against gabbro (10% dykes). In the former case the faults appear to have acted as loci for upward serpentinite diapirism; thus NW of Haql serpentinite intervenes between gabbro, intruded by some dolerite dykes, and red pillow lavas. Analogous relationships involving serpentinite diapirism along faults parallel to the ridge-axis have been recorded on the M. A. R. (Bonatti, 1976). These major faults may have provided passageways for the significant hydrothermal circulation necessary to produce the observed dyke-lava metamorphism.

B1-2 The cumulate-harzburgite boundary is a surface of shearing and gabbro-gabbro pegmatite-dolerite intrusion (W. of Jabal Hamra, Jabal Shabbah). Both processes may have occured in the near-axis environment, before cooling and "welding" together occurs and while significant amounts of magma were available.
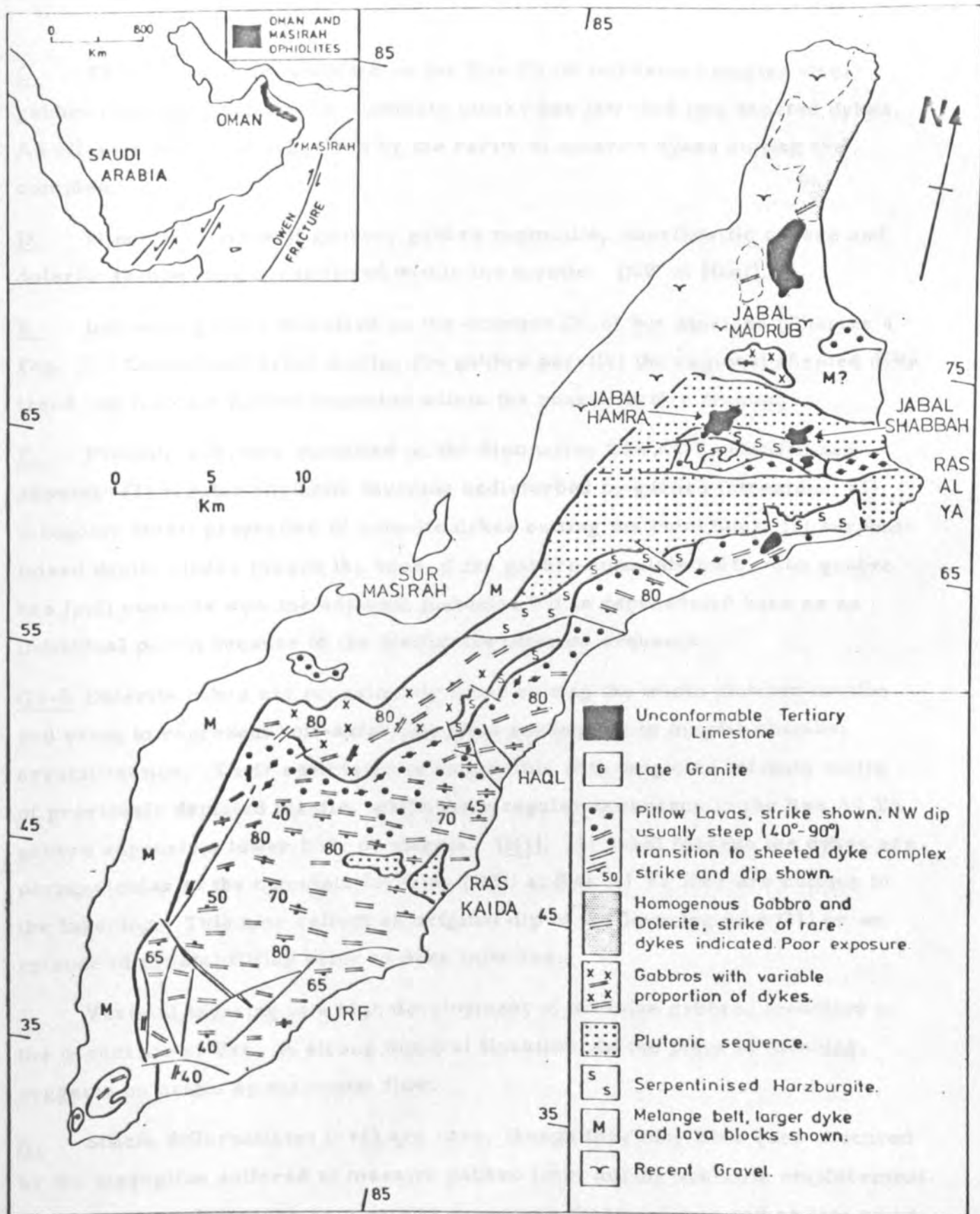
FIG.2. Geological map of Masirah Island showing the distribution of the main lithologies and showing the localities used in the cross-section of Fig.1.

C.   This intrusion is modelled on the Ras Kaida intrusive complex where gabbro containing ultramafic cumulate blocks has intruded into sheeted dykes. An off-axis timing is suggested by the rarity of dolerite dykes cutting the complex.

D.   Minor intrusions of gabbro, gabbro pegmatite, anorthositic gabbro and dolerite trapped and crystallised within the mantle.   (NW of Haql).

E.   Intrusive gabbro modelled on the example SE of Sur Masirah (Chapter 4 : Fig. 2).   Occasional dykes cutting the gabbro parallel the regional sheeted dyke trend and indicate gabbro intrusion within the zone of active tension.

F.   Plutonic sequence modelled on the distinctive Ras Al Ya Gabbro and showing: (1) regular rhythmic layering undisturbed by gabbro intrusions; (2) a regular small proportion of dolerite dykes cutting the cumulates; (3) serpentinised dunite blocks toward the base of the gabbro cumulate unit.   The gabbro has fault contacts with the adjacent plutonics but is represented here as an individual pluton because of the distinctive internal sequence.

G1-2 Dolerite dykes are occasionally found cutting the whole plutonic section and seem to represent "off-axis" intrusion subsequent to magma chamber crystallisation.   Their chemistry is compatible with origin as off-axis melts of previously depleted mantle, while their regular occurence in the Ras Al Ya gabbro suggests a lower body of magma   (H1).   At Jabal Madrub the dykes are perpendicular to the cumulate layering (G2); at Ras Al Ya they are oblique to the layering.   This may reflect an original dip of the layering (see G1) or an episode of crustal tilting prior to dyke injection.

J.   Vertical layering in a high development of massive gabbro, modelled on the occurence at Urf.   A strong mineral lineation, in the plane of layering, suggests an origin by magmatic flow.

K.   Silicic differentiates (+++) are rare, though they may have been obscured by the disruption suffered at massive gabbro level during ophiolite emplacement. The only examples occur as a narrow screen to sheeted dykes and as late veins cutting magmatic gabbro breccias.   The breccia represents repeated gabbro intrusion and may reflect (1) a zone of crustal weakness which attracted the through-put of magma or (2) the contact of two magma chambers.

L.   Significant variation in the depth of the dyke-gabbro transition is indicated by the outcrops W. of Sur Masirah where large ($\sim$1 km) exposures of sheeted dykes alternate with massive gabbro intruded by only occasional dolerite dykes.

M.   Layering is best developed in the ultramafic cumulates (N. of Jabal Hamra). The gabbro cumulates possess a good lamination but layering is only sporadically developed.

N.   Gass and Smewing (1978) suggest that the hydrothermal metamorphism seen in ophiolites is probably imposed in the zone of active axial volcanism. The metamorphic facies developed in the Masirah Ophiolite are indicated below N. (Fig. 1) but no attempt is made to show the pattern of water circulation. The geothermal gradient has been estimated at 170-200°C/Km (Abbotts, 1978b; Chapter 4).

O.   The prescence of massive gabbro screens to within 300-400 m vertically of the first pillow lavas at Haql (860505) suggests axial underplating which is gradually isolated by continual dyke injection as the underlying magma chamber (P) solidifies.

P.   The relationships within the magma chamber are hypothetical. It has been suggested that underplating at the roof will be encouraged by convective cooling of the overlying upper crust (e.g. Cann 1974). Cumulate rock textures suggest crystal settling on the chamber floor whilst thermometry-barometry studies of the cumulates suggest crystallisation temperatures and pressures of $\sim$930°C and 1-2 Kb (3-6 km).

R.   The geochemistry of the bulk of the cumulate rocks suggests an open system where liquid fractionation is inhibited. Magma is probably semi-continuously supplied from beneath and released through the roof. The rare silicic rocks (K) may represent localised closures of the system and complete crystallisation.

S.   The LREE-enriched characteristics of the Masirah dykes and gabbros suggest 10-15% partial melting of the source peridotite before melt separation. This assumes a source with a flat, 2x chondrite REE pattern. Mass balance

calculations assuming a total magmatic fraction of 6Km thickness and 12.5% melting suggest the original prescence of ~40 Km of harzburgite. This may indicate melting in the spinel-lherzolite - lower plagioclase lherzolite stability fields. However gross approximations are involved here because of the lack of precise knowledge of the REE characteristics of the undepleted source.

TECTONIC ENVIRONMENT OF THE MASIRAH SPREADING AXIS

The study of any fully-developed ophiolite should consider the possibility of defining the type of constructive margin represented. The alternatives appear to be a major mid-ocean ridge, a smaller "Gulf of Aden" type spreading centre, or a back arc basin-island arc environment. In the case of Masirah the geological possibilities appear to be (1) correlation with the large Semail Ophiolite of the Oman Mountains and formation in the same Cretaceous ocean, situated to the NE of Arabia, as that ophiolite or (2) rejection of the correlation and generation during an early Indian Ocean spreading episode.

Chemical studies of the axis sequence dykes-lavas preclude the possibility of an island arc environment but are inconclusive in discriminating the spreading centre type. Of significance amongst the geological evidence schematically illustrated on Fig. 1 are the following:-

1.   a thick dyke unit (~1.8Km);

2.   common gabbro screens amongst the sheeted dykes and a gradual vertical transition from 100% dykes to 90-100% gabbro;

3.   the evidence of "off-axis" magmas in the late dykes, the Ras Kaida pluton, the dykes cutting the gabbro intrusion into sheeted dykes near Sur-Masirah and the occasional dolerite dykes cutting serpentinized harzburgite;

4.   the disrupted nature, which seems to reflect near axis faulting and related serpentinite diapirism.

Cann (1974) suggests that a thicker dyke unit is encouraged by slower spreading and the resulting depression of the crustal isotherms. In the case of

the MAR there appears to be a correlation between a slow rate of spreading, a rifted axial valley, and extensive serpentinite diapirism on both transforms and faults parallel to the ridge (Bonatti, 1976; Bonatti and Honnorez, 1976 and 1978; Dewey and Kidd, 1977). The extensive gabbro screens and evidence of "off-axis" magmas on Masirah may indicate a wide zone of intrusion.

Thus the Masirah Ophiolite appears to bear the characteristics of a slow-spreading, much faulted, ridge. Present day spreading axes exhibit similar features along both the MAR and also in the marginal basins of the Philippine Sea (Fountain et al, 1978), and the Sea of Japan - Shikoku Basin area (Kobayashi and Isezaki, 1976; Marsh, pers. comm). It appears that neither internal geology nor geochemistry can constrain the type of spreading-centre, largely because no discriminatory parameters have been set up by study of the modern equivalents.

NON-EQUIVALENCE OF THE MASIRAH AND SEMAIL OPHIOLITES

Previously it has been suggested that the Masirah Ophiolite should be correlated with the Semail Ophiolite of the Oman Mountains. This belief was based on geographical proximity and lithological similarity : both contain (serpentinised) harzburgite, "gabbros" composed of olivine $\pm$ plagioclase $\pm$ clinopyroxene, trondhjemites, a sheeted dyke complex and pillow lavas. Subsequently, however, it has been demonstrated that most ophiolites are formed of this association (Penrose Conference, 1972).

Comparison of Masirah with published and verbal reports of the Semail Ophiolite suggest the following distinct differences:

1. The Semail forms an enormous, largely intact, ophiolite resting on a horizontal thrust. A tectonic melange is developed along the thrust, whilst beneath this is an exotic limestone-pillow lava association and a sedimentary olistostrome unit. All units are sub-horizontal in attitude. In contrast the Masirah Ophiolite exhibits a disrupted nature, heavily faulted in directions perpendicular and parallel to the sheeted dykes and penetrated by serpentinite lenses. The melange which terminates the ophiolite to the west appears to be a vertical structure

and is formed largely of all ophiolitic components, with the "extras" of cherts and exotic limestones with associated pillow lavas. The structure appears to be oceanic in origin and disruption of the complex may have an origin both at and near the ocean ridge and during uplift as an ophiolite. All faults are sub-vertical and there is no evidence of thrusting. The contrast of the two ophiolites probably reflects a different mechanism of emplacement but also, possibly, a more rifted spreading centre at Masirah.

2. The Semail is thrust over Mesozoic sediments of the Hawasina formation, which include exotic limestones of Mid-late Permain and Late Triassic age (Glennie et al, 1974). The Mesozoic cherts and exotic limestones on Masirah are all Lower-Mid Cretaceous (Valanginian-Cenomanian : Glennie et al, 1974) and tectonically included within the vertical ophiolite melange.

3. The Masirah axis sequence has "typical" spreading centre trace element levels including moderately high Cr (mean of 44 = 303 ppm) and Ni (mean of 44 = 91 ppm) values. The Semail, in comparison, has significantly lower Ni-Cr levels (Pearce, pers. comm.) Low levels of Ni and Cr appear to be developed during wet melting of peridotite, one example being in the production of island arc tholeiite basalts. The higher Masirah levels may indicate melting away from the influence of subduction and the water that subduction introduces into the mantle.

4. The regular ENE-WSW sheeted dykes on Masirah contrast with the N-S trends found in the northern, and possibly southern, parts of the Semail Ophiolite (Smewing et al, 1977; Smewing, pers. comm.; Coleman, pers. comm.)

5. The Masirah Ophiolite has been intruded by a high-K granite which appears to be absent in the Semail (Aldiss, pers. comm).

It is suggested that these differences reflect distinct origins and emplacement histories for the two ophiolites.

PLACE OF ORIGIN AND EMPLACEMENT OF THE MASIRAH OPHIOLITE

Since it seems unlikely that the Masirah and Semail Ophiolite should
be correlated it is suggested that the Masirah ocean crust may have originated
during initial (?Mid-Late Cretaceous) ocean floor spreading involved in the
break-up of Gondwanaland (Abbotts, 1978b; Moseley and Abbotts, 1978;
Chapters 4 and 7). Unfortunately the extensive sediment cover of the adjacent
Arabian Sea - Owen Basin-Indus Cone has prevented the detailed study of the
basement of this margin of the Indian Ocean that has been made at the Australian
margin (e.g. Larson 1975 and 1976). Consequently little is known of the
details of the separation of India from Afro-Arabia. Nonetheless Fig. 3
indicates the apparent oceanic nature and Late Cretaceous-Lower Tertiary age,
of much of the northern Indian Ocean-Arabian Sea. It may be significant that
axis sequence chemistry and an absence of turbidite-type sediments both suggest
generation distant from subduction zone or continental landmass for Masirah.

It is suggested that ophiolite uplift into its present position was caused
by local compression at the plate boundary of continental Arabia and the
oceanic Indian Ocean plate (Moseley and Abbotts, 1978; Chapter 7). Both
plates moved northwards away from Antarctica in the Cretaceous-Tertiary
but movement may not have been completely parallel and could have involved
compression at the plate boundary. Relative movement during the Tertiary was
probably largely accommodated along the Owen Fracture (Whitmarsh et al, 1976)
but the importance of this structure becomes less clear in the Late Cretaceous-
Lower Tertiary. Without geophysical evidence it is not possible to tell if actual
emplacement onto continental crust has occured but the intrusive granites,
which appear to have been generated by melting of continental crust, may suggest
this.

FIG.3. Map of the northern Arabian Sea. Data sources:
(a) magnetic anomalies and transform faults. (McKenzie and
Sclater, 1971; Whitmarsh and others, 1974), (b) D.S.D.P.
stations and results (Whitmarsh and others, op.cit),
(c) bathymetry, gravity anomalies and earthquake epicentres.
(Geological and geophysical atlas of the Indian Ocean, 1975),
(d) seismic refraction studies and estimates of sediment
thickness (White and Klitgord, 1976; Farhoudi, 1977).
Dyke trends: Oman Mountains (Smewing et al, 1977; Smewing,
pers.comm.), Masirah (this study). Note the approximate
parallelism of the Masirah dykes and the melange with,
respectively, the Indian Ocean magnetic anomalies and transform
faults. Owen Basin magnetic anomalies : Whitmarsh (1978, in press).

FIG.1. Interpretive cross-section of the constructive margin at which the Masirah Ophiolite was formed. Section is at right angles to the ridge axis and therefore to the sheeted dykes. Relationships shown at A-T are discussed in the text. Thicknesses of the units are calculated from the maximum exposed thickness and the average unit dip.

APPENDICES

1. Representative petrographic descriptions of each rock-type

2. Microprobe analyses : technique and results

3. Modal analyses

4. Cumulus-intercumulus phases : type and order of crystallisation

5. Location maps of analysed samples

6. Whole-rock geochemistry : analytical techniques and results

7. References

APPENDIX 1.   REPRESENTATIVE PETROGRAPHICAL DESCRIPTIONS

Note: Locations of all samples used for chemical and petrographic analysis are shown in Appendix 5, maps A-H.   Each description here is headed by a rock collection number (e.g. MA136) and a location map letter (e.g. A).   Definitive mineral names and compositions are provided by microprobe analysis. Modal analyses of further specimens are presented in Appendix 3. There is a continual transition throughout all of the gabbroic rocks described here.

1.   Serpentinised harzburgite - e.g. MA136 (A)   Plate A.1.a.

Macroscopic : green-black serpentine matrix to rectangular bronze bastites (after orthopyroxene; $\leq$ 6 x 4 mm).

Microscopic, general : advanced serpentinization (99%) has destroyed any igneous texture.

Mode : Serpentine (+ magnetite) after olivine = 73.3 (8.9), "bastite" = 17.3, spinel = 0.2.

Olivine : rare relicts (1-2%, < 0.02 mm).

Serpentine : mesh texture; narrow cross fibres ($\sim$ 15%) through "massive"type.   Chrysotile + lizardite (XRD).   Cross-fibre veinlets have magnetite grains concentrated along centres. Bastites form perfect orthopyroxene pseudomorphs, preserve cleavage and clinopyroxene exsolution lamellae; isolated or group with larger spinel grains; rectangular to irregular shape.

Spinel : dark brown-black; small irregular grains $\leq$ 0.03 mm, rarely $\leq$ 1.75 mm.

Deformation : narrow cataclased serpentine   bands ($\leq$ 0.1 mm), rotated kinked bastites.

Plate A. 1. 1
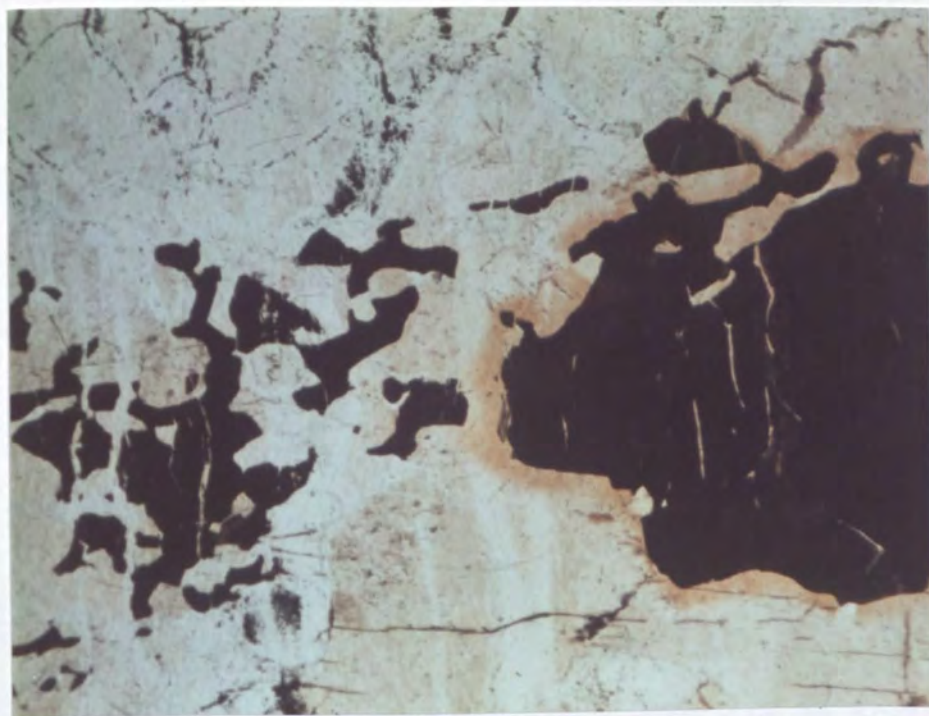
(a)   Unusually large chrome spinel grain in serpentinised harzburgite. X101. ppl. X12.5
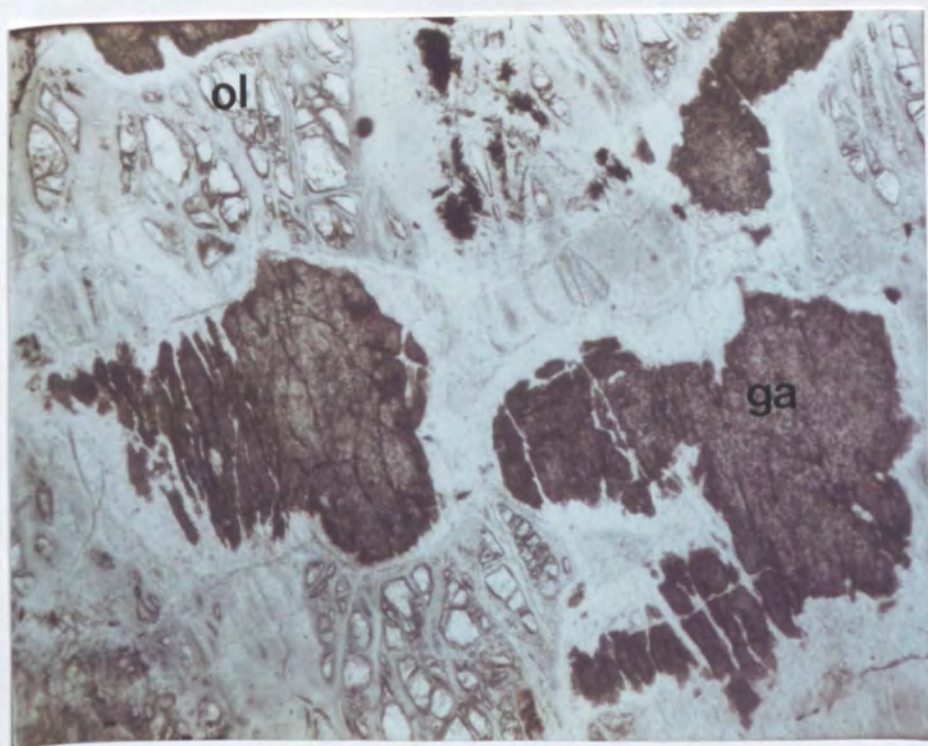
(b)   Rodingite reaction in a plagioclase-bearing dunite. The plagioclase is transformed into a hydro-garnet rimmed by chlorite-amphibole. The olivine occurs as relicts in serpentinite. MA217 ppl. X12.5

2. Serpentinised dunite - e.g. MA2 (B)   Plate A.1.b.

Macroscopic : rounded brown-black serpentinised olivines, 1-5 mm,

in minor grey intercumulus plagioclase-diopside.

Mode : olivine (F087) 47.9, serpentine (after olivine) 31.3,

plagioclase 6.6, diopsidic clinopyroxene 7.0, chromite 5.1.

Olivine : rounded grains, unzoned, weak elongation and alignment,

0.75-3 mm. 50% serpentinization.

Plagioclase : unzoned, intercumulus, xenomorphic, 4-5 mm.   70%

rodingitized (Degree of rodingitization correlates with that

of serpentinization.)

Clinopyroxene : fresh, poikilitic, 2-4 mm, irregular distribution,

unzoned, light-brown, minor exsolved orthopyroxene, contemp-

oraneous with plagioclase.

Spinel : precedes olivine, anhedral equant grains < .5 mm.

3. Clinopyroxene troctolite e.g. X130 (B)   Plate A.2.a.

Macroscopic : rhythmic layering, 10-12 mm scale, of cumulus

olivine $\lesssim$ cumulus plagioclase. Olivine defines weak

lamination, plagioclase plates good lamination, both parallel

layering.

Mode : olivine (F085) 29, serpentine 31, plagioclase (An85) 27,

diopside 12, ore 1. (Olivine rich-layer).

Olivine : as under dunite, rounded cumulus grains.

Plagioclase : subhedral cumulus plates, elongate parallel

albite-carlsbad twins (010), mean size = 3 x 1.5 mm ($\lesssim$ 5 x 3 mm),

fractured by cracks radiating from serpentinised olivines,

unzoned, fresher than in dunites.

Clinopyroxene : as under dunite, poikilitic, intercumulus.

Plate A. 1. 2
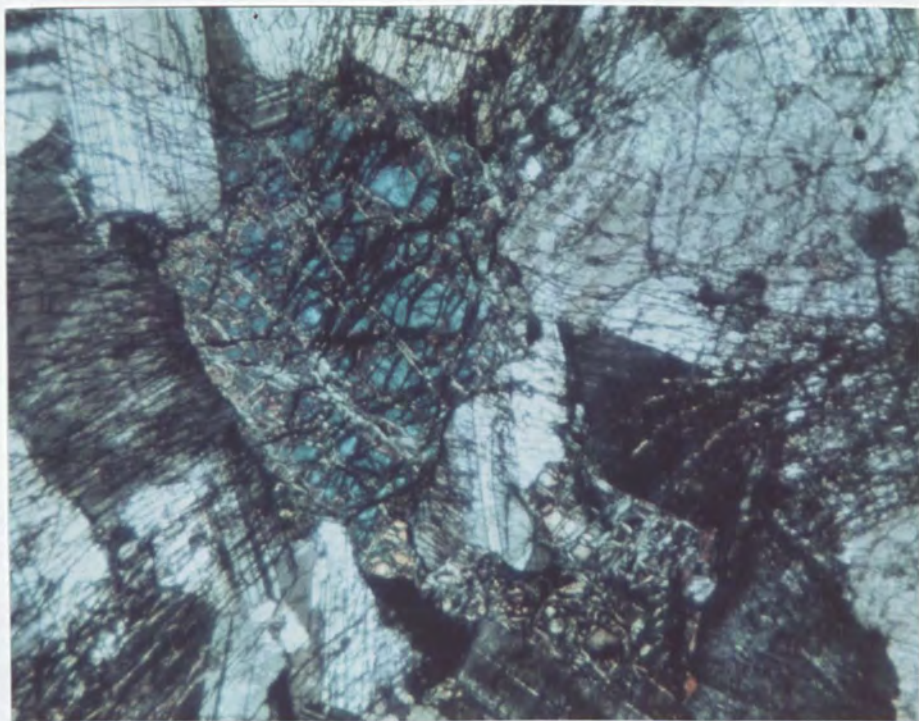
(a)   Olivine-plagioclase relationships in a clinopyroxene-
       troctolite. Minor olivine serpentinization is shown to
       be an expansive process by the radial fractures of
       the plagioclase grains. X272. Xp. X5.
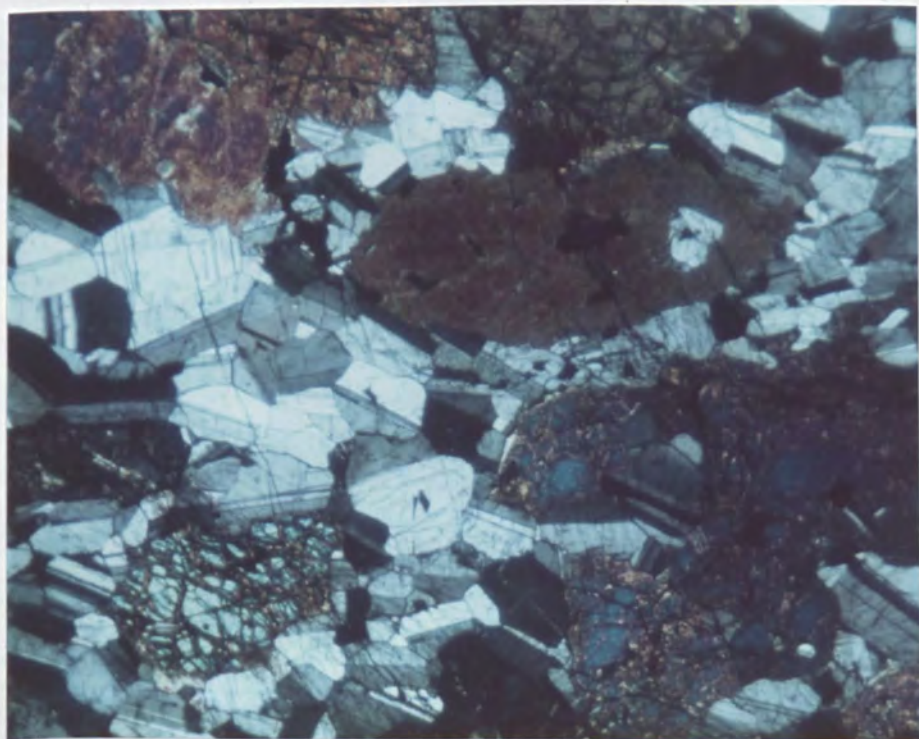
(b)   Olivine gabbro showing good igneous lamination
       defined by olivine, plagioclase and clinopyroxene.
       MA21. Xp. X5.

4. <u>Olivine-gabbro e.g. X131 (B)</u>   Plate A.2.b.

Macroscopic : rhythmic layering, 8-10 mm scale, 3-phase

cumulate (ol, pl, cpx), homogenous types also occur; good

mineral lamination defined by plagioclase (010) plates, elliptical

olivine crystals, diopside plates; lamination parallels layering.

Mi roscopic general : mode of little use in layered rocks; all

3 phases subhedral with straight crystal boundaries; fresher

as olivine decreases in abundance.

Olivine : 3-4 mm long axis, common simple twins, serpentinization

20%.

Plagioclase : fresh plates with good alignment parallel

layering, variable size (l = 0.5 - 4 mm, l/w = 4:1), hair-line

fractures with cataclasis common, minor rim zoning (An85-82).

Diopside : plates unzoned, < 7 x 2 mm.

5. <u>Pyroxene leucogabbro e.g. MA126 (C)</u>   Plate A.3.a.

Macroscopic : pale grey, unlayered but laminated,

anorthositic with minor green clinopyroxene.

Microscopic general : coarse (4-6 mm) hypidiomorphic,

plagioclase > diopside cumulate.

Mode : plagioclase (An69) 75, diopside 17, uralitic amphibole

(actinolite + hornblende) 8.

Plagioclase : dominates rock, subhedral tabular plates aligned,

6 x 1.5 mm, rare small intercumulus grains (< 0.3 mm), minor

rim zoning.

Diopside : anhedral-subhedral stumpy prisms, 5 x 1.5 x 1 mm,

elongate //c, poor alignment, single 100 twins common.

Plate A. 1. 3.
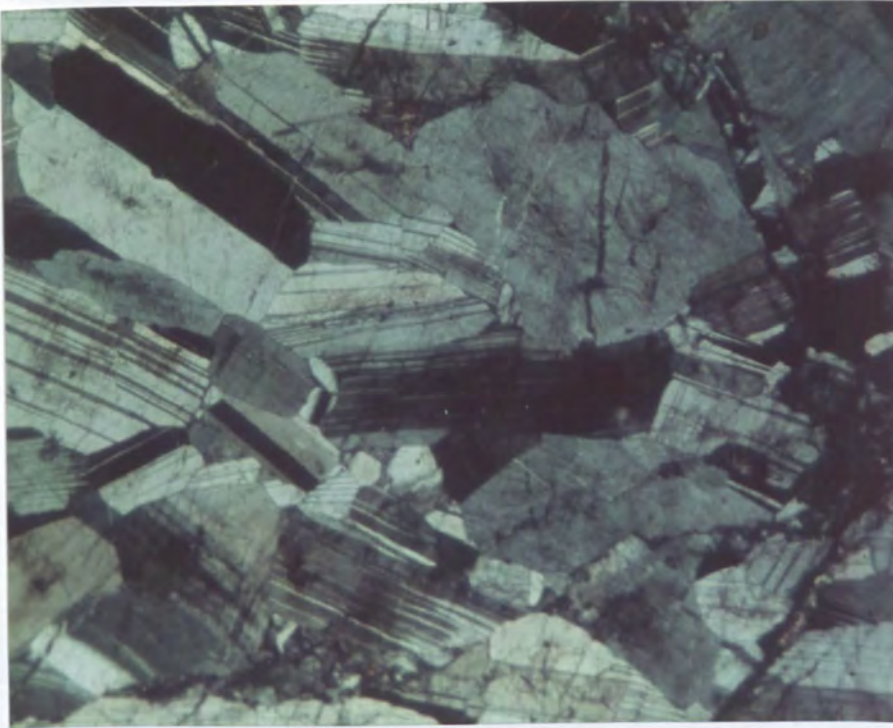
(a)   Anorthositic gabbro showing good igneous lamination.
      X268.   xp.   X12. 5
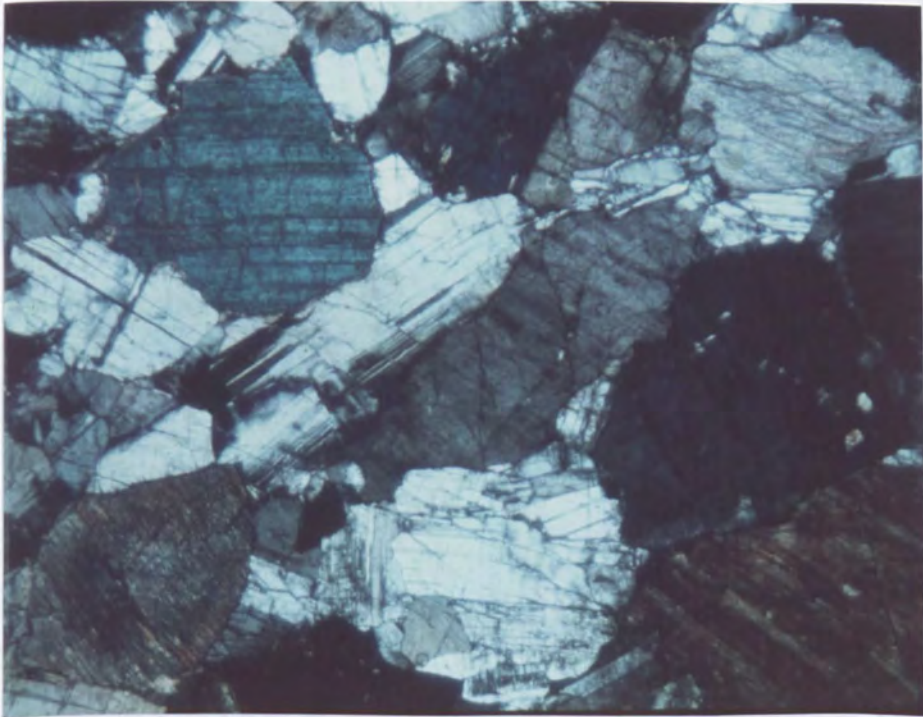
(b)   Pyroxene gabbro with xenomorphic granular texture.
      MA54   xp.   X5.

Deformation : narrow fractures common, tend to sub-parallel, some with minor cataclasis, displacement and granulation of crystals, chlorite and epidote veining along some.

Uralitization : minor (30%), attacks clinopyroxene margins and along cleavage; actinolite, actinolitic hornblende and hornblende (all green). Some samples show more extensive replacement.

6. <u>Pyroxene gabbro e.g. X186 (C)</u>   Plates A.3.b., A.4.a.

Macroscopic : medium-coarse, massive, grey gabbro.

Microscopic general : xenomorphic granular (some samples, usually cut by dykes, are coarsely sub-ophitic).

Mode : diopside = 35, plagioclase (An83) = 51, hornblende (secondary) = 14.

Plagioclase : anhedral, mutually interfering boundaries, 3 x 1.5 mm, no alignment, rim normal zoning (An83-77).

Diopside : anhedral prisms to poikilitic, 4 x 2 mm, common 100 twins and good 100 cleavage; minor (< 30%) uralitization (green hornblende > actinolite).

Deformation : hair-line fractures, sub-parallel, associated kinking of cleavage and twinning or slight granulation (< 0.1 mm).

7. <u>Pyroxene gabbro - MA276 (C)</u>

Macroscopic : medium grain, grey gabbro; screen between dolerite dykes.

Microscopic general : sub ophitic texture.

Plate A. 1. 4.
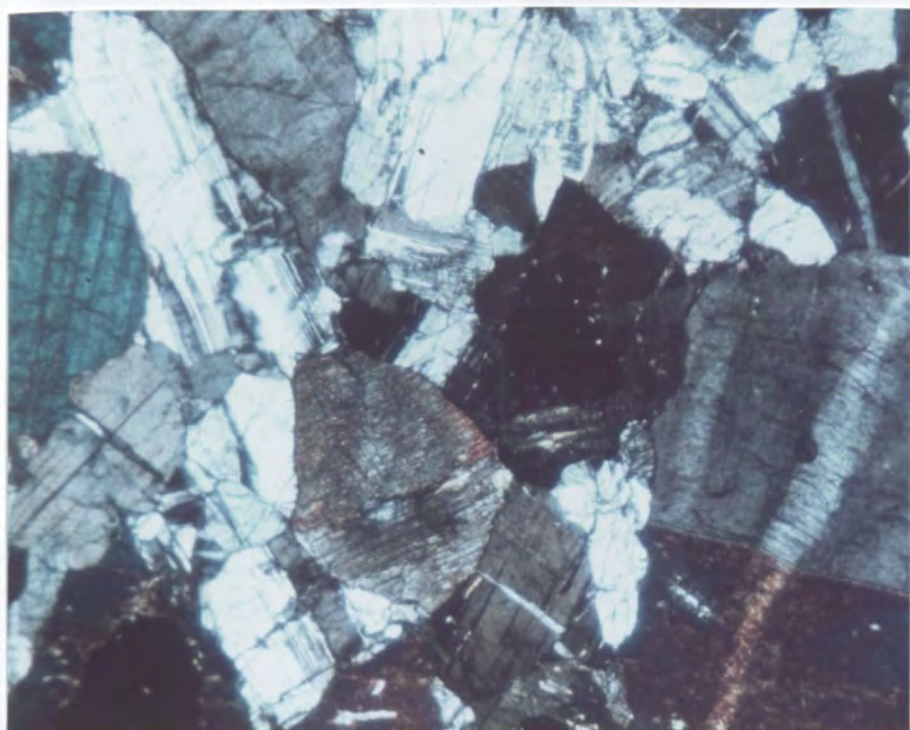
(a) Pyroxene gabbro with xenomorphic granular texture.
Deformation has caused kink-banding of the bottom
right clinopyroxene grain.   MA54 xp.   X5.
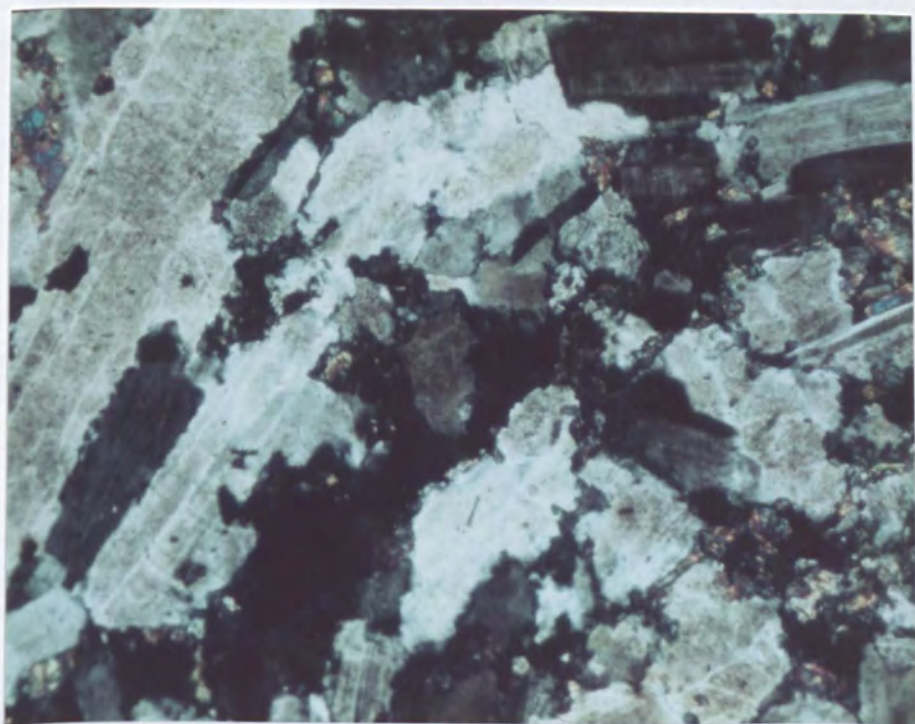
(b) Tonalite composed predominately of saussuritized
plagioclase with minor interstitial epidote.
MA417 xp.   X12.5

Plagioclase : subhedral, straight boundaries, 010 elongation but no alignment.

Diopside : anhedral poikilitic plates partially enclosing plagioclases, 6 x 5 mm.

Hornblende : brown primary hornblende crystallised late, prismatic, grows out from diopside crystals but is not replacing them.

Opaque : rare, equant, ilmenite grains ($<$0.5 mm).

8. Pyroxene gabbro - MA272 (C)

Macroscopic : medium-coarse, grey gabbro; layering developed (discontinuous), parallel lamination and good mineral lineation of diopside and plagioclase (rare).

Microscopic : excellent lineation of 20% diopside prisms.

Plagioclase : as above but plates aligned.

Diopside : 7.0 x 1.0 x 1.0 mm, long axes aligned, minor rim uralitization, larger size than plagioclase (= few nucleation centres), subhedral, 100 twinning.

Deformation : hair-line fractures common.

9. Tonalite - MA417 (D)   Plate A.4.b.

Macroscopic : medium grain, pink screen in sheeted dyke complex, similar petrographically to leucogabbro (5).

Mode : plagioclase 80, epidote 13, amphibole 7.

Plagioclase : subhedral aligned plates, 2-3 mm, partially interlocking.

Epidote : anhedral, interstitial, $<$ 0.5 mm. (A similar sample from a gabbroic breccia contained tiny ($\sim$0.1 mm), high relief, zircons).

10. Trondhjemite - X308 (D)

Macroscopic : 3 cm wide vein cutting grey massive gabbro
which is intruded by < 10% dolerite dykes.

Mode : plagioclase (albitic) = 47, quartz = 41, calcite + epidote
= 12.

Plagioclase : large (3-4 mm) crystals in a fine-grain quartz
matrix; sutured margins and quite porphyroblastic in appearance;
strong zoning.

Quartz : fine-grain (0.2 - 0.3 mm) and granulated.

Veining : quartz-epidote and calcite veins follow lines of
concentrated cataclasis.

11. Uralitised gabbro e.g. MA246 (C)   Plate A.5.a.

Macroscopic : unlayered, medium-coarse, grey-green gabbro
intruded by dolerite dykes; greener appearance = altered
plagioclase + uralitic amphibole.

Microscopic general : xenomorphic granular.

Mode : plagioclase (An71) = 60, clinopyroxene = 10, secondary
amphibole = 30.

Plagioclase : 0.5-2 mm, anhedral, interfering boundaries with
pyroxene, 50% saussuritization,   concentrated along rock
fractures, normal zoning (An71-61).

Clinopyroxene : relicts (< 0.3 mm) in green uralitic
actinolitic hornblende and hornblende.

Amphibole : xenomorphic areas occupied by fibrous amphibole
(< 5 mm), minor fibrous chlorite intergrown.

Plate A. 1. 5.
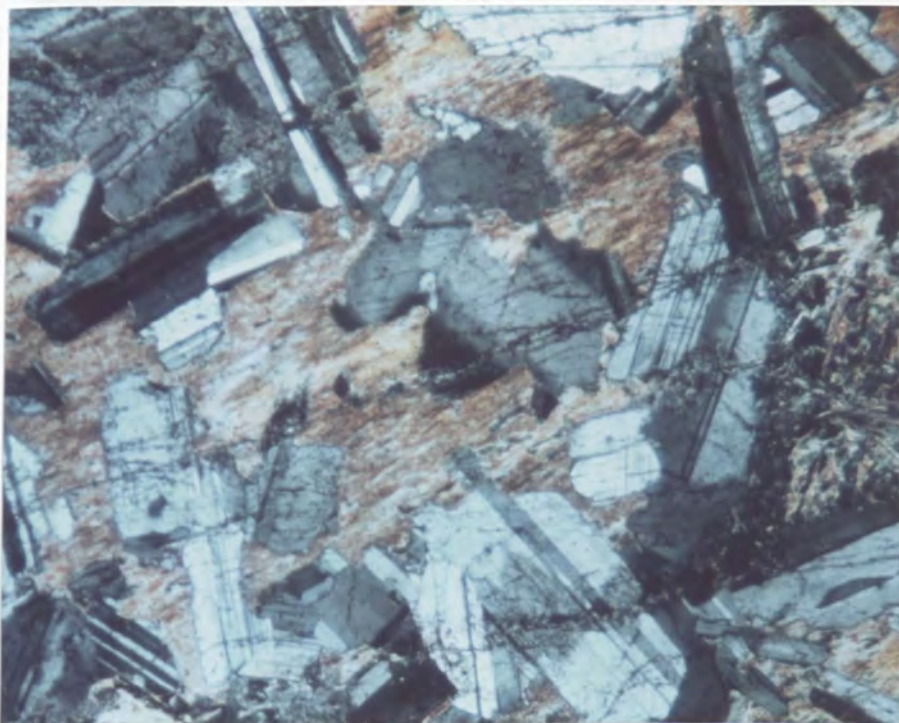
(a)   Uralitized ophitic gabbro. (Screen to sheeted dolerite
dykes). Fresh plagioclase laths within extensive
uralitic amphibole. X156. xp. X12.5
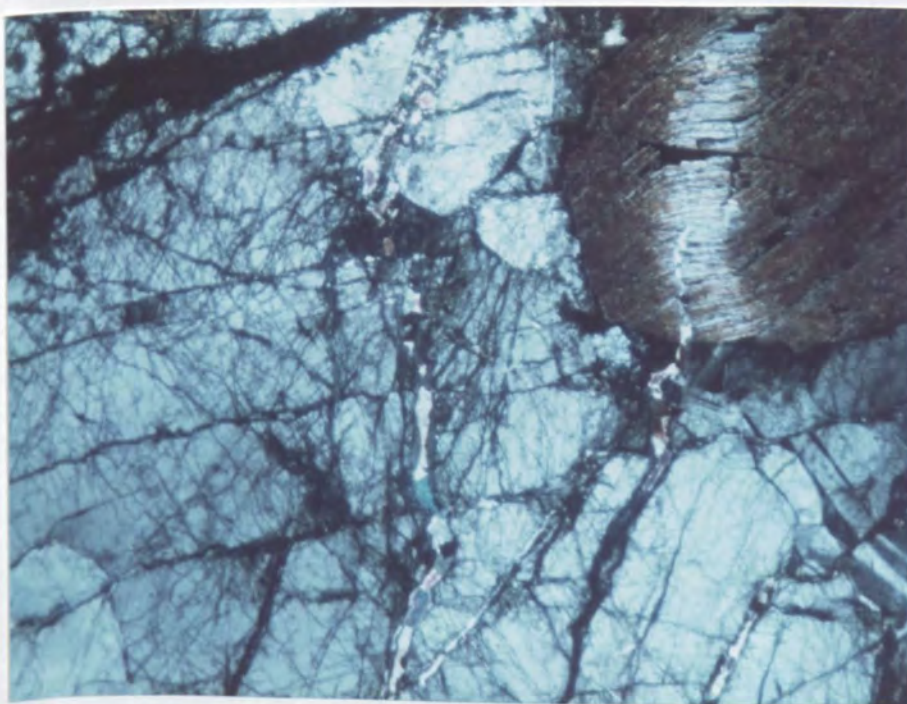
(b)   Gabbro pegmatite containing clinopyroxene (top-right) and
plagioclase and showing evidence of mechanical deformation.
From a narrow vein in serpentinised harzburgite.
MA217. xp. X5.

Deformation : subparallel shear-planes cause diopside

kinking; quartz-epidote veins follow some of these, saussuriti-

zation is concentrated along them.

Note: A variant of this rock type contains very fresh, small

(< 0.4 mm), anhedral, plagioclase accompanying the same

uralitized clinopyroxene. The plagioclase grains occur in

aggregates with mutual triple-junction boundaries and have a

recrystallised appearance.

12. <u>Clinopyroxene gabbro pegmatite e.g. MA127 (A)</u>   Plate A.5.b.

Macroscopic : pegmatitic grain-size, black (uralitized) clino-

pyroxene (10-30 mm) and grey-white plagioclase (4-8 mm).

Microscopic, general : xenomorphic, large clinopyroxene plates

partially enclose smaller plagioclase.

Mode : clinopyroxene = 20, secondary amphibole = 33,

plagioclase = 47. (Due to large grain-size, these are very

approximate.)

Plagioclase : anhedral with irregular and rounded boundaries,

much deformed by fractures with associated cataclasis, 60%

saussuritization. No apparent zoning.

Clinopyroxene : subhedral plates (30 x 10 x 10 mm), 60%

uralitization from crystal edges and along cleavage and basal

parting.

Hornblende : occasional fibrous chlorite is associated.

Deformation : hair-line fractures, some widening into zones

(< 0.5 mm) of cataclasis; related kink-banding and deformation

twins in clinopyroxene; fractures followed by quartz-calcite

veining.

Opaque : occasional small ($<$ 0.4 mm) oxidised grain.

Note: (1) occasional grain size $<$ 250 mm (2) similar gabbro pegmatites intrude the mantle serpentinites, the cumulates and the massive gabbro unit (3) occasional varieties possess a strong mineral foliation and a flaser-gabbro appearance (4) there is a transition to coarse anorthosites, with only minor uralitic amphibole accompanying the plagioclase plates.

13. Metadolerite dyke of the sheeted dyke complex e.g. MA286 (E)

Plates A.6.a,b; A.7.a.

Macroscopic : fine-medium grain, homogeneous and massive, grey-green, plagiophyric with rectangular white plagioclase phenocrysts (2-4 mm) = 2%

Groundmass mode : secondary amphibole (+ clinopyroxene relicts) = 36 (+ 14), plagioclase = 43, opaque (ilmenite) = 7. Sub-ophitic to intergranular.

Plagioclase phenocrysts : tabular, 2.5 - 4 mm x 2 mm (1/w = 2 is indicative of slow growth), zone of resorbtion followed by further zoned growth. Core = An85, rim = An53 (similar to groundmass laths). Core saussuritization $>$ rim.

Groundmass plagioclase : subhedral-euhedral laths in uralitic matrix; laths form an interlocking network, each elongate // 010 (a = 0.1 - 0.8 mm, b = 0.05 - 0.03 mm, c = 0.2 - 2.0 mm; 1/w = 4-16 = rapid growth); normally zoned (An67-27); 10-50 % saussuritization concentrated in calcic core.

Groundmass clinopyroxene : original sub-ophitic with plagioclase, now relicts in amphibole.
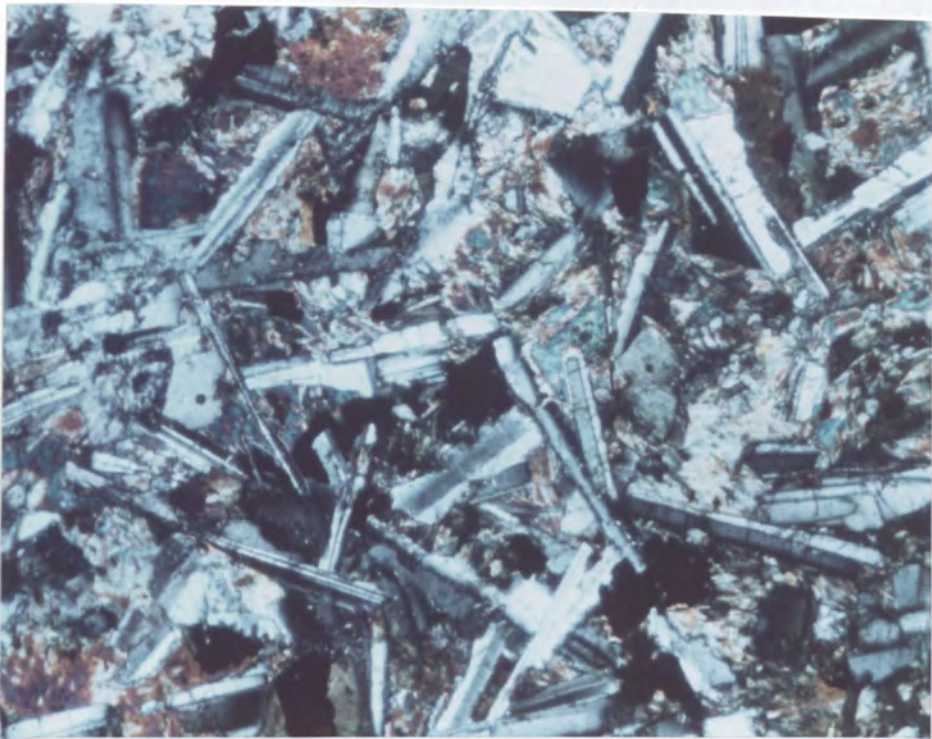
(a) Texture of metadolerite of the sheeted dyke complex.
Zoned plagioclase laths, clinopyroxene relicts in
uralitic amphibole, and Fe-Ti ore.   X134 xp.   X12.5

(b) Same metadolerite in plane polarized light.
X134 ppl.   X12.5

Plate A. 1. 7
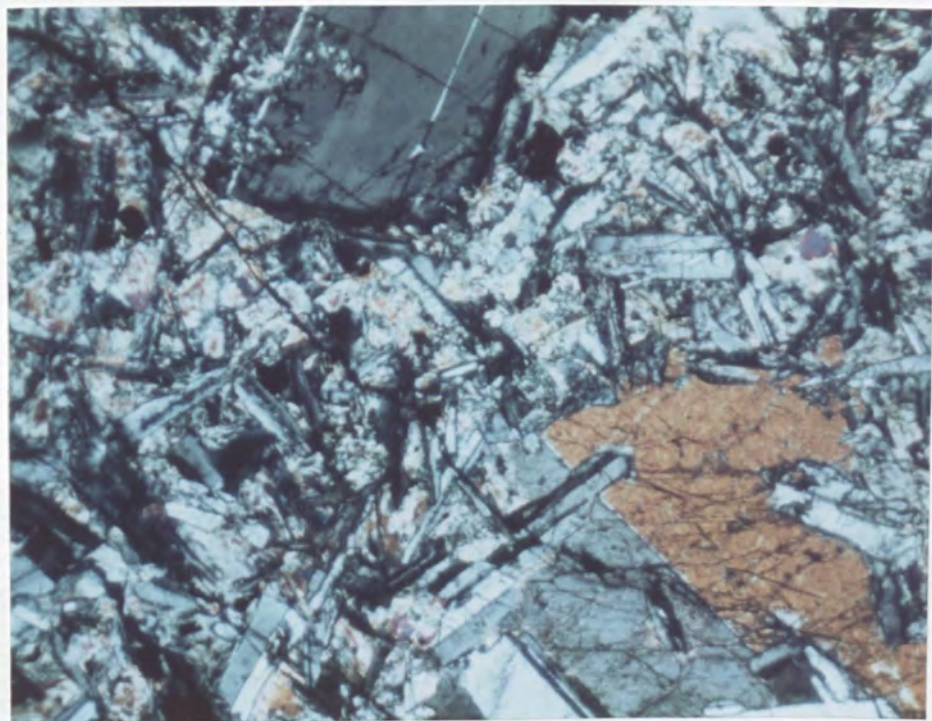
(a) Plagioclase and diopside phenocrysts in a metadolerite.
     MA214. xp. X12.5
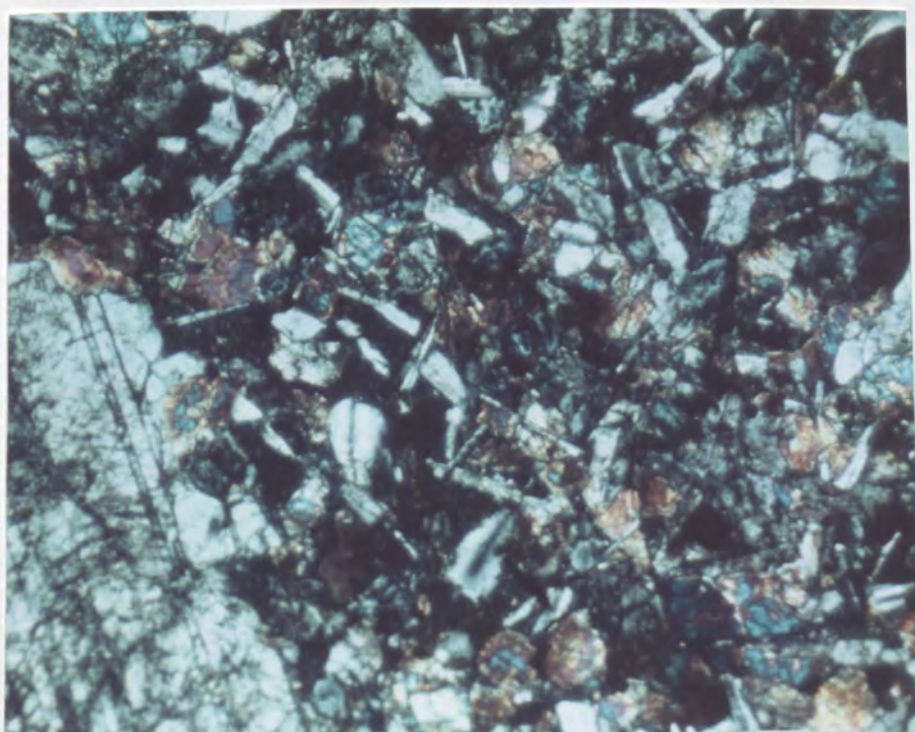
(b) Intersertal basalt lava with plagioclase phenocryst.
     Green pillow lava unit. MA113. xp. X12.5

Uralitic amphibole : fibrous - finely prismatic; actinolite - actinolitic hornblende.

Chlorite : rare, fine grain, fibrous areas ($<$ 0.5 mm), probably recrystallised mesostasis.

Opaque : equant grains or squat prisms (0.1-0.5 mm).

Sphene : rare irregular grains ($<$ 0.2 mm).

Veining : quartz and epidote (0.1-0.4 mm width).

Note: (1) the dyke groundmass is extremely uniform as described; the main variation in the dykes is in the type(s) and proportion(s) of the phenocryst phases; there is a variation from aphyric (MA367, map E) to plagiophyric with 49% phenocrysts (MA424, map E). Additionally olivine and clinopyroxene occur occasionally. Plagioclase phenocrysts = 33% of samples, olivine and clinopyroxene = 5% of samples and only $<$ 2% modally. Olivine ($<$ 1.5 mm) usually corroded and pseudomorphed by actinolite/chlorite. Clinopyroxene fresher.

Note: (2) Dykes uniform as described in areas of 20% to 100% concentration.

14. <u>Metadolerite dyke of sheeted dyke complex e.g. X187 (E)</u>

Macroscopic : contact of dolerite dyke and 8" wide gabbro screen; dyke very fine grain and black, gabbro = medium-coarse, pyroxene gabbro.

Microscopic general : irregular contact, 2-3 mm selvages of dolerite into gabbro; dolerite very fine-grain ($<$ 0.01 mm), aphyric.

Groundmass plagioclase : tiny subhedral laths (long axis $\sim$ .005 mm), zoned, appear fresh.

Groundmass clinopyroxene : difficult to estimate clinopyroxene:
uralitic amphibole proportion but both present.

Opaque : tiny equant grains (<.005 mm).

Note: X160 contains 2 similar chilled margins to the 50 cm wide
dyke.

15. <u>Green pillow lava e.g. MA114 (F)</u>   Plate A.7.b.

Macroscopic : well-formed pillowed flow, pillows 40 cm diameter,
outer 4 mm = darker "glassy" rim, interior = greenish. Radial
fractures sub-perpendicular to margin. Plagiophyric-phenocrysts =
even distribution.

Mode : olivine phenocrysts = 2%, plagioclase phenocrysts = 7%,
clinopyroxene = 5%, amphibole=4%, plagioclase=26%, chlorite 11%,
opaque = 8%, remainder = 36% = fine-grain and altered.

Microscopic general : porphyritic, intergranular groundmass =
plagioclase laths in fibrous amphibole-chlorite; fresh areas
with clinopyroxene show originally sub-ophitic.

Plagioclase phenocrysts : single or glomerophyric aggregates
(6-8 crystals), $\leq$ 4 mm, extensive saussuritization, l/w = 2-4,
subhedral plates.

Groundmass plagioclase : subhedral laths, 0.4-0.5 mm long,
interlocking, l/w = 6-10 = more rapid growth, saussuritized,
zoning still visible.

Groundmass clinopyroxene : relicts within uralitic amphibole-
chlorite.

Groundmass opaque : anhedral to prismatic grains (< 0.3 mm),
dark-red (= oxidised?).

Veining : epidote (< 0.5 mm width).

16. Red pillow lava core e.g. X245 (F)

Macroscopic : well-formed pillowed form; pillows 80 cm diameter; outer 3-5 mm = dark green glassy rim, interior = purplish-grey. Radial fractures are sites of calcite mineralisation; plagiophyric.

Mode : olivine phenocrysts = 4%, plagioclase phenocrysts (An86) = 21.5%, plagioclase laths = 13%, rest = 63.5% (= oxidised altered groundmass of opaque + "smectite" + calcite + zeolite).

Plagioclase phenocrysts : glomerophyric aggregates (3-20 crystals), variation fresh - complete saussuritization, l = 4 mm, l/w = 3-6; resorbed zone followed by further growth.

Olivine phenocrysts : straight-sided, 1-2 mm, pseudomorphed = calcite + ? serpentine.

Groundmass plagioclase : fresh interlocking laths $\leqslant$ 0.1 mm (l/w = 6-25 = rapid growth).

Groundmass opaque : small (< 0.05 mm) equant oxidised grains.

Groundmass ? smectite : golden-yellow secondary areas, associated with calcite, fibrous chlorite, fibrous zeolite.

Vesicles: $\leqslant$ 0.75 mm, infilled with calcite or zeolite.

Veining : calcite veins < 0.2 mm, rare quartz.

17. Red pillow lava rim e.g. MA139 (F)   Plate A.8.a.

Macroscopic : as for X245, sample from 5 cm into 70 cm diameter pillow, inward of glassy rim.

Mode : olivine phenocrysts = 1%, plagioclase phenocrysts = 26%, clinopyroxene phenocrysts = 2%, groundmass plagioclase = 18%, remaining 53% = very fine grain, altered, inc.opaque, calcite, smectite, zeolite (largely visible in veins and vesicles).

Plate A. 1. 8
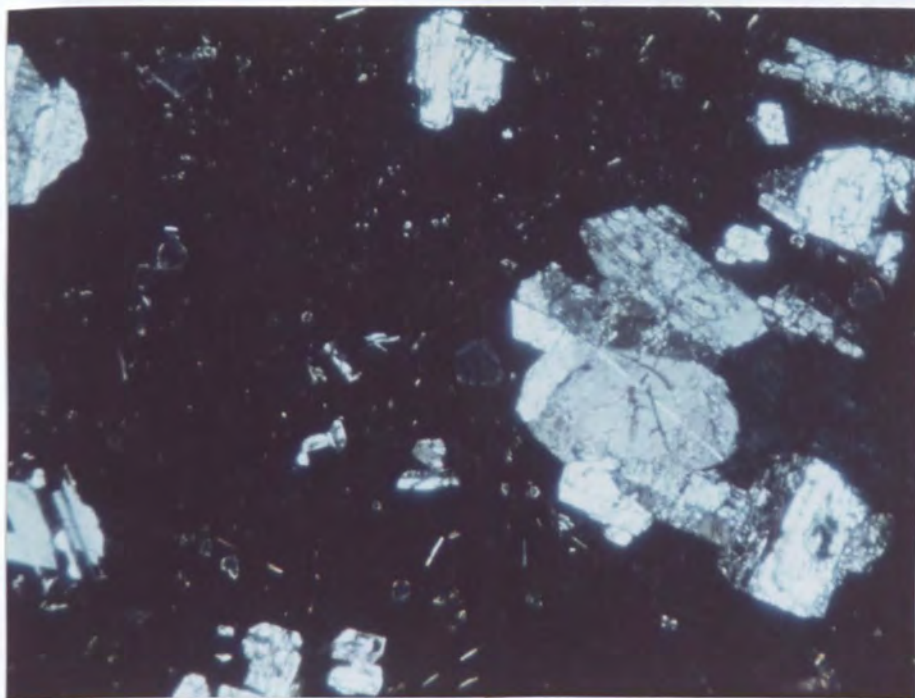
(a)   Fine-grained rim of pillow from red pillow lava unit.
       Single and glomerophyric aggregates of plagioclase
       phenocrysts. Groundmass with plagioclase microlites.
       MA143. xp. X5.
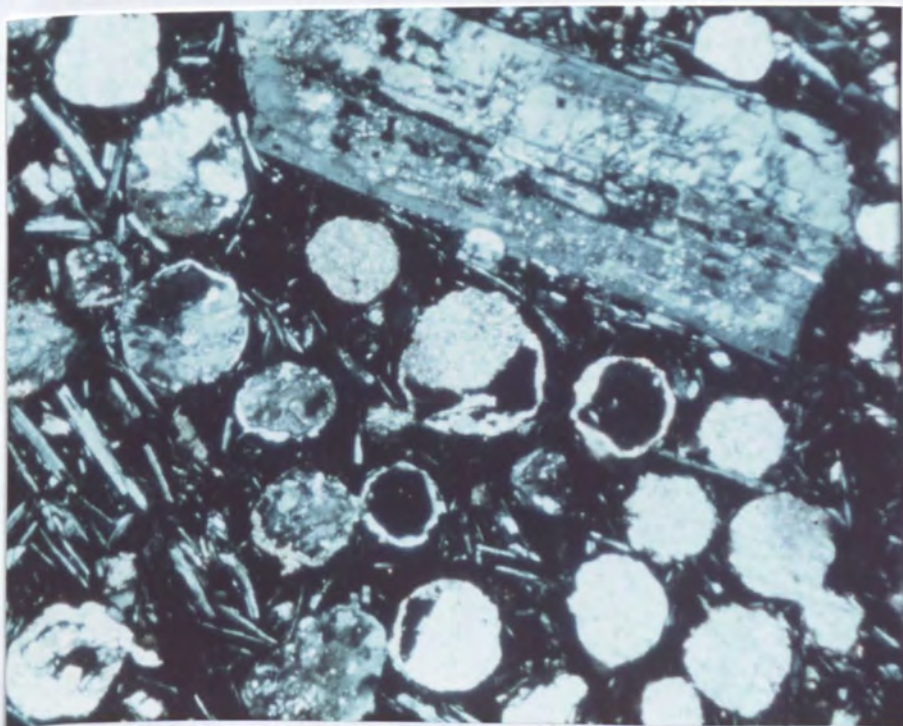
(b)   Highly vesicular plagiophyric basalt of the Melange
       Lava Group. Calcite infill of vesicles. Fine-grain
       groundmass with plagioclase laths. MA339 xp. X5.

Plagioclase phenocrysts : aggregate and size as for X245 above, extensive saussuritization.

Olivine phenocrysts : 1-1.5 mm, pseudomorphed by calcite + serpentine.

Clinopyroxene phenocrysts : 1-2 mm, fresh, euhedral.

Groundmass : quench plagioclase microlites with hollow cross-sections and "belt-buckle" shapes, 1 < 0.01 mm, 1/w ～ 20 (typical of quench plagioclase); in very fine-grain dark matrix.

Note: all transitions are visible from MA139 (= quenched vitrophyric outer zone) to X245 (= holocrystalline, sub-ophitic interior). The transition involves increasing groundmass plagioclase size, change from quench microlites to rapidly-grown laths, and growth of other groundmass phases.

18. Melange basalt e.g. MA354 (F)   Plate A.8.b.

Macroscopic : sheared pillowed basalt substrate below limestone block.

Microscopic general : plagiophyric, groundmass dominated by fluidal alignment of plagioclase laths.

Mode : plagioclase phenocrysts = 2%, groundmass plagioclase = 52%, groundmass opaque = 6%, secondary calcite = 6%, rest = 34%.

Plagioclase phenocrysts : 2-3 mm, subhedral plates, completely saussuritized or replaced by calcite.

Groundmass plagioclase : fine-grain laths (≤ 0.01 mm), strong alignment, flow around phenocrysts, set in matrix of small oxidised opaque grains (< 0.01 mm) and altered ? mesostasis.

Vesicles : large size (≤ 4 mm), zeolite and calcite infill.

<u>Note</u>: One similar, though finer grain, specimen contained ～ 30% calcite-filled vesicles.

19. <u>Shinzi Group basalt e.g. X220A1 (F)</u>

Macroscopic : orange-brown massive basalt occurring in sheets 1.5-6.0 m thick.

Microscopic general : sparsely plagiophyric, groundmass dominated by fluidal alignment of plagioclase laths.

Mode : plagioclase microphenocrysts 4, plagioclase 47, opaque 5 fine grain altered Fe-Mg mineral or mesostasis 44.

Plagioclase microphenocrysts : single and glomerophyric aggregates (4-10 crystals), euhedral-subhedral plates (1.5 x 0.75 mm), marginal resorption, 90% saussuritization. Narrow rim of oscillatory zoning visible.

Plagioclase laths : 0.5 x 0.05 mm, strong alignment and flow around phenocrysts, strongly zoned.

Opaque : brown oxidised grains, anhedral to prismatic (< 0.1 mm, rarely < 1 mm).

Rest : too fine for identification except occasional clear interstitial quartz grains (< 0.5 mm); occurrence of quartz in narrow veins suggests secondary.

Deformation : bands of shearing cause kinking of plagioclase laths, pre quartz veining.

20. <u>Shinzi Group trachyte e.g. X219 (F)</u>   Plate A.9.a.

Macroscopic : massive light brown flow.

Microscopic general : plagiophyric, groundmass = trachytic texture of plagioclase laths.
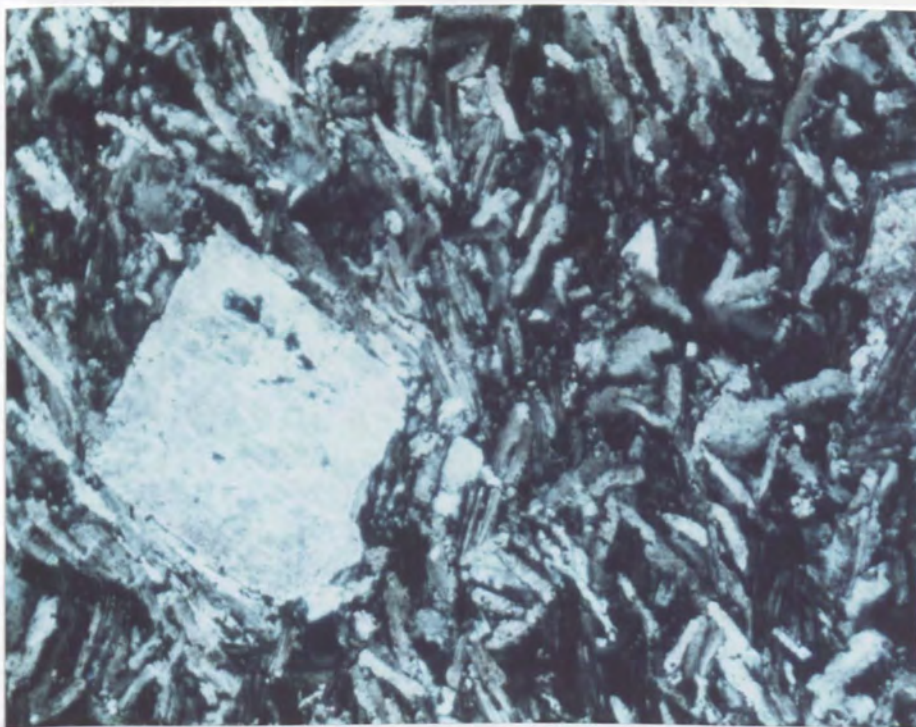
Plate A. 1. 9

(a)   Fluidal textured trachyte with plagioclase phenocryst.
X219 xp.   X12.5

(b)   Cataclased granite : orthoclase and plagioclase
"porphyroblasts" in a granulated quartz matrix.
MA44.   xp.   X5

Plate A. 1. 9
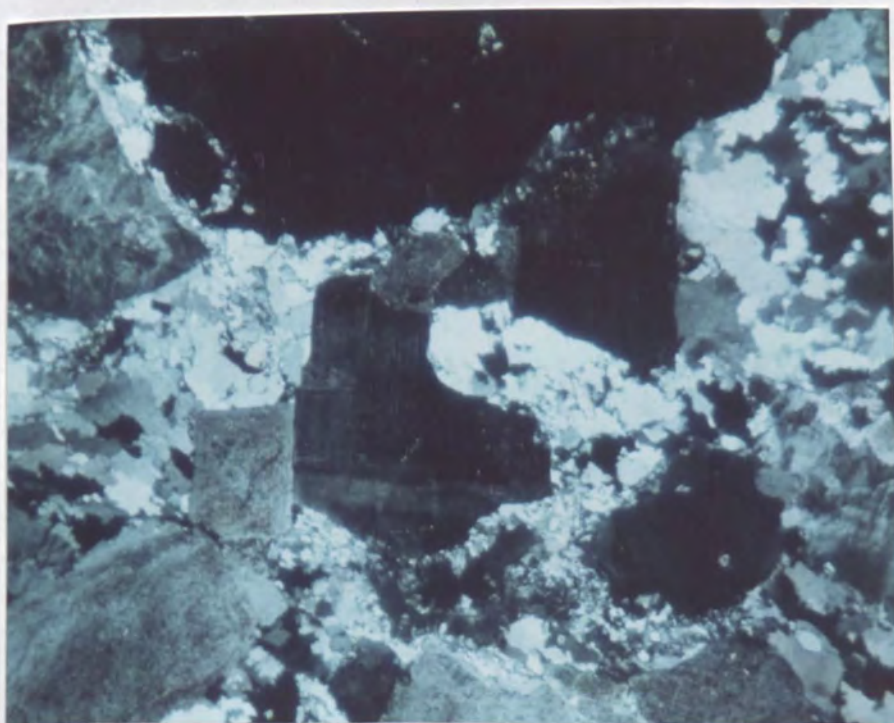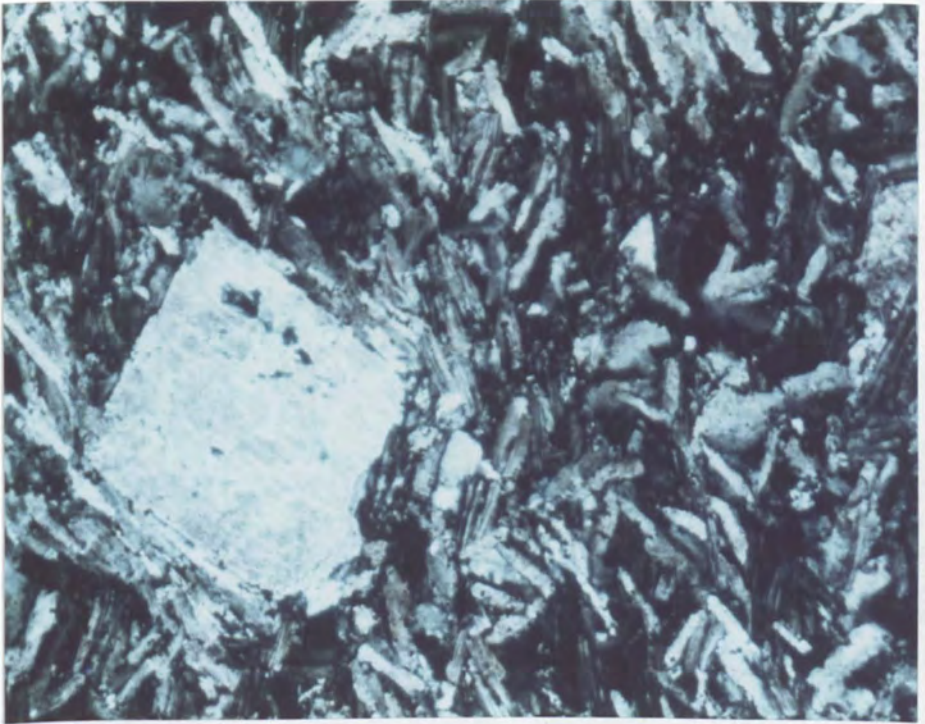
(a)   Fluidal textured trachyte with plagioclase phenocryst.
X219 xp. X12.5
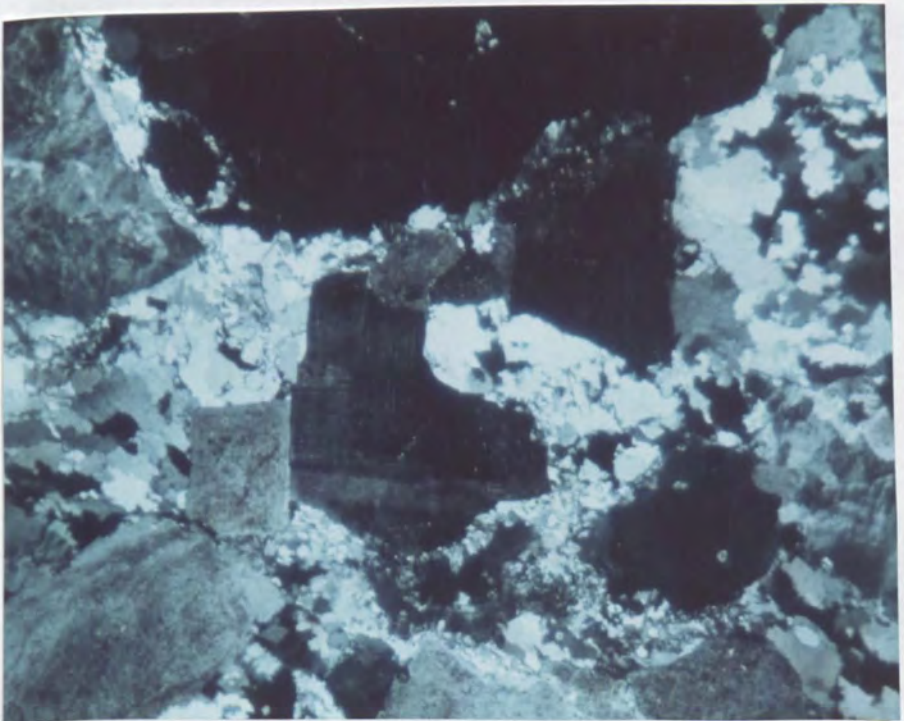
(b)   Cataclased granite : orthoclase and plagioclase
"porphyroblasts" in a granulated quartz matrix.
MA44. xp. X5

Plagioclase phenocrysts : single and rare, euhedral, saussuritized.

Plagioclase laths : 0.5 x 0.1 mm, strong alignment, zoned.

Quartz : interstitial clear areas.

21. Granite e.g. MA37 (G)

Macroscopic : leucocratic, quartzo - felspathic with < 5% small biotite flakes.

Mode : quartz = 39%, orthoclase = 39%, plagioclase = 21% biotite 1%.

Microscopic general : Xenomorphic-hypidiomorphic granular.

Quartz : anhedral grains, strain-shadowed (0.8-2.0 mm), occasionally in areas (4 x 3 mm) of several grains; rare graphic intergrowth with orthoclase, grain boundaries weakly sutured.

Orthoclase : anhedral-subhedral plates (2-3 mm), usually untwinned, rarely perthitic, minor suturing of grain boundaries.

Plagioclase : subhedral (2-3 mm), more altered than orthoclase = cloudy in P.P.L., twinned (albite ≫ carlsbad > pericline), limited rim zoning.

Biotite : small flakes (< 0.4 mm), even distribution throughout, 50% alteration to chlorite and opaque.

22. Granite, cataclased variety e.g. MA44 (G) Plate A.9.b.

Macroscopic : leucocratic, quartzo-felspathic rock, strong shearing causes almost mylonitic appearance with foliation defined by streaked-out biotite.

Microscopic general : protomylonitic texture.

Mode : quartz = 44%, orthoclase = 34%, plagioclase = 20%, biotites = 2%.

Quartz : granulated, sutured, interlocking, fine-grained (< 0.1-0.2 mm).

Felspar : both orthoclase and plagioclase, as described above, form porphyroblasts (< 3 mm) in the granulated quartz matrix; sutured grain boundaries.

Biotite : extensively streaked out and wrapped around felspar porphyroblasts.

Note: there is a transition, through an intermediate micro-breccia stage, between these 2 varieties.

APPENDIX 2 : ELECTRON MICROPROBE ANALYSIS

TECHNIQUE

Mineral analyses were carried out on the Cambridge Instruments Microscan V electron microprobe analyzer at the University of Leicester. Operating conditions consisted of an electron gun voltage of 15 kV, an X-ray emergence angle of $75°$, and a specimen current of approximately 0.02 mA. obtained on the Cu surround of the Faraday Cage. The main machine parameters for the analyzed elements are listed in Table 1. Analyses were carried out by focused beam on carbon-coated, polished, thin sections, the standards and thin sections being coated simultaneously. The elements were analyzed in pairs, commencing with the more volatile Na and K. Standard peaks were measured at the start and finish of each pair of elements and a linear correction made for drift. Three counts of 20 seconds were used for each element, per analysis point, except for Na and K where 5 counts of 10 seconds were made.

Corrections to the raw data were made with a version of the programme MAGIC IV. (Microprobe Analysis General Intensity Corrections; J.W. Colby, Bell Telephone Labs., Pennsylvania), modified for geological use by R.N. Wilson, Geology Department, Leicester University. The programme corrects the raw intensities for dead time, background, absorption (Heinrich, Duncomb-Shields, Philibert), characteristic fluorescence (Reed), backscatter loss (Duncomb), and ionization-penetration loss (Philibert-Tixier). Oxygen was not analyzed and its concentration is determined in the programme by stoichiometry using assumed

Table 1 : Cambridge Instruments Microscan V Electron Micro-probe Analyzer : machine parameters

Angles$^\circ$ 2Θ

Element		Standard	Crystal	Counter	Peak	Bkgd. Std.	Bkgd. Spec.	Threshold E(v)	Window Gatewidth ΔE(v)
CHANNEL 1									
K	Kα	CH14(synthetic)	Q$_3$	Flow	68-04	±2	±2	1.6	1.0
Ca	Kα	Wollastonite(natural)	Q$_3$	Flow	60-19	±2	+1,-2	1.8	1.0
Ti	Kα	CH15(ilmenite)	Q$_3$	Flow	48-33	±2	±2	2.3	1.0
Fe	Kα	Fe(pure)	LiF 200	Sealed	57-29	±2	±2	3.5	1.0
Mn	Kα	Rhodonite(natural)	LiF 200	Sealed	62-56	±2	±2	3.5	1.0
Ni	Kα	Ni(pure)	LiF 200	Sealed	48-38	±2	±2	4.2	1.0
CHANNEL 2									
Na	Kα	Jadeite(natural)	RAP	Flow	54-15	+2,-3	+2,-3	0.5	0.5
Si	Kα	Wollastonite(natural)	KAP	Flow	31-05	±2	±2	1.0	0.5
Al	Kα	Jadeite(natural)	RAP	Flow	37-14	+2,-3	+2,-3	0.8	0.5
Mg	Kα	MgO(synthetic)	RAP	Flow	44-30	+2,-3	+2,-3	0.6	0.5
Cr	Kα	Cr(pure)	LiF 200	Sealed	69-19	±2	±2	2.8	1.0

RAP - Rubidium acid phthalate   KAP - Potassium acid phthalate

LiF 200 - Lithium fluoride.

stoichiometric oxide proportions input with the initial data.

The olivine, pyroxene and amphibole analyses are average analyses of 2 to 6 spots on 2 or 3 grains in each thin section. These minerals were essentially unzoned. The plagioclase analyses are single spot analyses because zoning invalidates averaged values. Zoning is monitored by the presentation of core and edge, and occasionally intermediate, analyses. Up to 12 points in any one grain were analyzed when strong zoning was found.

Most of the analyses are accurate to within 2% and the lower limits of detection range from about 0.02 to 0.05 wt. %. (Clark, 1978). Total iron is calculated as FeO except for plagioclase and the Fe-Ti oxides.

Appendix 11 - Microprobe analyses and mineral recalculations
of major mineral phases

A. Olivine

Sample no.	Olivine gabbros				
	X78	X355	MA76	X131	X272
SiO2	40.73	42.19	40.98	40.15	39.33
FeO	14.14	12.70	12.53	12.92	19.75
MgO	45.95	47.74	47.51	46.68	42.60
CaO	0.04	0.05	0.04	0.04	0.06
MnO	0.22	0.22	0.19	0.19	0.33
NiO	0.21	0.29	0.24	0.22	0.20
Cr2O3	0.00	0.02	0.01	0.02	0.00
Total	101.29	103.21	101.31	100.22	102.27
O=	4	4	4	4	4
Si	1.005	1.013	1.002	0.997	0.985
Fe	0.292	0.254	0.257	0.268	0.414
Mg	1.689	1.708	1.732	1.728	1.595
Ca	0.001	0.001	0.001	0.001	0.001
Mn	0.005	0.004	0.004	0.004	0.007
Ni	0.004	0.006	0.005	0.004	0.004
Fo	85.3	87.0	87.7	86.6	79.5

B. <u>Pyroxene</u>

Sample no.	Olivine gabbros X78		X355	MA76	X131	X272
	OPX	CPX	CPX	CPX	CPX	CPX
SiO2	54.95	52.53	52.99	52.90	52.43	51.42
TiO2	0.28	0.52	0.24	0.37	0.35	0.97
Al2O3	1.63	2.58	2.65	2.95	3.32	2.81
Cr2O3	0.44	0.75	1.04	0.93	1.05	0.50
FeO	9.11	4.06	3.79	3.70	3.71	5.32
MnO	0.24	0.19	0.16	0.12	0.14	0.14
MgO	31.23	16.57	17.20	17.38	16.62	15.76
CaO	1.42	22.51	22.67	22.86	22.19	22.47
Na2O	0.01	0.29	0.38	0.29	0.31	0.43
K2O	0.00	0.00	0.01	0.00	0.00	0.00
Total	99.31	99.99	101.13	101.51	100.13	99.80
O=	6	6	6	6	6	6
Si	1.944	1.923	1.917	1.906	1.911	1.900
Al	0.056	0.077	0.083	0.094	0.089	0.100
Al	0.012	0.034	0.030	0.031	0.054	0.022
Ti	0.007	0.014	0.007	0.010	0.010	0.027
Cr	0.012	0.022	0.030	0.026	0.030	0.122
Fe	0.270	0.124	0.115	0.112	0.113	0.164
Mn	0.007	0.006	0.005	0.004	0.004	0.004
Mg	1.647	0.904	0.927	0.933	0.903	0.868
Ca	0.054	0.883	0.879	0.882	0.867	0.889
Na	0.001	0.020	0.027	0.020	0.022	0.031
K	–	–	0.001	–	–	–
Mg	83.6	46.2	48.3	45.8	46.0	45.1
Fe	13.7	6.5	6.0	5.8	8.0	8.6
Ca	2.7	47.3	45.7	48.4	46.0	46.3
	Bron-zite	Diop-side	Diop-side	Diop-side	Diop-side	Diop-side

E. Pyroxene

Sample no.	Pyroxene gabbros				
	MA14	MA17	MA54	MA67 [+]	MA126
	CPX	CPX	CPX	CPX	CPX
SiO_2	51.24	51.63	52.31	51.00	52.91
TiO_2	0.38	0.53	0.50	0.71	0.52
Al_2O_3	3.62	3.17	2.33	2.75	2.11
Cr_2O_3	1.11	1.05	0.72	0.53	0.21
FeO	3.90	3.81	3.85	6.29	5.21
MnO	0.16	0.13	0.14	0.17	0.15
MgO	15.84	16.40	16.69	15.55	16.16
CaO	22.54	23.46	22.92	22.25	22.20
Na_2O	0.28	0.20	0.28	0.37	0.50
K_2O	0.02	0.01	0.01	0.02	0.04
Total	99.10	100.38	99.75	99.65	100.01
O≡	6	6	6	6	6
Si	1.895	1.889	1.921	1.897	1.942
Al	0.105	0.111	0.079	0.103	0.058
Al	0.053	0.026	0.022	0.018	0.033
Ti	0.011	0.015	0.014	0.020	0.014
Cr	0.033	0.030	0.021	0.016	0.006
Fe	0.121	0.117	0.118	0.196	0.160
Mn	0.005	0.004	0.004	0.005	0.005
Mg	0.873	0.894	0.914	0.862	0.884
Ca	0.893	0.920	0.902	0.886	0.873
Na	0.020	0.014	0.020	0.027	0.036
K	0.001	-	0.001	0.001	0.002
Mg	46.3	46.3	47.3	44.3	46.1
Fe	6.4	6.1	6.1	10.1	8.4
Ca	47.3	47.6	46.6	45.6	45.5
	Diopside	Diopside	Diopside	Salite	Diopside

Note: + = dyke screen

B. Pyroxene

Sample no.	Pyroxene gabbros			
	MA175	MA182	X186[+]	MA246[+]
	CPX	CPX	CPX	CPX
SiO_2	51.32	51.61	51.26	51.36
TiO_2	0.35	0.88	0.80	0.66
Al_2O_3	3.46	2.94	2.87	2.56
Cr_2O_3	1.26	0.36	0.12	0.31
FeO	3.10	6.39	5.19	7.96
MnO	0.09	0.24	0.16	0.25
MgO	16.21	15.33	15.84	14.63
CaO	22.13	21.97	22.87	21.47
Na_2O	0.28	0.32	0.32	0.39
K_2O	-	-	0.04	-
Total	98.20	100.04	99.45	99.61*
O≡	6	6	6	6
Si	1.905	1.907	1.900	1.918
Al	0.095	0.093	0.100	0.082
Al	0.056	0.035	0.025	0.031
Ti	0.010	0.024	0.022	0.018
Cr	0.037	0.011	0.003	0.009
Fe	0.096	0.197	0.161	0.249
Mn	0.003	0.007	0.005	0.008
Mg	0.897	0.844	0.875	0.814
Ca	0.880	0.870	0.908	0.859
Na	0.020	0.023	0.023	0.028
K	-	-	0.002	-
Mg	47.9	44.2	45.0	42.4
Fe	5.1	10.3	8.3	12.9
Ca	47.0	45.5	46.7	44.7
	Diopside	Salite	Diopside	Salite

Note: + = dyke screen

* total includes 0.02 NiO

B.Pyroxene

Sample no.	Dolerite dykes MA50[1]	MA50[2]	MA214[3]
SiO2	52.87	51.99	52.14
TiO2	0.24	0.20	0.38
Al2O3	2.91	3.83	3.79
Cr2O3	0.55	1.24	0.85
FeO	4.23	3.55	3.93
MnO	0.15	0.12	0.11
MgO	18.37	17.85	17.99
CaO	20.44	20.86	20.75
Na2O	0.19	0.20	0.23
K2O	-	0.01	0.01
Total	99.95	99.86	100.19
O=	6	6	6
Si	1.922	1.893	1.894
Al	0.078	0.107	0.106
Al	0.047	0.057	0.056
Ti	0.007	0.006	0.010
Cr	0.016	0.036	0.024
Fe	0.129	0.108	0.119
Mn	0.005	0.004	0.004
Mg	0.996	0.969	0.973
Ca	0.796	0.814	0.808
Na	0.013	0.014	0.016
K	-	-	-
Mg	51.8	51.2	51.2
Fe	6.7	5.8	6.3
Ca	41.5	43.0	42.5
	Endiopside	Endiopside	Endiopside

[1] unzoned microphenocryst

[2] unzoned phenocryst

[3] unzoned phenocryst

C. Plagioclase

Sample no.	Olivine gabbros					
	X78 – Core	X78 Edge	X355 – Core	X355 Edge	MA76 – Core	MA76 Edge
SiO2	47.03	47.49	47.59	47.19	48.14	47.51
Al2O3	30.29	30.31	31.90	31.69	33.02	33.21
Fe2O3*	0.23	0.24	0.25	0.26	0.23	0.31
CaO	17.15	16.79	17.16	17.32	17.02	17.19
Na2O	1.90	2.06	1.91	1.64	1.98	1.96
K2O	0.04	0.04	0.02	0.02	0.03	0.03
Total	96.65	96.91	98.84	98.11	100.42	100.21
O≡	32	32	32	32	32	32
Si	8.952	9.001	8.848	8.838	8.798	8.716
Al	6.795	6.770	6.990	6.996	7.113	7.181
Fe	0.033	0.034	0.035	0.036	0.032	0.042
Ca	3.498	3.409	3.419	3.476	3.333	3.380
Na	0.702	0.757	0.690	0.594	0.700	0.699
K	0.010	0.009	0.006	0.005	0.007	0.008
Or						
Ab	17	18	17	15	17	17
An	83	82	83	85	83	83

* Total iron as Fe2O3

C. Plagioclase

| Sample no. | Olivine gabbros | | | | |
	X131 - Core	X131 Edge	X272 - Core	X272 Edge	X272 Core
SiO2	48.02	48.01	49.32	49.65	48.60
Al2O3	33.43	32.99	31.21	31.20	32.28
Fe2O3	0.29	0.30	0.45	0.27	0.50
CaO	17.54	17.13	15.37	14.83	15.75
Na2O	1.74	2.04	2.86	3.16	2.60
K2O	0.03	0.04	0.06	0.07	0.04
Total	101.06	100.52	99.27	99.28	99.77
O≡	32	32	32	32	32
Si	8.773	8.777	9.091	9.135	8.925
Al	7.165	7.108	6.781	6.787	6.987
Fe	0.040	0.041	0.063	0.038	0.069
Ca	3.417	3.356	3.036	2.923	3.099
Na	0.613	0.725	1.022	1.125	0.925
K	0.007	0.010	0.013	0.016	0.009
Or					
Ab	15	18	25	28	23
An	85	82	75	72	77

C. Plagioclase

Sample no.	Pyroxene gabbros & leucogabbros					
	MA14 – Core	MA14 Edge	MA17 – Core	MA17 Edge	MA54 – Core	MA54 Edge
SiO_2	45.45	45.45	48.14	48.05	46.58	48.59
Al_2O_3	33.72	33.49	33.09	33.15	32.37	32.60
Fe_2O_3	n.d.	n.d.	n.d.	n.d.	n.d.	n.d.
CaO	16.73	18.52	16.44	16.50	16.96	13.94
Na_2O	1.74	1.90	2.31	2.25	1.94	2.31
K_2O	0.03	0.03	0.04	0.05	0.02	0.02
Total	97.67	99.39	100.01	100.00	97.87	97.45
O≡	32	32	32	32	32	32
Si	8.548	8.465	8.821	8.806	8.745	9.040
Al	7.474	7.351	7.145	7.161	7.162	7.148
Fe	–	–	–	–	–	–
Ca	3.372	3.695	3.226	3.241	3.412	2.779
Na	0.635	0.688	0.819	0.800	0.705	0.834
K	0.008	0.008	0.008	0.011	0.004	0.004
Or						
Ab	16	16	20	20	17	23
An	84	84	80	80	83	77

C. Plagioclase

Sample no.	Pyroxene gabbros & leucogabbros					
	MA67 – Core	MA67 Edge	MA126[+]– Core	MA126 Edge	MA182 – Core	MA182 Edge
SiO_2	48.11	49.88	51.32	51.41	48.95	49.08
Al_2O_3	32.18	31.09	30.88	30.83	32.12	32.32
Fe_2O_3	n.d.	n.d.	0.23	0.11	0.39	0.40
CaO	16.65	15.39	14.21	14.15	16.31	15.24
Na_2O	2.26	2.96	3.56	3.69	2.43	2.59
K_2O	0.03	0.06	0.04	0.03	0.05	0.24
Total	99.23	99.38	100.24	100.22	100.24	99.87
O≡	32	32	32	32	32	32
Si	8.891	9.166	9.321	9.336	8.952	8.988
Al	7.009	6.734	6.610	6.599	6.923	6.975
Fe	–	–	0.032	0.015	0.054	0.055
Ca	3.297	3.031	2.765	2.754	3.196	2.991
Na	0.810	1.055	1.252	1.300	0.861	0.920
K	0.007	0.015	0.009	0.007	0.011	0.056
Or						1
Ab	20	26	31	32	21	24
An	80	74	69	68	79	75

[+] Screens between dolerite dykes

C. Plagioclase

| Sample no. | Pyroxene gabbros & leucogabbros | | | | | |
	X186[+] - Core	X186 Edge	MA246[+] - Core	MA246 Edge	X268 - Core	X268 Edge
SiO_2	48.08	49.03	50.75	53.20	51.51	50.94
Al_2O_3	32.87	32.56	30.93	29.55	29.85	30.09
Fe_2O_3	n.d.	n.d.	0.36	0.40	n.d.	n.d.
CaO	16.12	16.09	14.71	12.83	13.64	14.00
Na_2O	2.53	2.64	3.37	4.45	3.55	3.61
K_2O	0.03	0.04	0.05	0.06	0.12	0.13
Total	99.64	100.37	100.16	100.48	98.68	98.76
O≡	32	32	32	32	32	32
Si	8.842	8.942	9.246	9.608	9.478	9.387
Al	7.124	6.999	6.642	6.289	6.472	6.534
Fe	-	-	0.050	0.055	-	-
Ca	3.176	3.144	2.871	2.482	2.689	2.764
Na	0.904	0.935	1.190	1.558	1.265	1.289
K	0.008	0.010	0.011	0.013	0.029	0.030
Or					1	1
Ab	22	23	29	39	32	32
An	78	77	71	61	67	67

[+] Screens between dolerite dykes

C. Plagioclase

Sample no.	Pyroxene gabbro	
	MA175 —	MA175
	Core	Edge
SiO_2	46.74	46.96
Al_2O_3	31.60	31.34
Fe_2O_3	n.d.	n.d.
CaO	17.26	17.03
Na_2O	1.76	1.78
K_2O	0.02	0.02
Total	97.38	97.14
O≡	32	32
Si	8.821	8.876
Al	7.028	6.981
Fe	–	–
Ca	3.491	3.448
Na	0.645	0.653
K	0.005	0.005
Or		
Ab	16	16
An	84	84

C. Plagioclase

Sample no.	Dolerite dykes					
	MA50[1] Core	MA50[2] Core	MA50[3]- Core	MA50 Edge	MA50[4]- Core	MA50 Edge
SiO_2	54.45	54.12	48.65	51.18	48.21	55.80
Al_2O_3	26.92	26.96	31.48	29.04	30.61	26.02
Fe_2O_3	0.68	0.72	0.38	0.60	0.40	0.59
CaO	11.50	11.28	15.69	13.86	16.39	10.30
Na_2O	5.05	5.02	1.53	3.64	2.12	5.09
K_2O	0.09	0.08	0.03	0.05	0.03	0.08
Total	98.68	98.17	97.76	98.36	97.75	97.88
$O\equiv$	32	32	32	32	32	32
Si	9.983	9.969	9.067	9.479	9.042	10.246
Al	5.818	5.853	6.915	6.338	6.767	5.630
Fe	0.093	0.099	0.054	0.084	0.056	0.082
Ca	2.259	2.226	3.132	2.750	3.295	2.026
Na	1.795	1.793	0.553	1.306	0.769	1.813
K	0.020	0.020	0.006	0.011	0.006	0.018
Or	1	1				
Ab	44	44	15	32	19	47
An	55	55	85	68	81	53

1 - 2 Groundmass laths   3 - 4 Zoned phenocrysts

C. Plagioclase

Sample no.	Dolerite dykes				
	MA214[5]- Core	MA214[6] Edge	MA214[7] Core	MA214[8]- Core	MA214 Edge
SiO_2	51.13	54.73	55.61	47.58	52.77
Al_2O_3	29.45	28.37	27.65	33.33	29.38
Fe_2O_3	n.d.	n.d.	n.d.	n.d.	n.d.
CaO	13.61	11.07	10.47	17.17	12.65
Na_2O	3.74	5.42	5.76	1.85	3.89
K_2O	0.02	0.07	0.04	0.01	0.02
Total	97.95	99.66	99.52	99.94	98.70
$O\equiv$	32	32	32	32	32
Si	9.483	9.908	10.058	8.736	9.659
Al	6.436	6.052	5.893	7.213	6.338
Fe	-	-	-	-	-
Ca	2.704	2.148	2.030	3.377	2.481
Na	1.345	1.902	2.020	0.660	1.381
K	0.006	0.016	0.009	0.003	0.004
Or					
Ab	33	47	50	16	36
An	67	53	50	84	64

5 - 6 - 7 Groundmass laths   [8] Zoned phenocryst

C. Plagioclase

Sample no.	Dolerite dykes			
	MA214[9]- Core	MA214 Edge	X214[10] Core	X214[11] Core
SiO_2	47.60	47.40	52.91	53.15
Al_2O_3	33.10	33.57	27.75	27.50
Fe_2O_3	n.d.	n.d.	n.d.	n.d.
CaO	16.93	17.06	12.05	11.79
Na_2O	1.91	1.89	4.71	4.66
K_2O	0.01	0.02	0.10	0.12
Total	99.55	99.95	97.53	97.22
$O\equiv$	32	32	32	32
Si	8.768	8.704	9.819	9.881
Al	7.186	7.264	6.070	6.025
Fe	-	-	-	-
Ca	3.342	3.356	2.396	2.347
Na	0.681	0.675	1.695	1.681
K	0.002	0.006	0.024	0.028
Or			1	1
Ab	17	17	41	41
An	83	83	58	58

[9]Phenocryst   [10] - [11]Groundmass laths

C. Plagioclase

Sample no.	Dolerite dykes MA266 - Core	MA266[12] Edge	MA266[13] Core	MA266[14] Core
SiO_2	54.94	61.68	53.12	56.45
Al_2O_3	26.57	26.24	27.31	25.50
Fe_2O_3	n.d.	n.d.	n.d.	n.d.
CaO	11.02	4.72	11.99	9.37
Na_2O	5.32	6.85	4.60	5.65
K_2O	0.09	0.13	0.07	0.11
Total	97.93	99.62	97.08	97.08
$O \equiv$	32	32	32	32
Si	10.111	10.873	9.890	10.408
Al	5.763	5.451	5.992	5.541
Fe	-	-	-	-
Ca	2.173	0.891	2.392	1.850
Na	1.899	2.343	1.662	2.019
K	0.022	0.029	0.016	0.026
Or	1	1		1
Ab	46	72	41	52
An	53	27	59	48

12 - 13 - [14] Zoned groundmass laths

C. Plagioclase

Sample no.	Red pillow lavas		
	X245P1[1] − Core	X245P1 Edge	X245P1[2] Core
SiO_2	47.07	47.80	47.85
Al_2O_3	33.16	32.00	32.29
Fe_2O_3	n.d.	n.d.	n.d.
CaO	17.64	16.58	16.83
Na_2O	1.62	2.16	1.99
K_2O	0.02	0.04	0.04
Total	99.52	98.58	99.00
$O \equiv$	32	32	32
Si	8.695	8.891	8.863
Al	7.217	7.014	7.049
Fe	−	−	−
Ca	3.491	3.304	3.340
Na	0.582	0.779	0.714
K	0.006	0.009	0.010
Or			
Ab	14	19	18
An	86	81	82

[1]Slightly zoned phenocryst   [2]Unzoned microphenocryst

D. Amphibole

Sample no.	Pyroxene gabbros & leucogabbros					(including dyke screens[+])	
	MA54		X186[+]	MA126[+]		MA246[+]	
	1	2		1	2	1	2
SiO_2	44.77	47.34	43.71	54.31	46.99	51.70	47.29
TiO_2	0.04	0.07	3.31	0.19	0.42	0.49	0.37
Al_2O_3	13.34	9.42	12.35	2.98	10.45	4.14	10.81
Cr_2O_3	0.04	0.18	0.20	0.12	0.03	0.12	-
FeO	9.77	8.53	8.03	6.70	8.58	12.20	11.26
MnO	0.17	0.16	0.11	0.13	0.12	0.18	0.10
MgO	14.79	16.23	15.47	20.05	16.79	15.43	14.61
CaO	12.64	12.52	12.25	12.42	11.84	12.07	12.06
Na_2O	2.51	1.64	2.31	0.59	2.04	0.73	2.60
K_2O	0.08	0.08	0.65	0.08	0.24	0.02	0.11
NiO	n.d.	n.d.	n.d.	n.d.	n.d.	n.d.	n.d.
Total	98.15	96.17	98.39	98.39	97.57	97.08	99.22
$O\equiv$	23	23	23	23	23	23	23
Si	6.451	6.884	6.278	7.624	6.745	7.497	6.754
Al	1.549	1.116	1.722	0.376	1.255	0.503	1.246
Al	0.716	0.499	0.369	0.116	0.512	0.204	0.574
Ti	0.005	0.008	0.358	0.020	0.045	0.054	0.039
Cr	0.005	0.021	0.023	0.013	0.004	0.014	-
Fe	1.177	1.037	0.964	0.786	1.030	1.480	1.345
Mn	0.021	0.020	0.013	0.015	0.015	0.022	0.012
Mg	3.176	3.517	3.313	4.195	3.592	3.335	3.111
Ca	1.951	1.951	1.885	1.868	1.821	1.875	1.846
Na	0.702	0.462	0.644	0.161	0.566	0.206	0.721
K	0.015	0.014	0.119	0.015	0.044	0.003	0.020
Mg	50.4	54.1	53.8	61.3	55.8	49.9	49.4
Fe	18.7	15.9	15.6	11.4	16.0	22.1	21.3
Ca	30.9	30.0	30.6	27.3	28.2	28.0	29.3
[1]	Horn-blendic	Horn-blendic	Horn-blendic	Actin-olitic	Horn-blendic	Actin-olitic horn-blende	Horn-blendic

[1] Actinolitic = Al replacement of Si in unit formula = < 0.500
   Hornblendic = Al   "   of Si in unit formula = > 0.500
                                                        < 2.000
                                   following Deer et al, 1963.

D. Amphibole

Sample no.	Dolerite dykes				
	MA50	MA214	X214	MA266	
				1	2
SiO_2	51.69	50.20	43.19	48.61	49.61
TiO_2	0.35	0.56	3.38	0.42	0.70
Al_2O_3	3.95	5.60	10.83	4.64	6.28
Cr_2O_3	0.08	0.23	0.07	0.02	0.09
FeO	17.60	13.65	11.23	15.56	14.58
MnO	0.48	0.23	0.17	0.27	0.27
MgO	13.44	14.39	13.81	14.60	13.25
CaO	9,89	11.82	11.77	11.65	12.20
Na_2O	0.56	0.63	2.42	0.51	0.49
K_2O	0.09	0.07	0.57	0.08	0.04
NiO	n.d.	n.d.	n.d.	0.07	0.03
Total	98.11	97.38	97.45	96.42	97.54
$O\equiv$	23	23	23	23	23
Si	7.557	7.317	6.362	7.252	7.256
Al	0.443	0.683	1.638	0.748	0.744
Al	0.238	0.280	0.243	0.067	0.338
Ti	0.038	0.062	0.374	0.047	0.078
Cr	0.009	0.026	0.009	0.003	0.010
Fe	2.151	1.664	1.383	1.941	1.784
Mn	0.059	0.028	0.021	0.034	0.033
Mg	2.928	3.126	3.032	3.246	2.889
Ni	-	-	-	0.008	0.003
Ca	1.549	1.846	1.858	1.862	1.911
Na	0.159	0.178	0.691	0.149	0.140
K	0.016	0.013	0.107	0.016	0.007
Fe	32.4	25.1	22.1	26.1	27.1
Mg	44.2	47.1	48.3	47.5	43.9
Ca	23.4	27.8	29.6	26.4	29.0
	Actin- olitic	Actin- olitic horn- blende	Horn- blendic	Actin- olitic horn- blende	Actin- olitic horn- blende

E. Fe-Ti oxides

Sample no.	Gabbro screen		Dyke
	MA246	MA246	MA214
	Mt	Ilm	Ilm
SiO2	0.15	0.07	n.d.
FeO	30.62	44.19	42.54
Fe2O3	61.29	0.64	0.62
TiO2	0.76	51.97	48.06
Al2O3	0.36	0.05	1.44
Cr2O3	2.93	0.05	0.04
MnO	0.07	2.40	0.73
MgO	-	0.06	0.80
Total	96.18	99.43	94.23
O ≡	32	32	32
Si	0.063	0.020	-
Fe	29.594	10.144	10.187
Ti	0.236	10.589	10.280
Al	0.177	0.018	0.482
Cr	0.956	0.010	0.009
Mn	0.023	0.552	0.177
Mg	0.002	0.024	0.340
$T^{o}C$		340	

Mt – magnetite   Ilm – ilmenite
FeO, Fe2O3, $T^{o}C$ calculated from Buddington & Lindsley, 1964.

APPENDIX 3 Modal Analyses

Quantitative point-count analyses include at least 1,000 points and are shown as percentages. Multiple analyses provide a check on reproducibility. Qualitative analyses indicate major rock-forming phases. Included are most samples for which whole-rock or mineral chemistry analyses are presented. Sample locations are shown in Appendix 5; a brief field description is included here.

3A. SERPENTINITES & CLINOPYROXENITE

Sample No.	n.	Serpentine & Opaque * after Olivine		Bastite Serpentine after Orthopyroxene	Clinopyroxene	Spinel	Field description
MA 11		X	X	X		X	Serpentinite block in gabbro.
MA 31	1500	73.3	8.9	17.3		0.5	Serpentinite block in gabbro.
	1500	77.4	6.8	13.4		2.6	
	1500	74.7	7.3	17.1		0.9	
MA 100	1175	83.8	8.1	4.3	0.9	2.9	Extensive area of weathered serpentinite
X 101		X	X	X		X	Serpentinite cut by gabbro dykes
MA 103	1400	76.1	7.2	14.7		2.0	Extensive area of weathered serpentinite
MA 110	1365	74.0	9.9	9.5	4.0	2.6	As above
MA 117	1600	82.6	6.7	8.3		2.4	Serpentinite beneath dunite cumulate
MA 135	1000	75.0	8.8	15.4		0.8	Serpentinite cut by gabbro
MA 136	1482	74.6	7.8	15.9		1.7	As above
X 220		X	X	X		X	As above
X 6					X		Dyke in serpentinised harzburgite

Note: * Qualitative XRD analysis, following the method of Aumento (1970), indicates lizardite and chrysotile, with the former dominant.

3B. PLAGIOCLASE DUNITES & MELA-OLIVINE GABBROS[1]

Sample No.	n.	Olivine	Ortho-pyroxene	Clino-pyroxene	Amphi-bole	Plagio-clase	Opaque	Serpentine & Magnetite after Olivine	Field Description
MA 2	2000	51.4		8.3		5.4	7.9	27.0	Dunite cumulate block
MA 16		X		X		X			Layered gabbros
MA 16A	2150	39.4				25.6	4.6	30.4	Ultramafic cumulate
M 16B	2200	24.6				22.0	2.7	50.7	As above
M 20		X		X		X	X	X	As above
X 78		X	X	X		X	X		Layered cumulates
X130	2000	23.1		12.1		26.7	1.0	31.3	As above
	2000	27.7		9.7		28.0	2.4	32.2	
MA174		X		X		X	X	X	Interlayered ultramafic gabbro cumulates.
MA217	2150	42.1				40.0		17.9	Block in harzburgite
X224		X	X			X		X	Block in px-gabbro
X233	2000	47.9		7.0	2.1	6.6	5.1	31.3	Layered cumulates
MA251		X		X	X	X	X		Ultramafic hill cut by gabbro pegmatite
X280	2000			5.7		20.7	0.2	73.4	Block in gabbro
	2000			1.0		21.2	0.6	77.2	
	2000			2.9		25.0	-	72.1	

Note: [1] In all plutonic samples, and particularly gabbro pegmatites, coarse grain-size and layering inhomogeneities reduce precision of modal analyses. To partly counteract this n. was increased.

Sample No.	n.	Olivine	Ortho-pyroxene	Clino-pyroxene	Amphi-bole	Plagio-clase	Opaque	Serpentine & Magnetite after Olivine	Field Description
X283		X		X		X	X		Layered cumulates
X286	1800	1.8		0.7		83.1		14.4	As above
X355	2200	11.7	1.5	17.9		31.0		37.9	Layered cumulates
MA378	2150	55.4		2.1		25.1		18.4	Block in gabbro cumulates
	2150	49.6		4.1		26.4		19.9	

Note: [1] In all plutonic samples, and particularly gabbro pegmatites, coarse grain-size and layering inhomogeneities reduce precision of modal analyses. To partly counteract this n. was increased.

3C. LEUCO-OLIVINE GABBROS

Sample No.	n.	Olivine	Ortho-pyroxene	Clino-pyroxene	Amphi-bole	Plagio-clase	Opaque	Serpentine & Magnetite after Olivine	Field Description
MA 21		X		X		X			Layered cumulates
X 71	2000	17.7	3.1	2.9	3.4	72.9			"
MA 76	1750	7.0		9.7		63.2		20.1	Layered cumulates, intruded by dolerite dykes
	1750	7.6		12.8		63.0		16.4	
	1750	10.9		11.0		65.1		13.0	
X131		13.1		12.1		55.4		9.4	Layered cumulates
X156	2100	0.8		13.5	18.9	63.4	3.4		
X160		X		X	X	X	X		Gabbro (50%) cut by dolerite dykes (50%)
MA175	2000	3.4		26.9	8.8	60.9			Layered cumulates
X180	2000	4.7		27.9		67.4			Gabbro cut by dolerite dykes
X235		X		X	X	X			Gabbro cut by rare dolerite dykes
X272		16.4		9.1		69.8		4.7	Layered cumulates
X287	2000	22.8	2.6	3.7		70.9			"

212

3D. PLUTONICS: "LEUCO GABBROS" (AL203 > 21%)

Sample No.	n.	Clinopyroxene	Amphibole	Plagioclase	Opaque	Epidote	Sphene	Rest	Field Description
MA 9	1900	18.7	1.2	80.1					Homogenous gabbro
X 10			X	X					Pegmatite
MA 14		X	X	X	X				Coarse homogenous gabbro
M 21				X				X	As above
M 22		X	X	X					As above
MA 57		X	X	X				X	Cumulate cut by dolerite dykes
MA 98		17.4	7.9	74.7					Homogenous gabbro
MA 99	2000	19.6		76.1		4.3			Homogenous gabbro
X120	1850	14.4	12.2	73.4					Homogenous gabbro
MA126		X	X	X					Layered cumulate
X132	2000	2.0	6.1	89.9		2.0			Homogenous gabbro
	2000	6.7	9.8	81.7		1.8			
MA173	2100	24.6		85.4					Layered cumulate
X189°		X	X	X					Screen to dolerite dykes
X247	1750	16.2	13.7	70.1					Gabbro (90%) cut by dykes
	1750	17.6	5.9	76.5					Homogenous area
X268			X	X	X	X			Layered cumulate

Note: ° Gabbro screens

3D. contd. PLUTONICS: "LEUCO GABBROS" (AL203 > 21%)

Sample No.	n.	Clinopyroxene	Amphibole	Plagioclase	Opaque	Epidote	Sphene	Rest	Field Description
X241		X	X	X					Vein in gabbro
MA276°	1750		14.9	85.1					Layered cumulate cut by
	1750		9.8	90.2					dolerite dykes (10%)
X288				X*					Layered cumulates
MA376	1950	7.1	3.5	88.4		1.0			Layered cumulates
MA433		X		X					Brecciated gabbro
MA444	1950			87.7		11.9	0.4		Screen to dolerite dykes

Note: * Complete rodingitization   ° Gabbro screens

Sample No.	n.	Clinopyroxene	Amphibole(s)	Plagioclase	Opaque	Epidote	Chlorite	Rest	Field Description
M 6		X	X	X	X	X			Layered cumulate
MA 7	1900	26.1	9.8	64.1					Pegmatite intrusion in cumulates
MA 8	2200	32.3	2.1	65.6					Homogenous gabbro
M 9			X	X	X				X[*1]	Homogenous gabbro
MA 17	2000	37.6		62.4					Layered cumulate
M 23C[o]	2000	26.7	15.7	57.6					Screen to dolerite dykes
M 23D[o]		X	X	X	X				Screen to dolerite dykes
X 26			X	X	X	X	X	X[*2]	Xenolith in granite
MA 30A		X	X	X			X		
M 31	2000		35.7	64.3					Xenolith in granite
X 34	2050		48.7	47.4			3.9		Xenolith in granite
X 40			X	X	X				Homogenous massive gabbro
M 46			X	X	X				Homogenous massive gabbro
M 47	2000	33.1	8.3	58.6					Layered cumulate
M 48		X	X	X					Layered cumulate
MA 53	1950	37.8	6.4	49.6		4.3	1.9		Homogenous cumulate

Note: *1 Apatite

*2 Includes biotite, quartz, apatite

3E. PLUTONICS : GABBROS (INC. SCREENS TO DOLERITE DYKES[o]) contd.

Sample No.		Clinopyroxene	Amphibole(s)	Plagioclase	Opaque	Epidote	Chlorite	Rest	Field Description
MA 54	2000	34.9	13.8	51.3					Layered cumulate cut by rare thin dolerite dykes
	2000	38.4	11.0	50.6					
MA 65	2200	26.6	1.9	61.5					Layered cumulate cut by rare dolerite dykes
MA 67		X	X	X					Layered cumulate cut by rare dolerite dykes
MA 73	1800	1.9	35.8	61.5	0.8				Layered cumulate cut by rare dolerite dykes
MA 96		X	X	X					Homogenous gabbro
X102				X				X	Sheet in serpentinite (harzburgite)
MA124		X	X	X	X	X			Homogenous gabbro
MA130	2000	31.7	8.4	59.9					Homogenous gabbro cut by gabbro pegmatite
MA151		X	X	X		X			Pegmatite in harzburgite
MA154		X	X	X					Screen to dolerite dykes (50%)
MA182	2000	25.4	10.5	64.1					Layered cumulate
X186[o]		X	X	X					6" screen to dolerite dykes (80%)
X195[o]		X	X	X					Gabbro with dolerite xenoliths

Sample No.	n.	Clinopyroxene	Amphibole(s)	Plagioclase	Opaque	Epidote	Chlorite	Rest	Field Description
MA205[o]			X	X					Screen to dolerite dykes
MA238[o]		X	X	X					Layered gabbro cut by dolerite dykes, layering and dykes parallel.
MA246[o]		X	X	X	X				Homogenous massive gabbro
MA250		X	X	X	X		X		Gabbro cut by dolerite dykes (50%)
MA254[o]	1750	18.4	12.7	68.9					Screen to dolerite dykes (60%)
MA260[o]	1750	17.4	19.4	63.2					Screen to dolerite dykes (50%)
X263[o]		X	X	X					Gabbro cut by dolerite dykes (80%)
X265	1900	15.8	4.9	72.8		6.5			
	1900	17.9	2.1	72.9		7.1			Layered cumulates
	1900	13.1	5.5	79.4		2.0			
X270	2150	30.5		68.6	0.4		0.5		Layered cumulates,
MA272[o]	2000	9.6	30.3	60.1					Screen to dolerite dykes (90%)
	2000	12.8	28.9	58.3					
	2000	7.8	34.1	58.1					
X294		X	X	X			X		Massive gabbro

3E. PLUTONICS : GABBROS (INC. SCREENS TO DOLERITE DYKES°) contd.

Sample No.	n.	Clinopyroxene	Amphibole(s)	Plagioclase	Opaque	Chlorite	Q_3	Rest	Field Description
X308	2000			64.1			32.3	3.6[1]	6" vein intruding darker gabbro
MA321			X	X					Mylonised outcrop
X347				X		X		X[2]	Pink lense in massive gabbro
X349			X	X	X				Basic mylonite
MA365°	2000	22.9	20.7	56.4					Gabbro cut by dolerite dykes (30%)
MA372		X	X	X					Layered cumulate
MA407				X				X[3]	Matrix to darker gabbro in magmatic gabbro breccia.
MA417°	1950			80.2				19.8[4]	Screen to dolerite dykes (90%)

Note: *1 Epidote
*2 Thulite (Manganese zoisite)
*3 Plagioclase total includes some k-felspar, rest = sphene, epidote, minor zircon
*4 Mainly epidote > amphibole

3F.   GABBRO PEGMATITES

Sample No.	n.	Clinopyroxene	Amphibole[1]	Plagioclase	Opaque	Rest[2]	Field Description
M 3		X	X	X			Extensive area in gabbros
X 4	1900	14.1	37.8	48.1			Veins cutting serpentinite (harzburgite)
MA 7A		X	X	X	X		Vein cutting gabbro cumulate
X 11	2000		44.5	54.8	0.7		Extensive area in cumulate gabbros
MA32A		, X	X	X	X	X	Intruding massive gabbro, intruded by granite
MA109	2000	19.4	32.0	47.7	0.9		Boss in serpentinite (harzburgite)
MA127	1900	20.2	32.9	47.7			Small hills through alluvium
	1900	14.0	40.3	45.7			
	1900	21.3	29.7	49.0			
MA150	1900		53.3	46.7			Sheared outcrop in serpentinite (harzburgite)
MA168		X		X			Homogenous, massive, area
MA297			X	X		X	Coarse screens cut by dolerite dykes

Note: *1 Includes obvious "uralitic" pale green fibrous amphibole and dark green-brown prismatic amphibole which might be primary.

*2 Includes epidote-zoisite, sphene, quartz, epidote

3G. METADOLERITES, MAINLY OF SHEETED DYKE COMPLEX

| | | PHENOCRYSTS | | | GROUNDMASS | | | | |
| | | Olivine *1 | Plagioclase | Clinopyroxene | Amphibole(& clinopyroxene relicts) | Plagioclase | Opaque | Sphene | |
Sample No.	n.								Field Description
M 17	1500				54.3	42.0	3.7		Dykes intrude gabbro
	1500				51.1	46.9	2.0		(screens ~ 30%)
	1500				52.9	42.7	4.4		
M 23A					X	X	X		As above
M 23B					X	X	X		As above
X 29	1450				54.3	41.6	1.0	3.1	Xenolith in granite
MA 33					X	X	X	X	Xenolith in granite
MA 42	1500		1.7		48.7	44.4	3.3	1.9	Xenolith in granite
X 43	1400		5.4		55.7	31.7	7.2		Low hills through alluvium
MA 46					X	X	X	X	Massive outcrop
MA 50				X	X	X	X		Massive outcrop
MA 53		X <	X		X	X	X		Massive outcrop
MA 58	1600	0.9			56.1	37.6	5.4		Dykes (5%) intruding layered cumulates
MA 60					X	X	X		Dykes (5%) intruding layered cumulates

Note: *1 Olivine phenocrysts pseudomorphed by amphibole - chlorite
*2 Dolerite dykes cutting green pillow lavas

3G. contd. METADOLERITES, MAINLY OF SHEETED DYKE COMPLEX

		PHENOCRYSTS			GROUNDMASS				
Sample No.	n.	Olivine *1	Plagioclase	Clinopyroxene	Amphibole(& clinopyroxene relicts)	Plagioclase	Opaque	Sphene	Field Description
X134	1490		7.6		49.6	34.0	8.8		Low hills of 100% dykes
X142					X (X)	X	X		Low hills of 100% dykes
X176	1400				49.7	47.4	2.7		Massive dolerite
	1400				55.6	41.1	3.3		
	1400				49.1	46.3	4.6		
MA206	1500		4.9		19.7(18.2)	50.1	6.0		Dykes (90%) with gabbro screens (10%)
X214			X		X	X	X		Block in ultramafic cumulates
MA214	1600		4.6	0.6	45.1	42.2	7.4		Dykes (40%) intruding gabbro (60%)
	1600		2.7		50.1	39.4	7.8		
	1600		4.8		46.4	43.1	5.7		
X215					X (X)	X	X		Block in ultramafic cumulates

Note: *1   Olivine phenocrysts pseudomorphed by amphibole - chlorite
      *2   Dolerite dykes cutting green pillow lavas

3G. contd. METADOLERITE DYKES, MAINLY OF SHEETED DYKE COMPLEX

Sample No.	n.	Olivine	Plagio-clase	Clino-pyroxene	Amphibole (& clinopyroxene relicts)	Chlorite	Plagio-clase	Opaque	Sphene	Field Description
		PHENOCRYSTS			GROUNDMASS					
MA236	2000				51.4		46.5	2.0		Dykes (30%) intruding sheared layered cumulates.
MA257					X		X	X		Dykes (70%) with gabbro screens
MA266					X (X)		X	X		Dykes (80%) with gabbro screens
MA286	1400				36.1 (14.3)		43.2	6.4		Massive outcrop below
	1400				40.9 (11.7)		40.4	7.0		limestone exotic
X307	1900				- (38.3)		52.4	9.3		Bosses in serpentinite (harzburgite)
MA320			X		X		X	X		Low hill in alluvium, massive outcrop
X324					(X)	X	X	X		Sinuous dykes (20%) in green pillow lavas
X342					X		X	X	X	Block in melange
MA363					49.7 (3.7)		44.7	1.9		Dykes (30%) intruding massive gabbro
MA367	1724				53.8		41.1	2.6	2.5	Dykes (90%) with massive gabbro screens

Sample No.	n.	PHENOCRYSTS				GROUNDMASS				Field Description
		Olivine	Plagio-clase	Clino-pyroxene	Amphibole (& clinopyroxene relicts)	Chlorite	Plagio-clase	Opaque	Sphene	
MA370		X		X	X (X)	X	X	X		Dyke in gabbro cumulate
MA410		X			X (X)	X	X	X		(Dykes (90%) with green
MA411			X		X		X	X		(pillow lava screens
										(
MA413	1300		1.8		40.1 (11.4)		44.1	2.6		Dykes (50%) cutting serpent-inite (harzburgite)
MA419					X		X	X	X	Massive block in melange
MA424	1316		49.8		29.5		18.8	2.0	0.4	100% dykes
MA450	1400		17.4		44.4		29.3	8.9		100% dykes, 1cm ↔ 3m width
	1400		11.7		47.3		36.0	5.0		
	1400		16.0		47.9		32.2	3.9		

3H. RED PILLOW LAVAS

Sample No.	n	PHENOCRYSTS/MICROPHENOCRYSTS				GROUNDMASS			Field Description
		Olivine	Plagioclase	Clino-pyroxene	Opaque	Plagioclase laths	Chlorite	Matrix[1]	
MA139	1600	1.3	18.3			15.0		65.4	Core. Tightly filling elliptical
	1600	0.2	21.9			20.1		57.8	pillows. Diameter 0.3-1.0m.
	1600	0.7	14.4			16.2		68.7	
MA139A	1500	2.1	17.4			11.7		68.8	Margin of above pillow
MA142	1696	0.9	25.5	0.9		17.7		54.8	Core from adjacent pillow to MA139
MA143			X			X	X	X	Core from adjacent pillow to MA139
MA143A		X	X		X	X		X	Margin from adjacent pillow to MA139
X245			X			X		X	Margin. Extensive area of pillowed lavas
X245A	1800	3.5	21.5			12.7		62.3	Margin. As above
X245B			X			X		X	Core. As above
MA435			X			X		X	Margin. Vescular brecciated pillows
MA437						X		X	Core. Pillow 0.6-0.9m. dia. cut by rare dykes

Note: [1] Includes oxidised opaque ± calcite ± smectite ± zeolite. Same minerals occur in veins, vesicles.

- 224 -

3H. contd. RED PILLOW LAVAS

Sample No.	n.	PHENOCRYSTS/MICROPHENOCRYSTS				GROUNDMASS			Field Description
		Olivine	Plagioclase	Clino-pyroxene	Opaque	Plagioclase laths	Chlorite	Matrix [*1]	
MA439			13.7	2.4		24.1		59.8	Core. Pillow lava with inter-calated thin limestone
MA440			X			X		X	Core. Pillowed, locally hyaloclastic.
MA461			X	X		X	X	X	Vesicular, pillowed to massive
MA464			15.0			21.4		63.6	Core. Pillow lava cut by rare dykes

Note: *1 Includes oxidised opaque $\pm$ calcite $\pm$ smectite $\pm$ zeolite. Same minerals occur in veins, vesicles.

3I. GREEN PILLOW LAVAS

Sample No.	n.	PHENOCRYSTS/MICROPHENOCRYSTS				GROUNDMASS						Field Description
		Olivine	Plagio-clase	Clino-pyroxene	Opaque	Clino-pyroxene	Amphi-bole	Plagio-clase laths	Chlorite	Opaque	Remainder	
MA112	1604	0.7	11.6					30.8		5.0	51.9	Low hills, rubbly, splitic, veined by calcite
MA113		X	X		X	X		X	X		X	As above, better pillows
MA114	1500	1.9	7.4			5.1	4.2	25.7	11.1	8.1	26.5	Pillows with good chilled margins
MA232		X	X	X		X		X		X	X	0.6-0.9m pillows, calcite veining
X326		1.2	9.0	1.7				32.3	8.7		47.1	90% pillow lavas cut by dykes

3J. MELANGE LAVAS

Sample No.	n.	PHENOCRYSTS		GROUNDMASS				SECONDARY		Field Description
		Plagio-clase	Clino-pyroxene	Clino-pyroxene	Plagio-clase	Opaque	Rest *2	Zeolite	Calcite	
X346				X	X	X	X			Block, pillowed
MA354	1500				53.5 *1	6.4	34.4		5.7	Low hills, vesicular, massive.
MA356				X	X	X		X	X	Low hills, amygdoloidal lava
MA420		X	X	X	X	X	X		X	Massive, basalt

Note: *1   felspar laths too fine in MA354 to postively identify species
       *2   fine matrix, individual minerals not identified; includes epidote and chlorite in MA420

3K. SHINZI GROUP VOLCANICS

Sample No.	n.	PHENOCRYSTS Plagioclase	Clinopyroxene	Clinopyroxene	Amphibole	GROUNDMASS Plagioclase *1	Quartz *2	Opaque	Chlorite *3	Rest *5	Calcite *2	Field Description
X219A		X				X	X	X		X	X	(2-6m thick sheets
X219B	1500					50.4	2.1	8.9		35.0	3.6	((dykes? flows?) of (dolerite. Aphyric
X219C		X				X	X	X		X	X	(to plagiophyric.
X219D	1600					55.7		6.2	5.1	33.0		(Some paler, (medium-grained
X219E		X				X		X	X	X	X	(more leucocratic (keratophyre.
X220A		X				X	X	X		X		(2-6m thick sheets
X220A1	1400	3.6				47.2	1.5	4.7		33.0		(dipping at 40°, (massive, fine- (grained.
X222		X		X		X		X	X	X	X	(
X222A	1400	15.8		17.7 *4		55.2		6.6	1.6		3.2	(Vesicular pillowed
	1400	9.4		24.7		51.5		8.3	4.1		2.0	) lava, sometimes
	1400	9.0		27.0		48.4		9.8	0.3		5.5	) brecciated.
MA339		X				X				X	X	(

Note:
*1 Felspar laths frequently too fine to positively identify species
*2 Occurs in matrix and as occasional veins
*3 Occurs in matrix and occasionally in vesicles
*4 Includes some amphibole alteration
*5 Dark, fine-grain matrix

3K. contd. SHINZI GROUP VOLCANICS

		PHENOCRYSTS				GROUNDMASS						
Sample No.	n.	Plagio-clase	Clino-pyroxene	Clino-pyroxene	Amphi-bole	Plagio-clase *1	Quartz *2	Opaque	Chlorite *3	Rest *5	Calcite *2	Field Description
MA425A		X	X	X		X		X	X			(Pillowed lavas cut
MA425B		X	X			X		X		X	X	(by narrow dykes. (Many massive
MA426	1500	1.1			23.1	57.8		17.9				(structureless
MA427		X				X	X	X		X	X	(outcrops. (

Note: *1 Felspar laths frequently too fine to positively identify species
*2 Occurs in matrix and as occasional veins
*3 Occurs in matrix and occasionally in vesicles
*5 Dark, fine-grain matrix

3L. GRANITES

Sample No.	n.	Quartz	Orthoclase	Plagioclase	Biotite (inc. chlorite & opaque replacement)	Sphene	Epidote	Calcite	Field Description
M 12		X	X	X					Highly xenolithic (gabbro)
X 24	1612	44.5	31.9	24.5	1.1				Dolerite/gabbro xenoliths and host rock
MA 28		X	X	X	X				20% granite veins intruding massive gabbro
M 29		X	X	X	X				
N 30B	1500	42.0	30.8	23.9	1.7				(Narrow veins cutting
	1500	45.7	29.1	22.5	2.7				(gabbro - gabbro
	1500	44.9	32.4	20.9	1.8				(pegmatite
MA 30B	1177	40.9	37.9	15.6			2.7	2.9	Gabbro intruded by gabbro pegmatite intruded by 10-50% granite veins
X 33		X	X	X	X				(Gabbro host. Granite
X 34		X	X	X	X				(contains gabbro-dolerite
X 35		X	X	X	X				(xenoliths, some partially
X 37	1200	39.1	36.0	21.4	3.5				(absorbed.
MA 37	1512	38.6	38.6	21.3	1.3				Granite veins, stocks cutting gabbro, gabbro pegmatite
MA 44	1477	43.5	33.9	19.8	2.9				As above

3L. contd. GRANITES

Sample No.	n.	Quartz	Orthoclase	Plagioclase	Biotite (inc. chlorite & opaque replacement)	Sphene	Epidote	Calcite	Field Description
X 86	1500	42.6	34.3	21.1	2.0				Mylonised, sheared
	1500	38.1	34.5	24.3	3.1				contact with serpentinite (harzburgite).
MA120A		X	X	X	X				Stocks of 4.5 cu.m. cutting serpentinite (harzburgite)
MA360		X	X	X	X	X			(Granite containing 10-20%
MA360A		X	X	X	X				(gabbro xenoliths
MA455	1500	40.2	38.7	20.1	1.0				Pods in serpentinite (harzburgite)

4. Cumulus and intercumulus phases in some plutonic cumulate rocks

Sample no.	Cumulus phases[1]	Intercumulus phases[2]
MA2	Cr→Ol	Pl. Cpx.
MA9	Pl. Cpx.	
MA17	Ol→Pl,Cpx.	
MA21	Ol. Pl. Cpx.	
MA53	Pl. Cpx.	
MA54	Pl. Cpx.	
MA65	Pl. Cpx.	
MA67	Pl. Cpx.	
X 71	Ol. Pl.	Cpx.
MA76	Ol. Pl. Cpx.	
X78	Ol. Pl. Cpx.	
X124	Pl. Cpx. Mt.	
X130	Cr→Ol	Pl. Cpx.
X131	Ol. Pl.	Cpx.
X132	Pl.	Cpx.
MA174	Cr→Ol	Pl. Cpx.
MA175	Ol. Pl.	Cpx.
MA182	Pl. Cpx.	
X189	Pl. Cpx.	
MA217	Ol	Pl
X224	Ol. Pl.	
X355	Ol. Pl.	Cpx.

Note: [1] Arrows indicate the order of precipitation where determinable.

[2] Commonly represented by pl-cpx overgrowths. Difficult to decide if common minor intercumulus amphibole is primary or secondary.

APPENDIX 5 Sample location maps

The maps show:

(a)   The outcrop pattern of each major rock-type

(b)   The approximate location of analyzed samples of that rock-type

SERPENTINITES

X-14

MA-100/108/110

MA-128/135/136

MA-31

X-152

A
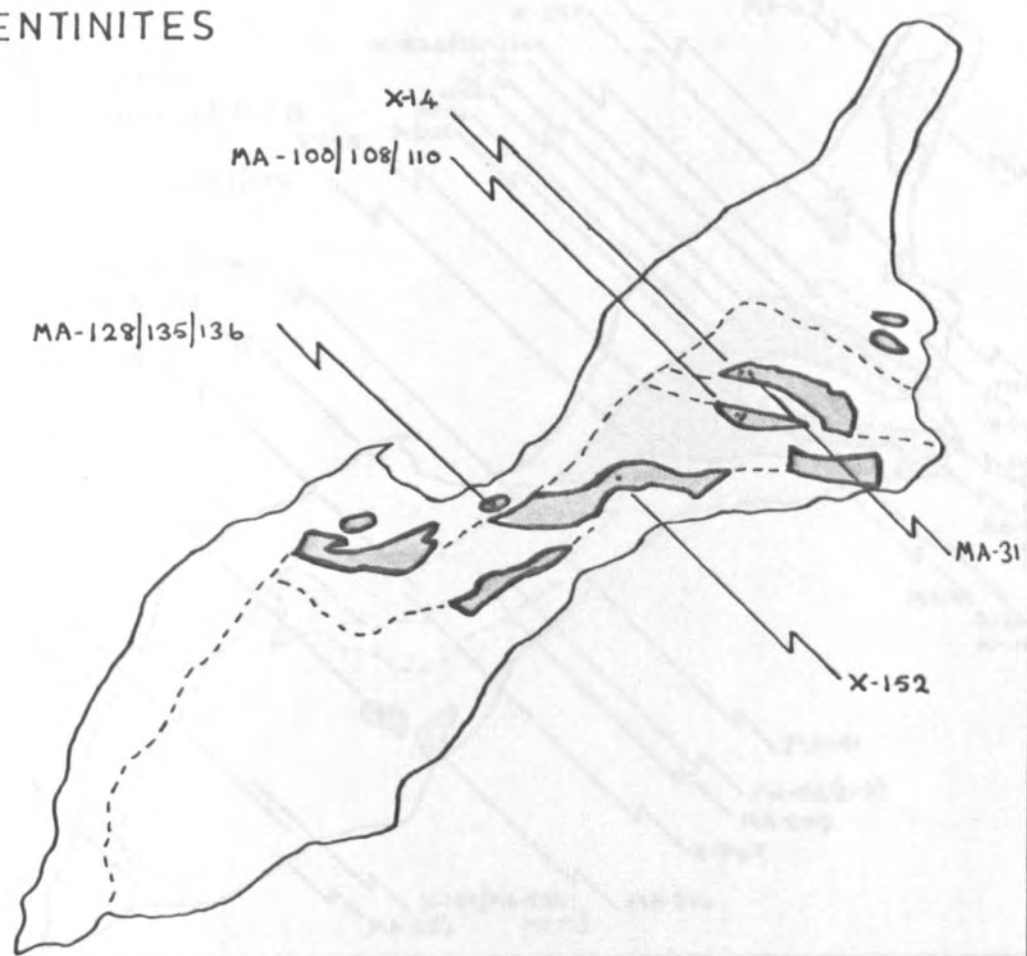
GABBRO : 1
Dunite, troctolite, olivine gabbro.

X-69/78

MA-2

X-129/150/131

X-280

MA-76
X-355

MA-122

MA-251

X272

B
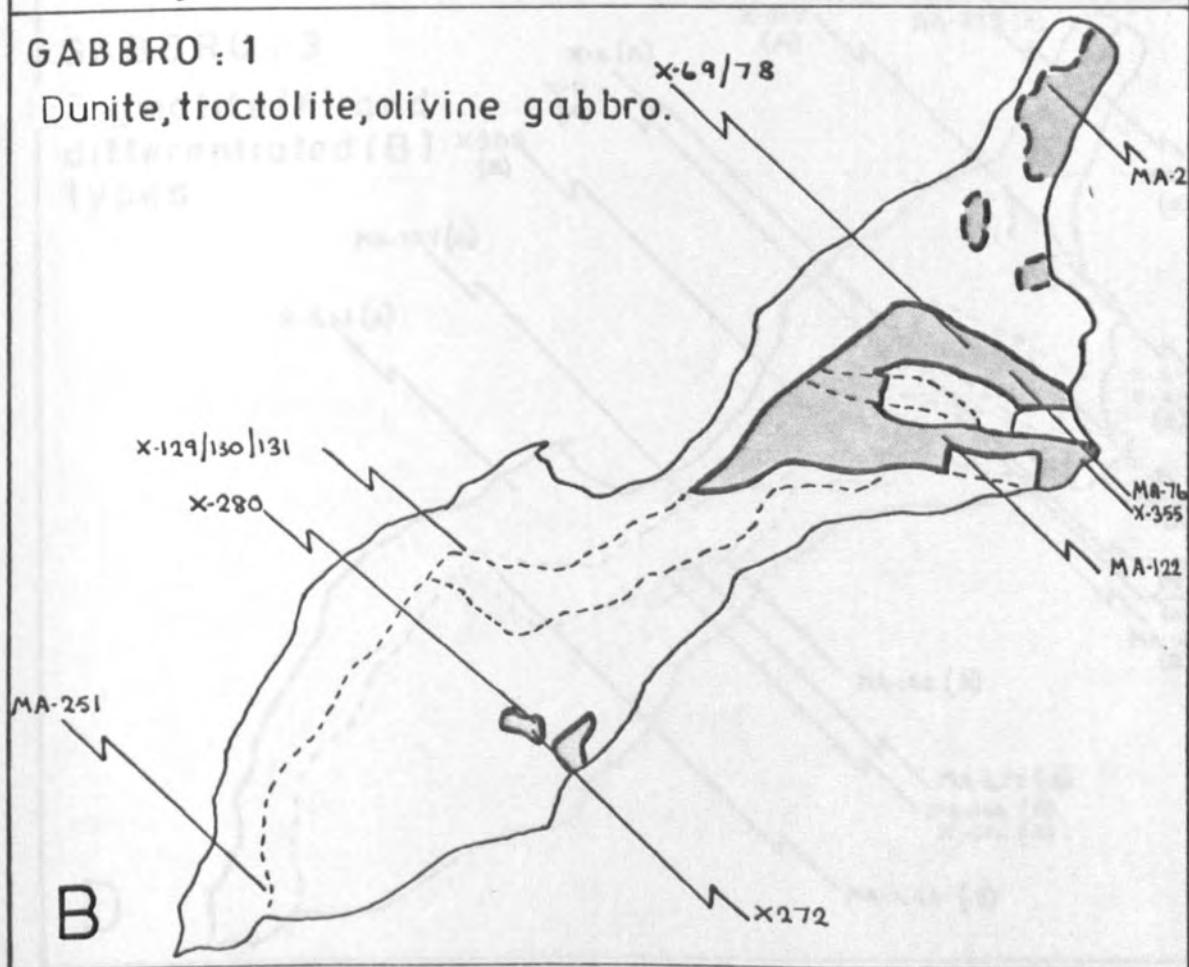
GABBRO: 2
Pyroxene and
hornblende gabbro

X-238
X-297
X-264/265/266
X-71
MA-9
MA-11
MA-14
MA-25
X-120
MA-168/173/175
MA-132/124/126/127
MA-182
MA-438
X-286/287/288
X-186/189
MA-250/MA 246
MA-254

MA-47
X-40
MA-427
X-349
MA-71
MA-73
57
MA-59
61
66
MA-99
X-109
X-110
MA-151
MA-154 (1-3)
MA-205
X-247
X-189/MA-276/MA 272
MA-283
MA-376
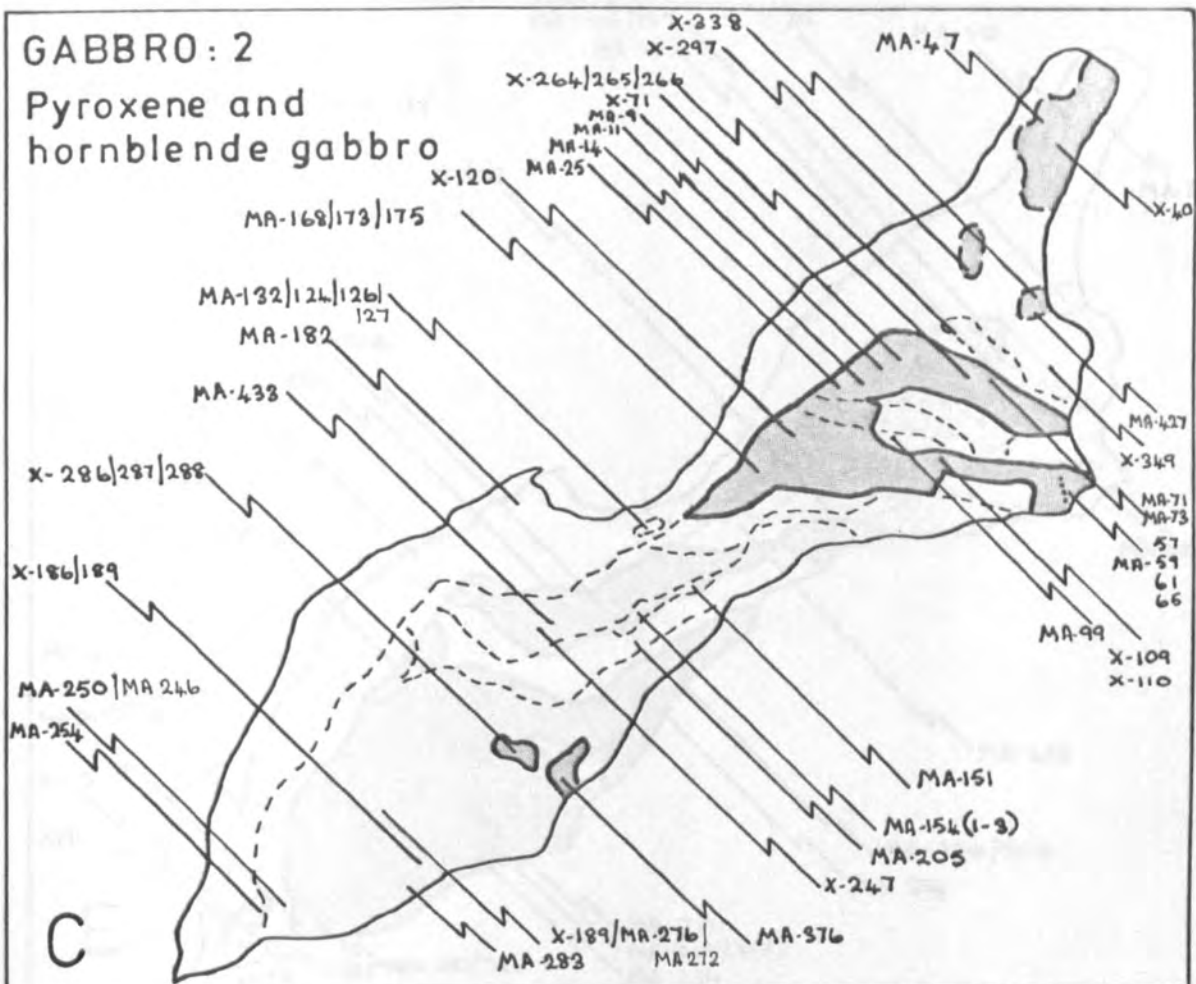
C

GABBRO: 3
Pegmatite (A) and
differentiated (B)
types

X-217 (A)
X-4 (A)
X-11 (A)
X308 (B)
MA-127 (A)
X-241 (A)

MA-323 (A)
MA-321 (B)
X-219
X-219AI (B)
X-205 (A)
X-27 (A)
X-106A (B)
MA-120 (B)
MA-150 (A)
MA-417 (B)
MA-164 (A)
X-114 (A)
MA-444 (B)
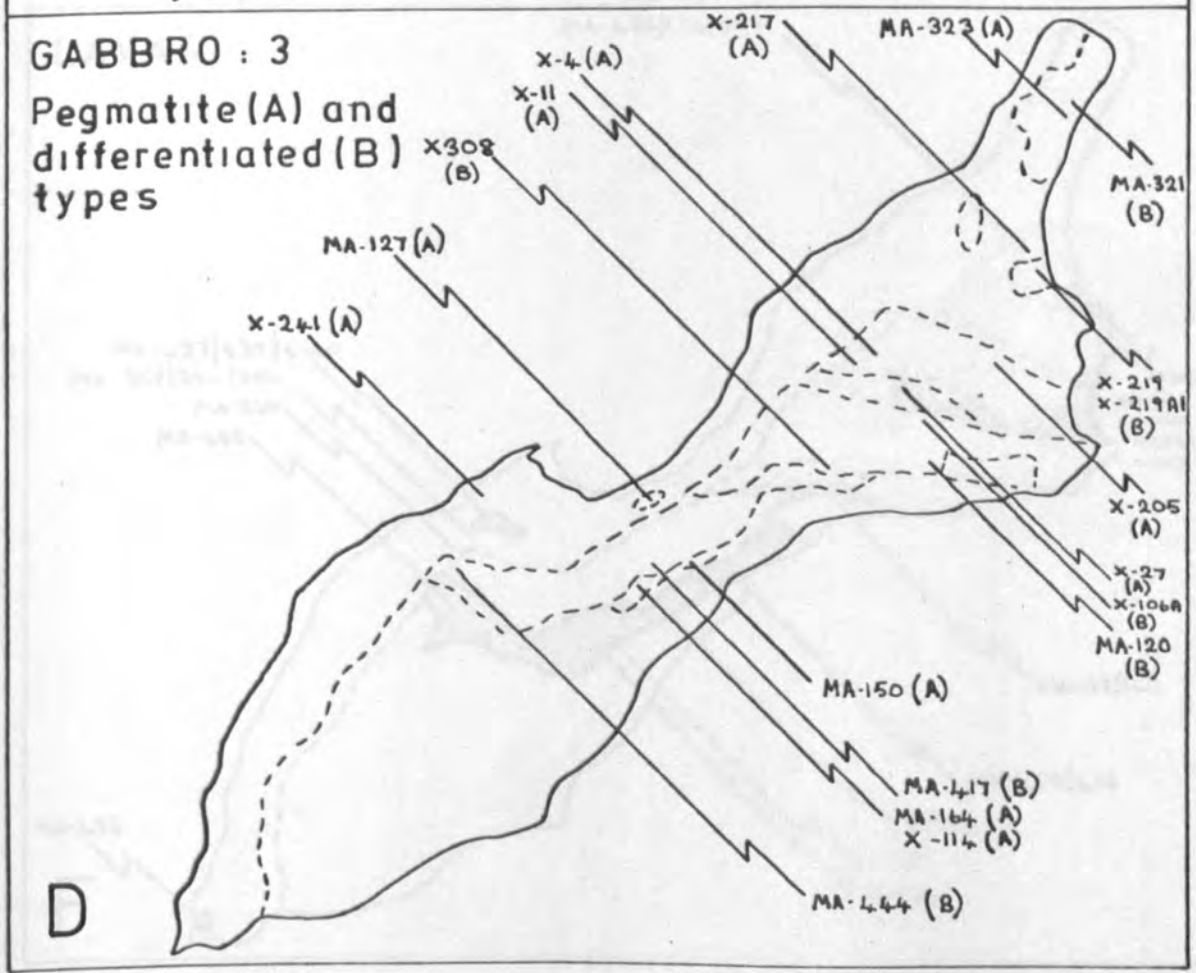
D

DOLERITE
Outcrop pattern of
sheeted dykes

MA-366/367
MA-75
X-214
MA-50
MA-320
X-207
X-324
MA-183
X-239
MA-286
MA-58
MA-424
MA-257
X-178
X-176
MA-413
MA-206/208
MA-214
E
X-179
X-183 MA-257/266
MA-271
MA-248/X-187
MA-236

LAVAS
MA-425/426/427
X-219A
MA-437/439/440
MA-352/354/356
MA-346
MA-448
X-220A
X-220B
X-222A
X-223
MA-139/142
MA-422
MA-400/401
X-323
X-328
F
X-330

GRANITES

MA-42 X-26
MA-44 X-29
X-86
MA-358

MA-33/
MA-35/
MA-37
MA-29
MA-46
MA-120A

G

OTHERS

MA-79/80
chert

X-16
pyroxenite

thulitic X-347
vein

X-a

amphibolite

H

APPENDIX 6 Whole-rock geochemistry : analytical techniques and results

Sample preparation

Major and trace element analysis by X-ray fluorescence techniques requires a general method of sample preparation.

The size of sample crushed depended on the grain size of that rock. In general this amounted to 1-2kg, more in the case of the pegmatites to avoid mineralogical bias. Samples were first split into pieces (2-3 cm^3) using an hydraulic jaw splitter and then crushed to chips (1 cm^3) by a fly-press fitted with hardened steel crushing surfaces. During these two operations the obvious weathered crusts were removed. The chips were crushed to a coarse powder in a "Tema" tungsten-carbide swing mill. A random 50cc sample was taken and ground for three one-minute intervals, each grinding being followed by 45 seconds of cooling. 15gms of the resulting fine powder were mixed with 25-45 drops of "Mowiol" organic binder and the resulting paste compressed in a polished tungsten carbide die at a pressure of 20 tons/in^2 to produce 46mm diameter powder pellets. These were dried for 24 hours before analyzing and care was taken throughout their handling that the surface to be irradiated was uncontaminated.

A representative selection of samples were also prepared as fusion beads. 0.8gm of fine rock powder were mixed with 4.0gm of 80% lithium metaborate - 20% lithium tetraborate (Johson-Malthey Spectroflux 100B) and fused for 20 minutes in a Pt/Au crucible at 1150°C in a vertical tube furnace. 46mm glass discs were then pressed in aluminium moulds using equipment similar to that described by Harvey et al (1973). The discs were cooled and annealed in a heated asbestos block before storing in sealed poly-propylene bags in a dessicator to prevent atmospheric contamination.

Analysis

Major and trace elements were analyzed by X-ray fluorescence spectrometry using the University of Birmingham Philips PW1450 Automatic Spectrometer with a PW1466 sixty position sample charger. Three tubes

are used - chromium, tungsten and molybdenum - for the determination of up to 27 elements. Tables A6.1, A6.2 and A6.3 show the machine conditions for the three tube programmes. A ratio technique was used to eliminate all but short term drift, which was monitored and corrected using a series of identical pellets on each run. Four internal reference standards per run were used to monitor long term precision. The counts produced by the spectrometer were recorded on paper roll and paper tape and processed by computer using programs written by P.D. Marsh.

The machine was calibrated by a combination of international standard values (Flanagan, 1973; Jackson and Strelow, 1975) and spiking techniques. The details of calibration are described by Leake et al (1969). Potential errors, due to mineralogical effects, are inherent in the use of powder pellets for major element analysis. Representative samples were selected to cover the composition range of Masirah rocks. These were analysed in parallel with standard beads and the determined concentrations used to establish calibrations for the remaining pellet samples.

Three international standard values are presented in Table A6.4 to monitor machine accuracy. Precision is high, especially in the case of the elements with higher atomic weights and replicate analyses of the gabbro MA254 are presented in Table A6.5 to illustrate the precision. Lower limits of detection, as determined by the formulae in Jenkins and De Vries (1967) are:-

Y	2 ppm	Ni	2 ppm
Sr	1 ppm	Cr	2 ppm
Rb	1 ppm	Ce	3 ppm
Th	3 ppm	La	2 ppm
Pb	3 ppm	Zr	2 ppm
Ga	2 ppm	Nb	1 ppm
Ba	4 ppm		

Norms and analytical listings were created by using programmes written by Dr. A.E. Wright, Dr. J. Tarney and Mr. B.L. Weaver.

Presentation

Major elements are given in percentages. Iron is assigned in the mafic and ultramafic rocks so that $Fe_2O_3/FEO = 0.15$. MnO is determined in

Table A6.1

Spectrometer Conditions for the CR-Programme

Element	Line	Peak $^\circ 2\theta$	Background(s)		Crystal	Detector	Coll.	KV	mA	Time(Peak)
Ti	$K\alpha_{1,2}$	36.54	+3.16		PE	F	f	50	20	4 secs.
Ca	Kα	45.06	-1.80		PE	F	f.	20	10	4
K	Kα	50.58	+3.75		PE	F	f	60	30	4
Si	Kα	108.94	+3.00		PE	F	C	60	30	20
Al	Kα	144.75	-4.80		PE	F	C	60	30	20
P	Kα	140.92	+2.70		GE	F	C	60	30	20
Fe	Kα	85.74	+4.83		LIF 220	F	f	60	30	10
Mn	Kα	62.98	+3.02		LIF 200	F	f	60	30	20
Mg	Kα	45.21	-2.30	+3.20	TLAP	F	f	60	30	20
Na	Kα	55.20	-2.20	+1.30	TLAP	F.	C	40	45	40
S	Kα	75.74	-2.64		PE	F	C	60	30	20
CL	Kα	65.32	+2.00		PE	F	C	60	30	20

Table A6.2

Spectrometer Conditions for the W-Programme

Element	Line	Peak $^\circ 2\theta$	Background(s)		Crystal	Detector	Coll.	KV	mA	Time(Peak)
Ni	$K\alpha_{1,2}$	71.25	WLL		LIF 220	F	f	60	30	20 secs
Cr	$K\alpha_{1,2}$	107.13	-2.22		LIF 220	F	f	60	30	20
Ce	$L\beta_1$	111.68	-1.75		LIF 220	F	c	60	30	20
La	$L\alpha_1$	138.95	-2.20		LIF 220	F	c	60	30	20
W	$L\beta$	53.48	-1.18		LIF 220	S	f	60	30	20
Zr	$K\alpha_{1,2}$	32.04	-0.94	+0.57	LIF 220	S	f	60	30	20
Nb	$K\alpha_{1,2}$	30.36	+0.74	-0.55	LIF 220	S	f	60	30	20

Table A6.3

Machine Conditions for the Mo-Programme

Element	Line	Peak $^{\circ}2\theta$	Background(s)		Crystal	Detector	Coll.	KV	mA	Time(Peak)
Y	$K\alpha_1$	33.83	-0.85	$+0.93$	LIF 220	S	f	60	30	20 secs
Sr	$K\alpha_1$	35.79	-1.03	$+0.84$	LIF 220	S	f	60	30	20
Rb	$K\alpha_1$	37.92	-1.29	$+0.90$	LIF 220	S	f	60	30	20
Th	$L\alpha_1$	39.22	-0.40	$+0.80$	LIF 220	S	f	60	30	20
Pb	$L\beta_2$	40.35	-0.33	$+0.90$	LIF 220	S	f	60	30	20
Mo	Compton	30.10	-1.66		LIF 220	S	f	60	30	20
Ga	$K\alpha_1$	56.12	-1.82	$+1.28$	LIF 220	F + S	f	60	30	20
Zn	$K\alpha_1$	60.50	$+1.27$		LIF 220	F + S	f	60	30	20
Cu	$K\alpha_1$	65.52	$+1.04$		LIF 220	F + S	f	60	30	20
Ba	$L\beta_1$	128.67	$+2.69$		LIF 220	F	c	60	30	20

	Diabase W1		Basalt JB1		Granite G2	
	Abbey 1978	B'ham 1977 XRF	Abbey 1978	B'ham 1977 XRF	Abbey 1978	B'ham 1977 XRF
SiO2	52.72	52.02	52.62	52.84	69.19	69.31
TiO2	1.07	1.02	1.34	1.32	0.50	0.48
Al2O3	14.87	15.54	14.62	14.65	15.35	15.67
Fe2O3(t)	11.10	10.71	9.01	9.33	2.67	2.73
MnO	0.17	0.17	0.15	0.16	0.04	0.04
MgO	6.63	6.08	7.76	7.06	0.77	0.81
CaO	10.98	10.77	9.35	8.67	1.98	1.88
Na2O	2.15	2.38	2.79	2.85	4.06	4.25
K2O	0.64	0.73	1.42	1.56	4.52	4.56
P2O5	0.14	0.14	0.26	0.25	0.14	0.11
	100.47	99.56	99.32	98.69	99.22	99.84
Ni	78	72	135	125	6	3
Cr	120	113	400	396	7	11
Ce	23	22	67	65	150	161
La	12	19	36	52	100	102
Zr	105	106	155	175	300	356
Nb	9.5	5	-	37	14	31
Y	25	21	26	24	12	12
Sr	190	193	440	459	480	466
Rb	21	21	41	41	168	168
Th	2.4	2	9	10	24	31
Pb	7.8	8	14	8	29	30
Ga	16	17	17	21	23	25
Zn	86	79	83	82	85	70
Ba	160	188	490	562	1850	2055

Table A6.5 : replicate analyses of gabbro MA254

	1	2	3	4
SiO_2	47.54	47.38	47.54	47.41
TiO_2	0.18	0.16	0.18	0.17
Al_2O_3	19.55	18.84	19.53	18.97
$Fe_2O_3(t)$	4.06	4.09	4.31	4.11
MnO	0.09	-	0.10	0.11
MgO	11.08	10.93	11.01	11.00
CaO	14.41	14.54	14.48	14.60
Na_2O	1.72	1.73	1.79	1.74
K_2O	0.33	0.33	0.29	0.28
P_2O_5	0.01	0.01	0.01	0.02
	98.97	98.01	99.24	98.37
Ni	128	123	128	127
Cr	588	604	594	589
Ce	3	2	3	2
La	2	2	5	3
Zr	18	19	21	21
Nb	2	1	1	1
Y	4	3	4	5
Sr	210	214	200	208
Rb	2	2	2	4
Th	3	3	1	3
Pb	3	2	2	3
Ga	14	14	14	15
Zn	13	17	23	17
Ba	34	27	34	31

Note: - not determined

approximately 50% of samples, otherwise shown as 0.00. In the ultramafic rocks ignition loss during heating to 1150°C is quoted. Twenty-seven representative gabbros, dolerites and lavas gave ignition losses ranging 1.28 - 4.65% with a mean of 2.71%. These values support the analysis totals of 96.0 - 99.0%.

Trace elements are given as p.p.m. A negative value indicates a content below the lower limit of detection. Within the rock-groups the analyses are ordered by increasing Zr.

Within the various gabbros the screens in the sheeted dyke complex are distinguished by a cross (+).

SERPENTINISED HARZBURGITES

ROCK NO	X14	MA100	MA135	MA110	MA125	X152	MA108	MA31
SIO2	41.90	42.10	40.21	40.58	40.72	41.88	40.65	42.77
TIO2	0.01	0.01	0.01	0.01	0.01	0.01	0.01	0.01
AL2O3	1.51	1.37	0.58	0.36	0.52	0.48	0.37	0.48
FE2O3	1.16	1.20	1.18	1.19	1.16	1.26	1.18	1.17
FEO	7.63	7.92	7.81	7.84	7.62	3.31	7.79	7.69
MNO	0.00	0.00	0.12	0.17	0.11	0.15	0.17	0.10
MGO	34.74	32.93	35.45	34.07	35.65	34.22	34.35	38.44
CAO	0.49	0.58	0.18	0.73	0.23	0.22	0.52	0.15
NA2O	0.05	0.05	0.07	0.21	0.06	0.05	0.04	0.05
K2O	0.01	0.01	0.01	0.01	0.01	0.02	0.01	0.01
P2O5	0.00	0.00	0.00	0.00	0.00	0.00	0.00	0.00
H_2O*	13.21	13.46	13.76	14.15	13.90	14.90	15.37	10.12
TOTAL	100.71	99.63	99.38	99.82	99.99	101.50	100.46	100.99

TRACE ELEMENTS IN PPM

NI	2077	2336	2505	2337	2556	2449	2390	2456
CR	3843	3100	3539	3453	3321	3243	3171	3478
ZN	30	33	44	37	57	42	42	35
GA	4	-2	-2	-2	-2	-2	-2	-2
RB	-1	-1	-1	-1	-1	-1	-1	1
SR	14	10	10	15	23	12	11	59
V	-2	-2	-2	-2	-2	-2	-2	-2
ZR	1	1	3	3	4	4	5	8
NB	-1	-1	1	2	1	-1	2	-1
BA	11	-4	7	4	8	14	1	10
LA	-2	-2	1	1	2	2	3	2
CE	-3	3	7	3	5	8	7	6
PB	-3	-3	-3	1	1	2	2	3
TH	-3	-3	-3	-3	-3	-3	1	-3

ELEMENT RATIOS

ZR/NB	-1.	-1.	3.	1.	4.	-4.	2.	-8.
BA/SR	0.79	-0.40	0.70	0.27	0.35	1.17	0.09	0.17
CE/YN	3.7	-3.7	-8.6	-3.7	-6.1	-9.8	-8.6	-7.3
FE*/MG	0.32	0.35	0.32	0.34	0.31	0.36	0.33	0.29

CIPW NORMS

Q	0.0	0.0	0.0	0.0	0.0	0.0	0.0	0.0
NE	0.0	0.0	0.0	0.0	0.0	0.0	0.0	0.0
OR	0.1	0.1	0.1	0.1	0.1	0.1	0.1	0.1
AB	0.5	0.5	0.7	2.1	0.6	0.5	0.4	0.5
AN	2.8	3.3	1.0	0.0	1.3	1.2	0.9	0.8
DI	0.0	0.0	0.0	3.4	0.0	0.1	1.7	0.0
HY	46.0	51.7	39.7	39.1	41.0	48.9	43.6	39.5
OL	48.1	42.2	56.4	53.4	55.1	47.2	51.4	57.2
MT	1.9	2.0	2.0	2.0	2.0	2.1	2.0	1.9
ILM	0.0	0.0	0.0	0.0	0.0	0.0	0.0	0.0
AP	0.0	0.0	0.0	0.0	0.0	0.0	0.0	0.0

SERPENTINISED HARZBURGITES

ROCK NO   MA136

SIO2	41.95
TIO2	0.02
AL2O3	0.72
FE2O3	1.14
FEO	7.50
MNO	0.12
MGO	37.62
CAO	0.18
NA2O	0.08
K2O	0.01
P2O5	0.01
H_2O*	10.12
TOTAL	99.47

TRACE ELEMENTS IN PPM

NI	2601
CR	3359
ZN	52
GA	-2
RB	-1
SR	8
Y	1
ZR	20
NB	-1
BA	12
LA	3
CE	5
PB	2
TH	3

ELEMENT RATIOS

ZR/NB	-20.
BA/SR	1.50
CE/YN	12.2
FE*/MG	0.29

CIPW NORMS

Q	0.0
NE	0.0
OR	0.1
AB	0.8
AN	0.9
DI	0.0
HY	38.8
OL	57.4
MT	1.8
IL*	0.0
AP	0.0

PLUTONICS - PICRITES+TROCTOLITES

ROCK NO	X355	X69	MA2	X129	MA76A	X233	X280	X130
SIO2	44.08	41.37	39.23	42.29	42.23	39.99	40.89	41.03
TIO2	0.08	0.04	0.07	0.07	0.10	0.10	0.05	0.06
AL2O3	12.90	9.27	3.77	13.73	6.89	4.02	9.00	4.64
FE2O3	0.62	1.01	1.47	0.73	0.92	1.43	0.74	1.22
FEO	4.09	6.68	9.69	4.81	6.09	9.46	4.86	8.04
MNO	0.00	0.00	0.17	0.00	0.00	0.20	0.13	0.17
MGO	21.72	28.84	33.27	23.36	30.83	28.35	22.37	27.99
CAO	12.43	8.14	1.06	9.88	8.52	3.99	7.83	4.59
NA2O	1.04	0.76	0.04	1.19	0.58	0.23	0.44	0.29
K2O	0.02	0.02	0.01	0.04	0.02	0.01	0.33	0.01
P2O5	0.00	0.01	0.00	0.01	0.01	0.01	0.00	0.01
H_2O*	nd	nd	10.98	nd	nd	10.43	11.43	10.00
TOTAL	96.98	96.14	99.76	96.11	96.19	98.22	98.07	98.05

TRACE ELEMENTS IN PPM								
NI	546	808	1429	644	914	1496	890	1174
CR	1729	1145	3041	547	2644	2493	1288	1592
ZN	21	30	59	25	27	51	31	40
GA	8	9	5	9	7	6	7	6
RB	1	-1	-1	-1	-1	1	-1	-1
SR	65	138	4	168	186	68	134	64
Y	-2	-2	-2	-2	-2	-2	-2	-2
ZR	2	4	5	5	6	7	9	10
NB	1	-1	1	-1	-1	1	-1	1
BA	4	-4	5	15	4	10	9	4
LA	-2	2	-2	-2	-2	3	2	-2
CE	-3	4	-3	-3	3	8	5	-3
PB	-2	-3	4	-3	14	-3	-3	-3
TH	-3	-3	-3	-3	-3	-3	-3	-3

ELEMENT RATIOS								
ZR/NB	2.	-4.	5.	-5.	-6.	7.	-9.	10.
BA/SR	0.06	-0.03	1.25	0.09	0.02	0.15	0.07	0.06
CE/YN	3.7	-4.9	3.7	3.7	-3.7	-9.8	-6.1	3.7
FE*/MG	0.28	0.34	0.43	0.30	0.29	0.49	0.32	0.42

CIPW NORMS								
Q	0.0	0.0	0.0	0.0	0.0	0.0	0.0	0.0
NE	3.7	3.2	0.0	4.2	2.4	0.0	0.0	0.0
OR	0.1	0.1	0.1	0.2	0.1	0.1	2.3	0.1
AB	2.2	0.7	0.4	2.8	0.7	2.2	4.3	2.8
AN	31.4	22.7	5.9	33.3	16.9	11.3	24.9	12.9
DI	25.4	15.2	0.0	14.0	21.4	8.9	15.8	10.3
HY	0.0	0.0	31.7	0.0	0.0	25.1	14.1	26.4
OL	36.0	56.4	57.3	44.3	56.9	49.9	37.4	45.5
MT	0.9	1.5	2.4	1.1	1.4	2.4	1.2	2.0
ILM	0.2	0.1	0.1	0.1	0.2	0.2	0.1	0.1
AP	0.0	0.0	0.0	0.0	0.0	0.0	0.0	0.0

PLUTONICS - PICRITES+TROCTOLITES

ROCK NO	Y78	MA251
SIO2	43.41	42.01
TIO2	0.11	0.47
AL2O3	6.08	5.59
FE2O3	1.10	1.34
FEO	7.25	8.83
MNO	0.16	0.20
MGO	21.85	26.19
CAO	8.54	5.14
NA2O	0.73	0.37
K2O	0.02	0.18
P2O5	0.01	0.05
H$_2$O*	7.86	6.56
TOTAL	97.12	96.93

TRACE ELEMENTS IN PPM
NI	795	1202
CR	1840	2764
ZN	38	49
GA	7	6
RB	-1	2
SR	57	35
Y	2	8
ZR	10	40
NB	2	7
BA	2	49
LA	2	4
CE	5	10
PB	-3	-3
TH	-3	-3

ELEMENT RATIOS
ZR/NB	5.	6.
BA/SR	0.04	1.40
CE/YN	6.1	3.1
FE*/MG	0.49	0.49

CIPW NORMS
Q	0.0	0.0
NE	0.0	0.0
OR	0.1	1.2
AB	6.9	3.5
AN	14.8	14.5
DI	25.9	10.7
HY	19.0	26.2
OL	31.2	40.8
MT	1.8	2.1
ILM	0.2	1.0
AP	0.0	0.1

PLUTONICS - OLIVINE GABBROS

ROCK NO	MA122	MA76	X131	X272
SIO2	46.03	46.40	47.23	44.71
TIO2	0.11	0.11	0.14	0.14
AL2O3	14.79	18.92	16.73	16.86
FE2O3	0.58	0.37	0.40	0.85
FEO	3.82	2.47	2.62	5.61
MNO	0.00	0.06	0.07	0.11
MGO	17.81	13.62	15.00	16.44
CAO	13.80	15.23	15.84	11.37
NA2O	1.04	1.30	1.20	1.36
K2O	0.02	0.05	0.04	0.04
P2O5	0.00	0.00	0.00	0.00
TOTAL	98.00	98.53	99.27	97.49

TRACE ELEMENTS IN PPM

NI	394	307	309	416
CR	1452	1820	209	462
ZN	18	11	11	29
GA	9	11	12	12
RB	-1	-1	-1	-1
SR	88	158	124	139
Y	-2	2	2	2
ZR	6	11	11	12
NB	-1	3	-2	2
BA	5	9	9	10
LA	2	3	-2	-2
CE	3	4	-3	5
PR	-3	-3	-3	-3
TH	-3	-3	-3	-3

ELEMENT RATIOS

ZR/NB	-6.	4.	-5.	6.
BA/SR	0.06	0.06	0.07	0.07
CE/YN	-3.7	4.9	-3.7	6.1
FE*/MG	0.31	0.27	0.26	0.50

CIPW NORMS

Q	0.0	0.0	0.0	0.0
NE	1.0	2.2	2.2	0.4
OR	0.1	0.3	0.2	0.2
AB	7.1	7.1	6.1	11.0
AN	36.4	46.3	40.4	40.8
DI	26.5	24.0	30.5	13.6
HY	0.0	0.0	0.0	0.0
OL	27.8	19.3	19.6	32.4
MT	0.9	0.5	0.6	1.3
ILM	0.2	0.2	0.3	0.3
AP	0.0	0.0	0.0	0.0

PLUTONICS - GABBRO ANORTHOSITES(AL2O3>21%)

ROCK NO	X288	MA376	MA276[+]	MA433	X287	MA99	MA59	MA427
SIO2	42.90	46.27	44.96	45.32	44.43	46.93	47.27	48.22
TIO2	0.07	0.11	0.10	0.06	0.08	0.08	0.10	0.19
AL2O3	24.65	24.30	27.03	24.84	21.13	22.08	23.31	23.55
FE2O3	0.13	0.45	0.45	0.30	0.45	0.20	0.27	0.34
FEO	0.86	2.98	1.58	2.01	2.98	1.35	1.75	2.23
MNO	0.02	0.00	0.00	0.00	0.06	0.00	0.04	0.00
MGO	6.85	7.86	6.16	9.26	14.60	9.48	9.79	6.32
CAO	22.22	14.64	15.17	12.96	13.25	15.18	16.42	16.34
NA2O	0.49	2.13	2.32	2.34	1.31	2.39	1.40	2.12
K2O	0.03	0.22	0.13	0.29	0.03	0.15	0.03	0.28
P2O5	0.00	0.00	0.01	0.02	0.00	0.00	0.00	0.01
TOTAL	98.22	98.96	97.91	97.40	98.32	97.84	100.38	99.60

TRACE ELEMENTS IN PPM

NI	91	109	86	134	339	129	123	77
CR	265	445	256	34	385	965	568	616
ZN	15	13	10	10	13	8	16	14
GA	8	16	14	17	13	12	14	17
RB	-1	1	1	3	-1	-1	-1	1
SR	116	209	199	255	125	329	157	229
Y	-2	-2	-1	-2	-2	-2	-2	4
ZR	8	8	9	10	10	10	10	10
NB	-1	-1	1	3	-1	-1	2	2
BA	7	15	18	37	10	71	10	33
LA	2	-2	2	2	3	-2	-2	-2
CE	3	-3	3	3	5	3	-3	3
PR	-3	3	-3	-3	3	-3	3	-3
TH	-3	-3	-3	-3	-3	-3	-3	-3

ELEMENT RATIOS

ZR/NB	-8.	-8.	9.	3.	-10.	-10.	5.	5.
BA/SR	0.06	0.07	0.09	0.15	0.08	0.22	0.06	0.14
CE/YN	-3.7	3.7	-7.3	-3.7	-6.1	-3.7	3.7	1.8
FE*/MG	0.18	0.56	0.42	0.32	0.30	0.21	0.26	0.52

CIPW NORMS

Q	0.0	0.0	0.0	0.0	0.0	0.0	0.0	0.0
NE	2.3	4.2	6.4	4.8	2.7	5.8	1.8	3.3
OR	0.0	1.3	0.8	1.8	0.2	0.9	0.2	1.7
AB	0.0	10.4	8.2	11.4	6.3	9.9	8.5	12.0
AN	66.1	56.7	64.3	57.9	52.6	50.2	57.0	54.1
DI	13.0	13.4	9.9	6.3	11.3	21.1	19.1	21.7
HY	0.0	0.0	0.0	0.0	0.0	0.0	0.0	0.0
OL	9.0	13.1	9.5	17.1	26.1	11.6	12.9	6.4
MT	0.2	0.7	0.7	0.4	0.7	0.3	0.4	0.5
ILM	0.1	0.2	0.2	0.1	0.2	0.2	0.2	0.4
AP	0.0	0.0	0.0	0.0	0.0	0.0	0.0	0.0

PLUTONICS - GABBRO ANORTHOSITES(AL2O3>21%)

ROCK NO	MA61	X71	MA14	MA173	MA132	MA98	X120	X247
SIO2	47.01	44.95	45.40	45.47	47.03	45.41	44.67	47.36
TIO2	0.09	0.05	0.07	0.07	0.10	0.10	0.14	0.24
AL2O3	23.53	22.18	26.93	25.46	26.92	21.79	21.69	21.59
FE2O3	0.22	0.38	0.19	0.21	0.22	0.34	0.46	0.45
FEO	1.47	2.49	1.28	1.39	1.47	2.27	3.02	2.94
MNO	0.04	0.05	0.04	0.04	0.04	0.06	0.07	0.08
MGO	10.07	12.22	8.24	9.19	5.90	12.50	12.60	8.63
CAO	16.23	13.63	15.87	17.92	14.25	14.95	13.60	14.72
NA2O	1.23	1.50	1.86	0.81	2.82	1.35	1.43	2.31
K2O	0.06	0.04	0.03	0.01	0.06	0.04	0.04	0.06
P2O5	0.00	0.00	0.00	0.00	0.00	0.01	0.01	0.01
TOTAL	99.75	97.49	99.91	100.57	98.81	98.82	97.73	98.39

TRACE ELEMENTS IN PPM

NI	188	247	192	196	57	238	218	97
CR	901	384	861	1324	162	820	404	371
ZN	16	10	16	4	17	10	16	20
GA	14	12	14	13	18	11	15	19
RB	-1	-1	-1	-1	-1	-1	-1	-1
SR	54	220	222	299	261	200	205	255
Y	-2	-2	-2	-2	-2	-2	2	4
ZR	11	13	13	15	15	19	19	21
NB	2	-1	-1	1	1	3	2	-1
BA	7	7	13	2	19	11	15	25
LA	2	2	2	3	-2	-2	2	3
CE	4	3	3	5	-3	-3	3	5
PB	3	-3	-3	3	-3	5	-3	-3
TH	-3	-3	-3	-3	-3	-3	-3	-3

ELEMENT RATIOS

ZR/NB	5.	-13.	-13.	15.	15.	6.	9.	-21.
BA/SR	0.13	0.03	0.06	0.01	0.07	0.05	0.07	0.10
CE/YN	-4.9	-3.7	-3.7	-6.1	3.7	3.7	3.7	3.1
FE*/MG	0.21	0.30	0.23	0.22	0.36	0.27	0.35	0.50

CIPW NORMS

Q	0.0	0.0	0.0	0.0	0.0	0.0	0.0	0.0
NE	0.9	2.1	5.6	3.0	4.8	3.0	2.3	3.2
OR	0.4	0.2	0.2	0.1	0.4	0.2	0.2	0.4
AB	8.8	9.2	5.5	1.3	15.3	5.9	8.2	13.9
AN	58.1	55.0	65.1	65.4	61.3	53.9	53.9	49.2
DI	17.8	11.3	10.8	18.1	8.1	16.7	12.0	19.9
HY	0.0	0.0	0.0	0.0	0.0	0.0	0.0	0.0
OL	13.6	21.5	12.4	11.6	9.6	19.5	22.5	12.3
MT	0.3	0.6	0.3	0.3	0.3	0.5	0.7	0.7
ILM	0.2	0.1	0.1	0.1	0.2	0.2	0.3	0.5
AP	0.0	0.0	0.0	0.0	0.0	0.0	0.0	0.0

PLUTONICS - GABBRO ANORTHOSITES(AL2O3>21%)

ROCK NO	X268	MA126	X10	X338
SIO2	50.07	49.30	50.48	46.61
TIO2	0.16	0.17	0.17	0.29
AL2O3	28.22	23.71	25.04	21.48
FE2O3	0.20	0.35	0.20	0.48
FEO	1.34	2.30	1.33	3.16
MNO	0.03	0.05	0.00	0.00
MGO	3.02	6.32	3.42	8.39
CAO	12.79	13.15	12.68	11.84
NA2O	4.08	3.23	4.19	3.02
K2O	0.22	0.09	0.17	0.88
P2O5	0.01	0.01	0.02	0.02
TOTAL	100.14	98.68	97.70	96.17

TRACE ELEMENTS IN PPM

NI	41	83	19	75
CR	42	141	34	225
ZN	7	14	13	18
GA	23	18	21	19
RB	1	-1	-1	10
SR	360	297	563	361
Y	2	4	4	6
ZR	25	27	27	33
NB	-1	1	1	4
BA	42	43	106	119
LA	3	3	5	3
CE	3	3	16	6
PB	-3	-3	6	-3
TH	-3	-3	-3	-3

ELEMENT RATIOS

ZR/NB	-25.	27.	27.	8.
BA/SR	0.12	0.14	0.19	0.33
CE/YN	3.7	1.8	9.8	2.4
FE*/MG	0.65	0.53	0.57	0.55

CIPW NORMS

Q	0.0	0.0	0.0	0.0
NE	4.8	2.3	3.9	6.5
OR	1.3	0.5	1.0	5.4
AB	25.6	23.4	29.1	14.5
AN	58.0	50.6	50.2	44.1
DI	4.4	12.4	11.4	13.5
HY	0.0	0.0	0.0	0.0
OL	5.4	9.9	3.8	14.6
MT	0.3	0.5	0.3	0.7
ILM	0.3	0.3	0.3	0.6
AP	0.0	0.0	0.0	0.0

PLUTONICS - GABBROS

ROCK NO	X297	MA65	MA9	X286	MA175	X189	MA71	X186
SIO2	46.04	46.37	47.39	42.61	46.17	49.68	45.30	48.63
TIO2	0.12	0.18	0.18	0.05	0.09	0.34	0.10	0.24
AL2O3	19.49	17.18	18.53	20.59	18.69	13.89	20.68	18.13
FE2O3	0.45	0.59	0.39	0.29	0.33	0.60	0.34	0.63
FEO	3.30	3.89	2.61	1.92	2.15	4.39	2.23	4.17
MNO	0.00	0.00	0.00	0.03	0.05	0.00	0.05	0.00
MGO	12.24	13.89	11.52	13.16	13.98	12.14	13.19	9.04
CAO	14.53	13.62	16.02	17.34	15.57	13.75	14.70	12.85
NA2O	1.65	1.61	1.79	0.75	1.49	2.45	1.47	2.79
K2O	0.12	0.09	0.05	0.03	0.10	0.09	0.10	0.12
P2O5	0.00	0.01	0.01	0.00	0.00	0.00	0.00	0.01
TOTAL	97.94	97.43	98.49	96.77	98.62	97.33	98.16	96.66

TRACE ELEMENTS IN PPM

NI	195	237	176	253	271	109	286	143
CR	736	705	1130	85	1931	324	1084	363
ZN	20	24	15	10	7	19	19	14
GA	15	14	12	15	10	11	14	17
RB	1	-1	-1	-1	-1	-1	1	2
SR	215	175	142	192	138	167	175	196
Y	-2	3	4	5	-2	7	-2	7
ZR	8	8	8	10	10	10	11	11
NB	1	-1	2	2	-1	1	1	-2
BA	41	16	16	13	22	21	21	24
LA	-2	-2	2	3	3	-2	3	-2
CE	-3	-3	4	3	4	-3	3	-3
PB	-3	-3	-3	-3	-3	-3	-3	-3
TH	-3	-3	-3	-3	-3	-3	-3	-3

ELEMENT RATIOS

ZR/NB	8.	-8.	4.	5.	-10.	10.	11.	-5.
BA/SR	0.19	0.09	0.11	0.07	0.16	0.13	0.12	0.12
CE/YN	3.7	-2.4	2.4	1.5	-4.9	-1.0	-3.7	-1.5
FE*/MG	0.39	0.41	0.33	0.21	0.23	0.52	0.25	0.68

CIPW NORMS

Q	0.0	0.0	0.0	0.0	0.0	0.0	0.0	0.0
NE	3.2	1.5	3.6	3.6	4.6	0.7	4.0	1.1
OR	0.7	0.5	0.3	0.0	0.6	0.5	0.6	0.7
AB	8.4	11.2	8.7	0.0	4.2	20.1	5.4	22.5
AN	46.4	40.4	43.0	54.5	44.6	27.4	50.5	37.9
DI	21.6	22.9	29.7	15.6	26.5	34.0	18.8	22.5
HY	0.0	0.0	0.0	0.0	0.0	0.0	0.0	0.0
OL	18.8	22.2	13.7	21.2	18.6	15.8	20.1	14.0
MT	0.7	0.9	0.6	0.4	0.5	0.9	0.5	0.9
ILM	0.2	0.4	0.3	0.1	0.2	0.7	0.2	0.5
AP	0.0	0.0	0.0	0.0	0.0	0.0	0.0	0.0

PLUTONICS - GABBROS

ROCK NO	MA57	MA154.1	X266	X265	MA168	MA25	MA238	MA154.3
SIO2	46.21	48.63	47.27	49.33	48.41	47.11	48.53	48.65
TIO2	0.12	0.26	0.26	0.30	0.20	0.17	0.22	0.26
AL2O3	21.01	15.32	18.75	18.15	14.41	16.17	16.82	15.31
FE2O3	0.33	0.65	0.72	0.48	0.48	0.51	0.45	0.65
FEO	2.18	4.28	4.76	3.15	3.18	3.37	2.94	4.29
MNO	0.05	0.00	0.00	0.00	0.00	0.08	0.07	0.00
MGO	12.25	12.70	10.12	9.17	13.91	14.17	12.10	12.70
CAO	15.40	13.52	13.90	14.93	16.24	15.06	15.56	13.41
NA2O	1.29	2.11	2.19	2.72	1.61	1.38	1.89	2.07
K2O	0.05	0.19	0.16	0.18	0.03	0.05	0.08	0.19
P2O5	0.01	0.01	0.01	0.01	0.01	0.00	0.01	0.01
TOTAL	98.90	97.67	98.14	98.42	98.48	98.07	98.76	97.54

TRACE ELEMENTS IN PPM

NI	217	193	116	102	191	211	180	191
CR	969	351	421	691	692	820	909	354
ZN	19	18	25	19	18	16	21	19
GA	13	13	16	16	13	14	15	15
RB	-1	1	1	1	-1	-1	1	1
SR	139	245	268	356	333	185	169	244
Y	-2	6	5	5	5	3	5	5
ZR	12	12	12	12	12	14	14	14
NB	-1	-1	-1	-1	-1	2	-1	-1
BA	16	30	36	33	17	16	24	22
LA	-2	2	-2	-2	-2	3	2	-2
CE	3	6	3	3	-3	3	3	-3
PB	-3	-3	-3	3	3	3	-3	-3
TH	-3	-3	-3	-3	-3	-3	-3	-3

ELEMENT RATIOS

ZR/NB	-12.	-12.	-12.	-12.	-12.	7.	-14.	-14.
BA/SR	0.12	0.12	0.13	0.09	0.05	0.09	0.14	0.09
CE/YN	-3.7	2.4	1.5	1.5	-1.5	2.4	1.5	-1.5
FE*/MG	0.26	0.49	0.69	0.50	0.33	0.35	0.35	0.49

CIPW NORMS

Q	0.0	0.0	0.0	0.0	0.0	0.0	0.0	0.0
NE	2.0	0.7	2.6	3.7	2.6	1.5	2.3	0.2
OR	0.3	1.1	1.0	1.1	0.2	0.3	0.5	1.2
AB	7.3	17.0	14.2	16.5	9.1	9.2	11.9	17.6
AN	52.0	32.5	41.6	37.4	32.5	38.5	37.6	32.7
DI	19.9	28.7	22.9	30.1	39.0	29.8	32.0	28.2
HY	0.0	0.0	0.0	0.0	0.0	0.0	0.0	0.0
OL	17.8	18.4	16.2	9.9	15.6	19.6	14.5	18.6
MT	0.5	1.0	1.1	0.7	0.7	0.8	0.7	1.0
ILM	0.2	0.5	0.5	0.6	0.4	0.3	0.4	0.5
AP	0.0	0.0	0.0	0.0	0.0	0.0	0.0	0.0

PLUTONICS - GABBROS

ROCK NO	MA7M	MA154.2	MA254+	MA47	MA272+	MA152	MA205+	X264
SIO2	46.27	47.21	47.54	47.05	49.42	48.90	49.05	45.05
TIO2	0.19	0.25	0.18	0.21	0.28	0.25	0.25	0.20
AL2O3	18.58	18.09	19.55	16.51	15.98	18.45	20.90	16.78
FE2O3	0.57	0.57	0.49	0.52	0.68	0.42	0.52	0.74
FEO	3.42	3.73	3.22	3.44	4.48	2.75	3.43	4.86
MNO	0.08	0.09	0.09	0.09	0.09	0.07	0.00	0.10
MGO	13.32	11.41	11.08	15.08	10.47	10.31	7.24	14.66
CAO	14.57	13.32	14.41	15.09	13.19	16.61	11.14	12.61
NA2O	1.40	2.22	1.72	1.16	2.36	1.86	3.89	1.39
K2O	0.06	0.19	0.73	0.06	0.13	0.05	0.28	0.13
P2O5	0.01	0.02	0.01	0.01	0.01	0.00	0.02	0.01
TOTAL	98.42	97.01	98.62	99.22	97.09	99.67	96.76	96.64

TRACE ELEMENTS IN PPM

NI	255	162	128	283	90	136	70	209
CR	1394	463	588	1063	345	1005	355	672
ZN	28	24	13	13	13	19	9	20
GA	14	14	14	12	17	9	15	15
RB	-1	1	2	-1	-1	-1	2	1
SR	163	211	210	124	187	175	213	209
Y	4	4	4	4	7	-2	3	5
ZR	16	17	18	18	18	19	10	10
NB	1	1	2	3	1	1	4	2
BA	18	17	34	12	28	12	41	35
LA	3	2	2	2	3	2	-2	3
CE	5	4	3	4	4	4	-3	4
PB	3	-3	3	-3	-3	5	-3	3
TH	-3	-3	3	-3	-3	3	-3	-3

ELEMENT RATIOS

ZR/NB	16.	17.	9.	6.	18.	19.	5.	9.
BA/SR	0.11	0.08	0.16	0.10	0.15	0.07	0.19	0.17
CE/YN	3.1	2.4	1.8	2.4	1.4	-4.9	-2.4	2.0
FE*/MG	0.38	0.48	0.43	0.33	0.63	0.39	0.69	0.49

CIPW NORMS

Q	0.0	0.0	0.0	0.0	0.0	0.0	0.0	0.0
NE	1.8	2.3	1.4	1.2	0.0	2.4	4.0	0.9
OR	0.4	1.2	2.0	0.4	0.8	0.3	1.7	0.8
AB	8.8	15.2	12.2	7.8	20.6	11.4	26.6	10.5
AN	44.9	40.0	45.3	40.0	33.6	42.0	40.0	40.5
DI	22.5	22.2	21.6	28.0	27.0	32.2	13.6	19.2
HY	0.0	0.0	0.0	0.0	3.7	0.0	0.0	0.0
OL	20.4	17.7	16.5	21.5	12.8	10.6	12.7	26.3
MT	0.8	0.9	0.7	0.8	1.0	0.6	0.8	1.1
ILM	0.4	0.5	0.3	0.4	0.5	0.5	0.5	0.6
AP	0.0	0.0	0.0	0.0	0.0	0.0	0.0	0.0

FLUTONICS - GARBROS

ROCK NO	X40	MA250	X340	X186[+]	MA11	MA73	MA124	MA151
SIO2	45.48	45.10	50.21	47.39	49.63	50.84	45.83	47.35
TIO2	0.22	0.18	0.41	0.41	0.58	0.80	5.68	0.50
AL2O3	17.84	18.21	14.47	16.99	13.41	16.25	11.41	15.78
FE2O3	0.68	0.69	0.76	0.65	0.73	0.73	1.25	0.66
FEO	4.46	4.56	5.02	4.31	4.83	4.82	8.23	4.34
MNO	0.00	0.09	0.00	0.10	0.14	0.00	0.00	0.12
MGO	13.08	14.05	11.90	11.31	11.33	8.31	8.11	0.91
CAO	13.55	11.97	11.52	14.69	12.88	12.22	16.61	16.01
NA2O	1.44	1.52	2.67	1.65	1.87	3.55	0.99	1.47
K2O	0.06	0.09	0.34	0.11	0.13	0.28	0.05	0.51
P2O5	0.01	0.01	0.03	0.01	0.03	0.05	0.02	0.07
TOTAL	96.82	96.47	97.33	97.62	95.56	97.85	98.18	96.72

TRACE ELEMENTS IN PPM

NI	187	246	266	123	71	69	36	134
CR	461	224	172	242	87	234	18	346
ZN	34	21	13	27	31	20	29	19
GA	16	13	18	14	15	18	18	17
RB	-1	-1	2	1	1	2	-1	3
SR	210	256	201	275	302	186	243	273
Y	5	2	17	7	12	22	28	23
ZR	20	23	30	32	43	54	56	66
NB	2	2	2	6	6	11	18	3
BA	25	52	57	65	77	68	93	144
LA	2	-2	4	2	3	5	5	-2
CE	3	-3	11	4	9	13	6	-3
PB	-3	4	-3	3	3	-3	6	4
TH	-3	-3	-3	-3	-3	-3	-3	-3

ELEMENT RATIOS

ZR/NB	10.	12.	15.	5.	7.	5.	3.	22.
BA/SR	0.12	0.20	0.28	0.24	0.25	0.37	0.38	0.53
CE/YN	1.5	-3.7	1.6	1.4	1.8	1.4	0.5	-0.3
FE*/MG	0.50	0.48	0.62	0.56	0.62	0.85	1.49	0.64

CIPW NORMS

Q	0.0	0.0	0.0	0.0	0.0	0.0	2.2	0.0
NE	1.0	0.2	0.0	0.5	0.0	1.4	0.0	1.8
OR	0.4	0.6	2.1	0.7	0.8	1.7	0.3	3.1
AB	10.7	13.0	23.2	13.4	16.6	28.1	8.5	9.5
AN	43.4	44.2	27.2	39.6	29.1	28.2	27.0	36.1
DI	20.7	13.8	25.0	28.0	30.0	26.8	45.2	36.4
HY	0.0	0.0	5.0	0.0	16.3	0.0	3.9	0.0
OL	22.4	26.9	15.6	16.2	4.9	11.0	0.0	10.9
MT	1.0	1.0	1.1	1.0	1.1	1.1	1.8	1.0
ILM	0.4	0.4	0.8	0.8	1.2	1.6	11.0	1.0
AP	0.0	0.0	0.1	0.0	0.1	0.1	0.0	0.2

PLUTONICS - GABBROS

ROCK NO	X109	X110	NA78
SIO2	48.99	48.97	46.11
TIO2	1.20	1.51	1.11
AL2O3	14.32	14.48	14.89
FE2O3	0.88	1.05	0.99
FEO	5.81	6.92	6.53
MNO	0.00	0.00	0.00
MGO	10.37	7.69	11.56
CAO	12.22	11.68	11.76
NA2O	2.58	3.32	2.16
K2O	0.21	0.34	0.36
P2O5	0.26	0.68	0.19
TOTAL	96.84	96.64	95.66

TRACE ELEMENTS IN PPM

NI	116	51	194
CR	172	22	487
ZN	50	58	57
GA	18	27	14
RB	2	-1	-1
SR	384	341	307
Y	20	68	20
ZR	94	94	106
NB	20	70	17
BA	123	185	142
LA	11	30	9
CE	25	73	28
PB	-3	3	-3
TH	3	-3	-3

ELEMENT RATIOS

ZR/NB	5.	1.	6.
BA/SR	0.32	0.54	0.46
CE/YN	3.1	2.6	3.4
FE*/MG	0.82	1.32	0.83

CIPW NORMS

Q	0.0	0.0	0.0
NE	0.0	0.0	0.4
OR	1.3	2.1	2.2
AB	22.5	29.1	18.3
AN	27.7	24.4	31.2
DI	26.6	25.2	22.9
HY	5.8	2.1	0.0
OL	11.7	11.0	20.7
MT	1.3	1.6	1.5
ILM	2.4	3.0	2.2
AP	0.6	1.7	0.5

PLUTONICS - GABBRO PEGMATITES

ROCK NO	MA127	MA164	X4	MA150	MA323	X114	X11	X217
SIO2	49.09	50.39	49.71	51.01	48.86	50.01	50.26	46.91
TIO2	0.41	0.45	1.03	0.51	0.66	0.52	0.83	1.83
AL2O3	13.27	20.16	14.11	13.45	18.80	16.33	15.04	15.52
FE2O3	0.72	0.53	1.92	0.81	0.81	0.74	0.82	0.71
FEO	4.78	3.52	6.09	5.35	5.31	4.91	5.42	4.69
MNO	0.12	0.07	0.00	0.13	0.12	0.08	0.14	0.00
MGO	12.57	5.68	10.50	11.23	8.46	10.00	10.32	11.26
CAO	13.62	12.45	12.62	11.41	13.34	11.90	12.15	11.30
NA2O	2.24	3.80	2.15	3.22	2.07	2.93	2.41	3.80
K2O	0.09	0.08	0.15	0.12	0.13	0.14	0.21	0.16
P2O5	0.01	0.02	0.29	0.03	0.05	0.03	0.09	0.54
TOTAL	96.92	97.15	98.57	97.27	98.61	97.59	97.69	96.72

TRACE ELEMENTS IN PPM

NI	152	40	76	183	80	131	75	166
CR	728	51	42	240	268	107	93	70
ZN	17	20	63	24	20	11	39	31
GA	14	20	17	18	17	17	16	27
RB	-1	-1	-1	-1	-1	2	1	-1
SR	213	294	341	305	119	362	300	328
Y	10	4	17	19	16	11	18	100
ZR	27	28	34	42	42	49	53	100
NB	2	5	13	3	3	5	17	25
BA	32	33	84	173	21	67	123	100
LA	2	2	5	4	3	3	7	11
CE	3	4	19	11	6	7	17	40
PB	-3	-3	-3	-3	4	-3	-3	3
TH	-3	-3	-3	-3	-3	4	-3	-3

ELEMENT RATIOS

ZR/NB	13.	6.	3.	14.	14.	10.	3.	4.
BA/SR	0.15	0.11	0.25	0.57	0.18	0.19	0.41	0.30
CE/YN	0.7	2.4	2.7	1.4	0.9	1.6	2.3	1.0
FE*/MG	0.56	0.91	0.96	0.70	0.92	0.72	0.77	0.61

CIPW NORMS

Q	0.0	0.0	0.0	0.0	0.0	0.0	0.0	0.0
NE	0.1	1.9	0.0	0.0	0.0	0.0	0.0	6.2
OR	0.5	0.5	0.9	0.7	0.8	0.8	1.3	1.0
AB	19.4	29.6	18.5	28.0	17.8	25.4	20.9	21.8
AN	26.7	38.8	28.8	22.5	42.2	31.8	30.3	25.7
DI	34.2	19.9	26.3	28.5	19.8	22.9	24.8	22.8
HY	0.0	0.0	15.2	3.0	8.4	2.8	12.1	0.0
OL	17.1	7.6	4.8	15.0	8.5	14.1	7.7	16.7
MT	1.1	0.8	2.8	1.2	1.2	1.1	1.2	1.1
ILM	0.8	0.9	2.0	1.0	1.3	1.0	1.6	3.6
AP	0.0	0.0	0.7	0.1	0.1	0.1	0.2	1.3

PLUTONICS - GABBRO PEGMATITES

ROCK NO	X27	X205
SIO2	51.02	44.50
TIO2	0.91	2.83
AL2O3	16.53	13.03
FE2O3	0.79	1.47
FEO	5.20	9.68
MNO	0.00	0.00
MGO	7.15	8.15
CAO	9.07	9.92
NA2O	4.15	4.28
K2O	1.13	0.39
P2O5	0.36	1.44
TOTAL	96.31	95.69

TRACE ELEMENTS IN PPM

	X27	X205
NI	35	77
CR	39	8
ZN	68	82
GA	20	25
RB	20	4
SR	392	244
Y	32	117
ZR	110	172
NB	36	68
BA	285	244
LA	22	50
CE	53	117
PB	-3	6
TH	4	-3

ELEMENT RATIOS

	X27	X205
ZR/NB	3.	3.
BA/SR	0.73	1.00
CE/YN	4.0	2.4
FE*/MG	1.07	1.74

CIPW NORMS

	X27	X205
Q	0.0	0.0
NE	1.0	6.5
OR	6.9	2.4
AB	34.6	25.9
AN	24.0	15.9
DI	16.5	21.0
HY	0.0	0.0
OL	13.2	17.0
MT	1.2	2.2
ILM	1.8	5.6
AP	0.9	3.6

PLUTONIC DIFFERENTIATES

ROCK NO	MA321	X308	MA120	MA417	X219A1	X106A	X219
SIO2	57.13	72.12	50.56	59.01	60.77	51.49	67.80
TIO2	0.16	0.20	1.45	0.55	0.58	1.96	0.42
AL2O3	22.91	14.82	18.32	18.77	15.05	18.41	13.42
FE2O3	0.99	0.91	7.94	2.87	6.72	7.71	5.33
FEO	0.00	0.00	0.00	0.00	0.00	0.00	0.00
MNO	0.02	0.00	0.13	0.00	0.00	0.16	0.10
MGO	3.03	0.54	4.89	1.80	2.39	4.63	1.39
CAO	5.44	2.25	9.19	4.04	1.98	7.74	1.74
NA2O	7.44	7.10	4.76	9.97	8.22	5.02	7.38
K2O	1.11	0.80	0.43	0.05	0.07	0.31	0.06
P2O5	0.02	0.03	0.24	0.10	0.08	0.20	0.06
TOTAL	98.25	98.77	97.91	97.16	95.86	97.63	97.70

TRACE ELEMENTS IN PPM

NI	40	1	19	5	-1	14	-1
CR	11	2	8	-1	-1	8	-1
ZN	10	3	67	4	88	69	28
GA	27	14	25	24	32	26	32
RB	18	14	3	-1	1	1	-1
SR	613	139	448	183	98	408	71
Y	18	54	64	57	61	57	59
ZR	75	88	308	711	745	745	784
NB	8	34	64	52	98	118	96
BA	647	281	295	87	49	316	137
LA	11	53	11	44	62	29	36
CE	26	86	50	88	129	68	100
PP	4	-3	-3	-3	-3	-3	3
TH	4	27	-3	17	15	-3	13

ELEMENT RATIOS

ZR/NB	9.	3.	5.	14.	8.	6.	8.
BA/SR	1.06	2.02	0.66	0.48	0.50	0.77	1.93
CE/YN	3.5	3.9	1.9	3.8	5.2	2.9	4.1
FE*/MG	0.38	1.96	1.89	1.85	3.26	1.93	4.45

CIPW NORMS

Q	0.0	23.5	0.0	0.0	6.5	0.3	20.5
NE	4.9	0.0	0.0	8.4	0.0	0.0	0.0
OR	6.7	4.8	2.6	0.3	0.4	1.9	0.4
AB	55.0	60.8	41.1	71.3	72.6	43.5	63.9
AN	26.3	6.3	27.9	6.5	4.1	27.4	3.4
DI	0.7	2.9	9.8	9.0	2.7	3.4	3.1
HY	0.0	0.0	2.7	0.0	4.9	10.2	2.1
OL	5.2	0.0	3.7	0.3	0.0	0.0	0.0
MT	0.0	0.0	0.0	0.0	0.0	0.0	0.0
ILM	0.0	0.0	0.3	0.0	0.0	0.4	0.2
AP	0.0	0.1	0.6	0.2	0.2	0.5	0.1

THULITIC VEIN, PYROXENITE, AMPHIBOLITE

ROCK NO	X347	X16	X0
SIO2	54.65	54.98	47.46
TIO2	0.20	0.04	0.22
AL2O3	24.13	1.09	13.73
FE2O3	0.99	0.66	0.69
FEO	0.00	0.00	4.56
MNO	0.00	0.02	0.11
MGO	1.00	20.16	16.58
CAO	11.10	21.90	14.23
NA2O	7.33	0.06	1.31
K2O	0.29	0.00	0.08
P2O5	0.00	0.00	0.01
TOTAL	99.69	98.91	98.98

TRACE ELEMENTS IN PPM

NI	1	271	327
CR	36	105	1286
ZN	-1	5	37
GA	33	-2	11
RB	1	-1	-1
SR	590	4	85
Y	3	-2	6
ZR	16	5	12
NB	1	2	2
BA	34	-4	25
LA	11	3	6
CE	17	4	19
PB	4	-3	3
TH	-3	-3	3

ELEMENT RATIOS

ZR/NB	16.	2.	6.
BA/SR	0.06	-1.00	0.29
CE/YN	13.8	-4.9	7.7
FE*/MG	1.15	0.04	0.40

CIPW NORMS

Q	0.0	0.6	0.0
NE	11.0	0.0	0.9
OR	1.7	0.0	0.5
AB	41.9	0.5	9.5
AN	32.2	2.7	31.7
DI	5.4	83.4	31.4
HY	0.0	12.1	0.0
OL	0.0	0.0	24.6
MT	0.0	0.0	1.0
IL*	0.0	0.1	0.4
AP	0.0	0.0	0.0

METADOLERITE DYKES

ROCK NO	MA248	MA424	MA58	X178	MA50	MA366	MA75	MA320
SIO2	48.91	48.12	44.22	47.89	46.90	46.52	43.56	48.47
TIO2	0.46	0.50	0.76	0.54	0.69	0.69	0.89	0.71
AL2O3	13.58	19.92	13.70	19.05	18.50	18.45	11.32	15.22
FE2O3	1.05	0.63	1.51	0.65	0.89	0.82	1.44	0.90
FEO	6.93	4.18	9.98	4.30	5.89	5.44	9.47	5.92
MNO	0.12	0.00	0.00	0.00	0.13	0.00	0.00	0.12
MGO	9.98	7.62	11.83	8.51	9.86	8.68	13.42	10.43
CAO	13.42	14.51	10.40	14.07	12.58	13.25	13.74	12.10
NA2O	2.30	2.10	1.95	2.01	1.70	2.18	1.15	2.15
K2O	0.12	0.26	0.08	0.20	0.11	0.07	0.04	0.18
P2O5	0.09	0.05	0.03	0.05	0.07	0.08	0.05	0.06
TOTAL	97.05	97.89	94.55	97.27	97.32	96.18	95.08	96.27

TRACE ELEMENTS IN PPM

NI	83	67	282	61	128	119	365	127
CR	274	195	326	328	358	323	414	413
ZN	12	16	61	13	26	25	66	12
GA	17	16	18	14	15	14	10	14
RB	1	2	-1	1	1	-1	-1	1
SR	141	254	80	239	111	120	94	160
Y	19	11	26	12	17	18	23	17
ZR	34	45	45	47	49	51	51	51
NB	5	7	3	4	5	3	2	5
BA	29	37	28	30	54	29	25	43
LA	2	-2	2	3	3	2	2	3
CE	7	5	5	8	7	6	5	6
PB	-3	-3	-3	3	-3	-3	4	-3
TH	-3	-3	-3	-3	-3	-3	-3	-3

ELEMENT RATIOS

ZR/NB	7.	6.	15.	12.	10.	17.	25.	10.
BA/SR	0.21	0.15	0.35	0.13	0.49	0.24	0.27	0.27
CE/YN	0.9	1.1	0.5	1.6	1.0	0.8	0.6	0.9
FE*/MG	1.02	0.80	1.24	0.74	0.87	0.92	1.03	0.83

CIFW NORMS

Q	0.0	0.0	0.0	0.0	0.0	0.0	0.0	0.0
NE	0.0	0.2	0.0	0.0	0.0	0.3	1.7	0.0
OR	0.7	1.6	0.5	1.2	0.7	0.4	0.2	1.1
AB	20.8	17.7	17.4	17.5	14.8	18.6	7.0	18.9
AN	26.8	45.1	30.0	43.6	43.7	42.0	26.9	32.6
DI	33.3	22.6	20.1	22.3	16.1	20.8	35.9	23.6
HY	1.3	0.0	1.1	1.9	9.1	0.0	0.0	10.0
OL	14.4	10.8	26.9	11.3	12.8	15.1	24.1	10.9
MT	1.6	0.9	2.3	1.0	1.3	1.2	2.2	1.4
ILM	0.9	1.0	1.5	1.1	1.3	1.4	1.8	1.4
AP	0.2	0.1	0.1	0.1	0.2	0.2	0.1	0.1

METADOLERITE DYKES

ROCK NO	MA214	X324	MA206	X239	MA367	MA413	MA266	MA236
SIO2	49.63	48.11	47.62	50.07	48.89	44.28	49.43	49.07
TIO2	0.88	0.95	0.91	1.05	1.13	0.90	1.11	1.15
AL2O3	14.71	14.84	16.10	13.01	14.35	14.47	12.93	13.64
FE2O3	1.00	1.00	1.00	1.16	1.20	1.00	1.24	1.04
FEO	6.60	6.60	6.66	7.64	7.90	6.60	8.20	6.83
MNO	0.15	0.00	0.14	0.14	0.15	0.00	0.18	0.12
MGO	9.86	9.75	9.43	9.62	9.29	13.85	9.62	10.09
CAO	12.47	10.75	11.92	11.04	11.34	13.28	11.32	12.64
NA2O	2.10	3.15	2.19	2.52	2.28	1.19	2.14	2.48
K2O	0.06	0.14	0.08	0.28	0.13	0.11	0.18	0.11
P2O5	0.07	0.05	0.09	0.09	0.11	0.13	0.10	0.14
TOTAL	97.53	95.34	96.14	96.62	96.77	95.81	96.45	97.31

TRACE ELEMENTS IN PPM

NI	109	142	102	84	79	266	60	98
CR	422	451	332	275	154	576	190	409
ZN	27	66	46	18	15	50	47	12
GA	15	15	15	18	18	15	18	16
RB	1	-1	-1	1	-1	-1	-1	2
SR	126	214	222	186	155	291	177	202
Y	19	23	22	26	29	18	27	22
ZR	56	68	70	71	77	82	82	87
NB	5	1	6	4	7	8	6	9
BA	19	61	160	54	61	38	76	29
LA	3	2	2	4	5	3	4	3
CE	10	7	15	8	12	11	10	13
PB	-3	-3	5	-3	-3	3	-3	-3
TH	-3	-3	-3	-3	-3	-3	-3	3

ELEMENT RATIOS

ZR/NB	11.	68.	12.	18.	11.	10.	14.	10.
BA/SR	0.15	0.29	0.72	0.29	0.39	0.13	0.43	0.14
CE/YN	1.3	0.7	1.7	0.8	1.0	1.5	0.9	1.4
FE*/MG	0.98	0.99	1.03	1.16	1.25	0.70	1.25	0.99

CIPW NORMS

Q	0.0	0.0	0.0	0.0	0.0	0.0	0.0	0.0
NE	0.0	0.3	0.0	0.0	0.0	0.4	0.0	0.0
OR	0.4	0.9	0.5	1.7	0.8	0.7	1.1	0.7
AB	18.2	27.5	19.3	22.1	19.9	9.7	18.8	21.6
AN	31.3	27.2	35.2	24.2	29.5	35.3	26.1	26.5
DI	25.5	22.9	20.8	25.9	22.7	26.1	25.6	29.8
HY	16.0	0.0	9.7	16.7	16.6	0.0	21.0	5.9
OL	5.2	17.8	11.0	5.5	6.3	24.2	3.2	11.4
MT	1.5	1.5	1.5	1.7	1.8	1.5	1.9	1.5
ILM	1.7	1.9	1.8	2.1	2.2	1.8	2.2	2.2
AP	0.2	0.1	0.2	0.2	0.3	0.3	0.2	0.3

METADOLERITE DYKES

ROCK NO	MA208	MA286	MA271	X307	X214*	MA183	X183	X179
SIO2	47.76	48.42	49.82	46.32	44.21	48.52	48.64	49.12
TIO2	1.14	1.18	1.14	1.03	1.36	1.34	1.32	1.45
AL2O3	13.69	14.43	12.57	15.93	14.31	14.28	13.15	14.56
FE2O3	1.19	1.14	1.10	1.12	1.00	1.04	1.08	1.03
FEO	7.87	7.53	7.24	6.82	6.58	6.87	7.14	6.82
MNO	0.00	0.17	0.00	0.00	0.00	0.16	0.00	0.14
MGO	9.64	9.44	10.20	10.11	13.36	11.52	11.17	9.08
CAO	11.33	11.98	12.26	11.07	11.46	11.40	9.63	11.09
NA2O	2.61	2.06	2.07	2.57	2.06	2.29	2.41	3.11
K2O	0.09	0.08	0.16	0.40	0.37	0.11	0.91	0.31
P2O5	0.11	0.11	0.14	0.17	0.18	0.16	0.19	0.22
TOTAL	95.43	96.54	96.70	95.54	94.89	97.69	95.64	96.93

TRACE ELEMENTS IN PPM

	MA208	MA286	MA271	X307	X214*	MA183	X183	X179
NI	103	107	86	134	242	169	118	100
CR	337	346	324	270	537	426	323	286
ZN	63	50	21	57	· 59	36	46	50
GA	16	18	17	18	15	16	15	20
RB	2	1	-1	3	1	-1	9	1
SR	175	204	169	249	704	202	299	279
Y	28	26	25	20	21	25	22	23
ZR	89	89	90	96	114	115	119	122
NB	5	5	11	15	13	13	15	19
BA	41	45	82	123	1777	80	195	114
LA	3	6	4	8	7	6	9	11
CE	13	9	17	21	19	17	18	25
PR	3	-3	3	-3	4	-3	4	3
TH	-3	-3	-3	-3	-3	-3	-3	-3

ELEMENT RATIOS

	MA208	MA286	MA271	X307	X214*	MA183	X183	X179
ZR/NB	18.	18.	8.	6.	9.	9.	8.	6.
BA/SR	0.23	0.22	0.49	0.49	2.52	0.40	0.65	0.41
CE/YN	1.1	0.8	1.7	2.6	2.2	1.7	2.0	2.7
FE*/MG	1.20	1.17	1.04	1.00	0.72	0.87	0.94	1.10

CIPW NORMS

	MA208	MA286	MA271	X307	X214*	MA183	X183	X179
Q	0.0	0.0	0.0	0.0	0.0	0.0	0.0	0.0
NE	0.0	0.0	0.0	0.9	3.1	0.0	0.0	0.0
OR	0.6	0.5	1.0	2.5	2.3	0.7	5.6	1.9
AB	23.1	18.1	18.1	21.1	12.6	19.8	21.3	27.1
AN	26.6	31.0	25.4	32.2	30.3	29.0	23.4	25.6
DI	25.6	24.2	29.5	19.5	23.2	22.3	20.4	24.0
HY	6.4	16.0	19.0	0.0	0.0	10.5	11.2	3.1
OL	13.4	6.0	2.8	19.7	24.0	13.1	13.4	13.4
MT	1.8	1.7	1.6	1.7	1.5	1.5	1.6	1.5
ILM	2.3	2.3	2.2	2.0	2.7	2.6	2.6	2.8
AP	0.3	0.3	0.3	0.4	0.4	0.4	0.5	0.5

* High Ba and Sr caused by Ca-Ba-Sr containing white
alteration mineral. XRF/XRD analysis of separated mineral
failed to give the identity.

METADOLERITE DYKES

ROCK NO	MA257	X176
SIO2	49.06	50.51
TIO2	1.60	1.40
AL2O3	12.37	13.85
FE2O3	1.29	0.99
FEO	8.50	6.53
MNO	0.00	0.13
MGO	9.77	10.17
CAO	10.49	8.34
NA2O	2.32	2.34
K2O	0.30	1.88
P2O5	0.18	0.17
TOTAL	95.88	96.31

TRACE ELEMENTS IN PPM

NI	83	80
CR	262	188
ZN	32	10
GA	19	17
RB	1	21
SR	169	375
Y	35	24
ZR	124	133
NB	11	12
BA	81	268
LA	5	7
CE	18	22
PB	-3	-3
TH	-3	-3

ELEMENT RATIOS

ZR/NB	11.	11.
BA/SR	0.48	0.71
CE/YN	1.3	2.2
FE*/MG	1.27	0.94

CIPW NORMS

Q	0.0	0.0
NE	0.0	0.0
OR	1.8	11.5
AB	20.5	20.6
AN	23.4	22.6
DI	24.0	15.6
HY	20.8	17.1
OL	3.8	8.1
MT	2.0	1.5
ILM	3.2	2.8
AP	0.4	0.4

GREEN PILLOW LAVAS

ROCK NO	X330	MA401	X326
SIO2	49.41	48.29	47.79
TIO2	1.05	0.99	1.08
AL2O3	13.71	16.35	15.51
FE2O3	1.06	0.95	1.06
FEO	6.97	6.24	6.99
MNO	0.00	0.00	0.00
MGO	9.18	8.87	8.59
CAO	10.44	8.86	10.12
NA2O	3.42	2.76	3.62
K2O	0.25	1.81	0.86
P2O5	0.09	0.00	0.01
TOTAL	95.58	95.12	95.63

TRACE ELEMENTS IN PPM

NI	139	99	129
CR	405	314	364
ZN	131	493	53
GA	14	16	17
RB	2	26	12
SR	172	211	273
Y	26	23	25
ZR	63	66	74
NB	-1	4	4
BA	68	257	146
LA	3	2	4
CE	7	8	9
PB	3	6	-3
TH	-3	-3	-3

ELEMENT RATIOS

ZR/NB	-63.	16.	18.
BA/SR	0.40	1.22	0.53
CE/YN	0.7	0.8	0.9
FE*/MG	1.11	1.03	1.19

CIPW NORMS

Q	0.0	0.0	0.0
NE	0.0	0.7	5.1
OR	1.5	11.2	5.3
AB	30.3	23.3	22.7
AN	22.3	28.3	24.6
DI	25.3	14.6	22.6
HY	1.9	0.0	0.0
OL	14.8	18.5	16.0
MT	1.6	1.4	1.6
ILM	2.1	2.0	2.1
AP	0.2	0.0	0.0

RED PILLOW LAVAS

ROCK NO	MA400	X249	X323	MA391	X245B1	X245C1	MA139	MA142
SIO2	47.30	47.87	48.29	47.90	46.81	47.38	48.96	48.29
TIO2	0.83	0.94	0.89	0.91	0.97	0.99	0.91	0.94
AL2O3	14.38	13.76	16.35	17.28	15.45	15.93	17.10	17.46
FE2O3	0.88	0.95	0.94	0.95	0.96	0.96	0.91	0.91
FEO	5.81	6.27	6.21	6.27	6.31	6.35	5.98	6.02
MNO	0.00	0.00	0.00	0.14	0.21	0.18	0.14	0.19
MGO	7.04	7.11	7.20	6.85	4.67	4.78	6.49	7.06
CAO	15.34	13.43	12.21	12.59	14.27	13.57	12.55	12.25
NA2O	3.11	3.35	3.14	2.88	3.65	3.74	3.25	2.76
K2O	0.36	1.06	0.89	0.87	0.94	0.96	1.07	1.01
P2O5	0.08	0.07	0.06	0.06	0.10	0.09	0.07	0.07
TOTAL	95.13	94.81	96.18	96.70	94.34	94.93	97.43	96.96

TRACE ELEMENTS IN PPM

NI	102	112	95	83	55	64	98	90
CR	344	391	347	314	289	310	316	312
ZN	56	60	58	34	47	52	35	59
GA	16	18	19	17	16	16	16	15
RB	4	13	11	11	13	12	16	15
SR	181	168	153	206	140	140	227	199
Y	20	22	24	23	24	23	22	21
ZR	57	57	58	63	66	66	67	67
NB	4	2	3	3	3	4	5	6
BA	40	41	22	49	43	42	36	63
LA	4	4	2	5	4	10	4	3
CE	8	10	6	6	14	11	10	11
PB	-3	4	-3	4	-3	-3	3	-3
TH	-3	-3	-3	-3	-3	-3	-3	-3

ELEMENT RATIOS

ZR/NB	14.	28.	19.	21.	22.	16.	13.	11.
BA/SR	0.22	0.24	0.14	0.24	0.31	0.30	0.16	0.32
CE/YN	1.0	1.1	0.6	0.6	1.4	1.2	1.1	1.3
FE*/MG	1.21	1.29	1.26	1.34	1.98	1.94	1.35	1.25

CIPW NORMS

Q	0.0	0.0	0.0	0.0	0.0	0.0	0.0	0.0
NE	8.0	8.2	4.1	3.6	11.1	9.9	4.9	2.4
OR	2.2	6.6	5.5	5.3	5.9	6.0	6.5	6.2
AB	12.8	14.7	20.0	18.5	12.2	15.0	19.1	19.6
AN	25.5	20.4	29.0	32.7	24.4	25.1	29.7	33.3
DI	43.7	40.0	27.2	25.6	41.1	37.1	27.5	23.5
HY	0.0	0.0	0.0	0.0	0.0	0.0	0.0	0.0
OL	4.5	6.5	10.8	10.9	1.6	3.2	9.0	11.7
MT	1.3	1.5	1.4	1.4	1.5	1.5	1.4	1.4
ILM	1.7	1.9	1.8	1.8	2.0	2.0	1.8	1.8
AP	0.2	0.2	0.1	0.1	0.3	0.2	0.2	0.2

RED PILLOW LAVAS

ROCK NO	X245P2	X245P2	X245P1	X245	X245A2	MA448	X245A1	MA44
SIO2	47.38	47.64	47.63	48.64	47.82	47.30	48.35	45.61
TIO2	1.04	1.06	1.05	1.05	1.16	1.21	1.22	0.95
AL203	16.34	16.37	16.32	17.06	16.70	15.00	17.08	17.85
FE203	1.01	1.02	1.02	1.01	1.08	1.09	1.16	0.83
FEO	6.65	6.76	6.78	6.64	7.14	7.20	7.65	5.46
MNO	0.19	0.18	0.19	0.24	0.19	0.00	0.18	0.00
MGO	4.48	4.65	4.66	6.24	4.53	5.42	4.65	6.96
CAO	12.73	12.66	12.61	12.51	10.26	11.46	9.42	10.84
NA2O	4.12	4.17	4.13	3.23	4.66	4.79	4.74	4.40
K2O	0.92	0.92	0.94	0.51	0.88	1.02	0.90	0.56
P205	0.11	0.10	0.10	0.08	0.09	0.13	0.09	0.09
TOTAL	94.97	95.53	95.43	97.21	94.51	94.62	95.44	93.55

TRACE ELEMENTS IN PPM

NI	52	55	55	67	59	53	59	44
CR	321	314	314	292	327	185	330	205
ZN	54	56	53	50	50	67	57	50
GA	14	15	14	17	16	17	16	19
RB	12	12	12	7	11	16	11	0
SR	132	142	140	208	145	225	150	608
Y	24	24	26	24	27	27	27	16
ZR	67	68	59	72	74	77	77	78
NB	6	4	5	5	6	5	6	7
BA	31	42	39	51	50	26	59	62
LA	5	5	5	4	5	3	6	4
CE	13	10	14	14	11	11	14	13
PB	-3	3	-3	-3	3	-3	-3	3
TH	-3	-3	-3	-3	-3	-3	-3	-3

ELEMENT RATIOS

ZR/NB	11.	17.	12.	14.	12.	15.	13.	11.
BA/SR	0.23	0.30	0.28	0.25	0.34	0.12	0.39	0.10
CE/YN	1.3	1.0	1.3	1.4	1.0	1.0	1.3	2.0
FE*/MG	2.17	2.13	2.13	1.56	2.31	1.95	2.41	1.15

CIPW NORMS

Q	0.0	0.0	0.0	0.0	0.0	0.0	0.0	0.0
NE	10.5	10.6	10.3	2.8	8.9	13.5	7.6	11.8
OR	5.7	5.7	5.8	3.1	5.5	6.4	5.6	3.5
AB	17.2	17.4	17.5	23.0	25.2	18.0	28.0	18.1
AN	24.6	24.3	24.3	31.4	23.3	17.3	23.8	29.2
DI	33.9	33.6	33.4	26.1	24.7	34.4	20.4	22.5
HY	0.0	0.0	0.0	0.0	0.0	0.0	0.0	0.0
OL	4.0	4.5	4.7	9.9	8.0	6.1	10.3	11.5
MT	1.5	1.5	1.5	1.5	1.7	1.7	1.8	1.3
ILM	2.1	2.1	2.1	2.1	2.3	2.4	2.4	1.9
AP	0.3	0.2	0.2	0.2	0.2	0.3	0.2	0.2

RED PILLOW LAVAS

ROCK NO	MA437	MA439	MA422
SIO2	43.98	45.44	47.66
TIO2	1.35	1.48	1.74
AL2O3	12.06	12.85	12.10
FE2O3	0.97	0.79	1.13
FEO	6.43	5.22	7.49
MNO	0.00	0.00	0.00
MGO	4.55	5.43	7.78
CAO	17.58	16.80	9.83
NA2O	2.68	3.19	3.67
K2O	2.30	1.97	1.57
P2O5	0.25	0.07	0.26
TOTAL	92.15	93.24	93.23

TRACE ELEMENTS IN PPM

NI	77	81	82
CR	189	86	170
ZN	53	57	68
GA	16	18	18
RB	46	18	16
SR	462	388	148
Y	20	22	27
ZR	134	159	161
NB	27	33	27
BA	276	314	207
LA	15	16	16
CE	32	37	36
PB	5	-3	4
TH	3	6	3

ELEMENT RATIOS

ZR/NB	5.	5.	6.
BA/SR	0.60	0.81	1.40
CE/YN	3.9	4.1	3.3
FE*/MG	2.07	1.41	1.41

CIPW NORMS

Q	0.0	0.0	0.0
NE	13.3	15.7	5.5
OR	2.9	10.0	10.0
AB	0.0	0.0	23.2
AN	15.3	16.0	12.8
DI	44.4	44.4	30.6
HY	0.0	0.0	0.0
OL	0.0	0.0	12.0
MT	1.5	1.2	1.8
ILM	2.8	3.0	3.5
AP	0.6	0.2	0.7

MELANGE LAVAS

ROCK NO	X346	MA352	MA356	MA354
SIO2	51.08	48.36	46.26	56.75
TIO2	2.17	1.88	2.10	2.16
AL203	14.39	13.18	12.98	16.14
FE203	0.93	0.54	0.77	0.51
FEO	6.13	3.55	5.11	3.35
MNO	0.00	0.00	0.12	0.20
MGO	6.30	3.82	5.36	2.01
CAO	5.49	11.92	13.33	8.35
NA20	6.35	3.46	3.39	3.96
K20	2.06	5.73	3.24	3.27
P205	0.28	0.43	0.57	0.76
TOTAL	95.18	92.87	93.23	97.46

TRACE ELEMENTS IN PPM

NI	76	90	54	2
CR	186	147	126	6
ZN	71	52	64	111
GA	19	16	20	23
RB	19	68	41	28
SR	115	344	258	459
Y	25	26	24	50
ZR	173	260	283	396
NB	34	70	82	105
BA	429	1303	513	457
LA	21	39	36	37
CE	41	77	72	106
PB	5	4	7	8
TH	3	11	12	11

ELEMENT RATIOS

ZR/NB	5.	4.	3.	4.
BA/SR	3.73	3.79	1.99	1.00
CE/YN	4.0	7.2	7.3	5.2
FE*/MG	1.43	1.36	1.40	2.44

CIPW NORMS

Q	0.0	0.0	0.0	5.7
NE	10.9	17.1	15.4	0.0
OR	12.8	34.8	20.5	19.8
AB	36.3	0.0	2.3	34.4
AN	4.9	3.8	11.4	17.0
DI	17.7	28.1	41.9	16.0
HY	0.0	0.0	0.0	0.0
OL	11.0	0.0	0.0	0.0
MT	1.4	0.8	1.2	0.8
ILM	4.3	3.8	4.3	4.2
AP	0.7	1.1	1.4	1.8

SHINZI GROUP

ROCK NO	X220A1	Y223	X222	MA425	X222A	X219A	MA427	X219A
SIO2	47.05	48.40	47.12	46.41	48.15	45.30	44.55	51.18
TIO2	1.74	2.05	2.10	2.34	2.35	2.98	2.31	1.92
AL2O3	15.41	13.40	13.55	14.47	13.86	12.62	12.46	14.87
FE2O3	1.11	1.12	0.98	1.21	1.07	1.22	1.07	1.30
FEO	7.30	7.42	6.44	8.02	7.07	8.08	7.04	8.60
MNO	0.00	0.14	0.15	0.00	0.00	0.00	0.00	0.14
MGO	5.26	9.02	5.91	10.42	6.17	7.43	5.70	3.77
CAO	13.87	8.41	11.92	6.88	9.75	9.73	14.96	7.81
NA2O	2.25	3.56	3.49	3.38	4.36	2.20	2.46	3.31
K2O	1.20	2.05	2.56	1.69	2.08	2.13	0.91	0.86
P2O5	0.29	0.32	0.45	0.72	0.48	0.57	0.79	0.72
TOTAL	95.48	95.89	94.67	95.54	95.34	92.26	92.25	94.48

TRACE ELEMENTS IN PPM

NI	62	99	64	76	59	26	24	-1
CR	83	264	146	126	138	25	10	-1
ZN	54	72	63	62	61	73	66	161
GA	22	18	18	18	18	23	27	30
RB	22	22	36	27	31	33	30	11
SR	448	384	494	560	518	272	484	301
Y	23	27	26	31	31	37	33	67
ZR	163	209	240	248	273	293	331	480
NB	30	44	52	56	59	67	86	60
BA	225	433	603	461	425	471	30	486
LA	18	16	16	38	31	40	54	37
CE	40	44	54	77	67	82	111	89
PB	4	5	4	-3	4	-3	13	-3
TH	-3	3	6	6	4	5	14	-3

ELEMENT RATIOS

ZR/NB	5.	5.	5.	4.	5.	4.	4.	7.
BA/SR	0.50	1.13	1.22	0.82	0.82	1.73	0.06	1.61
CE/YN	4.2	4.0	5.1	6.1	5.3	5.4	8.2	3.2
FE*/MG	2.03	1.20	1.60	1.13	1.68	1.59	1.81	3.34

CIPW NORMS

Q	0.0	0.0	0.0	0.0	0.0	0.0	0.0	5.5
NE	1.9	4.4	11.2	1.8	9.5	0.0	5.1	0.0
OR	7.4	12.6	16.0	10.5	12.9	13.6	5.8	5.4
AB	16.4	23.4	10.6	26.6	21.1	20.2	13.1	29.6
AN	29.7	15.2	14.5	20.2	12.7	19.8	22.0	24.5
DI	33.2	21.3	36.6	8.7	28.4	23.2	43.1	9.8
HY	0.0	0.0	0.0	0.0	0.0	1.2	0.0	17.6
OL	5.5	16.7	4.4	24.0	7.9	12.5	2.4	0.0
MT	1.7	1.7	1.5	1.8	1.6	1.9	1.7	2.0
ILM	3.5	4.1	4.2	4.7	4.7	6.1	4.8	3.9
AP	0.7	0.8	1.1	1.8	1.2	1.5	2.0	1.8

SHINZI GROUP

ROCK NO	MA426	X220A
SIO2	56.47	64.82
TIO2	0.70	0.20
AL2O3	13.92	16.52
FE2O3	1.05	0.43
FEO	6.96	2.85
MNO	0.00	0.00
MGO	5.31	0.14
CAO	3.24	0.61
NA2O	5.18	7.23
K2O	2.29	3.81
P2O5	0.13	0.02
TOTAL	95.25	96.63

TRACE ELEMENTS IN PPM

NI	-1	-1
CR	-1	-1
ZN	76	81
GA	34	42
RB	29	64
SR	143	37
Y	71	93
ZR	633	1286
NB	85	182
BA	391	92
LA	55	101
CE	120	196
PB	-3	5
TH	11	29

ELEMENT RATIOS

ZR/NB	7.	7.
BA/SR	2.73	2.49
CE/YN	4.1	5.1
FE*/MG	1.92	29.80

CIPW NORMS

Q	0.0	5.1
NE	0.0	0.0
OR	14.2	23.3
AB	46.0	63.3
AN	8.4	1.4
DI	6.4	1.4
HY	20.8	4.3
OL	0.9	0.0
MT	1.6	0.6
ILM	1.4	0.4
AP	0.3	0.0

GRANITES

ROCK NO	MA120A	MA37	MA455	X35	X33	MA44	X86	MA28
SIO2	75.98	74.97	75.47	74.95	73.31	74.70	74.66	75.05
TIO2	0.10	0.10	0.08	0.05	0.17	0.06	0.07	0.15
AL2O3	13.16	13.50	14.12	13.91	13.77	13.63	14.01	13.57
FE2O3	0.56	0.74	0.56	0.58	1.57	0.70	0.72	1.08
FEO	0.00	0.00	0.00	0.00	0.00	0.00	0.00	0.00
MNO	0.01	0.01	0.00	0.02	0.04	0.02	0.02	0.02
MGO	0.29	0.40	0.19	0.14	1.07	0.11	0.18	0.49
CAO	0.59	0.57	0.72	0.61	1.58	0.50	0.85	1.09
NA2O	4.00	3.76	4.43	3.62	3.74	3.83	3.86	3.53
K2O	4.58	5.20	5.23	5.75	4.49	5.34	4.95	4.49
P2O5	0.01	0.01	0.01	0.01	0.01	0.00	0.01	0.02
TOTAL	99.28	99.26	100.81	99.64	99.75	98.89	99.33	99.49

TRACE ELEMENTS IN PPM

NI	-1	-1	-1	-1	8	-1	-1	3
CR	4	5	-1	6	28	4	6	9
ZN	4	3	1	2	10	3	3	5
GA	13	13	15	14	16	16	17	14
RB	67	77	106	102	95	85	101	60
SR	72	56	29	40	72	30	34	96
Y	6	3	7	10	9	9	11	6
ZR	31	54	60	72	72	92	98	102
NB	23	27	48	53	81	48	73	53
BA	2970	798	459	137	348	224	183	994
LA	83	23	28	20	23	29	18	65
CE	103	35	41	35	37	45	30	89
PR	4	5	3	6	7	6	6	6
TH	50	17	27	42	34	39	43	46

ELEMENT RATIOS

ZR/NB	1.	2.	1.	1.	1.	2.	1.	2.
BA/SR	41.25	14.25	15.83	3.42	4.83	7.47	5.38	10.35
CE/YN	41.9	28.5	14.3	8.6	10.0	12.2	6.7	36.2
FE*/MG	2.24	2.15	3.42	4.81	1.70	7.39	4.64	2.56

CIPW NORMS

Q	33.5	31.6	27.7	30.5	29.5	31.1	31.4	34.4
NE	0.0	0.0	0.0	0.0	0.0	0.0	0.0	0.0
OR	27.3	31.0	30.7	34.1	26.6	31.9	29.5	26.7
AB	34.1	32.1	37.2	30.7	31.7	32.8	32.9	30.0
AN	3.5	2.9	3.2	3.0	7.5	2.6	4.2	5.5
DI	0.0	0.0	0.1	0.0	0.0	0.0	0.0	0.0
HY	0.7	1.0	0.4	0.3	2.7	0.3	0.5	1.2
OL	0.0	0.0	0.0	0.0	0.0	0.0	0.0	0.0
MT	0.0	0.0	0.0	0.0	0.0	0.0	0.0	0.0
ILM	0.0	0.0	0.0	0.0	0.1	0.0	0.0	0.0
AP	0.0	0.0	0.0	0.0	0.0	0.0	0.0	0.0

GRANITES

ROCK NO	X37	MA358
SIO2	74.13	73.61
TIO2	0.12	0.09
AL2O3	13.82	14.30
FE2O3	1.68	1.00
FEO	0.00	0.00
MNO	0.03	0.01
MGO	0.61	0.21
CAO	1.30	0.99
NA2O	4.43	4.72
K2O	3.35	4.33
P2O5	0.01	0.02
TOTAL	99.48	99.28

TRACE ELEMENTS IN PPM

NI	1	-1
CR	8	6
ZN	23	3
GA	17	19
PB	56	60
SR	73	92
Y	8	0
ZR	103	138
NB	93	56
BA	218	658
LA	50	30
CE	76	47
PB	5	5
TH	50	20

ELEMENT RATIOS

ZR/NB	1.	2.
BA/SR	2.99	7.15
CE/YN	23.2	12.8
FE*/MG	3.20	5.53

CIPW NORMS

Q	32.0	27.3
NE	0.0	0.0
OR	19.9	25.8
AB	37.7	40.2
AN	6.5	5.0
DI	0.0	0.0
HY	1.5	0.5
OL	0.0	0.0
MT	0.0	0.0
ILM	0.1	0.0
AP	0.0	0.0

APPENDIX 7: REFERENCE LIST

ABBOTTS, I. L., 1978a. High-potassium granites in the Masirah ophiolite of Oman. Geol. Mag., in press. (Chapter 7)

ABBOTTS, I. L., 1978b. Intrusive processes at ocean ridges; evidence from the sheeted dyke complex of Masirah, Oman. Submitted to Tectonophysics. (Chapter 4)

ABBOTTS, I. L., 1978c. Geochemistry of the pillow lavas and sheeted dyke complex of Masirah Island, Oman. Submitted to Earth Planet. Sci. Lett. (Chapter 5)

ABBOTTS, I. L., 1978d. Masirah plutonic rocks; an exposure of oceanic lower crust. (Chapter 3)

ALBURQUERQUE, C. A. R. de, 1971. Petrochemistry of a series of granitic rocks from Northern Portugal. Bull. Geol. Soc. Am., 82, 2783-2798.

ALBURQUERQUE, C. A. R. de, 1977. Geochemistry of the tonalitic and granitic rocks of the Nova Scotia southern plutons. Geochem. cosmochim. Acta., 41, 1-14.

ALBURQUERQUE, C. A. R. de, 1978. Rare earth elements in 'Younger' granites, Northern Portugal. Lithos, 2, 219-229.

ALDISS, D., 1978. Plagiogranites and associated plutonic rocks of various ophiolite complexes. Unpubl. Ph.D thesis, Open University.

ALLEMANN, F. and PETERS, T., 1972. The ophiolite-radiolorite belt of the North Oman mountains. Eclogae. Geol. Helvetiae, 65, 657-697.

ALLEN, C. R., 1975. Petrology of a portion of the Troodos Plutonic Complex, Cyprus. Ph.D. thesis, Univ. of Cambridge.

ARTH, J. G., and BARKER, F., 1976. Rare earth partitioning between hornblende and dacitic liquid and implications for the genesis of tonalitic-trondhjemitic magmas. Geol., 4, 534-537.

AUMENTO, F., 1970. Serpentine mineralogy of ultrabasic intrusions in Canada and on the Mid-Atlantic Ridge. Geol. Surv. Can. Paper 69-53, 51pp.

AUMENTO, F., and LOUBAT, H., 1971. The Mid-Atlantic Ridge near $45^{\circ}N$: serpentinised ultramafic intrusions. Can. J. Earth Sci., 8, 631-663.

BAILEY, E. H. and BLAKE, M. C. J., 1974. Major chemical characteristics of Mesozoic Coast Range Ophiolite in California. Journ. Res. U.S. Geol. Surv., 2, 637-656.

BAKER, I., 1969. Petrology of the volcanic rocks of Saint Helena Island, S. Atlantic. Bull. Geol. Soc. Am., 80. 1283-1310.

BAKER, P. E., 1976. The South Sandwich Islands II Petrology and Geochemistry. Brit-Antarct. Sci. Rept. in press.

BARNES, I., O'NEIL, J. R., AND TRESCASES, J. J., 1978. Present-day serpentinization in New Caladonia, Oman and Yugoslavia. Note in Geochim. Cosmochim. Acta., 42, 144-146.

BASS, M. N., MOBERLY, R., RHODES, J. M., SHIH, C-Y., and CHURCH, S. E., 1973. Volcanic rocks cored in the central Pacific. Init. Repts. Deep Sea Drilling Project, leg. 17, 429-505.

BATIZA, R., 1977. Petrology and chemistry of Guadalupe Island; An alkalic sea mount on a fossil ridge crest. Geol., 5, 860-764.

BEAMAN, D.R., and ISASI, J. A. 1971. Electron beam microanalysis. Material Research and Standards, 11, 1-31.

BECKINSALE, R.D., 1974. Rb-Sr and K-Ar age determinations and oxygen isotope data for the Glen Cannel granophyre, Isle of Mull, Argyllshire, Scotland. Earth Planet. Sci. Lett., 22, 267-274.

BECKINSALE, R.D., FYFE, W. S., and SMEWING, J. D., 1974. O18 enriched ophiolitic metabasic rocks from E. Liguria (Italy), Pindos (Greece) and Troodos (Cyprus). Contrib. Mineral. Petrol., 47, 41-62.

BONATTI, E., 1973. Origin of offsets of the Mid-Atlantic Ridge in fracture zones. J. Geol., 81, 144-186.

BONATTI, E., 1975. Metallogenesis at oceanic spreading centres. Ann. Rev. Earth and Planetary Sci., 3, 401-403.

BONATTI, E., 1976. Serpentinite protrusions in the oceanic crust. Earth. Planet. Sci. Lett., 32, 107-113.

BONATTI, E., 1978. Vertical tectonism in oceanic fracture zones. Earth.Planet. Sci. Lett., 37, 369-379

BONATTI, E., HARRISON, C. G. A., FISHER, D. E., HONNOREZ, J., SCHILLING, J. G., STIPP, J. J., ZENTILLI, M., 1977. Easter volcanic chain (south-east Pacific) a mantle hot line. J. Geophys. Res., 82, 2457-2478.

BONATTI, E., and HONNOREZ, J., 1976. Sections of the earths crust in the equatorial Atlantic. J. Geophys. Res., 81, 4104-4116.

BONATTI, E., HONNOREZ-GUERSTEIN, M. B., HONNOREZ, J., and STERN, C., 1976. Hydrothermal pyrite concretions from the Romanche Trench (equatorial Atlantic): metallogenesis in oceanic fracture zones. Earth. Planet. Sci. Lett., 32, 1-10.

BONATTI, E., ZERBI, M., KAY, R., and RYDELL, N., 1976.
Metalliferous deposits from the Apennine
ophiolites; Mesozoic equivalents of modern
deposits from oceanic spreading centres.
Geol. Soc. Am. Bull., 87, 83-94.

BOYD, F. R., ENGLAND, J. L., and DAVIS, B. T. C., 1964.
Effect of pressure on the melting and poly-
morphism of enstatite, $MgSiO_3$. J. Geophys. Res.,
69, 2101-2109.

BRONGNIART, A., 1827. Classification et caracteres mineralogiques
des roches homogenes et heterogenes.
F. G. Levrault., Paris.

BROWN, G. C., 1977. Mantle origin of some Cordilleran granites.
Nature, 265, 21-24.

BRUHN, R. L., STERN, C. R., and DE WIT, M. J., 1978. Field and
geochemical data bearing on the development
of a Mesozoic volcano-tectonic rift zone and
back-arc basin in southernmost South America.
Earth Planet. Sci. Lett., 41, 32-47.

BUDDINGTON, A. F., and LINDSLEY, D. H., 1964. Iron-titanium
oxide minerals and synthetic equivalents.
J. Petrol., 5, 310-357.

BUMA, G., FREY, F. A., and WONES, D. R., 1971. New England
granites; trace element evidence regarding
their origin and differentiation. Contrib.
Mineral. Petrol., 31, 300-320.

CANN, J. R., 1970. New model for the structure of the ocean
crust. Nature, 266, 928-930.

CANN, J. R., 1971. Major element variations in ocean-floor
basalts. Phil. Trans. Roy. Soc. Lond., A268,
495-505.

CANN, J. R., 1974. A model for oceanic crustal structure
developed. Geophys. J. R. Astron. Soc., 39,
169-187.

CARNEY, J. N. and WELLAND, M. J. P., 1974. Geology and mineral
resources of the Oman Mountains.
London Inst. Geol. Sci. Gt. Brit. Rept., 27, 50pp.

CHRISTENSEN, N. I., 1970. Composition and evolution of the
oceanic crust. Marine Geol., 8, 139-154.

CHRISTENSEN, N. I., 1972. The abundance of serpentinites in the
oceanic crust. J. Geol., 80, 709-719.

CHRISTENSEN, N. I., 1978. Ophiolites, seismic velocities and
oceanic crustal structure. Tectonophysics, 47,
131-157.

CHRISTENSEN, N. I., and SALISBURY, M. R., 1975. Structure and constitution of the lower oceanic crust. Rev. Geophys. Space. Phys., 13, 57-86.

CHURCII, W. R., and RICCIO, L., 1977. Fractionation trends in the Bay of Islands ophiolite of Newfoundland: polycyclic cumulate sequences in ophiolites and their classification. Can. J. Earth Sci., 14, 1156-1165.

CLIFFORD, T. N., Rooke, J. N., and ALLSOPP, H. L., 1969. Petrochemistry and age of the Franzfontein granite rocks of northern south-west Africa. Geochim, cosmochim, Acta., 33, 973-986.

COISH, R. A. 1977. Ocean floor metamorphism in the Betts Cove Ophiolite, Newfoundland. Contr. Mineral. Petrol. 60, 255-270.

COLEMAN, R. G., 1967. Low-temperature reaction zones and alpine ultramafic rocks of California, Oregan, and Washington. U. S. Geol. Surv. Bull., 1247, 1-49.

COLEMAN, R. G., 1971. Plate tectonic emplacement of upper mantle peridotites along continental edges. J. Geophys. Res., 76, 1212-1222.

COLEMAN, R. G., 1977. Ophiolites. Ancient oceanic lithosphere? Springer Verlag - 239pp.

COLEMAN, R. G., and KEITH, T. E., 1971. A chemical study of serpentinization, Burrow Mountain, California. J. Petrol., 12, 311-328.

COLEMAN, R. G., and PETERMAN, Z. E., 1975. Oceanic plagiogranite. J. Geophys. Res. 80, 1099-1108.

CONDIE, K. C., 1969. Petrology and geochemistry of the Laramie batholith and related metamorphic rocks of Pre-Cambrian age, eastern Wyoming. Bull. Geol. Soc. Am. 80, 57-82.

DAVIES, H. L., 1968. Papuan ultramafic belt. 23rd Intern. Geol. Congr. Sect. 1, 209-220.

DAVIES, H. L., and SMITH, I. E., 1971. Geology of eastern Papua. Geol. Soc. Am. Bull, 82, 3299-3312.

DEWEY, J. F., 1974. Continental margins and ophiolite subduction: Appalachian Caledonian System, in, Burke, C.A., and Drake, C.L., eds., The Geology of Continental Margins: Springer Verlag, New York, p933-950.

DEWEY, J. F., 1976. Ophiolite obduction., Tectonophysics, V.31, 93-120.

DEWEY, J. F., and BIRD, J. M., 1971. Origin and emplacement of the ophiolite suite. Appalachian ophiolites in Newfoundland. J. Geophys. Res., 76, 3179-3206.

DEWEY, J. F., FOX, P. J., and KIDD, W. S. F., 1976. Geometry of plate accretion (abs.). Am. Geophus. Union Trans. V57, 331.

DEWEY, J. F., and KIDD, W. S. F., 1977. Geometry of plate accretion. Geol. Soc. Am. Bull., 88, 960-968.

DEWEY, J. F., PITMAN III, W. C., RYAN, W. B. F., and BONNIN, J., 1973. Plate tectonics and the evolution of the Alpine System. Geol. Soc. Am. Bull.,84, 3137-3180.

DICKEY, J. S. Jr, 1975. A hypothesis of origin for podiform chromite deposits. Geochim. Cosmochim Acta, 39, 1061-1074.

DICKINSON, W. R., 1966. Table mountain serpentinite extrusion in California Coast Ranges. Bull Geol. Soc. Am., 77, 451-72.

DIMROTH, E., COUSINEAU, P., LEDOC, M., and SANSCHAGRIN, Y., 1978. Structure and organisation of Archaen subaqueous basalt flows, Rouyn-noranda area, Quebec, Canada. Con. Journ. Earth. Sci., 15, 902-918.

DRAKE, M. J., and WEILL, D. F., 1975. Partition of Sr, Ba, Ca, Y, Eu^{2+}, Eu^{3+}, and other REE between plagioclase felspar and magmatic liquid: an experimental study. Geochim, Cosmochim. Acta. 39, 689-712.

ENGEL, A. E. J., ENGEL, C. J., and HAVENS, R. G., 1965. Chemical characteristics of oceanic basalts and the upper mantle. Geol. Soc. Am. Bull. 76, 719-723.

ENGEL, C., and FISHER, R. L., 1969. Lherzolite, anorthosite, gabbro and basalt dredged from the Mid-Indian Ocean Ridge. Sci., 166, 1136-1141.

ENGEL, C., and FISHER, R. L., 1975. Granitic to ultramafic rock complexes of the Indian Ocean ridge systems, western Indian Ocean. Bull. Geol. Soc. Am., 86, 1553-1578.

ENGLAND, R. N., and DAVIES, H. L., 1973. Minerology of ultramafic cumulates and tectonics from eastern Papua. Earth. Planet. Sci. Lett., 17, 416-425.

ERLANK, A. J. and E. J. D, 1976. The significance of imcompatible elements in Mid-Atlantic Ridge basalts from 45°N with particular reference to Zr/Nb. Contr. Mineral. Petrol., 54, 281-291.

EWING, M., EITTREIM, S., TRUCHAN, M., and EWING, J.I., 1969. Sediment distribution in the Indian Ocean. Deep Sea Res., 16, 231-248.

FARHOUDI, G. and KARIG, D.E., 1977. Makran of Iran and Pakistan as an active arc system. Geol., 5, 664-668.

FLOYD, P.A. and WINCHESTER, J.A., 1975. Magma type and tectonic setting discrimination using immobile elements. Earth Planet. Sci. Lett., 27, 211-218.

FOX, P.J., SCHREIBER, E., ROWLETT, H. and McCAMY, K., 1976. The geology of the Oceanographer Fracture Zone; a model for fracture zones. J. Geophys. Res., 81, 4117-4128.

FREY, F.A., BRYAN, W.B., and THOMPSON, G., 1974. Atlantic Ocean floor: geochemistry and petrology of basalts from Legs 2 and 3 of the Deep Sea Drilling Project. J. Geophys. Res., 79, 5507-5527.

FREY, F.A., CHAPPELL, B.W., and ROY, S.D., 1978. Fractionation of rare-earth elements in the Tuolumne Intrusive Series, Sierra Nevada batholith, California. Geol., 6, 239-242.

GASS, I.G., 1968. Is the Troodos massif of Cyprus a fragment of Mesozoic Ocean floor? Nature, 220, 39-42.

GASS, I.G., 1977. Origin and emplacement of ophiolites. in Volcanic processes in ore genesis. (The Institution of Mining and Metallurgy and the Geol. Soc. Lond.), 72-76.

GASS, I.G., and GIBSON, I.L., 1969. The structural evolution of the rift zones in the Middle East. Nature, 221, 926-930

GASS, I.G., and SMEWING, J.D., 1973. Intrusion, extrusion and metamorphism at constructive margins; evidence from the Troodos Massif, Cyprus. Nature, 242, 26-29.

GASS, I.G., and SMEWING, J.D., 1978. Ophiolites: obducted oceanic lithosphere. The Sea., Vol. 7, in press

GASS, I.G., SMITH, A.G., and VINE, F.J., 1975. Origin and emplacement of ophiolites in Geodynamics today. (London: The Royal Soc. 1975)

GEALEY, W.K., 1977. Ophiolite obduction and geologic evolution of the Oman Mountains and adjacent areas. Geol. Soc. Am. Bull., 88, 1183-1191

GLENNIE, K.W., BOEUF, M.G.A., HUGHES CLARKE, M.W., MOODY-STUART, M., PILAAR, W.F.H., and REINHARDT, B.M., 1973. Late Cretaceous nappes in the Oman Mountains and their geologic evolution. Am. Assoc. Petrol. Geol. Bull., 57, 5-27.

GLENNIE, K.W., BOEUF, M.G.A., HUGHES CLARKE, M.W., MOODY-STUART, M.,
PILAAR, W.F.H., and REINHARDT, B.M., 1974.
Geology of the Oman Mountains. Verh. K. ned.
geol. mijnb. Genoot., 31, 423pp.

GOODE, A.D.T., 1976. Small-scale primary cumulus igneous layering
in the Kalka Layered Intrusion, Giles Complex,
Central Australia. J. Petrol. 17. 379-397.

GRAPES, R.H., 1975. Actinolite-Hornblende pairs in metamorphosed
gabbro, Hidaka Mountains, Hokkaida.
Contr. Mineral. Petrol., 49, 125-140

GREEN, O.H. and HIBBERSON, W., 1970. The instability of
plagioclase in peridotite at high pressure.
Lithos., 1, 209-221.

GREENBAUM, D., 1972. Magmatic processes at ocean ridges;
evidence from the Troodos massif, Cyprus.
Nature, Phys. Sci., 238, 18-21.

GREENWOOD, J.E.G.W., HADLEY, D.G., ANDERSON, R.E., FLECK, R.J.,
and SCHMIDT, D.L., 1975. Late Proterozoic
cratonization in south-western Saudi Arabia.
U.S.G.S. Saudi Arabian Proj. Rept. 196, 23pp.

GREENWOOD, J.E.G.W. and LONEY, P.E., 1968. Geology and mineral
resources of the Trucial Oman Range.
Rept. Inst. Geol. Sci. London (Overseas Division),
108pp.

GUILLON, J.H., 1975. Les massifs peridotiques de Nouvelle-
Caledonie Memoires. Orstom, 76, 119pp. Paris.

HAHN-WEINHEIMER, P. and ACKERMANN, H., 1967. Geochemical
investigation of differentiated granite plutons
of the southern Black Forest. II. The zoning
of the Marlsburg granite pluton as indicated
by the elements titonium, zirconium, phosphorous,
strontium, barium, rubidium, potassium, and
sodium. Geochim. cosmochim. Acta, 31, 2197-218.

HANSON, G.N., 1977. Evolution of the sub-oceanic mantle.
Jl. Geol. Soc. Lond. 134, 235-253.

HANSON, G.N., 1978. The application of trace elements to the
petrogenesis of igneous rocks of granitic
composition. Earth Planet. Sci. Lett., 38,
26-43.

HART, S.R., 1971. K,Rb,Cs, Sr and Ba contents and Sr isotope
ratios of ocean-floor basalts. Phil. Trans.
Roy. Soc. Lond., A268, 573-588.

HAWKINS, J.W., 1974. Geology of the Lau Basin, a marginal sea
behind the Tonga Arc, in Burke, C.A., and
Drake, C.L., eds., The Geology of Continental
Margins: Springer-Verlag, New York, p.505-520.

HAWKINS, J.W., 1976. Petrology and geochemistry of basaltic rocks of the Lau Basin. Earth Planet Sci. Lett., 28, 283-298.

HEKINIAN, R., 1968. Rocks from the mid-ocean ridge in the Indian Ocean. Deep Sea Res., 15, 195-213.

HERTOGEN, J. and GIJBELS, R., 1971. Instrumental Neutron Activation Analysis of rocks with a low-energy Photon detector. Anal. Chim. Acta., 56, 61-82.

HEWINS, R.H., 1975. Pyroxene geothermometry of some granulite facies rocks. Contrib. Mineral. Petrol., 50, 205-209.

HIGGINS, M.W., 1971. Cataclastic rocks. Prof. Pap. U.S. geol. surv., 687, 1-95.

HIMMELBERG, G.R. and LONEY, R.A., 1973. Petrology of the Vulcan Peak alpine peridotite, S.W. Oregon. Bull. Geol. Soc. Am., 84, 1585-1600.

HONNOREZ, J. and KIRST, P., 1976. Petrology of rodingites from the equatorial Mid-Atlantic Ridge fracture zones and their tectonic significance. Contr. Mineral. Petrol., 49, 233-257.

IRVINE, T.N., 1970. Crystallization sequences in the Muskox intrusion and other byered intrusions. I. Olivine-pyroxine-plagioclase relations. Geol. Soc. S.Africa, Sp. Pub. 1, 441-476.

IRVINE, T.N., and BARAGAR, W.R.A., 1971. A guide to the chemical classification of the common volcanic rocks. Can. J. Earth Sci., 8, 523-548.

IRVING, T.N. and FINDLAY, T.C., 1972. Alpine-type peridotite with particular reference to the Bay of Islands igneous complex. Publ. Earth Phys. Br. 423, Rept. Energy, Mines, Resources, Canada, 97-128.

JACKSON, E.D., 1967. Ultramafic cumulates in the Stillwater, Great Dyke and Bushveld intrusions: in Wyllie, P.J. ed., Ultramafic and related rocks, John Wiley & Sons, New York. p.20-38.

JACKSON, E.D., GREEN II, H.W., and MOORES, E.M., 1975. The Vourinos ophiolite, Greece: cyclic units of lineated cumulates overlying harzburgite tectonite. Bull. Geol. Soc. Am., 86, 390-398.

JAKES, P. and GILL, J., 1970. Rare earth elements and the island arc tholeiite series. Earth Planet. Sci. Lett., 9, 17-28.

KAY, R.W., and SENECHAL, R.G., 1976. The rare earth geochemistry of the Troodos ophiolite complex. Jour. Geophys. Res., 81, 964-970

KEITH, T.E.C., MUFFLER, L.J.P., and CREMER, M., 1968.
Hydrothermal epidote formed in the Salton Sea
geothermal system, California. Am. Mineral.,
53., 1635-1644.

KEMPE, D.R.C. and SCHILLING, J.G., 1974. Discovery Tablemount
basalt: petrology and geochemistry.
Contrib. Mineral. Petrol., 44, 101-115.

KIDD, W.S.F., DEWEY, J.F., and BIRD, J.M., 1978. The Mings
Bight Ophiolite Complex, Newfoundland:
Appalachian oceanic crust and mantle.
Can. Journ. Earth Sci., 15, 781-805.

KOLBE, P., and TAYLOR, S.R.T., 1966. Geochemical investigation
of the granitic rocks of the Snowy Mountains
area, New South Wales. J. Geol. Soc. Aust.,
13, 1-25.

KUSHIRO, I., 1965. Clinopyroxene solid solutions at high
pressures. Carnegie Inst. Year Book 64, 112-117.

KUSHIRO, I. and YODER, H.S.Jr., 1965. The reactions between
forsterite and anorthite at high pressures.
Carnegie Inst. Year Book 64, 89-94.

KUSHIRO, I., SYONO, Y. and AKIMOTO, S., 1968. Melting of a
peridotite nodule at high pressures and
high water pressures. J. Geophys. Res., 73,
6023.

KUSHIRO, I., YODER, H.S., and NISHIKAWA, M., 1968. Effect of
water on the melting of enstatite.
Geol. Soc. Am. Bull., 79, 1685-1692.

LARSEN JR., E.S., 1948. Batholith and associated rocks of
Corona, Elsinore and San Luis Rey quadrangles,
southern California. Mem. Geol. Soc. Am., 29,
1-160.

LAUGHTON, A.S., 1966. The Gulf of Aden. Phil. Trans. Roy. Soc.
A, 259, 150-163.

LEEMAN, W.P., 1976. Petrogenesis of McKinney (Snake River)
olivine tholeiite in light of rare-earth
element and Cr/Ni distributions.
Geol. Soc. Am. Bull., 87, 1582-1586.

LEES, G.M., 1928. The geology and tectonics of Oman and of
part of south-eastern Asia. Q. Jl. Geol.
Soc. Lond., 84, 585-670.

LE PICHON, X., and HEIRTZLER, J.R., 1968. Magnetic anomolies
in the Indian Ocean and sea-floor spreading.
J. Geophys. Res., 73, 2101-2117.

LONEY, R.A., HIMMELBERG, G.R. and COLEMAN, R.G., 1971. Structure and petrology of the alpine-type peridotite at Burro Mountain, California, U.S.A. Jour. Petrol., 12, 245-310.

MACDONALD, R., UPTON, B.G.J. and THOMAS, E.J., 1973. Potassium and fluorine-rich hydrous phase co-existing with peralkaline granite in south Greenland. Earth Planet. Sci. Lett., 18, 217-22.

MACGREGOR, I.D., 1974. The system $MgO-Al_2O_3-SiO_2$ & solubility of Al_2O_3 in enstatite for spinel and garnet peridotite compositions. Am. Min., 59, 110-119.

McKENZIE, C.B. and CLARKE, D.B., 1975. Petrology of the South Mountain batholith Nova Scotia. Can. J. Earth Sci., 12, 1208-18.

McKENZIE, D. and SCHLATER, J.G., 1971. The evolution of the Indian Ocean since the Late Cretaceous. Geophys. J. Roy. Astro. Soc., 25, 437-528.

MALPAS, J., 1978. Magma generation in the upper mantle, field evidence from ophiolite suites, and application to the generation of the oceanic lithosphere. Phil. Trans. Roy. Soc. Lond. A., 288, 527-546.

MATTHEWS, D.H., 1966. The Owen Fracture Zone and the northern end of the Carlsburg Ridge. Phil. Trans. Roy. Soc. Lond. Ser. A., 259, 172-186.

MELSON, W.G., and THOMPSON, G., 1971. Petrology of a Transform fault zone and adjacent ridge segments. Phil. Trans. Roy. Soc. Lond. A., 268, 423-441.

MENZIES, M. and ALLEN, C., 1974. Plagioclase lherzolite-residual mantle relationships within two Eastern Mediterranean ophiolites. Contrib. Mineral. Petrol., 45, 197-213.

MENZIES, M., BLANCHARD, D., BRANNON, J., and KOROTEV, R., 1977. Rare earth geochemistry of fused ophiolitic and alpine lherzolites. Contrib. Mineral. Petrol., 64, 53-75.

MIYASHIRO, A., 1973. The Troodos ophiolitic complex was probably formed in an island arc. Earth Planet Sci. Lett., 19, 218-24.

MIYASHIRO, A., 1978. Nature of Alkalic Volcanic rock series. Contrib. Mineral. Petrol, 66, 91-104.

MIYASHIRO, A., SHIDO, F., and EWING, M., 1969. Composition and origin of serpentinites from the Mid-Atlantic Ridge. Contrib. Mineral. Petrol., 23, 117-127.

MIYASHIRO, A., SHIDO, F., and EWING, M., 1970. Petrologic models for the Mid-Atlantic Ridge. Deep Sea Res., 17, 109-123.

MIYASHIRO, A., SHIDO, F. and EWING, M., 1971. Metamorphism in
        Mid-Atlantic Ridge near 24° and 30°N.
        Phil. Trans. Roy. Soc. Lond. A. 268, 589-604.

MOORES, E.M., 1973. Plate tectonic significance of Alpine Peri-
        dotite types. Implications of continental
        drift to the earth sciences, II, ed. Tarling, E.D.
        and Runcorn, S.K.

MOORES, E.M., and MACGREGOR, I.D., 1972. Types of alpine
        ultramafic rocks and their implications for
        fossil plate interactions, in studies in
        Earth and Space Sciences. Geol. Soc. Am. Mem.,
        132, 209-223.

MOORES, E.M., and VINE, F.J., 1971. The Troodos Massif, Cyprus
        and other ophiolites as oceanic crust;
        evaluation and implications.
        Phil. Trans. Roy. Soc. Lond. A., 268, 443-466.

MORTON, D.M., 1959. The geology of Oman. Proc. Fifth Wld.
        Cong., New York, section 1, paper 14.

MOSELEY, F., 1969. The Upper Cretaceous ophiolite complex of
        Masirah Island, Oman. Geol. J., 6, 293-306.

MOSELEY, F., 1973. Diapiric and gravity tectonics in the Pre-
        Betic (Sierra Bernia) of south-east Spain.
        Bol. Geol. y Minero Espana, 84, 114-126.

MOSELEY, F., and ABBOTTS, I.L., 1978. The ophiolite melange
        of Masirah, Oman; diapir, transform, wrench
        or thrust? Submitted to Geol. Soc. Lond.
        (Chapter 8).

NAGASAWA, H., 1970. Rare earth concentrations in zircons and
        apatites and their host dacites and granites.
        Earth. Plant. Sci. Lett., 9, 359-364.

NEARY, C.R., GASS, I.G. and CAVANAGH, R.J., 1976. Granitic
        association of north-eastern Sudan.
        Bull. Geol. Soc. Am., 87, 1501-1512.

NISBET, E. and PEARCE, J.A., 1973. TiO_2 and a possible guide to
        past oceanic spreading rates. Nature. 246,
        468-470.

NOCKOLDS, S.R. and ALLEN, R., 1953. The geochemistry of some
        igneous rock series. Geochim. cosmochim. Acta.,
        4, 105-42.

O'CONNOR, J.T., 1965. A classification of quartz-rich
        igneous rocks based on felspar ratios.
        U.S. Geol. Surv. Prof. Paper., 525B, B79-84.

O'HARA, M.J., 1967. Mineral parageneses in ultrabasic rocks. In Ultramafic and related rocks, 393-403. Ed. P.J. WYLLIE. Wiley & Sons, London.

O'HARA, M.J., 1977a. Geochemical evolution during fractional crystallisation of a periodically refilled magma chamber. Nature, 266, 503-507.

O'HARA, M.J., 1977b. Thermometry and borometry of Scourie gneisses. J. Geol. Soc.

OSBOURNE, E.F. and TAIT, D.B., 1952. The system diopside-forsterite-anorthite. Am. J. Sci. Bowen Volume, 413-433

PEARCE, J.A., 1975. Basalt geochemistry used to investigate past environments on Cyprus. Tectonophysics. 25, 41-67

PEARCE, J.A., 1978. Petrogenetic studies of metabasalts using immobile trace elements. J. geol. Soc. Lond., 135, 592.

PEARCE, J.A. and CANN, J.R., 1971. Ophiolite origin investigated by discriminant analyses using Ti, Zr and Y. Earth Planet. Sci. Lett., 12, 339-349.

PEARCE, J.A. and CANN, J.R., 1973. Tectonic setting of basic volcanic rocks using trace element analyses. Earth Planet. Sci. Lett., 19, 290-300.

PEARCE, J.A. and FLOWER, M.F.J., 1978. The relative importance of petrogenetic variables in magma genesis at accreting plate margins, a preliminary investigation. J. geol. Soc. Lond., 134, 103-127.

PRICE, R.C. and TAYLOR, S.R., 1977. The rare earth element geochemistry of granite, gneiss and migmatite from the Western Metamorphic Belt of south-eastern Australia. Contr. Mineral Petrol., 62, 249-63.

RALEIGH, C.B., 1967. Tectonic implications of serpentinite weakening. R. Astro. Soc. Geophys. J., 14, 113-118.

REED, F.R.C., 1949. The Geology of the British Empire. 2nd ed. Edward Arnold.

REINHARDT, B.M., 1969. Ophiolites in the Oman Mountains Geosyndine. Schweiz. Min. Pet. Mitt., 49, 1-30.

REODER, P.L. and EMSLIE, R.F., 1970. Olivine-liquid equilibrium. Contrib. Mineral. Petrol., 29, 275-289.

RHODES, J.M., BLANCHARD, D.P., RODGERS, K.V., JACOBS, J.W., and BRANNER, J.C., 1976. Petrology and chemistry of basalts from the Nazca Plate: Part 2-major and trace element chemistry. Init. Rept. Deep Sea Drilling Project. 34, 239-244.

RONA, P.A and RICHARDSON, E.S., 1978. Early Cenozoic global plate reorganisation. Earth Planet. Sci. Lett., 40, 1-11.

SALISBURY, M.H., and CHRISTENSEN, N.I., 1978. The seismic velocity structure of a traverse through the Bay of Islands Ophiolite Complex, Newfoundland, an exposure of ocean crust and upper mantle. J. Geophys. Res., 83. 805-818.

SAUNDERS, A.D. and TARNEY, J., 1978. Geochemistry of basalts from the back-arc spreading centre in the Scotia Sea. Submitted to Geochim. Cosmochim. Acta.

SAUNDERS, A.D., TARNEY, J., STERN, C.R., and DAZIEL, I.W.D., 1978. Geochemistry of Mesozoic marginal basin floor igneous rocks from southern Chile. Bull. geol. Soc. Am. (in press).

SCHNETZLER, C.C. and PHILPOTTS, J.A., 1970. Partition coefficients of rare earth elements between igneous matrix material and rock forming mineral phenocrysts. Geochim. Cosmochim. Acta, 34, 331-340.

SCOTT, R.B., MALPAS, J., RONA, P.A., and UDINTSEV, G., 1976. Duration of hydrothermal activity at an oceanic spreading centre, Mid-Atlantic Ridge (lat. 26°N). Geology, 4, 233-236.

SCOTT, R.B., RONA, P.A., McGREGOR, B.A. and SCOTT, M.R., 1974. TAG Hydrothermal field. Nature, 251, 301-302.

SHIDO, F., MIYASHIRO, A. and EWING, M., 1971. Crystallization of abyssal tholeiites. Contr. Mineral. Petrol. v.31, p.251-266.

SIMONIAN, K.O., 1975. Metamorphism of the Troodos Massif, Cyprus. Unpubl. Ph.D. thesis, Open University.

SIMONIAN, K.O. and GASS, I.G., 1978. Arakapas Fault Belt, Cyprus: a fossil transform fault. Bull. Geol. Soc. Am., 89, 1220-1230.

SMEWING, J.D. and POTTS, P.J., 1970. Rare earth abundances in basalts and metabasalts from the Troodos Massif, Cyprus. Contrib. Mineral. Petrol., 57, 245-258.

SMEWING, J.D., SIMONIAN, K.O., and GASS, I.G., 1975. Metabasalts from Troodos Massif, Cyprus: genetic implication deduced from petrography and trace element geochemistry. Contr. Mineral. Petrol., 51, 49-64.

SMEWING, J.D., SIMONIAN, K.O., ELBOUSHI, I.M. and GASS, I.G., 1977. Mineralized fault zone parallel to the Oman ophiolite spreading axis. Geology, 5, 534-538.

SMITH, T.E., 1974. The geochemistry of the granite rocks of Halifax County, Nova Scotia. Con. J. Earth. Sci. 11., 650-6.

SPOONER, E.T.C, and FYFE, W.S., 1973. Sub-sea floor metamorphism, heat and mass transfer. Contr. Mineral. Petrol., 42, 287-304.

STONELY, R., 1974. On the origin of ophiolite complexes in the southern Tethys region. Tectonophysics, 25, 303-322.

STRECKEINSEN, A., 1976. Classification of plutonic rocks. Earth Sci. Rev., 12, 1-38.

SUN, S.S. and NESBIT, R.W., 1978. Geochemical regularities and genetic significance of ophiolitic basalts. Geol. (in press)

TARNEY, J., SAUNDERS, A.D., WEAVER, S.D., 1977. Geochemistry of volcanic rocks from the island arcs and marginal basins of the Scotia Arc Region. In: Island Arcs, Deep Sea Trenches and Back-Arc Basins. Maurice Ewing Series 1, 367-377. Ame. Geophys. Union.

TARNEY, J., SAUNDERS, A.D., WEAVER, S.D., DONNELLAN, N.C.B., HENDRY, G.L. Minor element geochemistry of basalts from Leg 49, North Atlantic Ocean. In J.R. Cann, B. Luyendyk et al, Initial Rept. Deep Sea Drilling Project, 49, Washington (U.S. Government Printing Office) in press.

TAYLOR, P.T., 1968. Interpretation of the northern Arabian Sea aeromagnetic survey. Earth Planet. Sci. Lett., 4, 222-236.

THOMPSON, G., BRYAN, W.B., FREY, F.A., DICKEY, J.S. and SUEN, C.J., 1976. Petrology and geochemistry of basalts from DSDP Leg 34, Nazca Plate. Init. Rept. Deep Sea Drilling Project, vol. 34. Washington (U.S. Government Printing Office) p. 215-226.

THOMPSON, G. and MELSON, W.G., 1970. Boron contents of serpentinites and metabasalts in the oceanic crust; implications for the boron cycle in the oceans. Earth Planet. Sci. Lett., 8, 61-65.

THOMPSON, G., and MELSON, W.G., 1972. The petrology of oceanic crust across fracture zones in the Atlantic Ocean: evidence for a new kind of sea-floor spreading. J. Geol., 80, 526-538.

THOMPSON, R.N., 1968. Tertiary granites and associated rocks of the Manxo area, Isle of Skye. Q. Jl. geol. Soc. Lond., 124, 349-85.

U.S.S.R. ACADEMY OF SCIENCES, 1975. Geological and Geophysical Atlas of the Indian Ocean.

VARNE, R. and RUBEN ACH, M.J., 1973. Geology of Macquarie Island in relation to tectonic environment. In: The Western Pacific island arcs, marginal seas, geochemistry. COLEMAN, P.J. ed. (Nedlands University of Western Australia Press, 1973), 535-41.

WAGER, L.R. and BROWN, G.M., 1967. Layered igneous rocks. W. J. Freeman & Co., San Francisco.

WEAVER, S.D., SAUNDERS, A.D. and TARNEY, J. Mesozoic-Cenozoic volcanism in the South Shetland Islands and the Antarctic Peninsula : geochemical nature and plate tectonic significance. In: Third Symposium on Antarctic Geology and Geophysics. ed CRADDOCK, C. Madison Univ. Winconsin. (in press)

WEAVER, S.D., SCEAL, J.S.C., GIBSON, I.L., 1972. Trace element data relevant to the origin of trachytic and pantelleritic lavas in the East African rift system. Contrib. Mineral. Petrol., 36, 181-194.

WELLAND, M.J.P., 1975. Late Cretaceous nappes in the Oman Mountains and their geological evolution: discussion. Bull. Am. Ass. Petrol. Geol. 59, 1686-1688.

WELLAND, M.J.P. and MITCHELL, A.H.G., 1977. Emplacement of the Oman Ophiolite: a mechanism related to subduction and collision. Bull. Geol. Soc. Am, 88, 1081-1088.

WELLS, P.R.A., 1977. Pyroxene thermometry in simple and complex systems. Contrib. Mineral. Petrol. 62, 129-139.

WENNER, D.B. and TAYLOR, H.P. Jr., 1971. Temperatures of serpentinisation of ultramafic rocks based on O^{18}/O^{16} fractionation between co-existing serpentine and magnetite. Contrib. Mineral. Petrol., 32, 165-185.

WEST, S., 1974. The geology of the Danco Coast, Graham Land. Br. Antarctic Surv. Sci. Rep., 84, 57pp.

WHITE, R.S. and KLITGORD, K., 1976.   Sediment deformation
                and plate tectonics in the Gulf of Oman.
                Earth Planet. Sci. Lett., 32, 199-209.

WHITMARSH, R.B. and others (shipboard crew), 1972.
                Init. Rept. DSDP, Leg 23.   Washington
                (U.S. Government Printing Office), 809-819.

WILSON, H.H., 1969.   Late Cretaceous eugeosynclinal
                sedimentation, gravity tectonics and
                ophiolite emplacement in the Oman Mountains,
                South-East Arabia.   Bull. Am. Ass. Petrol.
                Geol., 53, 626-71.

WOOD, B.J. and BANNO, S., 1973.   Garnet-orthopyroxene and
                orthopyroxene-clinopyroxene relationships
                in simple and complex systems.   Contrib.
                Mineral. Petrol., 42, 109-124.

WOODCOCK, N.H. and ROBERTSON, A.H.F., 1977.   Origins of some
                ophiolite-related metamorphic rocks of the
                "Tethyan" belt.   Geol., 5, 373-376.

YAGI, K., 1967.   Silicate systems related to basaltic rocks.
                In: Basalt Treatise, 359-400. HESS, H.H.
                and POLDERVAART, A. eds., Interscience,
                London.

YODER, H. S. Jr., 1952.   The $MgO-Al_2O_3-SiO_2-H_2O$ system and
                the related metamorphic facies.   Am.J.Sci.
                Bowen Vol., 569-627.